

FINAL REPORT

EVALUATION OF BRIDGE DECK DELAMINATION INVESTIGATION METHODS

Project IC-H1, 95/96

Report No. ITRC FR 95/96-1

Prepared by

Henrique L. M. dos Reis

and

Matthew D. Baright

Department of General Engineering
University of Illinois at Urbana-Champaign
Urbana, Illinois

July 1998

Illinois Transportation Research Center
Illinois Department of Transportation

ILLINOIS TRANSPORTATION RESEARCH CENTER

This research project was sponsored by the State of Illinois, acting by and through its Department of Transportation, according to the terms of the Memorandum of Understanding established with the Illinois Transportation Research Center. The Illinois Transportation Research Center is a joint Public-Private-University cooperative transportation research unit underwritten by the Illinois Department of Transportation. The purpose of the Center is the conduct of research in all modes of transportation to provide the knowledge and technology base to improve the capacity to meet the present and future mobility needs of individuals, industry and commerce of the State of Illinois.

Research reports are published throughout the year as research projects are completed. The contents of these reports reflect the views of the authors who are responsible for the facts and the accuracy of the data presented herein. The contents do not necessarily reflect the official views or policies of the Illinois Transportation Research Center or the Illinois Department of Transportation. This report does not constitute a standard, specification, or regulation.

Neither the United States Government nor the State of Illinois endorses products or manufacturers. Trade or manufacturers' names appear in the reports solely because they are considered essential to the object of the reports.

Illinois Transportation Research Center Members

Bradley University
DePaul University
Eastern Illinois University
Illinois Department of Transportation
Illinois Institute of Technology
Lewis University
Northern Illinois University
Northwestern University
Southern Illinois University at Carbondale
Southern Illinois University at Edwardsville
University of Illinois at Chicago
University of Illinois at Urbana-Champaign
Western Illinois University

Reports may be obtained by writing to the administrative offices of the Illinois Transportation Research Center at 200 University Park, Edwardsville, IL 62025 [telephone (618) 650-2972], or you may contact the Engineer of Physical Research, Illinois Department of Transportation, at (217) 782-6732.

1. Report No. ITRC FR 95/96-1		2. Government Accession No.		3. Recipient's Catalog No.	
4. Title and Subtitle Evaluation of Bridge Deck Delamination Investigation Methods				5. Report Date July 1998	
				6. Performing Organization Code	
7. Author(s) Henrique L.M. dos Reis and Matthew D. Baright				8. Performing Organization Report No.	
9. Performing Organization Name and Address University of Illinois at Urbana-Champaign Department of General Engineering 104 South Mathews Urbana, Illinois 61801				10. Work Unit No. (TRAIS)	
				11. Contract or Grant No. IC-H1, 95/96	
12. Sponsoring Agency Name and Address Illinois transportation Research Center 200 University Park, Room 2210 Edwardsville, IL 62025				13. Type of Report and Period Covered Final Report August 1996 to January 1998	
				14. Sponsoring Agency Code	
15. Supplementary Notes					
16. Abstract An objective view of the relative advantages and limitations of the nondestructive testing and evaluation methods that are currently used in the inspection of bridge decks is presented and discussed. The three main nondestructive testing technologies that were evaluated are impact-echo, ground penetrating radar, and infrared thermography. Nondestructive testing and evaluation procedures, including methodology and equipment to evaluate concrete bridge decks with asphalt overlays, are also presented and discussed. Current results indicate that a combination of ground penetrating radar and infrared thermography would provide the best methodology for evaluating the structure integrity, e.g., delaminations, of concrete bridge decks with overlays. Furthermore, current results also indicate that the impact-echo method shows promising future development towards the nondestructive evaluation of bridge superstructures.					
17. Key Words Bridge Decks, Overlays, Delaminations, Debonds, Impact-Echo, Ground Penetrating Radar, Infrared Thermography, Chain drag, Bridge Rehabilitation, Damage			18. Distribution Statement No Restrictions. This document is available to the public through the National Technical Information Service (NTIS), Springfield, Virginia 22161		
19. Security Classif. (of this report) Unclassified		20. Security Classif. (of this page) Unclassified		21. No. of Pages 275	22. Price



FINAL REPORT

EVALUATION OF BRIDGE DECK DELAMINATION INVESTIGATION METHODS

Project IC-H1, 95/96

Report No. ITRC FR 95/96-1

Prepared by

Henrique L. M. dos Reis

and

Matthew D. Baright

Department of General Engineering

University of Illinois at Urbana-Champaign

Urbana, Illinois

July 1998

Illinois Transportation Research Center

Illinois Department of Transportation

1870-1875

1876-1880

1881-1885

ACKNOWLEDGMENTS

The authors would like to acknowledge the support and advice from Dr. Steven J. Hanna from the Illinois Transportation Research Center and from Mr. Thomas J. Domagalski from the Illinois Department of Transportation (IDOT). The authors would also like to acknowledge Professor Neil M. Hawkins for his technical discussions and advice. Special thanks are due to Mr. Eugene Smania from IDOT, District 3, for spending many days chain dragging bridge decks across Illinois; his enthusiasm and willingness to share his experience proved invaluable. The assistance of Mr. George Ramia and Mr. Merle Dickey of IDOT, District 4, for providing information concerning bridge decks around Peoria is very much appreciated. Thanks are due to the men and women of IDOT Districts 3, 4, and 9 who provided traffic control for safety during inspection. The authors are also grateful to Mr. Anthony J. Alongi and Mr. Kevin J. Stephanski from Penetradar Corporation, to Mr. Jerry W. Eales and Mr. Daniel D. Ulrikson from RUST Environment & Infrastructure, and to Mr. Larry D. Olson from Olson Engineering, for performing the ground penetrating radar inspection, the thermal imaging inspection, and the impact-echo inspection, respectively.



EXECUTIVE SUMMARY
EVALUATION OF BRIDGE DECK
DELAMINATION INVESTIGATION METHODS

Project IC-H1, 95/96
Report No. ITRC FR 95/96-1

INTRODUCTION

Cost effective bridge deck rehabilitation makes it necessary to locate the areas in need of repair to accurately estimate the quantity of deteriorated concrete. Since the bituminous overlay prevents visual identification of these areas, nondestructive testing and evaluation techniques are essential. Conventional nondestructive testing techniques, such as sounding by hammer and chain drag, do not fare well on asphalt covered decks, primarily due to the inefficient coupling of energy between the asphalt overlay and the concrete. They are usually effective only after the asphalt overlay has been removed. Destructive testing methods such as core samples are effective when a large number of random samples are obtained, which is both costly and unnecessarily damaging to the bridge deck. Recently, nondestructive testing and evaluation techniques, such as impact-echo, ground penetrating radar, and infrared thermography, have shown promise for the noninvasive evaluation of the damage accumulation in concrete bridge decks overlaid with asphalt concrete wearing surfaces. The motivation of this study is to evaluate the advantages and limitations of the nondestructive testing and evaluation methods that are currently used to inspect bridge decks with asphalt overlays. A comprehensive literature review of these methods can be found in the technical report.

EXPERIMENTAL STUDY

Selection and Description of the Bridges

To ensure a comprehensive evaluation of the nondestructive testing and evaluation methods, nine bridge decks in varying states of decay were selected - the bridges were chosen with an increasing state of damage ranging from bridges with minimal reinforcing steel corrosion and few delaminations to bridges with widespread delaminations and showing previous rehabilitation work. In this manner, the selected nondestructive testing techniques could be evaluated based on their ability to locate delaminations and deterioration as well as on their susceptibility to falsely report delaminations and deterioration that does not exist. Although the actual conditions of the bridges were not known prior to testing, a reasonable guess was made based upon construction and maintenance dates and other information regarding the history of each bridge as well as visual inspection.

Table 1 provides a summary of general information of the nine bridge decks. For the description of the nine bridges and their selection procedure, the author is referred to technical report. In the technical report, the authors provide an overview of the general structural condition of each bridge based upon field observations made during testing and removal of the asphalt overlay. The conditions of the nine bridges provided a broad range of structural damage. All bridges were inspected using infrared thermography and ground penetrating radar. Only one bridge, structure number 100-005, was completely scanned using the impact-echo test method. Furthermore, only bridge number 100-005 was tested using the spectral analysis of surface waves method.

Experimental Procedure

Three different companies independently evaluated the nine bridge decks throughout central and southern Illinois in their pre-rehabilitation state during the summer of 1997. Each company is a recognized leader in its respective field. Penetradar Corporation performed the ground penetrating radar inspection, Rust Environment & Infrastructure performed the infrared thermography inspection, and Olson Engineering performed the impact-echo and the spectral analysis of surface waves inspection. Each test was performed independently of the others and before the asphalt overlays were removed. Each of the three companies submitted a report detailing their findings for this study.

Each of these test methods has a different inspection speed. Impact-echo, due to the prototypical nature of the inspection equipment, required a day to inspect a typical bridge deck. Infrared thermography can inspect a deck in one to two hours. Ground penetrating radar can inspect a bridge in less than an hour. These time estimates do not include the time required for data processing. During all inspections, the lanes were closed to traffic, and the inspection rate was no greater than 5 mph (8.1 km/h). However, infrared and radar inspections can be performed at normal traffic speeds without lane closings, which would certainly result in degradation of data quality. Vibrations caused by traffic have little effect on any of the three test methods. Impact-echo used a simple high-pass filter to filter out the low frequency vibrations averaging 10 Hz. During impact-echo testing, a sample point was taken once approximately every 3 inches (0.08 m). There was a one foot spacing between each line of testing. For ground penetrating radar inspection, a waveform was digitized approximately once every 3-6 inches (0.08- 0.18 m), with a 3 feet (0.92 m) spacing between antennas. Infrared thermography provided a full field digitized view of the pavement with a temperature measurement of at least one half-inch resolution.

After the nondestructive testing and evaluation of the bridge decks was completed, the asphalt overlays were removed from the bridge decks. Using the chain dragging method along with the sand/hammering test method, surveys of the delaminated areas of the bare concrete bridge decks were then performed by a technical expert with several years of experience. In this manner, unbiased and independent surveys of delaminated areas of the bridge decks were obtained. These surveys of delaminated areas detected by chain dragging and by the sand/hammering method were verified by visual inspection after the delaminated concrete was removed, and provided the base-line measurements with which the measurements of the chosen nondestructive testing methods were compared.

EXPERIMENTAL RESULTS AND DISCUSSION

Table 2 summarizes the total area of delaminations for all bridge decks. Using the chain drag method, 12383.0 ft² (1150.4 m²) of delaminated area, i.e., 13.0% of the total bridge deck area, was found. The infrared thermography survey found 8748.9 ft² (812.8 m²) of delaminated area, 9.2% of the total area of all the decks. The ground penetrating radar survey found 13993.4 ft² (1300.0 m²) of delaminated area, 14.7% of the total area of all the decks. Table 3 summarizes the total number of individual delaminations found for all bridge decks. The chain drag survey found 179 individual delaminations. The infrared thermography survey found 66 delaminations, 36.9% of the number found by the chain drag survey. The ground penetrating radar survey found 91 delaminations, 50.8% of the number found by the chain drag survey. Table 4 summarizes the total number of major delaminations found for all bridge decks. Major delaminations are those having a delaminated area of at least 10 ft² (0.9 m²). The chain drag survey found 22 major individual delaminations. The infrared thermography survey found 15 major individual delaminations, 68.2% of the number found by the chain drag survey. The ground penetrating radar survey found 15 major individual delaminations, 77.3% of the number found by the chain drag survey.

For the complete set of plots of the delaminated areas in the bridge decks found by infrared thermography, ground penetrating radar, impact echo, and the chain drag method, the reader is referred to the technical report. The spectral analysis of surface waves was used only point-by-point

on the bridge deck number 100-0005, and the results correlated with visual examination of corresponding cores extracted from the deck. Furthermore, only the structure number 100-0005 was completely scanned using the impact-echo method. While the impact-echo test method is reported here, the reader is referred to the technical report for discussion of the results obtained using the spectral analysis of surface waves and impact-echo test methods.

Tables 2-4 show the total delaminated area in need of repair for each bridge deck estimated by each method. It was observed that ground penetrating radar and infrared thermography easily detect large delaminated areas having wide crack widths. Smaller, deeper, delaminated areas, less than 10 ft² (0.9 m²), are more difficult for these methods, particularly for the infrared thermography. Because of its nature, impact-echo should theoretically detect even the smallest defect; the theoretical limitation of detectable crack separation width is small compared to practical requirements.

For the decks with large areas of delamination, both ground penetrating radar and infrared thermography did well estimating the total rehabilitation area. On the decks with small, individual delaminated areas, infrared thermography frequently underestimated the total area in need of repair and ground penetrating radar tended to overestimate the total area in need of repair. It was observed that each test is susceptible to report false delaminations to some degree. Infrared thermography reported fewer false indications of delaminations -- the majority of errors were on the conservative side, mis-identifying delaminations as debonds between concrete and the asphalt overlay. Ground penetrating radar reported a larger number of small delaminations where none were found by chain drag or visual inspection.

The presence of reinforcing steel in bridge decks has little effect on these test methods. Reinforcing steel has no significant effect on infrared thermography. Ground penetrating radar can detect the presence of reinforcing steel and determine its depth. Impact-echo can also detect and determine the depth of reinforcing steel. Steel abutment joints have very little effect on infrared thermography and impact-echo. However, results indicate that ground penetrating radar is affected by steel abutment joints; there is a high incidence of false indications surrounding the steel joints -- it appears that as the antenna approaches the steel joints, the radar pulse is affected by the presence of the large amount of ferrous material.

The ability of each test method to detect shallow versus deep delaminations and to distinguish debonding of the asphalt overlay from shallow delaminations was also evaluated. Ground penetrating radar detects shallow and deep delaminations with equal accuracy. Because depth is precisely determined, there is no confusion between shallow delaminations and debonding. Impact-echo theoretically detects shallow and deep delaminations with equal accuracy. Practically, the currently used impact-echo test method is often unable to distinguish between debonding and shallow delaminations because the dominant mode of vibration is flexural. Flexural vibrations have a low frequency and dominate the response of shallow delaminations and debonds. Infrared thermography theoretically can not distinguish a shallow delamination from a debond. Practically, the two can be distinguished by noting certain particular characteristics, such as size and shape, and by cross correlating the test results with visual observation of core samples. Only ground penetrating radar can inspect a concrete deck for delaminations with a debonded asphalt layer -- debonding of the asphalt layer prevents inspection of the underlying concrete by the infrared thermography and impact-echo methods. Following are some of the advantages and disadvantages of each test method.

Infrared Thermography -- Its Current Observed Advantages and Disadvantages

Infrared thermography provides a full field view of the bridge deck. Infrared thermography is repeatable provided solar conditions are consistent; otherwise, testing performed during different conditions may produce different results. There is no sampling during data collection; resolution is limited only by the digitization of the camera. Infrared can provide accurate size and shape delineation of large areas of delamination. Boundaries can be determined accurately to within an

inch or less. Infrared is relatively quick. A three lane, 300 ft (92 m) bridge can be inspected in less than one hour. Infrared is most accurate for large delaminations. In this study, infrared gave very few false indications of delaminated concrete.

Infrared thermography cannot make a determination of flaw depth, thereby making discernment between delaminations and debonds challenging. Infrared cannot accurately inspect small surface or subsurface regions which have been patched with asphalt or concrete. Infrared has specific weather criteria -- testing is not viable during periods of adverse weather including cloudiness or precipitation. In addition, inspection can only reliably be performed between the hours of 10 a.m. and 4 p.m. Infrared thermography requires a clear, sunny day; rain or snow prevents infrared inspection -- the best conditions for infrared inspection are cool nights followed by warm, sunny days. Infrared is adversely affected by several surface conditions such as debris, moisture, wearing, discoloration, and crack sealant. Infrared thermography requires a surface free of dirt and debris; wet pavement surfaces cannot be tested. In this study, infrared proved susceptible to underestimate the total area of the bridge deck in need of repair.

Ground Penetrating Radar -- Its Current Observed Advantages and Disadvantages

Ground penetrating radar is very repeatable, provided the movement of moisture in the bridge deck is minimal. Radar provides accurate depth information, allowing easy discernment between delaminations and debonds. Radar inspection can be performed at any time during the day or night. Radar inspection is relatively quickly. A three lane, 300 ft (92 m) bridge can be inspected in less than half an hour. Ground penetrating radar is not affected by the majority of adverse surface conditions -- it requires no surface preparation. Ground penetrating radar can be performed in most conditions provided rain or snow is not collecting on the bridge deck.

Ground penetrating radar does not provide a full field view. Currently, commercial available systems require a discrete antenna spacing and are limited by the speed of the data collection wave digitizer. Radar is sensitive to moisture in the bridge deck, and standing pools of water prevent deck inspection. Ground penetrating radar has shown in this study to give false indications of damaged concrete -- this is particularly evident around steel joints and abutments.

Impact-Echo -- Its Current Observed Advantages and Disadvantages

Impact-echo provides accurate depth information, allowing easy discernment between delaminations and debonds. Impact-echo inspection can be performed at any time during the day or night. Impact-echo is not affected by most adverse weather conditions, including standing water on the deck. Impact-echo requires no special weather considerations assuming heavy rain does not damage the electrical equipment. Future impact-echo data analysis techniques have the potential of providing additional information regarding materials characterization such as gradation, strength, and durability, i.e., life prediction.

The main limitation of the traditional impact echo method in this application is its inability to inspect the underlying concrete for delaminations under a debonded portion of the asphalt overlay; while this limitation could potentially be overcome by inspecting the bridge deck from the bottom side, it would clearly be cumbersome. Impact-echo does not provide a full field view -- it requires a point by point data collection system. Impact-echo is somewhat repeatable; currently, impact-echo repeatability is adversely affected by debris, crack sealant, surface roughness, and other irregularities on the surface of the deck which often lead to inconsistent impacts and inconsistent coupling of the roller transducers to the surface of the overlay. Impact-echo requires a surface free of large rocks allowing the transducers to roll smoothly across the asphalt. Impact-echo equipment for pavement inspection is in the early stages of development. Future design work is needed on data collection systems for field use -- current systems are too slow for practical use in testing bridge decks with asphalt overlays.

CONCLUSIONS

An objective view of the relative advantages and limitations of the nondestructive testing and evaluation methods that are currently used in the inspection of bridge decks is presented and discussed. The three main nondestructive testing methods that were evaluated are infrared thermography, ground penetrating radar, and impact-echo. While, infrared thermography and ground penetrating radar are widely used as stand alone test methods for rapid delamination detection in concrete bridge decks, it is recommended that a combination of both, i.e., infrared thermography and ground penetrating radar be used for the most accurate evaluation of the structural integrity, i.e., delaminations, of concrete bridge decks with asphalt overlays. Impact-echo, although showing promise in determining areas of concrete in need of rehabilitation, needs further development of field inspection equipment to make it feasible for practical use. However, current results also indicate that impact-echo test methods show promising future developments towards the nondestructive evaluation of bridge superstructures, and that it may provide additional important information regarding material characterization, damage evaluation, and life prediction.

It was observed that the chain drag method is very operator dependent and that not many operators are trained in this method. In the near future, the number of operators may be even smaller because of the normal process of personnel retirement, and because of the reluctance of younger personnel to develop and acquire the necessary knowledge by proper training. Current impact-echo technology can be developed into a low-cost, portable, and easy-to-operate instrument, that can replace the chain drag method, which is very operator dependent, and subject to misinterpretation. This portable battery-operated instrument can be designed to emit an alarming sound when a delamination is found. Because of relatively low cost, this instrument could be distributed to IDOT districts and be operated by personnel with relatively low training.

Table 1. Summary of Bridge Deck Survey

Structure	Route Carried	Structure Type	Year Constr.	Deck Survey	# Lanes	Lane Width feet (m)	Length feet (m)	Area ft ² (m ²)
057-0088	IL 9 over I-55	4 Span WF	1963 1974	1992	4	12 (3.66)	268 (81.7)	12,864 (1178)
090-0118	FAI 474 (EB)	3 Span Plate Girder	1979	1995	1	12 (3.66)	390 (118.9)	4,680 (435)
072-0106	FAI 474	Single Span Plate Girder	1973	1994	2	12 (3.66)	165 (50.3)	3,960 (368)
072-0107	FAI 474	same	1973	1994	2	12 (3.66)	161 (49.1)	3,864 (359)
072-0108	FAI 474	same	1973	1994	2	12 (3.66)	170 (51.8)	4,080 (379)
072-0109	FAI 474	same	1973	1994	2	12 (3.66)	164 (50.0)	3,936 (366)
072-0110	Ramp A FAI 74	Single Span Plate Girder	1973	1994	2	12 (3.66)	228 (69.5)	5,472 (508)
072-0111	FAI 474	3 Span Plate Girder	1973	1994	2	12 (3.66)	299 (91.1)	7,176 (667)
100-0005	FAI 57 (SB) over SBI 13	3 Span WF	1959/ 1975		3	15 (4.57)	154 (46.9)	6,930 (644)
TOTAL								52,962 (4920)

Table 2. Areas of proposed rehabilitation for all bridge decks

Test Method	Rehabilitation Area ft ² (m ²)	Rehabilitation Area x 100 Total Bridge Deck Area
Chain Drag	12383.0 (1150.4)	13.0%
Infrared Thermography	8748.9 (812.8)	9.2%
Ground Penetrating Radar	13993.4 (1300.0)	14.7%

Table 3. Number of individual delaminations for all bridge decks

Test Method	Number of Individual Delaminations Found	Percent of Delaminations Found by Chain Drag
Chain Drag	179	100%
Infrared Thermography	66	36.9%
Ground Penetrating Radar	91	50.8%

Table 4. Number of major delaminations (minimum 10 ft² (0.9 m²)) for all bridge decks

Test Method	Number of Individual Delaminations Found	Percent of Delaminations Found by Chain Drag
Chain Drag	22	100%
Infrared Thermography	15	68.2%
Ground Penetrating Radar	17	77.3%

TABLE OF CONTENTS

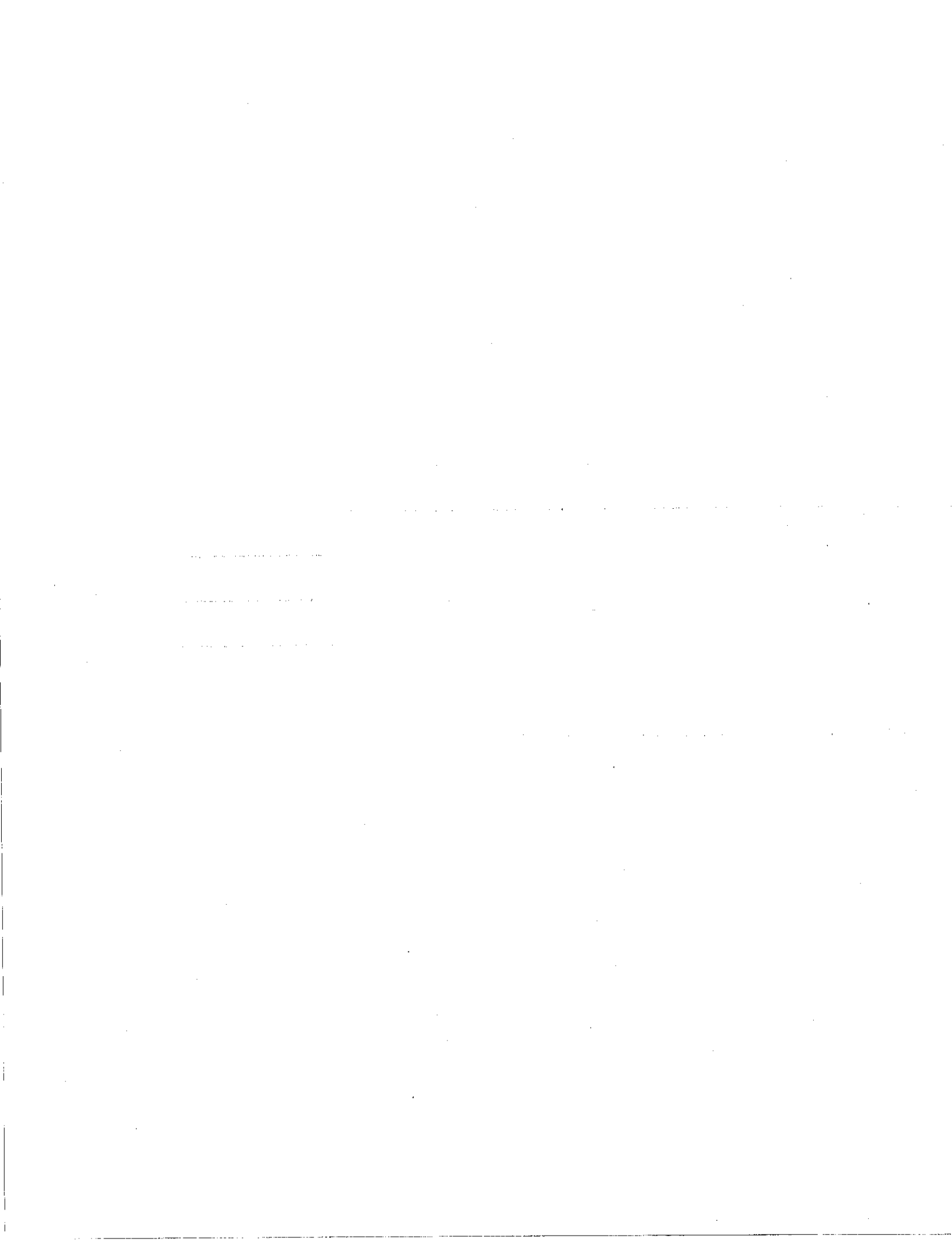
	Page
LIST OF TABLES	xi
LIST OF FIGURES	xiv
LIST OF SYMBOLS	xxiii
1.0 INTRODUCTION	1
1.1 Literature Review of Previous Work	4
1.1.1 Impact-Echo Literature Review of Previous Work.....	5
1.1.2 Ground Penetrating Radar Literature Review of Previous Work	9
1.1.3 Infrared Thermography Literature Review of Previous Work.....	14
1.1.4 Spectral Analysis of Surface Waves Literature Review of Previous Work	18
1.1.5 Chain Drag Survey Literature Review of Previous Work	20
1.2 Selection and Description of the Bridges.....	21
1.2.1 Description of Bloomington Structure Number 057-0088	22
1.2.2 Description of Peoria Structure Number 090-0118	24
1.2.3 Description of Peoria Structure Number 072-0106	26
1.2.4 Description of Peoria Structure Number 072-0107	26
1.2.5 Description of Peoria Structure Number 072-0108	27
1.2.6 Description of Peoria Structure Number 072-0109	27
1.2.7 Description of Peoria Structure Number 072-0110	30
1.2.8 Description of Peoria Structure Number 072-0111	32
1.2.9 Description of Marion Structure Number 100-0005.....	33
1.2.10 Summary Of Bridge Decks.....	35
2.0 THEORY OF INSPECTION METHODS.....	37
2.1 Theory of Impact-Echo	37
2.1.1 Principles of Stress Wave Propagation.....	37
2.1.2 Stress Wave Propagation and Impact-Echo	41
2.1.3 Data Analysis	43
2.1.4 Stress Wave Frequency Characteristics	45
2.2 Theory of Ground Penetrating Radar.....	46
2.2.1 Principles of Radar Propagation in Solids	47
2.2.2 Ground Penetrating Radar and Bridge Decks	50

2.3 Theory of Infrared Thermography	53
2.3.1 Principles of Infrared Radiation.....	53
2.3.2 Infrared Radiation and Bridge Decks.....	55
2.4 Theory of Spectral Analysis of Surface Waves	58
2.5 Theory of Chain Drag	62
3.0 NONDESTRUCTIVE FIELD INSPECTION OF BRIDGES.....	65
3.1 Impact-Echo Field Inspection.....	65
3.1.1 Impact-Echo Field Inspection Equipment	65
3.1.2 Impact-Echo Field Inspection Testing Method.....	70
3.1.3 Impact-Echo Hand Held Testing Equipment.....	70
3.1.4 Impact-Echo Field Inspection and Debonding vs. Delamination	73
3.1.5 Impact-Echo Field Inspection and Test Conditions.....	73
3.2 Ground Penetrating Radar Field Inspection.....	75
3.2.1 Ground Penetrating Radar Field Inspection Equipment	76
3.2.2 Ground Penetrating Radar Field Inspection Testing Method	79
3.2.3 Ground Penetrating Radar Field Inspection and Debonding vs. Delamination	80
3.2.4 Ground Penetrating Radar Inspection and Test Conditions.....	80
3.3 Infrared Thermography Field Inspection	82
3.3.1 Infrared Thermography Field Inspection Equipment.....	82
3.3.2 Infrared Thermography Field Inspection Testing Method.....	86
3.3.3 Infrared Thermography Field Inspection and Debonding vs. Delamination	87
3.3.4 Infrared Imaging of Debonds and Delaminations.....	88
3.3.5 Taking Cores During Infrared Inspection	90
3.3.6 Sounding During Infrared Inspection	92
3.3.7 Infrared Thermography Field Inspection and Test Conditions.....	93
3.4. Chain Drag Field Inspection	95
4.0 RESULTS	99
4.1 Results from Bloomington Structure Number 057-0088.....	99
4.1.1 Chain Drag Results from Bloomington Structure Number 057-0088	103
4.1.2 Infrared Thermography Results from Bloomington Structure Number 057-0088	104
4.1.3 Ground Penetrating Radar Results from Bloomington Structure Number 057-0088	104

4.2 Results from Peoria Structure Number 090-0118.....	105
4.2.1 Chain Drag Results from Peoria Structure Number 090-0118	107
4.2.2 Infrared Thermography Results from Peoria Structure Number 090-0118	108
4.2.3 Ground Penetrating Radar Results from Peoria Structure Number 090-0118	108
4.3 Results from Peoria Structure Number 072-0106.....	108
4.3.1 Chain Drag Results from Peoria Structure Number 072-0106	110
4.3.2 Infrared Thermography Results from Peoria Structure Number 072-0106	110
4.3.3 Ground Penetrating Radar Results from Peoria Structure Number 072-0106	111
4.4 Results from Peoria Structure Number 072-0107.....	111
4.4.1 Chain Drag Results from Peoria Structure Number 072-0107	113
4.4.2 Infrared Thermography Results from Peoria Structure Number 072-0107	114
4.4.3 Ground Penetrating Radar Results from Peoria Structure Number 072-0107	114
4.5 Results from Peoria Structure Number 072-0108.....	115
4.5.1 Chain Drag Results from Peoria Structure Number 072-0108	116
4.5.2 Infrared Thermography Results from Peoria Structure Number 072-0108	116
4.5.3 Ground Penetrating Radar Results from Peoria Structure Number 072-0108	117
4.6 Results from Peoria Structure Number 072-0109.....	117
4.6.1 Chain Drag Results from Peoria Structure Number 072-0109	120
4.6.2 Infrared Thermography Results from Peoria Structure Number 072-0109	121
4.6.3 Ground Penetrating Radar Results from Peoria Structure Number 072-0109	121
4.7 Results From Peoria Structure Number 072-0110.....	122
4.7.1 Chain Drag Results From Peoria Structure Number 072-0110	125
4.7.2 Infrared Thermography Results From Peoria Structure Number 072-0110	126
4.7.3 Ground Penetrating Radar Results From Peoria Structure Number 072-0110	126

4.8 Results from Peoria Structure Number 072-0111	127
4.8.1 Chain Drag Results from Peoria Structure Number 072-0111	129
4.8.2 Infrared Thermography Results from Peoria Structure Number 072-0111	130
4.8.3 Ground Penetrating Radar Results from Peoria Structure Number 072-0111	130
4.9 Results from Marion Structure Number 100-0005	131
4.9.1 Chain Drag Results from Marion Structure Number 100-0005.....	132
4.9.2 Infrared Thermography Results from Marion Structure Number 100-0005	132
4.9.3 Ground Penetrating Radar Results from Marion Structure Number 100-0005	133
4.9.4 Impact-Echo Results from Marion Structure Number 100-0005.....	133
4.9.5 Spectral Analysis of Surface Waves Results from Marion Structure Number 100-0005	137
4.10 Summary of All Results.....	137
5.0 DISCUSSION OF RESULTS	140
5.1 Discussion of Results from Bloomington Structure Number 057-0088.....	140
5.2 Discussion of Results from Peoria Structure Number 090-0118.....	142
5.3 Discussion of Results from Peoria Structure Number 072-0106.....	142
5.4 Discussion of Results from Peoria Structure Number 072-0107	143
5.5 Discussion of Results from Peoria Structure Number 072-0108.....	144
5.6 Discussion of Results from Peoria Structure Number 072-0109.....	144
5.7 Discussion of Results from Peoria Structure Number 072-0110.....	145
5.8 Discussion of Results from Peoria Structure Number 072-0111	146
5.9 Discussion of Results from Marion Structure Number 100-0005	147
5.10 Discussion of Results from All Bridges.....	151
5.11 Discussion of Major Issues in Nondestructive Testing of Bridge Decks	153
6.0 CONCLUSIONS AND RECOMMENDATIONS FOR FUTURE WORK.....	158

REFERENCES	162
APPENDIX A—CHAIN DRAG SURVEY RESULTS.....	170
APPENDIX B—INFRARED THERMOGRAPHY SURVEY RESULTS	181
APPENDIX C—GROUND PENETRATING RADAR RESULTS	191
APPENDIX D—IMPACT-ECHO AND SPECTRAL ANALYSIS OF SURFACE WAVES SURVEY RESULTS.....	211
APPENDIX E—CORE SAMPLES TAKEN DURING INFRARED INSPECTION	222
APPENDIX F—CHAIN DRAG DATA	231

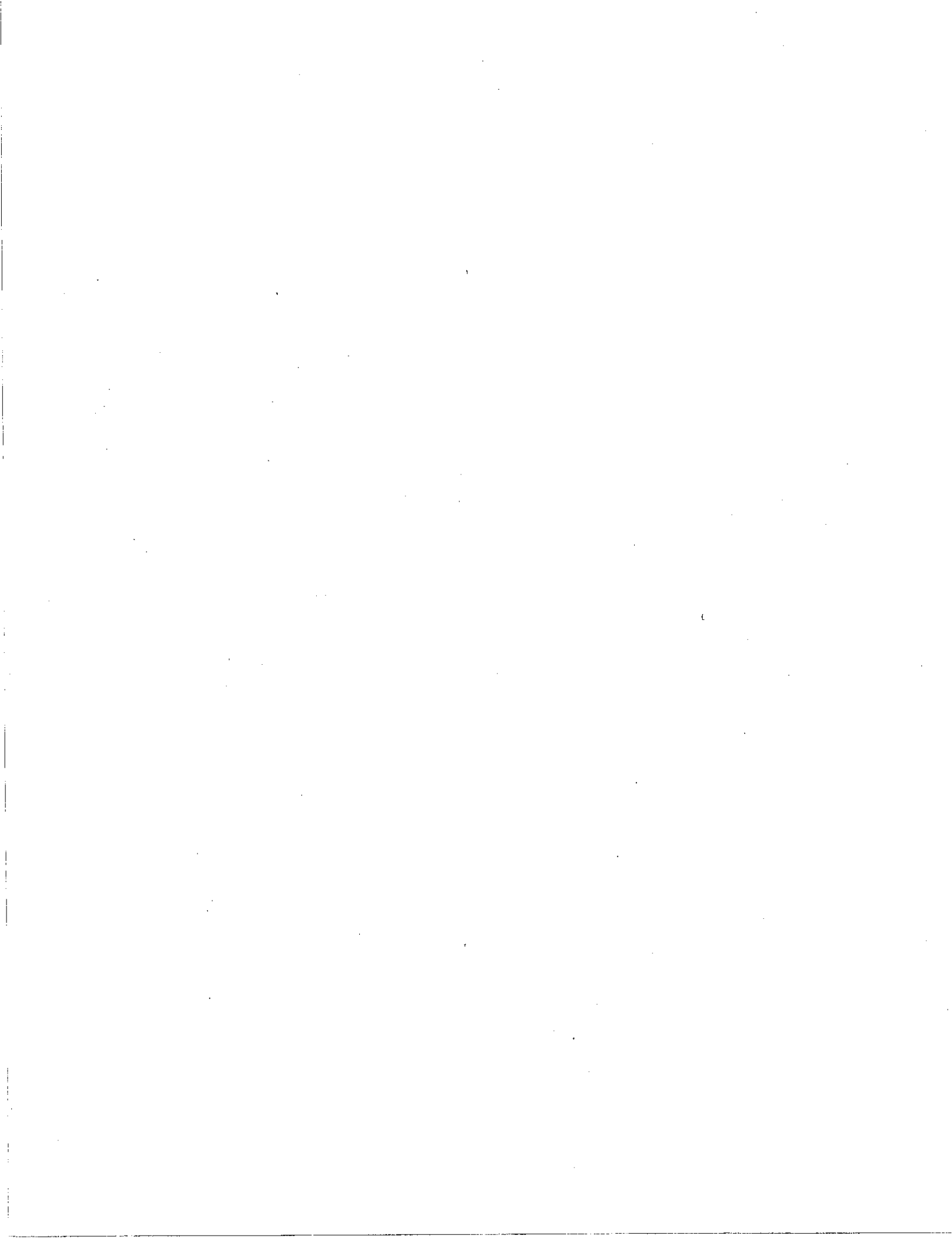


LIST OF TABLES

Table 1.1	Summary of Bridge Deck Survey	36
Table 2.1	Relative dielectric constants, ϵ_r , and reflection coefficients, R , of the three primary materials found in bridge decks ^{33,34,44}	51
Table 4.1	Areas of proposed rehabilitation for Bloomington Structure Number 057-0088 (eastbound).	100
Table 4.2	Areas of proposed rehabilitation for Bloomington Structure Number 057-0088 (westbound).	100
Table 4.3	Areas of proposed rehabilitation for Peoria Structure Number 090-0118.	106
Table 4.4	Individual delaminations for Peoria Structure Number 090-0118.	106
Table 4.5	Areas of proposed rehabilitation for Peoria Structure Number 072-0106.	109
Table 4.6	Individual delaminations for Peoria Structure Number 072-0106.	109
Table 4.7	Areas of proposed rehabilitation for Peoria Structure Number 072-0107.	112
Table 4.8	Individual delaminations for Peoria Structure Number 072-0107.	112
Table 4.9	Areas of proposed rehabilitation for Peoria Structure Number 072-0108.	115
Table 4.10	Individual delaminations for Peoria Structure Number 072-0108.	116
Table 4.11	Areas of proposed rehabilitation for Peoria Structure Number 072-0109.	118
Table 4.12	Individual delaminations for Peoria Structure Number 072-0109.	118
Table 4.13	Areas of proposed rehabilitation for Peoria Structure Number 072-0110.	122
Table 4.14	Individual delaminations for Peoria Structure Number 072-0110.	123
Table 4.15	Areas of proposed rehabilitation for Peoria Structure Number 072-0111.	127
Table 4.16	Individual delaminations for Peoria Structure Number 072-0111.	128
Table 4.17	Areas of proposed rehabilitation for Marion Structure Number 100-0005.	131

Table 4.18	Impact-echo scanner consistency with 10 inch (254 mm) depth for Marion Structure Number 100-0005.	135
Table 4.19	Areas of proposed rehabilitation for all bridge decks.	138
Table 4.20	Number of individual delaminations for all bridge decks except Bloomington Structure Number 057-0088 and Marion Structure Number 100-0005.	139
Table 4.21	Number of major delaminations (minimum 10 ft ²) for all bridge decks, excepting Bloomington Structure Number 057-0088 and Marion Structure Number 100-0005.	139
Table F-1	Chain drag survey field data for Bloomington Structure Number 057-0088 eastbound.	232
Table F-2	Chain drag survey field data for Bloomington Structure Number 057-0088 eastbound.	234
Table F-3	Chain drag survey field data for Bloomington Structure Number 057-0088 westbound.	235
Table F-3	Chain drag survey field data for Bloomington Structure Number 057-0088 westbound (Continued).....	236
Table F-4	Chain drag survey field data for Bloomington Structure Number 057-0088 westbound.	237
Table F-5	Chain drag survey field data for Peoria Structure Number 090-0118.	238
Table F-6	Chain drag survey field data for Peoria Structure Number 072-0106.	238
Table F-7	Chain drag survey field data for Peoria Structure Number 072-0106.	238
Table F-8	Chain drag survey field data for Peoria Structure Number 072-0107.	239
Table F-9	Chain drag survey field data for Peoria Structure Number 072-0107.	240
Table F-10	Chain drag survey field data for Peoria Structure Number 072-0108.	240
Table F-11	Chain drag survey field data for Peoria Structure Number 072-0108.	240
Table F-12	Chain drag survey field data for Peoria Structure Number 072-0109.	241

Table F-13	Chain drag survey field data for Peoria Structure Number 072-0109.	241
Table F-14	Chain drag survey field data for Peoria Structure Number 072-0110.	241
Table F-15	Chain drag survey field data for Peoria Structure Number 072-0110.	242
Table F-16	Chain drag survey field data for Peoria Structure Number 072-0111.	243
Table F-17	Chain drag survey field data for Peoria Structure Number 072-0111.	244
Table F-18	Chain drag survey field data for Marion Structure Number 100-0005.....	245



LIST OF FIGURES

Figure 1.1	Bloomington Structure Number 057-0088 bridge deck showing asphalt patching along abutment joints.....	23
Figure 1.2	Bloomington Structure Number 057-0088 bridge deck showing asphalt patching along longitudinal joints.	23
Figure 1.3	Bloomington Structure Number 057-0088 bridge deck view looking north.....	24
Figure 1.4	Peoria Structure Number 090-0118 bridge deck with no overlay looking south.....	25
Figure 1.5	Peoria Structure Number 090-0118 bridge deck with no overlay side view.	25
Figure 1.6	Peoria Structure Number 072-0109 bridge deck looking north.....	28
Figure 1.7	Peoria Structure Number 072-0109 bridge deck side view.	29
Figure 1.8	Peoria Structure Number 072-0109 bridge deck side view with Peoria Structure Number 072-0108 in background.	29
Figure 1.9	Underside of Peoria Structure Number 072-0109 bridge deck showing no major deterioration.	30
Figure 1.10	Peoria Structure Number 072-0110 looking west prior to removal of overlay.	31
Figure 1.11	Peoria Structure Number 072-0110 looking west following removal of overlay exposing milling marks in concrete bridge deck.	32
Figure 1.12	Marion Structure Number 100-0005 looking north before removal of overlay showing concrete surface patches.....	34
Figure 1.13	Underside of Marion Structure Number 100-0005 showing corrosion of superstructure and leaching of salts through transverse cracks in bridge deck.....	34
Figure 1.14	Underside of Marion Structure Number 100-0005 showing corrosion of reinforcement bars causing spalling and delamination of concrete.....	35

Figure 2.1	Reflection and refraction of stress waves given by Snell's Law.	39
Figure 2.2	Illustration of the impact-echo concept for a single layer system.....	41
Figure 2.3	Illustration of the impact-echo concept for a two layer system.	43
Figure 2.4	Typical time response and corresponding frequency spectrum of impact-echo signal.	44
Figure 2.5	Depth of inspection vs. frequency for typical compression wave velocity range in concrete.	46
Figure 2.6	Reflection and transmission of electromagnetic radar wave at a dielectric boundary.....	47
Figure 2.7	Transmission and reflection of radar pulses through a bridge deck ³³	52
Figure 2.8	Schematic diagram showing formation of a hot spot in overlaid bridge deck.....	55
Figure 2.9	Relationship between temperature of air, solid concrete, and delaminations to time of day ^{55,56}	57
Figure 2.10	Schematic diagram of spectral analysis of surface wave test method.	59
Figure 2.11	Illustration of the chain drag principle.....	63
Figure 2.12	Schematic diagram a typical debond leading to false readings during chain drag.....	64
Figure 3.1	Use of the impact-echo testing apparatus.	67
Figure 3.2	Closeup of the impact-echo testing apparatus.....	67
Figure 3.3	Front of the impact-echo testing apparatus showing distance wheel mounted ahead of transducer carts.....	68
Figure 3.4	Top view of a transducer cart with the rolling transducer mounted in the center.....	68
Figure 3.5	Side view of a transducer cart with the rolling emerging from the bottom.	69
Figure 3.6	Bottom view of a transducer cart with the rolling transducer mounted in the center.....	69

Figure 3.7	Hand held impact-echo testing apparatus.	71
Figure 3.8	Hand held impact-echo testing apparatus showing transducer pad at bottom.	72
Figure 3.9	Hand held impact-echo testing apparatus showing transducer pad at right and solenoid impactor at left.	72
Figure 3.10	Front view of the ground penetrating radar inspection van showing antennas in deployed position.	77
Figure 3.11	Front view of the ground penetrating radar inspection van showing antennas in stowed position.	77
Figure 3.12	Close up of the ground penetrating radar inspection antennas in deployed position.	78
Figure 3.13	Interior of the ground penetrating radar inspection van showing system power controls and data recorder.	78
Figure 3.14	Interior of the ground penetrating radar inspection van showing antenna power controls and oscilloscope.	79
Figure 3.15	The infrared inspection van with camera mount on front of van in stowed position.	84
Figure 3.16	The camera mount with infrared camera at right and visual camera at left.	85
Figure 3.17	Side view of camera mount with infrared camera.	85
Figure 3.18	Interior of infrared inspection vehicle showing two monitors and two VCRs for the visual and infrared images, respectively.	86
Figure 3.19	Coring of bridge deck during infrared inspection.	91
Figure 3.20	Apparatus used for chain drag survey.	97
Figure 3.21	Close up of apparatus used for chain drag survey.	98
Figure 4.1	Delaminated area on Blooming 057-0088 after removal of concrete showing corroded reinforcing bars.	101
Figure 4.2	Corroded and broken reinforcing bars on Bloomington Structure Number 057-0088 deck.	101

Figure 4.3	Close up of corroded and broken reinforcing bars on Bloomington Structure Number 057-0088 deck.....	102
Figure 4.4	Underside of Bloomington Structure Number 057-0088 deck showing corrosion of the superstructure.....	102
Figure 4.5	Deterioration of previous rehabilitation patch on Bloomington Structure Number 057-0088 deck.....	103
Figure 4.6	Peoria Structure Number 090-0118 deck showing excellent condition of pavement surface and abutment joint.	107
Figure 4.7	Peoria Structure Number 072-0107 after removal of west lane asphalt overlay.....	113
Figure 4.8	Peoria Structure Number 072-0109 after removal of west lane asphalt overlay.....	119
Figure 4.9	Peoria Structure Number 072-0109 potholes in concrete.	119
Figure 4.10	Peoria Structure Number 072-0109 close up of pothole in concrete.	120
Figure 4.11	Peoria Structure Number 072-0110 after removal of left lane overlay revealing milling gouges.....	124
Figure 4.12	Peoria Structure Number 072-0110 close up of milling gouges.....	124
Figure 4.13	Peoria Structure Number 072-0110 close up of milling gouges showing 1 inch (25.4 mm) depth.....	125
Figure A-1.	Bloomington Structure Number 057-0088 eastbound chain drag survey. Dark areas indicate delaminations.	171
Figure A-2.	Bloomington Structure Number 057-0088 westbound chain drag survey. Dark areas indicate delaminations.	172
Figure A-3.	Peoria Structure Number 090-0118 chain drag survey. Dark areas indicate delaminations.	173
Figure A-4.	Peoria Structure Number 072-0106 chain drag survey. Dark areas indicate delaminations.	174
Figure A-5.	Peoria Structure Number 072-0107 chain drag survey. Dark areas indicate delaminations.	175

Figure A-6.	Peoria Structure Number 072-0108 chain drag survey. Dark areas indicate delaminations.	176
Figure A-7.	Peoria Structure Number 072-0109 chain drag survey. Dark areas indicate delaminations.	177
Figure A-8.	Peoria Structure Number 072-0110 chain drag survey. Dark areas indicate delaminations.	178
Figure A-9.	Peoria Structure Number 072-0111 chain drag survey. Dark areas indicate delaminations.	179
Figure A-10.	Marion Structure Number 100-0005 chain drag survey. Dark areas indicate delaminations.	180
Figure B-1.	Bloomington Structure Number 057-0088 infrared thermography survey (from Rust final report ⁸⁷). Traffic is westbound in the north lanes, eastbound in the south lanes.	182
Figure B-2.	Peoria Structure Number 090-0118 infrared thermography survey (from Rust final report ⁸⁷).....	183
Figure B-3.	Peoria Structure Number 072-0106 infrared thermography survey (from Rust final report ⁸⁷).....	184
Figure B-4.	Peoria Structure Number 072-0107 infrared thermography survey (from Rust final report ⁸⁷).....	185
Figure B-5.	Peoria Structure Number 072-0108 infrared thermography survey (from Rust final report ⁸⁷).....	186
Figure B-6.	Peoria Structure Number 072-0109 infrared thermography survey (from Rust final report ⁸⁷).....	187
Figure B-7.	Peoria Structure Number 072-0110 infrared thermography survey (from Rust final report ⁸⁷).....	188
Figure B-8.	Peoria Structure Number 072-0111 infrared thermography survey (from Rust final report ⁸⁷).....	189
Figure B-9.	Marion Structure Number 100-0005 infrared thermography survey (from Rust final report ⁸⁷).....	190

Figure C-1.	Bloomington Structure Number 057-0088 eastbound ground penetrating radar delamination survey (from Penetradar final report ⁸⁸). Dark areas indicate delaminations.	192
Figure C-2.	Bloomington Structure Number 057-0088 eastbound ground penetrating radar scaling survey (from Penetradar final report ⁸⁸). Dark areas indicate delaminations.	193
Figure C-3.	Bloomington Structure Number 057-0088 westbound ground penetrating radar delamination survey (from Penetradar final report ⁸⁸). Dark areas indicate delaminations.	194
Figure C-4.	Bloomington Structure Number 057-0088 westbound ground penetrating radar scaling survey (from Penetradar final report ⁸⁸). Dark areas indicate delaminations.	195
Figure C-5.	Peoria Structure Number 090-0118 ground penetrating radar delamination survey (from Penetradar final report ⁸⁸). Dark areas indicate delaminations.	196
Figure C-6.	Peoria Structure Number 072-0106 ground penetrating radar delamination survey (from Penetradar final report ⁸⁸). Dark areas indicate delaminations.	197
Figure C-7.	Peoria Structure Number 072-0106 ground penetrating radar scaling survey (from Penetradar final report ⁸⁸). Dark areas indicate delaminations.	198
Figure C-8.	Peoria Structure Number 072-0107 ground penetrating radar delamination survey (from Penetradar final report ⁸⁸). Dark areas indicate delaminations.	199
Figure C-9.	Peoria Structure Number 072-0107 ground penetrating radar scaling survey (from Penetradar final report ⁸⁸). Dark areas indicate delaminations.	200
Figure C-10.	Peoria Structure Number 072-0108 ground penetrating radar delamination survey (from Penetradar final report ⁸⁸). Dark areas indicate delaminations.	201
Figure C-11.	Peoria Structure Number 072-0108 ground penetrating radar scaling survey (from Penetradar final report ⁸⁸). Dark areas indicate delaminations.	202
Figure C-12.	Peoria Structure Number 072-0109 ground penetrating radar delamination survey (from Penetradar final report ⁸⁸). Dark areas indicate delaminations.	203
Figure C-13.	Peoria Structure Number 072-0109 ground penetrating radar scaling survey (from Penetradar final report ⁸⁸). Dark areas indicate delaminations.	204
Figure C-14.	Peoria Structure Number 072-0110 ground penetrating radar delamination survey (from Penetradar final report ⁸⁸). Dark areas indicate delaminations.	205

Figure C-15.	Peoria Structure Number 072-0110 ground penetrating radar scaling survey (from Penetradar final report ⁸⁸). Dark areas indicate delaminations.....	206
Figure C-16.	Peoria Structure Number 072-0111 ground penetrating radar delamination survey (from Penetradar final report ⁸⁸). Dark areas indicate delaminations.	207
Figure C-17.	Peoria Structure Number 072-0111 ground penetrating radar scaling survey (from Penetradar final report ⁸⁸). Dark areas indicate delaminations.....	208
Figure C-18.	Marion Structure Number 100-0005 ground penetrating radar delamination survey (from Penetradar final report ⁸⁸). Dark areas indicate delaminations.	209
Figure C-19.	Marion Structure Number 100-0005 ground penetrating radar scaling survey (from Penetradar final report ⁸⁸). Dark areas indicate delaminations.....	210
Figure D-1.	Marion Structure Number 100-0005 impact-echo scanner test lines (from Olson final report ⁸⁹).	212
Figure D-2.	Marion Structure Number 100-0005 handheld impact-echo test at north side of corehole 1 (from Olson final report ⁸⁹).	213
Figure D-3.	Marion Structure Number 100-0005 handheld impact-echo test at north side of corehole 2 (from Olson final report ⁸⁹).	214
Figure D-4.	Marion Structure Number 100-0005 handheld impact-echo thickness plots from 0 to 31.5 feet (9.60 m) along east scan line1-channel 2 (from Olson final report ⁸⁹).	215
Figure D-5.	Marion Structure Number 100-0005 handheld impact-echo thickness plots from 32.0 to 80.0 ft (9.75 to 24.4 m) along east scan line1-channel 2 (from Olson final report ⁸⁹).	216
Figure D-6.	Marion Structure Number 100-0005 impact-echo scanner example of good results from center scan line 2, transducer channel 3 (from Olson final report ⁸⁹).	217
Figure D-7.	Marion Structure Number 100-0005 impact-echo scanner example of poor results from center scan line 2, transducer channel 4 (from Olson final report ⁸⁹).	218
Figure D-8.	Marion Structure Number 100-0005 impact-echo scanner example of good thickness results from center scan line 2, channel 3 (from Olson final report ⁸⁹).	219

Figure D-9.	Marion Structure Number 100-0005 impact-echo scanner example of poor thickness results from east scan line 1, channel 2 (from Olson final report ⁸⁹).	220
Figure D-10.	Marion Structure Number 100-0005 spectral analysis of surface waves experimental and theoretical dispersion curves at core 2 (from Olson final report ⁸⁹).	221
Figure E-1.	Core #1 from Peoria Structure Number 090-0118—solid (from Rust final report ⁸⁷).	223
Figure E-2.	Core #2 from Peoria Structure Number 072-0109—debonded (from Rust final report ⁸⁷).	223
Figure E-3.	Core #3 from Peoria Structure Number 072-0109—debonded and delaminated (from Rust final report ⁸⁷).	223
Figure E-4.	Core #4 from Peoria Structure Number 072-0107—debonded (from Rust final report ⁸⁷).	224
Figure E-5.	Core #5 from Peoria Structure Number 072-0107—debonded and delaminated (from Rust final report ⁸⁷).	224
Figure E-6.	Core #6 from Peoria Structure Number 072-0106—delaminated (from Rust final report ⁸⁷).	224
Figure E-7.	Core #7 from Peoria Structure Number 072-0106—debonded (from Rust final report ⁸⁷).	225
Figure E-8.	Core #8 from Peoria Structure Number 072-0108—debonded (from Rust final report ⁸⁷).	225
Figure E-9.	Core #9 from Peoria Structure Number 072-0108—debonded and delaminated (from Rust final report ⁸⁷).	225
Figure E-10.	Core #10 from Peoria Structure Number 072-0108—debonded (from Rust final report ⁸⁷).	226
Figure E-10A.	Core #10A from Peoria Structure Number 072-0108—debonded (from Rust final report ⁸⁷).	226
Figure E-11.	Core #11 from Peoria Structure Number 072-0111—delaminated (from Rust final report ⁸⁷).	226

Figure E-12.	Core #12 from Peoria Structure Number 072-0111—debonded (from Rust final report ⁸⁷).....	227
Figure E-13.	Core #13 from Peoria Structure Number 072-0111—delaminated (from Rust final report ⁸⁷).....	227
Figure E-14.	Core #14 from Peoria Structure Number 072-0110—delaminated (from Rust final report ⁸⁷).....	227
Figure E-15.	Core #15 from Peoria Structure Number 072-0110—delaminated (from Rust final report ⁸⁷).....	228
Figure E-16.	Core #16 from Marion Structure Number 100-0005—delaminated (from Rust final report ⁸⁷).....	228
Figure E-17.	Core #17 from Marion Structure Number 100-0005—solid (from Rust final report ⁸⁷).....	228
Figure E-18.	Core #18 from Marion Structure Number 100-0005—debonded (from Rust final report ⁸⁷).....	229
Figure E-19.	Core #19 from Marion Structure Number 100-0005—delaminated (from Rust final report ⁸⁷).....	229
Figure E-20.	Core #20 from Bloomington Structure Number 057-0088—delaminated (from Rust final report ⁸⁷).....	229
Figure E-21.	Core #21 from Bloomington Structure Number 057-0088—solid (from Rust final report ⁸⁷).....	230
Figure E-22.	Core #22 from Bloomington Structure Number 057-0088—rubble (from Rust final report ⁸⁷).....	230

LIST OF SYMBOLS

β	Angle of refraction
ε	Dielectric constant
ε_0	Dielectric constant of free space
ε_r	Relative dielectric constant
η_i	Electromagnetic impedance of material i
η_0	Electromagnetic impedance of free space
λ	Wavelength
μ_0	Magnetic permeability of free space
ν	Poisson's ratio
ρ	Mass density
θ	Angle of incidence
c	Electromagnetic wave velocity in a vacuum
f	Frequency
h	Planck's constant
k	Boltzmann's constant
t	Time
t_c	Contact time
C	Thermal contrast
C_h	Specific heat
C_p	Compressional stress wave velocity
C_r	Rayleigh stress wave velocity

C_s	Shear stress wave velocity
D	Depth
E	Young's modulus of elasticity
E_m	Emissivity of a material
E_0	Incident electromagnetic energy
E_r	Reflected electromagnetic energy
K	Thermal conductivity
$N_{\lambda,b}$	Spectral radiance of a black body, b , at a given wavelength, λ
R	Fraction of electromagnetic energy returned at dielectric boundary
R_n	Fraction of stress wave energy returned at material boundary
T	Temperature
V	Electromagnetic wave velocity in a material
Z_i	Specific acoustic impedance of material i



EVALUATION OF BRIDGE DECK DELAMINATION INVESTIGATION METHODS

1.0 INTRODUCTION

Cost effective bridge deck rehabilitation makes it necessary to locate the areas in need of repair in order to accurately estimate the quantity of deteriorated concrete in a bridge deck. Since the bituminous overlay prevents visual identification of these areas, nondestructive testing and evaluation techniques are essential.

Conventional nondestructive testing techniques, such as sounding by hammer and chain drag, do not fare well on asphalt covered decks, primarily due to the inefficient coupling of energy between the asphalt overlay and the concrete. They are usually effective only after the asphalt overlay has been removed. Destructive testing methods such as core samples are effective when a large number of random samples are obtained, which is both costly and unnecessarily damaging to the bridge deck. Recently, other nondestructive testing and evaluation techniques, such as impact-echo¹⁻³², ground penetrating radar³³⁻⁵⁶, and infrared thermography⁵⁴⁻⁷², have shown promise for the noninvasive evaluation of the damage accumulation in concrete bridge decks overlaid with asphalt concrete wearing surfaces. Each nondestructive evaluation method has its own set of advantages and limitations which are explored in detail in this study. It appears that currently no single technique is sufficient for accurate nondestructive evaluation of bridge decks. However, the combination of two or more of the currently available techniques may provide an approach which will yield an accurate evaluation of the state of damage of bridge decks with asphalt overlays.

Ground penetrating radar provides a noncontacting means to evaluate pavement joint deterioration, detection of voids beneath slabs, pavement layer thicknesses, and delamination profiles by sending a short electromagnetic pulse into the bridge deck and monitoring the returning signal. This is done at highway speeds and with reasonable measurement accuracy.

One of the limitations of ground penetrating radar is the significant effect that moisture has upon signal attenuation that, if not taken into consideration, affects the consistency of bridge deck concrete deterioration measurements between wet and dry conditions³⁶. In addition, ground penetrating radar provides only strips of data along the bridge deck length at predetermined antenna spacings.

Infrared thermography provides a means to identify delaminations in bridge decks by observing the temperature differential between delaminated and sound concrete, which exists under certain environmental conditions⁶⁴. Infrared thermography provides a field view of the delaminated area of the bridge deck and a noncontact means for evaluating bridge deck concrete pavements with relatively fast inspection rates. The drawbacks to infrared thermography are the relatively stringent weather requirements for accurate testing, and the inability to infer the depth of a delaminated or deteriorated area⁵⁶.

Impact-echo tests provide thickness profiles and detect voids, honeycombing, cracks, delaminations, and other damage in concrete bridge decks with asphalt overlays¹⁰. Using an impacting device, such as a solenoid tapper, a stress wave pulse in the bridge deck is generated and the returning pulse is monitored with a piezoelectric transducer. The returning stress wave pulses provide information about the integrity of the bridge deck. The primary difficulty of the impact-echo method is in obtaining measurements point by point without providing a field view of the bridge deck. Additionally, adequate coupling of the transducer to the bridge deck is required for reliable results. The impact-echo method is potentially more precise in the determination of layer thicknesses and flaw depths than ground penetrating radar³¹ and efforts are under way to automate data collection in order to generate a computer tomographic view of delaminations in concrete bridge decks³¹.

Three companies independently evaluated nine bridge decks throughout central and southern Illinois in their pre-rehabilitation state during the summer of 1997. A description of the bridges and the selection procedure are presented in following sections. Each company is a recognized leader in its respective field. Penetradar Corporation (c/o Mr. Anthony J. Alongi) performed the ground penetrating radar investigation of the bridge decks. Rust Environmental and Infrastructure (c/o Mr. Jerry W. Eales) performed the infrared thermography investigation of the bridge decks. Olson Engineering, Inc. (c/o Mr. Larry D. Olson) performed the impact-echo investigation of the bridge decks. Additionally, Mr Larry Olson briefly performed another nondestructive test—spectral analysis of surface waves, which is used to determine pavement layer thicknesses and properties. Each test was performed independently of the others and before the asphalt overlays were removed. Each of these companies submitted a report detailing their findings for this study.

During the late summer of 1997, the asphalt overlays were removed from the bridge decks by various Illinois Department of Transportation subcontractors. Chain drag surveys of the bare concrete bridge decks were subsequently performed by Mr. Eugene Smania of the Illinois Department of Transportation District Three and Mr. Matthew D. Baright of the University of Illinois. In this manner, an unbiased and independent survey of delaminated areas of the bridge decks was obtained, serving as the basis for comparison of the three nondestructive testing methods. This report details the comparisons of the three nondestructive testing methods to the results of the chain drag survey of the bare concrete bridge decks, and concludes that a combination of methodologies is the most effective in determining the state of damage in concrete bridge decks

1.1 Literature Review of Previous Work

This section provides an overview of previous research, experimentation, and comparisons of the three main nondestructive testing techniques used in this study—impact-echo, ground penetrating radar, and infrared thermography. While the review is not exhaustive, care was taken to obtain the most influential and frequently cited works in the corresponding testing disciplines. Each method has multiple applications outside of bridge deck inspection, and a cross section of these applications is presented. The majority of the works discussed pertain directly to concrete inspection with an emphasis on steel reinforced bridge decks. A number of works are evaluations of each method's ability to adequately provide information regarding the structural integrity of concrete bridge decks with asphalt overlays. In addition, some works directly compare the effectiveness of each method against each other, which is the spirit of this study.

Some general trends and observations about each testing method can be stated as a result of the literature review. The impact-echo method for concrete inspection has been in development since the mid 1980's, making it the youngest of the inspection technologies. While much laboratory research and field testing of the method has been performed, commercial use of impact-echo for the inspection of bridge decks has yet to become widespread. Ground penetrating radar has been used since the 1970's to inspect various forms of infrastructure, and seems to have the widest commercial following in bridge deck inspection. Infrared thermography, in use since the late 1970's, has just become commercially viable within the last decade for use as a bridge deck inspection tool due to recent improvements in the testing equipment.

Finally, a short discussion of the ASTM standard for inspecting bridge decks by sounding is presented. Sounding of bridge decks by impact devices such as a hammer or by dragging a length of chain across the deck is by far the oldest of inspection methods and its results were used in this study as the baseline measurements with which to compare the results of the other methods.

1.1.1 Impact-Echo Literature Review of Previous Work

The impact-echo technique for flaw detection was developed in the mid 1980's. Much of the pioneering work in the development of the technique was performed by M. Sansalone and N. Carino¹⁻⁴. This technique is thoroughly presented in a 1986 National Bureau of Standards report¹ (currently the National Institute of Standards and Technology, NIST). The report presents a basis for nondestructive flaw detection in heterogeneous solids, such as concrete, using transient stress wave propagation techniques. Exact analytical solutions of the response of an infinite plate to a point source of impact are presented and verified using finite element techniques. Finally, experimental testing equipment was developed to gather laboratory data which is presented in agreement with the analytical and numerical solutions. The results demonstrated the ability of the impact-echo technique to detect flaws, particularly planar voids, and to pinpoint their sizes and locations.

Further analytical and experimental work continued on the impact-echo technique in the late 1980s, again by M. Sansalone and N. Carino²⁻⁴. The depth of concrete slabs was determined using impact-echo^{1,2}. Through the use of a Fast Fourier Transform, the frequencies contained in the stress wave were shown to vary with the presence of defects. The depth of surface opening vertical cracks was determined experimentally using the impact-echo method and further signal

processing techniques³. Steel balls of varying diameter became the method of choice for generation of stress waves in concrete, since the frequency composition of the stress wave was determined by the time of contact^{3,4}. The time of contact of a steel ball striking the surface of a concrete slab is directly proportional to its diameter^{3,4}. Other sources were investigated, including hammers and spring loaded steel rods^{3,4}. Using experimentation and a finite element model, the impact-echo method was shown to detect honeycombing in concrete slabs³. These works provide the basis for the impact-echo technique for flaw detection.

The impact-echo method has been applied to a wide variety of concrete structures⁵⁻⁹. Initial work in structures of various geometries was performed using finite element methods⁵⁻⁹. Flat voids contained in thin and thick circular plates were proven detectable by the impact-echo method providing certain geometrical arrangements were considered⁵⁻⁶. The contact time of the impact must be small enough such that sufficient energy is contained in the frequencies reflected by the flaw⁵. The source, i.e. impactor, and receiver should be as close a possible⁵. Flaws are more easily detected when the ratio of flaw diameter to flaw depth is large⁵. For thick cylinders, stress wave reflections from deeper flaws may be hidden in reflections from the edges of the specimen⁶. Further finite element studies laid the groundwork for the impact-echo inspection of arbitrary geometries^{7,8} including concrete slabs containing layers of steel and plastic⁹. These previous works provide the basis for the use of the impact-echo method to inspect concrete slabs.

In 1989 M. Sansalone and N. Carino published a paper in which it was shown experimentally how the impact-echo method detected simulated delaminations in concrete slabs without and with asphalt concrete overlays¹⁰. The delaminations were simulated with pieces of plastic sheeting and also with corroded steel. The location of the delaminations were not known to the inspectors. All of the delaminations were successfully located and the depths of most

were accurately determined. The slabs were then overlaid with asphalt concrete and the test was rerun. The delaminations were again successfully located and the depths were determined. Additionally, it was shown that the thickness of the asphalt concrete overlay could be determined with the impact-echo data. Using a slight modification in the testing apparatus in which a steel disk was coupled to the asphalt surface, and impacted, the method worked better than impacting the soft asphalt directly. This work proved the experimental feasibility of detecting delaminations in concrete slabs without and with overlays. A second paper provides insights into how the presence of steel reinforcing bars can affect the impact-echo signals, but does not significantly affect the detection of delaminations¹¹.

The impact-echo method has been extended to other geometries. In particular, the inspection of concrete beams¹², columns¹², thick hollow cylinders¹³, thick circular and square bars¹⁴, and hollow cylinders surrounded by soil and rock^{15,16} has been studied. These studies have focused both on finite element analysis methods and experimental methods. The results show flaw detection capabilities similar to that of concrete slabs, although the geometrical effects are more difficult to analyze. Due to its versatility, the impact-echo method may be extended to other concrete structures in the future.

Determining the minimum crack width that can be detected using the impact-echo method is important to the detection of delaminations in concrete. Attempts have been made to determine the minimum crack width both numerically and experimentally^{17,18}. Artificially induced cracking in laboratory specimens shows that the impact-echo method can detect cracks with a width of approximately .000984 inches (0.025 mm)¹⁷. This figure was verified using numerical methods and fracture analysis¹⁸. The ability of the impact-echo method to detect very

small crack openings puts it well within range to detect the larger crack widths of concrete delaminations found in bridge decks.

The impact-echo method has been used to estimate strength and setting time of early-age concrete¹⁹⁻²¹. The velocity of propagation of a stress wave induced into the concrete by impact is related to the early-age strength of the concrete. The faster the stress wave propagates, the stronger the concrete is; the relation is exponential^{20,21}. From this relationship, setting times have been calculated in an effort to develop a standardized test to nondestructively determine the in-place strength of concrete²¹. The test should be limited to early-age concrete as the relationship between stress wave velocity and strength decreases with time²¹. An extensive experimental investigation has been performed by Pessiki and Johnson²².

Recent work on the impact-echo method includes using artificial intelligence to interpret signals²³. A neural network and expert system were used to detect and classify the presence and depth of flaws in concrete slabs. The experiment had some success, and future work will undoubtedly follow. Other attempts have been made to combine aspects of the impact-echo method with the pulse velocity and spectral analysis of surface waves methods for a comprehensive concrete inspection method²⁴. New methods are being devised to better control the character of the stress wave generated in the concrete. These methods include ultrasonic pulsers, impacts, tone-burst systems, and laser generation methods²⁵. With better control over the character of the stress wave, future systems will be able to extract more information from the impact-echo signals.

The ability to adequately and accurately detect the stress wave induced in concrete by impact is fundamental to the impact-echo techniques. Early laboratory work used a conical transducer developed by the National Bureau of Standards (NBS)²⁶⁻²⁹. Concrete presents an

interesting challenge since the frequency content of the stress waves involved are much lower than traditional ultrasonic inspection, yet much higher than geotechnical seismic phenomena. Improvements have been made over the years on the sensitivity and frequency response of the NBS transducer, leading to the recent development of a new transducer specifically for impact-echo applications by Larry Olson of Olson Engineering, Inc.³⁰. The new transducer compares favorably with the NBS transducer and a standard accelerometer used for impact-echo testing³⁰. Improvements on transducer design, particularly in rolling transducers, will improve the speed and accuracy of impact-echo testing.

The latest innovation in impact-echo testing of concrete structures involves the development of field equipment scanning systems, allowing a large area of concrete to be quickly and accurately scanned. Larry Olson of Olson Engineering, Inc. has developed a relatively high speed scanning system for concrete pipes and slabs as well as wooden beams^{31,32}. The system uses the recently developed rolling transducers to achieve high speed data collection. The results of previous work show that impact-echo scanning is a feasible technique to detect delaminations in concrete slabs and pipes. No previous work has been found on the use of high speed impact-echo testing of concrete slabs with asphalt overlays.

1.1.2 Ground Penetrating Radar Literature Review of Previous Work

The use of electromagnetic waves as a noninvasive technique to probe the ground, rock formations, pavements and other large structures came into use during the 1970's and early 1980's. The early use of ground penetrating radar as an inspection method for bridge decks was performed by G. Clemeña of the Virginia Highway and Transportation Research Council in 1985³³. This early work was compiled in a manual describing a basic testing procedure for

detection of delaminations in a reinforced concrete bridge deck with an asphalt overlay. The basic principles of ground penetrating radar are described, and guides on the survey procedure are provided, with the operation of a particular radar system and the interpretation and quantification of the radar results. A similar manual by G. Clemeña and others in 1986 serves as a basis for detecting voids in a jointed, reinforced concrete pavement³⁴. Although the system was able to nondestructively inspect five one-lane miles (1.6 km) of pavement per hour, the system was insensitive to shallow voids. Another early use of ground penetrating radar was the detection of subsurface cavities in karst topography in central Florida; these are areas where sinkhole development is possible³⁵. The radar system successfully penetrated 50 feet (15.24 m) of ground to detect voids. Since then the sensitivity of new radar systems has greatly increased.

More recent studies of ground penetrating radar as a method of bridge deck inspection have shown the technique to be quite suitable and useful as a noninvasive means for delamination detection³⁶⁻³⁸. In a field test of 22 bridges it was shown that ground penetrating radar was able to easily detect concrete delaminations caused by corrosion of the reinforcement bar³⁶. In addition, by measuring the attenuation of the radar signal, the feasibility of determining chloride content (corrosive to concrete) in highly permeable concrete was determined. Another laboratory test at Lawrence Livermore National Laboratory showed how imaging algorithms could be used to reconstruct various depth layers containing voids³⁷. Saarenketo et al³⁸ gave high marks to ground penetrating radar as a method for bridge deck inspection, citing the tediousness of radar signal interpretation as its largest drawback. The results of Saarenketo et al³⁸ are based upon a study involving ground penetrating radar applications for bridge deck evaluation in Finland.

Ground penetrating radar has been used in many widely varying applications, including mapping underground granite fractures^{39,40}, and pipelines⁴¹. Ground penetrating radar was used in the Underground Research Laboratory of Canada to assess the feasibility of permanent disposal of nuclear fuel waste deep underground^{39,40}. The ground penetrating radar was able to penetrate 16.4 to 32.8 feet (5 to 10 m) into the granite, and a map of the fracture planes was generated. Similarly, ground penetrating radar and advanced image processing techniques were used to map pipelines and the location of coffins at a grave site⁴¹. There are numerous applications of ground penetrating radar, other than bridge deck inspection, which will not be detailed here.

The basic procedures and guidelines for using ground penetrating radar to detect delaminations and determine pavement layer thicknesses are outlined in ASTM and AASHTO standards^{42,43}. The accuracy of the ground penetrating radar system test is dependent upon three components: radar system penetration, radar system resolution, and the dielectric constants. A typical ground penetrating radar system should have a minimum depth penetration of 20 inches (508 mm). The penetration depth is governed by radar system parameters (transmitted power, receiver sensitivity, signal processing), electromagnetic properties of the pavement materials, and environmental factors such as moisture content. A typical ground penetrating radar system is able to determine a layer thickness of 1 inch (25.4 mm) or greater to an accuracy of .2 inches (5.08 mm)⁴². The AASHTO provisional standard provides empirical guidelines for determining if the concrete is delaminated and reporting procedures for delaminations on the top and bottom of the steel reinforcing bars⁴³. These two reports provide the basis for a standardized test procedure.

Experimental laboratory work has been performed recently in an attempt to further the accuracy and precision of the ground penetrating radar method. Fundamental to accurate interpretation of ground penetrating radar signals is a knowledge of the electromagnetic properties of concrete. Theoretical models of the electromagnetic attenuation and magnetic properties of concrete have been devised based on the frequency, temperature, moisture content, chloride content, and concrete mix constituents⁴⁴. The models were verified through laboratory tests⁴⁴. Further research has been done on developing empirical mathematical models based on experimental results such that a simple backcalculation could be used to analyze the radar data and predict the condition of the concrete⁴⁵. Other studies show the ability of ground penetrating radar to successfully detect voids under various conditions--with and without steel reinforcement, with air cracks, with fresh water-filled cracks, and with saline water-filled cracks⁴⁶. Detailed theoretical and experimental studies have been performed on the effects of asphalt overlays and waterproofing membranes on ground penetrating radar's ability to detect voids and determine layer thicknesses⁴⁷. The results show that ground penetrating radar can overcome many different adverse conditions and still provide accurate results. Artificial intelligence such as neural networks have recently been used to interpret radar signals with much success, and further research is forthcoming⁴⁸. All of these studies serve to improve the accuracy of the ground penetrating radar method, and to explore new uses of this approach.

Recent studies have focused on the cost feasibility of ground penetrating radar over traditional inspection methods, such as coring^{49,50}. Results reveal that it is more cost effective to use ground penetrating radar for thickness determination in both project and network level calculations⁴⁹. A separate study showed a markedly improved estimation of rehabilitation costs using ground penetrating radar than other methods employed prior to radar use⁵⁰. The predicted

amount of deteriorated concrete using radar estimates was closer to the actual amount of concrete removed than Tennessee Department of Transportation officials were able to make prior to actual rehabilitation. These reports conclude that ground penetrating radar is quickly becoming a cost effective method for structural evaluation of bridge decks.

The most recent developments in ground penetrating radar equipment have been made by Road Radar Ltd. and Penetradar Corporation^{51,52}. Road Radar has improved thickness measurements by using a multi-antenna system which determines layer thickness as accurately as coring⁵¹. Penetradar claims a thickness measurement accuracy of 5-6%, a similar accuracy to coring. Both systems use advanced computer data acquisition systems and data processing algorithms.

In addition to improved computer equipment, considerable time and energy has been devoted to developing and tuning ground penetrating radar antennas. Typically these antennas are horn-shaped and custom-made by individual companies. The methods for tuning these antennas to provide the highest signal to noise ratio and to establish a flat response are closely guarded industry secrets. A quality source on the general principles and current research in ground penetrating radar and antenna systems is provided by Udpa et al⁵³. These technical articles discuss many aspects of ground penetrating radar systems at length.

Some experimental studies have also been performed in which there was a direct comparison of the ability to detect delaminations in concrete bridge decks between ground penetrating radar and infrared thermography⁵⁴⁻⁵⁶. Previous work performed on infrared thermography is detailed in the next section. The results of these studies generally conclude that the two technologies are complementary, each providing information the other does not. For example, ground penetrating radar gives accurate estimations of the depth of the delaminations,

while infrared thermography does not; and, infrared thermography provides a full field view, while radar does not. These similarities and differences are discussed in Chapter 5 of this study.

1.1.3 Infrared Thermography Literature Review of Previous Work

The history of infrared inspection can be traced back to the early 1800's. It was noted that the maximum temperature detected by a glass thermometer, when moved through a light spectrum created by a glass prism, occurred beyond the red band, where no radiation was visible. Subsequent investigations of emissive bodies laid the theoretical and experimental framework for the development of infrared thermography as a nondestructive investigative technique. One of the better sources detailing the theoretical and application aspects of thermographic inspection is the book by Maldague titled Nondestructive Evaluation of Materials by Infrared Thermography⁵⁷. In this reference, heat transfer modeling and finite element analysis of particular problems are presented. Practical applications discussed include infrared inspection of jet turbine blades, corrosion damage to pipes, delaminations in graphite epoxy composites, and aluminum laminates. Several image processing and data reduction processes are discussed as well as reliability issues. Maldague's book⁵⁷ provides significant, basic knowledge on infrared thermography.

Infrared thermography has been applied to a wide variety of nondestructive evaluation problems. The basic principle of thermographic inspection is the detection of temperature gradients across a volume of material where they are not anticipated under normal conditions. Frequently the term "hot spot" is used to indicate an area where the thermal load on the material is greater than expected. Considerable use of infrared inspection occurs in the commercial nuclear industry⁵⁸. A major application of infrared inspection is in the detection of delaminations

in various materials. Inspection of honeycomb and sandwich construction structures for delaminations proves to be an ideal application for infrared thermography^{59,61}. Carbon fiber reinforced plastics have been quickly inspected for hot spots, showing the locations where the top layer of material is improperly bonded to the honeycomb body⁵⁹. Glass-fiber reinforced plastic honeycombs sandwiched by aluminum plates have been inspected for delaminations as well⁶¹.

One of the attractive features of infrared inspection is the ease of data interpretation by looking at a thermogram and quickly locating hot spots as indications of defects. Fatigue cracks in metal structural members have been detected by infrared inspection^{60,61}. In these studies, the heat generated by cyclical loading of the cracks, were viewed as hot spots on the thermograms. The orientation of fiber reinforcement in composites can also be verified using infrared thermography⁶¹. In the mining industry, infrared thermography has been used to detect hazardous areas of loose rock⁶². Where there is a slight discontinuity in the transfer of heat, thermographic inspection is applicable.

The standard testing method for detecting delaminations in bridge decks using infrared thermography is detailed in the ASTM Standard D4788-88⁶⁴. The method can be used for both exposed and asphalt overlaid concrete, of up to 4 inches (101.6 mm) of thickness, bridge decks. The test consists of an infrared scanner and video recorder mounted on a vehicle. Delaminated areas appear as hot areas during the day and as cool areas during the night. A conventional video camera is also used to differentiate between areas where surface defects distort the infrared image. Delamination indications may also be locations where the overlay is separated from the underlying bridge deck. The infrared scanner must have a minimum resolution of .2 degrees Celsius and be mounted such that a minimum field view of 14 feet (4.27 m) is obtained. The

bridge deck must be clean and dry. A minimum 3 hours of direct sunlight must have been present to create the temperature differential required to detect delaminations. The minimum temperature difference for detection of delaminations is .5 degrees Celsius. An indicated, delaminations can be verified by using contact thermometer, sounding, and coring. Wind and temperatures below 0 degrees Celsius will decrease the temperature differential. An average detection rate of all delaminations is 80% to 90%. The ASTM document is the standard test procedure for inspection of concrete bridge decks with infrared thermography.

A number of studies have been performed over the years in an effort to gauge various aspects of the feasibility and accuracy of infrared thermographic inspection of bridge decks to detect delaminations in the concrete⁶⁵⁻⁶⁷. One study performed by the Indiana Department of Highways determined infrared inspection to be a viable alternative in the detection of delaminations⁶⁵. The infrared inspection was approximately 97 percent accurate in locating delaminated/debonded areas in comparison to the actual quantities of patching placed during construction⁶⁵. A study performed by the Vermont Agency of Transportation showed infrared inspection to have between 70 to 85 percent correlation with the results of inspection by sounding⁶⁶. The study concluded that infrared inspection can be a reasonably accurate, effective method for obtaining bridge deck condition information⁶⁶. A third study performed in Japan experimentally presented some limitations associated with thermographic inspection of concrete walls,⁶⁷ namely, delaminations smaller than approximately 8 inches (203.2 mm) on a side were difficult to detect⁶⁷. These studies indicate that although infrared thermographic inspection can be used to detect delaminations in concrete, care must be taken to address the practical difficulties that can arise during inspection.

A leading supplier of infrared thermography inspection equipment is Inframetrics. RUST Environment & Infrastructure (the principle infrared thermography subcontractor of this project) used the latest Inframetrics infrared thermal imaging equipment⁶⁹.

Although the sun radiates energy in both longwave and shortwave regions, the amount of energy radiated in each band is significantly different, resulting in interference in the shortwave region due to environmental noise⁶⁸. The equipment uses longwave infrared detectors to eliminate the false hot spots detected by shortwave systems in sunlit conditions^{68,69}. Advances in infrared thermography imaging equipment and improved temperature resolution have increased the accuracy of infrared nondestructive testing.

One of the latest applications of infrared thermography in infrastructure is the inspection of underground pipelines for water and gas leaks⁷⁰. The leaks are visualized as hot areas protruding from the pipeline. Sewer lines have also been inspected to locate areas where a leak in the line has caused erosion around the pipe, possibly leading to a cave in⁷⁰. New applications and guidelines are also being developed for the infrared inspection of masonry structures⁷². These inspections verify the integrity of precast panels and concrete block walls, and identify areas where insufficient building insulation results in energy losses⁷². Recent developments in pulse-echo thermal wave imaging use a modulated heat source launching heat waves into the object and monitoring the returning reflected waves with advance infrared cameras⁷¹. Using fast image processing techniques, quick inspection of injection molded automotive parts and aluminum aircraft parts have been performed⁷¹. These new developments are extending the useful applications of infrared thermography inspection.

Some experimental studies between ground penetrating radar and infrared thermography have been performed in order to compare their abilities to detect delaminations in concrete bridge

decks⁵⁴⁻⁵⁶. The results of these studies typically depict the two technologies as complementary, each providing information the other does not. For example, infrared thermography is able to provide a total areal inspection of the bridge deck while ground penetrating radar provides strips of data at predetermined intervals along the length of the deck. The similarities and differences, pertaining to this study, are discussed in Chapter 5.

1.1.4 Spectral Analysis of Surface Waves Literature Review of Previous Work

The spectral analysis of surface waves technique for pavement layer characterization was developed in the late 1970's and early 1980's. Much of the pioneering work in the development of the technique was performed by K. Stokoe and S. Nazarian^{74-83,86}. The spectral analysis of surface waves method is not intended to be used as a flaw detection technique, but as a means to characterize layer properties, such as thickness and modulus, through the depth of the pavement. The Ph.D. dissertation of S. Nazarian⁷⁴ presents the spectral analysis of surface waves method as an alternative to boreholes in determining the layer properties of soil deposits and pavements. This dissertation provides a step by step automated procedure from data collection to data analysis.

Further works by S. Nazarian and K. Stokoe performed at the Center for Transportation Research at the University of Texas at Austin added to and refined the spectral analysis of surface waves method^{75,76}. General results show the repeatability of the method in determining layer thicknesses and moduli⁷⁵. The testing setup known as the common-receiver-midpoint geometry was found to be the most accurate method⁷⁵. An exhaustive theoretical treatment of the surface waves method is presented⁷⁵. The data processing technique known as an inversion or backcalculation is detailed as well as theoretical investigations regarding the effect of different

material properties on the accuracy of the inversion method⁷⁶. These works lay the foundations for the use of the spectral analysis of surface waves method in determining layer properties in bridge decks.

A number of shorter works by S. Nazarian, K. Stokoe and others are found mainly in the Transportation Research Record⁷⁷⁻⁸¹. Early studies compared the accuracy of layer properties of the spectral analysis of surface waves method to properties obtained by deflection basins generated by falling weight deflectometers⁷⁷. Results of the common-receiver-midpoint geometry show that scatter in the data is reduced over the previous test setup⁷⁸. The inversion method is also tested to show the accuracy as compared to deflection basins⁷⁸. Layer properties of rigid pavements determined by the spectral analysis of surface waves method offer comparable results to deflection basins⁷⁹. Further refinement of the inversion algorithm, where iterative numerical solutions to the pavement profile are generated, show how an automated and fast testing method based on surface waves is developed⁸⁰. Finally, sensitivity tests were performed where the accuracy of the surface waves method for layer properties was established to be within 10 percent for the surface layer and 10 to 30 percent for below surface layers⁸¹. These papers establish the spectral analysis of surface waves method as a fast, reliable method for determining pavement layer properties.

Within the last decade, a number of papers have been presented specifying the variables most likely to affect the accuracy of the spectral analysis of surface waves method⁸²⁻⁸⁶. One of the most important factors affecting the method is the spacing between the two receiving transducers and the point of impact⁸². The common-receiver-midpoint geometry provides adequate filtering of low frequency components which could potentially cause errors in the inversion processing method⁸². Another factor effecting accuracy is the type of source used to

generate the surface waves in the pavement⁸⁴. Hammers of varying weights were tested to determine the optimum weight to generate the necessary range of frequencies within the pavement. It was found that light hammers (0.25 pounds [0.113 kg]) could not adequately generate low frequencies and heavy hammers (8 pounds [3.63 kg]) could not generate the necessary high frequencies. By combining the data from light and heavy hammers, adequate pavement layer properties could be determined⁸⁴. A similar study by D. Hiltunen⁸⁵ found similar results and concluded that no single source type is capable of determining completely accurate pavement properties. Finally, the influence of layer stiffnesses proved to be important in the accuracy of the spectral analysis of surface waves method⁸⁶. In the study, relatively stiff concrete was placed on soft soil of varying stiffnesses. It was found that bulk waves reflected by the concrete/soil interface can disrupt the backcalculation of layer properties. The most affected surface waves were those with wavelengths between 0.7 and 1.8 times the thickness of the concrete slab⁸⁶.

The spectral analysis of surface waves method is intended to be used to determine material properties of soil deposits and pavement layers. Very little work has been done on the application of this method to inspection of bridge decks, as the method is not intended to find specific flaws, such as delaminations, within a pavement.

1.1.5 Chain Drag Survey Literature Review of Previous Work

The standard test method for measuring delamination in concrete bridge decks by sounding is detailed in ASTM Standard D 4580-86⁷³. The procedure does not apply to bridge decks that have been overlaid with bituminous mixtures. The bridge can either be sounded with an impact device such as a hammer or steel rod, or be sounded by dragging a length of chain

across the surface of the concrete deck. Tapping with a hammer or other impact device creates a clear ringing sound heard over sound areas of the deck, and a dull or hollow sound is heard over delaminated areas. When dragging a chain across the deck, a faint ringing sound and clinking of the chain links is heard over solid areas of the deck, while hollow or lower frequency sounds described as “scratching” is heard over delaminated areas of the deck. Accuracy of data derived from chain dragging is strongly dependent on the expertise of the tester. A suspect area is marked with paint. A grid system is constructed with two perpendicular tape measures to record the beginning and ending lengths and widths of the delaminated areas. A scaled drawing of the deck is then made with the delaminated areas marked. The chain dragging procedure was used for this study and field observations of the testing are detailed in the experimental portion of this report.

1.2 Selection and Description of the Bridges

In order to ensure a comprehensive evaluation of the three nondestructive testing techniques, a wide variety of bridge decks in varying states of decay were evaluated. Specifically, bridges were chosen on a continuum of damage states ranging from bridges with minimal reinforcing steel corrosion and few delaminations to bridges with widespread delaminations and showing previous rehabilitation work. In this manner, the nondestructive testing techniques could be evaluated based on their ability to locate delaminations and deterioration, and to evaluate the susceptibility of each method to falsely report delaminations and deterioration that does not exist.

At the outset of this project, the Illinois Department of Transportation officials provided complete construction plans of fourteen potential bridges located in central and southern Illinois

for nondestructive inspection. In order to minimize cost, expedite testing and maximize damage variability, nine bridges were chosen. To reduce travel time and traffic control coordination, location was factored into the decision process such that the nine bridges were clustered into three main regions--Bloomington, Peoria, and Marion. Although the actual conditions of the bridges could not be known prior to testing, a reasonable guess could be made based upon construction and maintenance dates and other information supplied about the history of each bridge. Table 1.1 provides a summary of general information of the nine bridge decks. Each of the nine bridges are described below along with a brief overview of their general structural conditions based upon field observations made during testing and removal of the asphalt overlay.

1.2.1 Description of Bloomington Structure Number 057-0088

Located on State Highway 9 over Interstate 55/74, Structure Number 057-0088 located near Bloomington, Illinois carries three lanes of traffic in both the eastbound and westbound directions. It has a continuously reinforced portland cement concrete deck with an asphalt overlay. The overlay is composed of three layers: a woven geotextile fabric bonded to the surface of the concrete deck, a 0.5 to 1 inch (12.7 to 25.4 mm) layer of sand/tar mixture, and approximately 2 inches (50.8 mm) of asphalt concrete. The structure is approximately 268 feet (81.7 m) in length, comprised of the main span and two approach slabs on either end. The total area inspected is approximately 12,864 ft² (1195 m²). The deck was in poor condition with numerous areas of asphalt and concrete surface patching and very large areas of delamination and deteriorated concrete. Removal of the asphalt overlay revealed numerous concrete patches. Visual underside inspection showed minor deterioration with some corrosion of steel. Pictures of the structure are shown in Figure 1.1 through Figure 1.3.



Figure 1.1 Bloomington Structure Number 057-0088 bridge deck showing asphalt patching along abutment joints.



Figure 1.2 Bloomington Structure Number 057-0088 bridge deck showing asphalt patching along longitudinal joints.

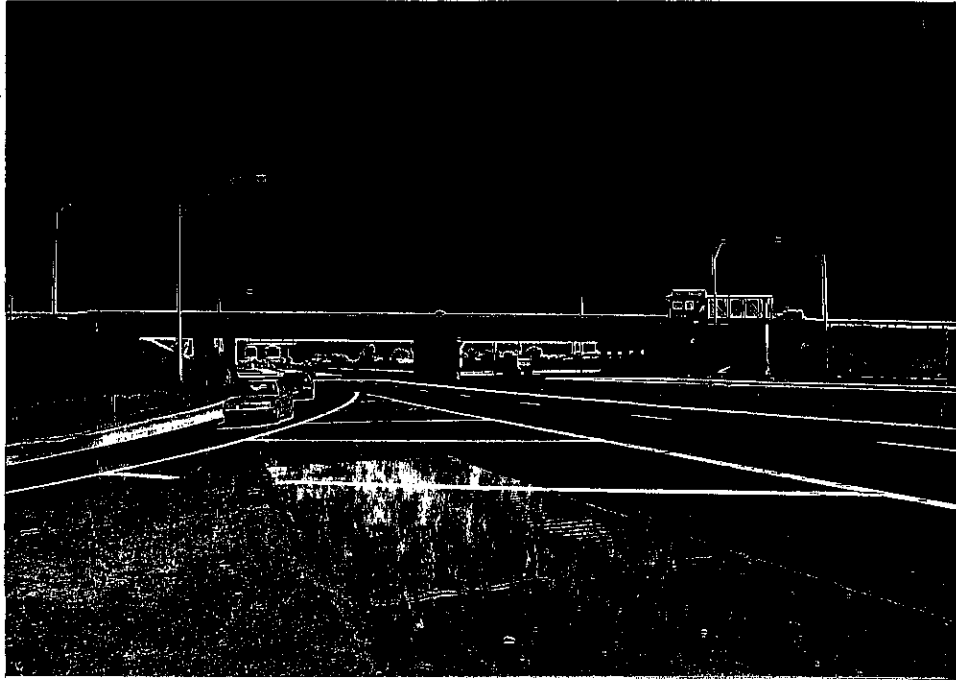


Figure 1.3 Bloomington Structure Number 057-0088 bridge deck view looking north.

1.2.2 Description of Peoria Structure Number 090-0118

Located on Interstate 474 eastbound ramp to Interstate 74 westbound over Interstate 474, Structure Number 090-0118 located east of Peoria, Illinois carries one lane of traffic in the southbound direction. It has a continuously reinforced portland cement concrete deck with no overlay. The structure is approximately 390 feet (118.9 m) in length, comprised of the main span and two approach spans on either end. The total area inspected is approximately 4,680 ft² (435 m²). The deck was in almost new condition. Visual underside inspection showed no major deterioration. Pictures of the structure are shown in Figure 1.4 and Figure 1.5.



Figure 1.4 Peoria Structure Number 090-0118 bridge deck with no overlay looking south.

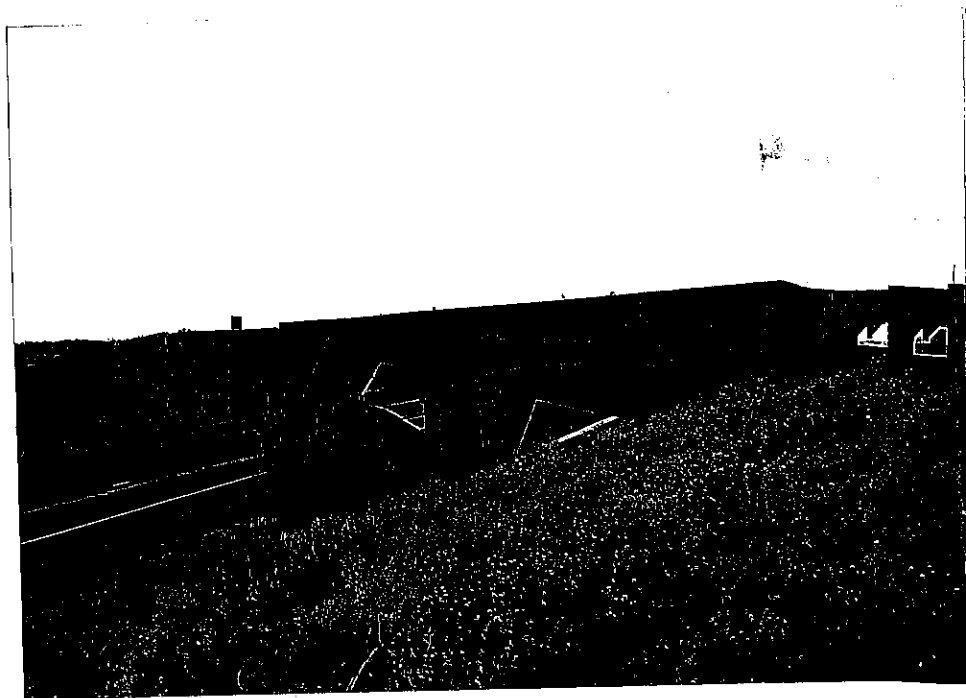


Figure 1.5 Peoria Structure Number 090-0118 bridge deck with no overlay side view.

1.2.3 Description of Peoria Structure Number 072-0106

Located on Interstate 474 southbound over Interstate 74 westbound, Structure Number 072-0106 located west of Peoria, Illinois carries two lanes of traffic in the southbound direction plus a merging ramp. It has a continuously reinforced portland cement concrete deck with an asphalt overlay. The overlay is composed of three layers: a woven geotextile fabric bonded to the surface of the concrete deck, a 0.5 to 1 inch (12.7 to 25.4 mm) layer of sand/tar mixture, and approximately 2 inches (50.8 mm) of asphalt concrete. The structure is approximately 165 feet (50.3 m) in length, comprised of the main span and two approach slabs on either end. The total area inspected is approximately 3,960 ft² (368 m²). The deck was in generally good condition with minor asphalt surface patching and a number of minor delaminations found upon removal of the asphalt overlay. Visual underside inspection showed no major deterioration. The structure is one of four similar structures composing the crossover of Interstate 474 over Interstate 74. Figure 1.6 through Figure 1.9 show these four structures.

1.2.4 Description of Peoria Structure Number 072-0107

Located on Interstate 474 northbound over Interstate 74 westbound, Structure Number 072-0107 located west of Peoria, Illinois, carries two lanes of traffic in the northbound direction plus a merging ramp. It has a continuously reinforced portland cement concrete deck with an asphalt overlay. The overlay is composed of three layers: a woven geotextile fabric bonded to the surface of the concrete deck, a 0.5 to 1 inch (12.7 to 25.4 mm) layer of sand tar mixture, and approximately 2 inches (50.8 mm) of asphalt concrete. The structure is approximately 161 feet (49.1 m) in length, comprised of the main span and two approach slabs on either end. The total area inspected is approximately 3,864 ft² (359 m²). The deck was in fair condition with minor

asphalt surface patching and a moderate number of delaminations found upon removal of the asphalt overlay. Visual underside inspection showed no major deterioration. The structure is one of four similar structures composing the crossover of Interstate 474 over Interstate 74. Figure 1.6 through Figure 1.9 show these four structures.

1.2.5 Description of Peoria Structure Number 072-0108

Located on Interstate 474 southbound over Interstate 74 eastbound, Structure Number 072-0108 located west of Peoria, Illinois carries two lanes of traffic in the southbound direction plus a merging ramp. It has a continuously reinforced portland cement concrete deck with an asphalt overlay. The overlay is composed of three layers: a woven geotextile fabric bonded to the surface of the concrete deck, a 0.5 inch to 1 inch (12.7 to 25.4 mm) layer of sand tar mixture, and approximately 2 inches (50.8 mm) of asphalt concrete. The structure is approximately 170 feet (51.8 m) in length, comprised of the main span and two approach slabs on either end. The total area inspected is approximately 4,080 ft² (379 m²). The deck was in excellent condition with minor asphalt surface patching and minimal delaminations found upon removal of the asphalt overlay. Visual underside inspection showed no major deterioration. The structure is one of four similar structures composing the crossover of Interstate 474 over Interstate 74. Figure 1.6 through Figure 1.9 show these four structures.

1.2.6 Description of Peoria Structure Number 072-0109

Located on Interstate 474 northbound over Interstate 74 eastbound, Structure Number 072-0109 located west of Peoria, Illinois carries two lanes of traffic in the northbound direction plus a merging ramp. It has a continuously reinforced portland cement concrete deck with an

asphalt overlay. The overlay is composed of three layers: a woven geotextile fabric bonded to the surface of the concrete deck, a 0.5 to 1 inch (12.7 to 25.4 mm) layer of sand tar mixture, and approximately 2 inches (50.8 mm) of asphalt concrete. The structure is approximately 164 feet (50.0 m) in length, comprised of the main span and two approach slabs on either end. The total area inspected is approximately 3,936 ft² (366 m²). The deck was in good condition with minor asphalt surface patching and a number of delaminations found upon removal of the asphalt overlay. Visual underside inspection showed no major deterioration. Pictures of the structure are shown in Figure 1.6 through Figure 1.9.



Figure 1.6 Peoria Structure Number 072-0109 bridge deck looking north.

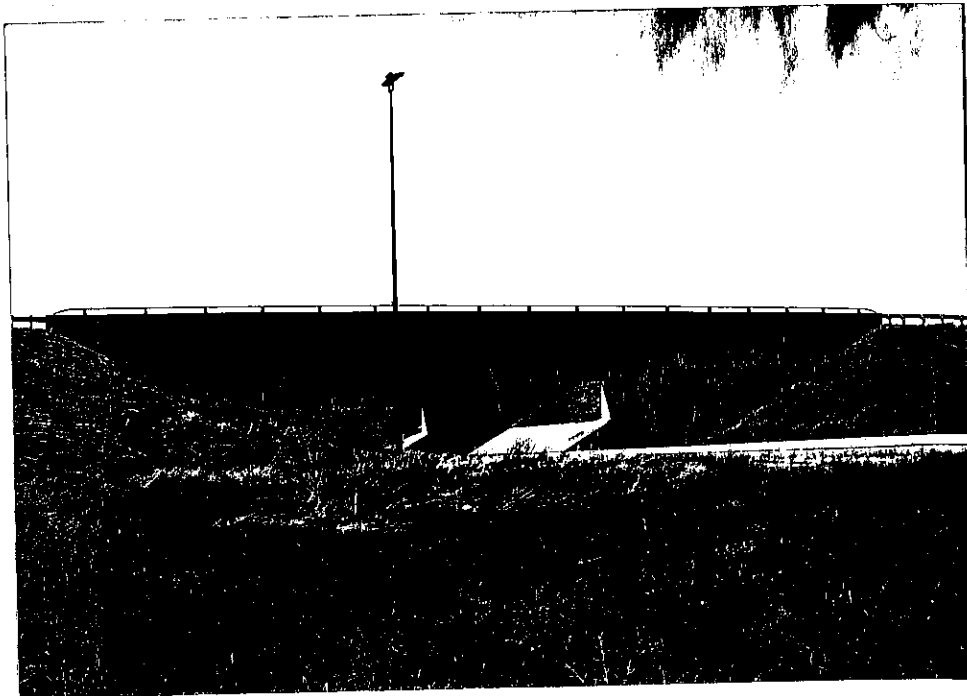


Figure 1.7 Peoria Structure Number 072-0109 bridge deck side view.

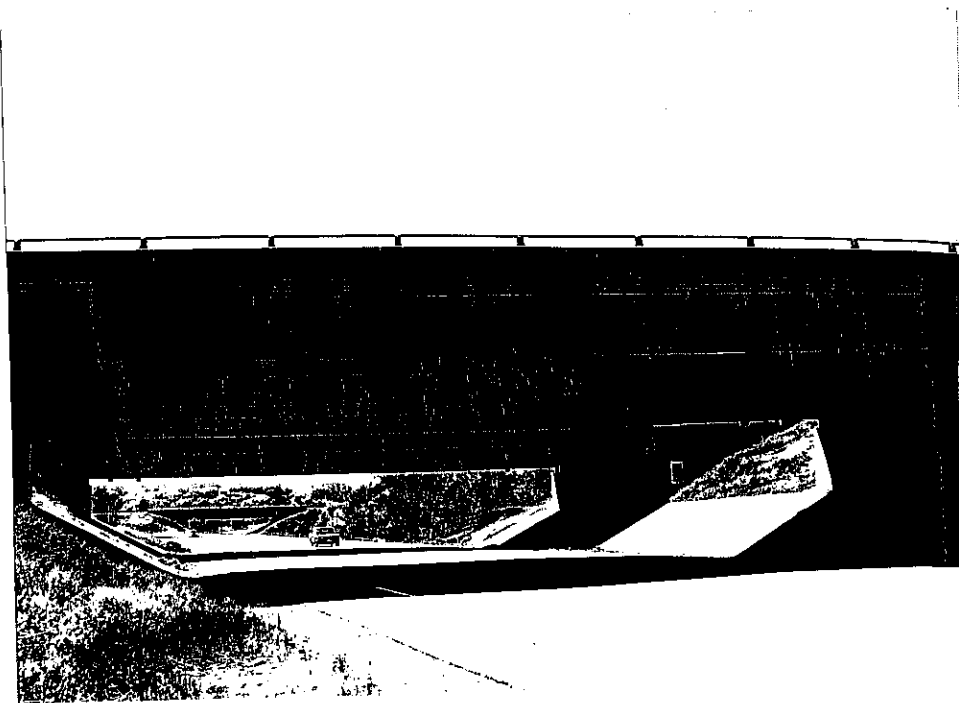


Figure 1.8 Peoria Structure Number 072-0109 bridge deck side view with Peoria Structure Number 072-0108 in background.

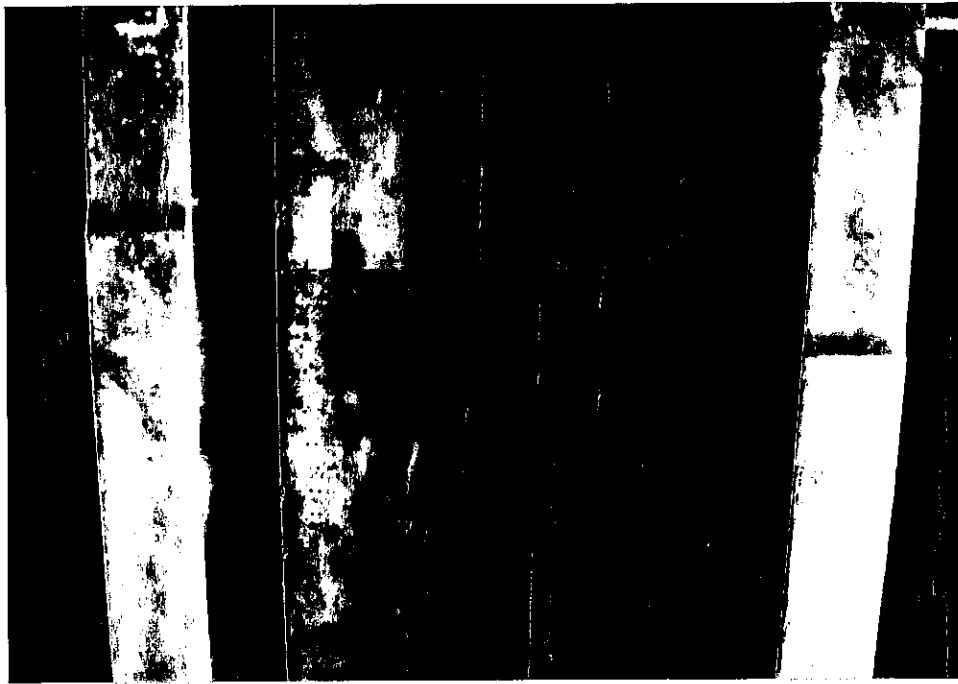


Figure 1.9 Underside of Peoria Structure Number 072-0109 bridge deck showing no major deterioration.

1.2.7 Description of Peoria Structure Number 072-0110

Located on Interstate 474 westbound over Interstate 74 eastbound, Structure Number 072-0110 located west of Peoria, Illinois carries two lanes of traffic in the westbound direction. It has a continuously reinforced portland cement concrete deck with an asphalt overlay. The overlay is composed of three layers: a woven geotextile fabric bonded to the surface of the concrete deck, a 0.5 inch to 1 inch (12.7 to 25.4 mm) layer of sand tar mixture, and approximately 2 inches (50.8 mm) of asphalt concrete. The structure is approximately 228 feet (69.5 m) in length, comprised of the main span and two approach slabs on either end. The total area inspected is approximately 5,472 ft² (508 m²). The deck was in fair condition with no asphalt surface patching and a number of delaminations found upon removal of the asphalt

overlay. After removal of the overlay, it was noted that the concrete deck had been milled with gouges up to 1 inch (25.4 mm) deep. Visual underside inspection showed no major deterioration. Pictures of the structure are shown in Figure 1.10 and Figure 1.11.

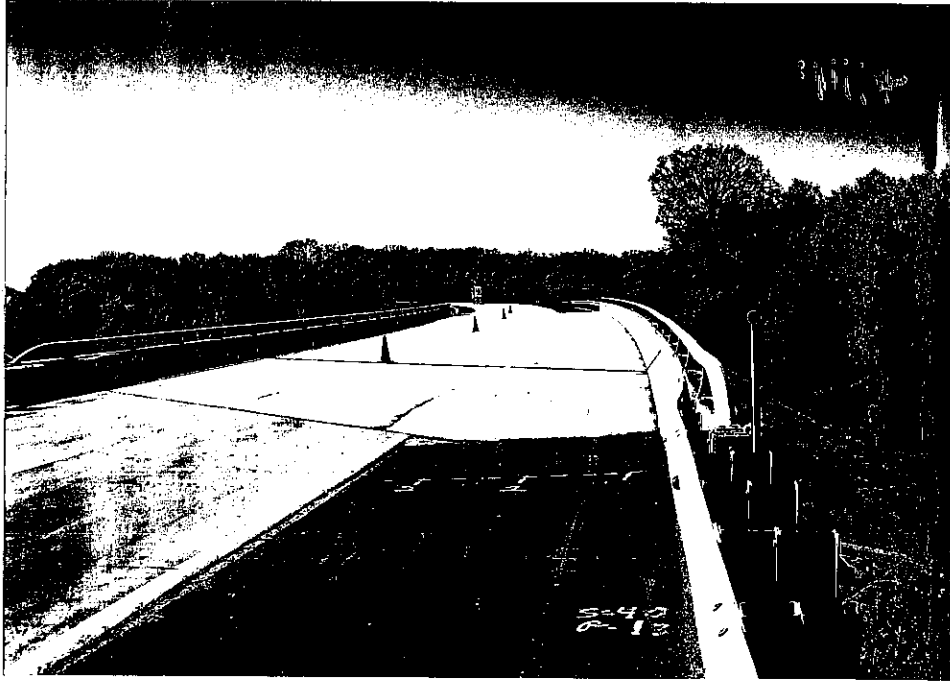


Figure 1.10 Peoria Structure Number 072-0110 looking west prior to removal of overlay.



Figure 1.11 Peoria Structure Number 072-0110 looking west following removal of overlay exposing milling marks in concrete bridge deck.

1.2.8 Description of Peoria Structure Number 072-0111

Located on Interstate 474 southbound over Interstate 74 eastbound, Structure Number 072-0111 located west of Peoria, Illinois carries two lanes of traffic in the southbound direction. It has a continuously reinforced portland cement concrete deck with an asphalt overlay. The overlay is composed of three layers: a woven geotextile fabric bonded to the surface of the concrete deck, a 0.5 to 1 inch (12.7 to 25.4 mm) layer of sand tar mixture, and approximately 2 inches (50.8 mm) of asphalt concrete. The structure is approximately 299 feet (91.1 m) in length, comprised of the main span and two approach slabs on either end. The total area inspected is approximately 7,176 ft² (667 m²). The deck was in fair condition with no asphalt surface patching and a number of delaminations found upon removal of the asphalt overlay. Visual underside inspection showed no major deterioration.

1.2.9 Description of Marion Structure Number 100-0005

Located on Interstate 57 southbound over Old State Highway 13, Structure Number 100-0005 located near Marion, Illinois carries three lanes of traffic in the southbound direction. It has a continuously reinforced portland cement concrete deck with an asphalt overlay. The overlay is composed of three layers: a woven geotextile fabric bonded to the surface of the concrete deck, a 0.5 to 1 inch (12.7 to 25.4 mm) layer of sand tar mixture, and approximately 2 inches (50.8 mm) of asphalt concrete. The structure is approximately 154 feet (46.9 m) in length comprised of the main span and two approach slabs on either end. The total area inspected is approximately 6,930 ft² (644 m²). The deck was in poor to very poor condition with numerous areas of asphalt and concrete surface patching and very large areas of delamination. Visual underside inspection showed major deterioration with exposed and corroded reinforcing steel and leaching of salts through transverse cracks in the deck. Pictures of the structure are shown in Figure 1.12 through Figure 1.14.



Figure 1.12 Marion Structure Number 100-0005 looking north before removal of overlay showing concrete surface patches.



Figure 1.13 Underside of Marion Structure Number 100-0005 showing corrosion of superstructure and leaching of salts through transverse cracks in bridge deck.



Figure 1.14 Underside of Marion Structure Number 100-0005 showing corrosion of reinforcement bars causing spalling and delamination of concrete.

1.2.10 Summary Of Bridge Decks

Table 1.1 depicts a summary of the bridge decks used in this study. A wide variety of deck deterioration conditions were found across the entirety of the study. This allows for comparison among the three main nondestructive testing techniques under a good sampling of field conditions.

Table 1.1 Summary of Bridge Deck Survey

Structure	Route Carried	Location	Structure Type	Year Constr.	Deck Survey	# Lanes	Lane Width feet (m)	Length feet (m)	Area feet ² (m ²)
057-0088	IL 9 over I-55	W. of Bloomington	4 Span WF	1963 1974	1992	4	12 (3.66)	268 (81.7)	12,864 (1178)
090-0118	FAI 474 (EB)	E. of Peoria	3 Span Plate Girder	1979	1995	1	12 (3.66)	390 (118.9)	4,680 (435)
072-0106	FAI 474	W. of Peoria	Single Span Plate Girder	1973	1994	2	12 (3.66)	165 (50.3)	3,960 (368)
072-0107	FAI 474	W. of Peoria	same	1973	1994	2	12 (3.66)	161 (49.1)	3,864 (359)
072-0108	FAI 474	W. of Peoria	same	1973	1994	2	12 (3.66)	170 (51.8)	4,080 (379)
072-0109	FAI 474	W. of Peoria	same	1973	1994	2	12 (3.66)	164 (50.0)	3,936 (366)
072-0110	Ramp A FAI 74	W. of Peoria	Single Span Plate Girder	1973	1994	2	12 (3.66)	228 (69.5)	5,472 (508)
072-0111	FAI 474	W. of Peoria	3 Span Plate Girder	1973	1994	2	12 (3.66)	299 (91.1)	7,176 (667)
100-0005	FAI 57 (SB) over SBI 13	S. of Marion	3 Span WF	1959/ 1975		3	15 (4.57)	154 (46.9)	6,930 (644)
								TOTAL	52,962 (4920)

2.0 THEORY OF INSPECTION METHODS

2.1 Theory of Impact-Echo

This section presents a concise description of the theory behind the impact-echo inspection method. For a more detailed mathematical development of this theory, consult the references cited at the end of this report¹⁻³². This discussion follows from Sansalone and Carino⁴.

2.1.1 Principles of Stress Wave Propagation

When a stress is applied suddenly to a medium, a displacement disturbance propagates through the medium at a finite velocity. This disturbance is known as a stress wave. There are three main types of stress waves: compression waves, shear waves, Rayleigh waves, plate waves, etc. Compression waves create particle displacements parallel to the direction of wave travel within the solid. Shear waves and Rayleigh waves create particle displacements perpendicular to wave travel. Both compression and shear waves travel within the medium, while Rayleigh waves travel along the surface of a solid medium.

Solutions to the wave equation in isotropic elastic media provide equations relating the material properties of a media to the velocity of wave propagation for the three types of stress waves. An accurate determination of the velocity of wave propagation is imperative to the impact-echo method. In infinite elastic solids, the compression wave velocity, C_p , is a function of Young's modulus of elasticity, E , Poisson's ratio, ν , and the mass density, ρ , as shown in Equation 2.1.

$$C_p = \sqrt{\frac{E(1-\nu)}{\rho(1+\nu)(1-2\nu)}} \quad (2.1)$$

In infinite elastic solid, the shear wave velocity, C_s , is given by Equation 2.2.

$$C_s = \sqrt{\frac{E}{2\rho(1-\nu)}} \quad (2.2)$$

Rayleigh waves propagate at a velocity, C_r , given by the approximate formula of Equation 2.3⁴.

$$C_r = \frac{0.87 + 1.12\nu}{1 + \nu} C_s \quad (2.3)$$

Of particular interest is the ratio of the three propagation velocities. Using the compression wave velocity, C_p , as a standard, and assuming a Poisson's ratio, ν , of 0.2 (concrete), the shear wave velocity, C_s , is 61% of the compression wave velocity, C_p , and the Rayleigh wave velocity, C_r , is 56% of the compression wave velocity, C_p . These values are significant when performing data analysis on impact-echo signals.

Much like light waves, stress waves will reflect and refract when incident upon dissimilar media. These are relevant phenomena when using the impact-echo technique to inspect layered systems such as bridge decks with asphalt overlays. Figure 2.1 illustrates the concepts of reflection and refraction.

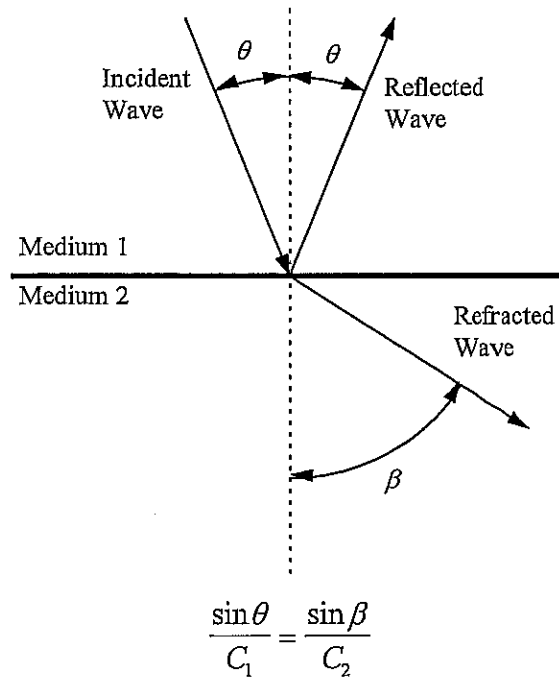


Figure 2.1 Reflection and refraction of stress waves given by Snell's Law.

As seen from Figure 2.1, when a stress wave is incident upon the boundary of two different mediums, part of the energy is reflected back at the incident angle, and the remainder of the energy is absorbed by the second material at an angle given by Snell's Law, Equation 2.4.

$$\frac{\sin \theta}{C_1} = \frac{\sin \beta}{C_2} \quad (2.4)$$

At greater angles of incidence, a more complicated phenomenon occurs involving the conversion of energy from one stress wave type, e.g. compression, to another stress wave type, e.g. shear. This phenomenon is not central to the impact-echo method; for a more complete discussion of mode conversions refer to the impact-echo references⁴.

The case where the angle of incidence, θ , is zero is important to impact-echo theory. In this case, both the angle of reflection, θ , and the angle of refraction, β , will also be zero. The amount of energy reflected and refracted when a stress wave is incident on a medium boundary is dependent upon the specific acoustic impedances of the two materials. The specific acoustic impedance of a material, Z , is given by Equation 2.5.

$$Z = \rho C_p \quad (2.5)$$

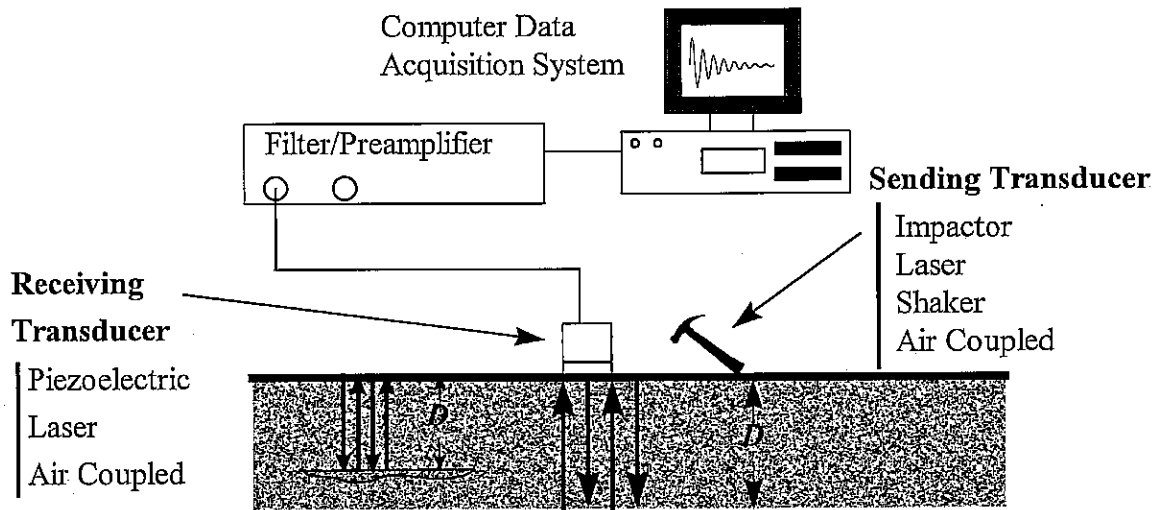
The specific acoustic impedance of a material is the product of the mass density, ρ , and the compression wave velocity, C_p . When the angle of incidence of a stress wave on two materials is zero, the ratio of the energy reflected by the boundary to the energy absorbed by the second material can be calculated using the specific acoustic impedances of the two materials, Z_1 , and, Z_2 , given by Equation 2.6.

$$R_n = \frac{Z_2 - Z_1}{Z_2 + Z_1} \quad (2.6)$$

The ratio, R_n , is the fraction of energy returned by the material boundary. If Z_1 is greater than Z_2 , then R_n is negative, indicating there is a phase change in the reflected stress wave. If Z_1 is less than Z_2 , then R_n is positive and there is no phase change in the reflected stress wave. The principle of reflection and refraction of stress waves is key to understanding the basic principle of the impact-echo method. The impact-echo method makes use of propagating stress waves reflecting and refracting off of discontinuities in concrete bridge decks as a means of defect detection.

2.1.2 Stress Wave Propagation and Impact-Echo

In the impact-echo test procedure, a sending transducer generates a stress wave pulse into the material to be inspected. The stress wave pulse travels into the material, is reflected by material interfaces or flaws, and is returned to the surface where it is monitored by a receiving transducer. Figure 2.2 illustrates the concept for a single, continuous slab of concrete.



$$D = C_p / 2f$$

D = distance to reflector

C_p = velocity of compression wave propagation

f = measured frequency

Figure 2.2 Illustration of the impact-echo concept for a single layer system.

Figure 2.2 shows that if the velocity of compression wave propagation, C_p , and the frequency, f , with which stress waves are reflected by an interface, are known through monitoring, then the depth, D , of the reflecting interface can be calculated. The depth, D ,

traveled by a stress wave pulse is a function of the round trip travel time, t , and velocity of propagation, C_p , given by Equation 2.7.

$$D = \frac{C_p t}{2} \quad (2.7)$$

By substituting the round trip travel time, t , with the frequency, f , of stress wave incidence on the surface of the material, an expression for interface depth is given by Equation 2.8.

$$D = \frac{C_p}{2f} \quad (2.8)$$

The frequency of successive stress wave pulses is easier to determine than the time between successive stress wave pulses; this is why Equation 2.8 is used instead of Equation 2.7.

Figure 2.3 shows the impact-echo concept for a two layer system (such as concrete with an asphalt overlay). Here the determination of the depth of the interface is slightly more complicated because there are two material layers with different material properties. Each layer has a different velocity of stress wave propagation, C_{p1} , and C_{p2} . The depth, D , of an interface in the second layer is given by Equation 2.9.

$$D = \frac{1}{2} \left[\frac{C_{p2}}{f_2} + \frac{C_{p1} - C_{p2}}{f_1} \right] \quad (2.9)$$

Equation 2.9 was derived in a similar manner as Equation 2.8 with two layers considered. The frequency, f_1 , corresponds to the successive round trips of stress waves reflecting off of the interface between layer 1 and layer 2. The frequency, f_2 , corresponds to the successive round trips of stress waves reflecting off either a flaw in layer 2 or the bottom of layer 2.

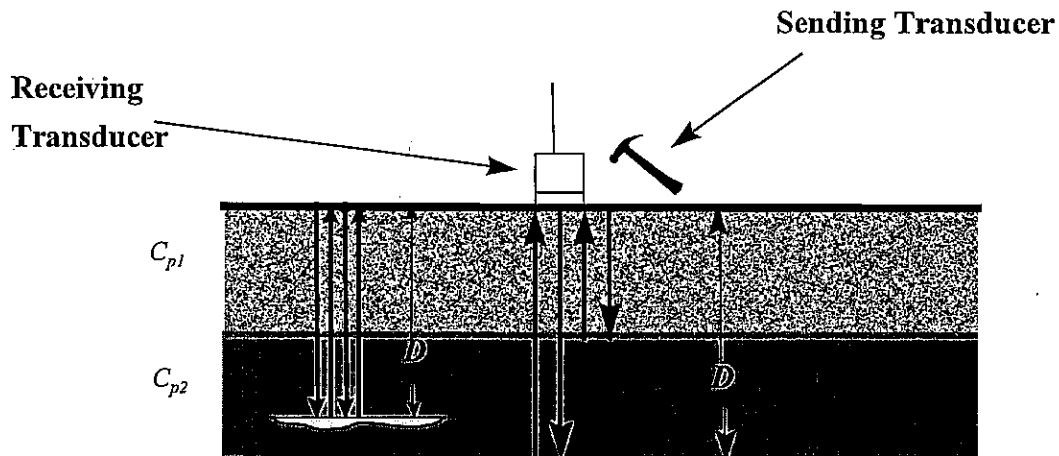


Figure 2.3 Illustration of the impact-echo concept for a two layer system.

The sending transducer of Figure 2.2 or Figure 2.3 can be any mechanism which generates stress waves of the proper frequency in the material. The most common sending method is a mechanical impact device such as a steel ball or spring loaded steel rod actuated by a solenoid. Current and future methods involve the use of high power lasers to generate stress waves by rapid thermal expansion and ablation of the material surface. Other methods of stress wave generation being investigated are the use of air coupled piezoelectric transducers and small, high frequency shakers. Piezoelectric transducers with a flat frequency response are commonly used to monitor the stress wave on the surface of the material. Other techniques use a laser interferometer or air coupled transducers to monitor stress wave propagation.

2.1.3 Data Analysis

The receiving piezoelectric transducer converts stress pulses into a voltage that can be recorded using an analog to digital board and a computer. As discussed in the preceding section, it is easier to determine the frequency of returning stress wave pulses than determining the time

between successive pulses, illustrated in Figure 2.4. The figure shows a typical time domain impact-echo signal as recorded by a piezoelectric transducer. Note the difficulty in determining the time between stress pulses. Figure 2.4 also shows the frequency domain of the signal converted by a Fast Fourier Transform (FFT) routine. The frequency domain clearly indicates the frequency at which maximum energy returns from the material. Note also the multiple peaks in the frequency domain. These may correspond to different material interfaces or flaws in the specimen. By using the main frequency, f , or other frequency peak from Figure 2.4, the depth of that returning stress wave can be calculated using Equation 2.8. If the system being inspected is layered, the depth of the reflection can be established using Equation 2.9. In this instance, two frequencies must be established, the frequency corresponding to the depth of the top layer, f_1 , and the frequency corresponding to the depth of the flaw or bottom layer, f_2 .

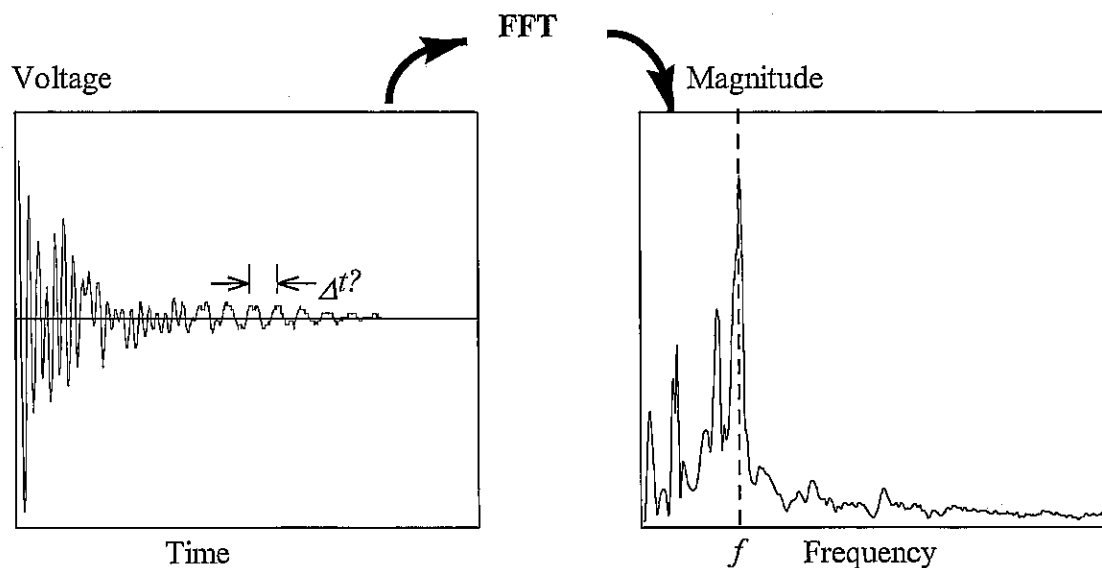


Figure 2.4 Typical time response and corresponding frequency spectrum of impact-echo signal.

2.1.4 Stress Wave Frequency Characteristics

The frequency range of stress wave energy generated by the impact is important for adequate flaw detection using the impact-echo method. Most energy is contained in frequencies less than $1.5/t_c$, where t_c is the impulse contact time. The stress pulse must contain a broad band frequency range with sufficient low frequency components necessary to penetrate the thickness of the concrete and reflect deep flaws and boundaries. In addition, the stress pulse must contain high frequency components to reflect shallow flaws. Figure 2.5 shows the depth of material that can be inspected at various frequencies within the range of compression stress wave velocities for concrete. To inspect a slab of concrete of a given thickness, a stress wave frequency range must be generated with the lowest frequency corresponding to the depth of the slab, and the highest frequency corresponding to the minimum desired thickness to be inspected. It is important that the receiving transducer have a flat frequency response in the frequency band of interest. A typical frequency range for impact-echo inspection of concrete bridge decks is 1000 Hz to 50,000 Hz. Therefore, the sampling rate of the analog to digital receiver must be at least 100,000 Hz as determined by the Nyquist criteria.

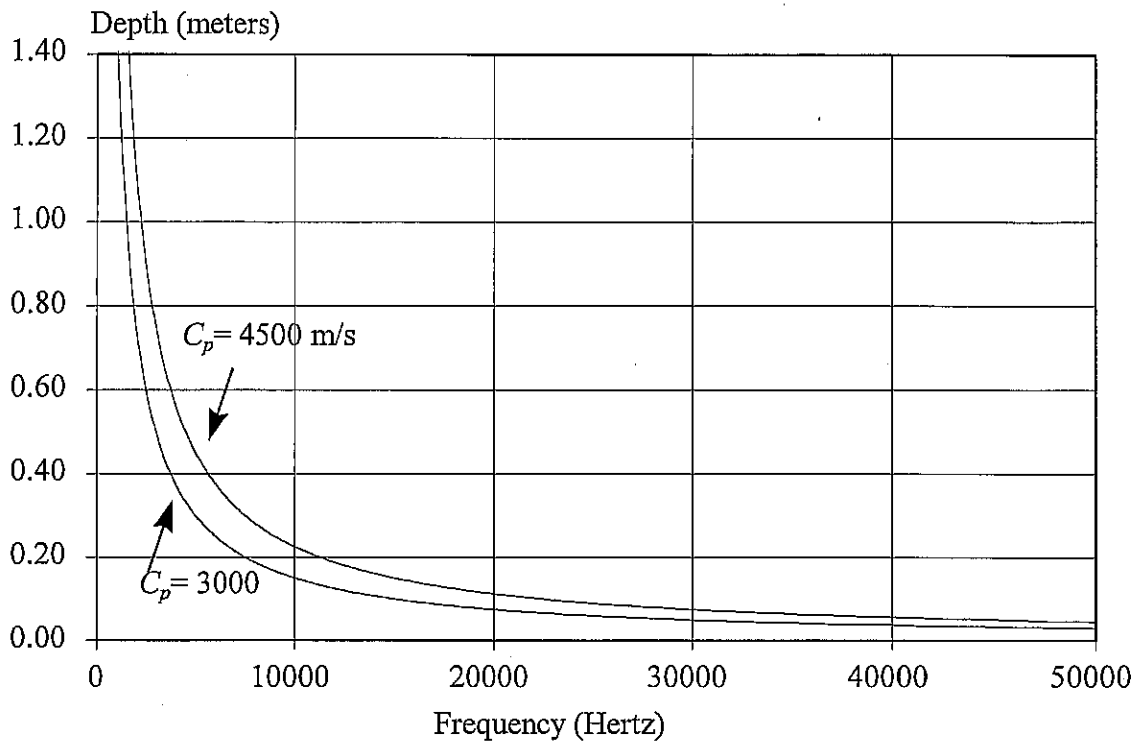


Figure 2.5 Depth of inspection vs. frequency for typical compression wave velocity range in concrete.

It should be stated that Equation 2.8 can be used to determine the velocity of the material if the depth is known. Therefore, during inspection, one test core of the concrete slab could be taken to determine the concrete velocity, which will give a more accurate determination of the depth of flaw or interface.

2.2 Theory of Ground Penetrating Radar

This section presents a concise description of the theory behind the ground penetrating radar inspection method. For a more detailed mathematical development of this theory, consult

the references at the end of this report³³⁻⁵⁶. Much of this discussion follows from Clemeña^{33,34} and is credited as such.

2.2.1 Principles of Radar Propagation in Solids

Suppose a microwave is incident upon a boundary of two materials each with different dielectric properties. Figure 2.6 shows the behavior of microwaves at a dielectric interface or boundary. Part of the energy incident upon the boundary will be reflected back into the material where the wave originated, and part of the energy will be transmitted into the second material and continue propagating in the incident direction. The amount of energy reflected and transmitted depends upon the dielectric properties of the two materials. The reflection coefficient, R , is related to the amount of original energy reflected back by the dielectric boundary. It is the ratio of reflected energy, E_r , to incident energy, E_0 . Equation 2.10 states this ratio to be determined by the material impedances, η_1 and, η_2 which are measured in ohms.

$$R = \frac{E_r}{E_0} = \frac{\eta_2 - \eta_1}{\eta_2 + \eta_1} \quad (2.10)$$

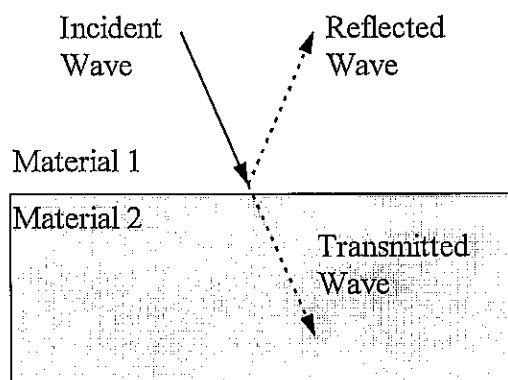


Figure 2.6 Reflection and transmission of electromagnetic radar wave at a dielectric boundary.

The impedance of a material, η , is related to its dielectric constant, ϵ (measured in henry/meters), by the magnetic permeability of free space, μ_0 , which is a universal constant ($4\pi \times 10^{-7}$ henry/meters). Equation 2.11 shows the relationship and is valid for nonmetallic materials such as soil and concrete. Metals are efficient conductors with zero wave impedance; therefore, they are perfect reflectors.

$$\eta = \sqrt{\frac{\mu_0}{\epsilon}} \quad (2.11)$$

The wave impedance of free space, η_0 , can be computed using the magnetic permeability of free space, μ_0 , and the dielectric constant of free space, ϵ_0 (8.85×10^{-12} farad/meters). Equation 2.12 shows this relationship.

$$\eta_0 = \sqrt{\frac{\mu_0}{\epsilon_0}} \quad (2.12)$$

For purposes of comparison, it is helpful to compare all the dielectric constants of materials to that of free space. Equation 2.13 shows how the relative dielectric constant, ϵ_r , is calculated from its absolute dielectric constant, ϵ .

$$\epsilon_r = \frac{\epsilon}{\epsilon_0} \quad (2.13)$$

By defining a relative dielectric constant, ϵ_r , it is now possible to rewrite Equation 2.11 in a different form. Equation 2.14 relates impedance, η , of a specific material to its relative dielectric constant, ϵ_r , using the impedance of free space, η_0 .

$$\eta = \frac{\eta_0}{\sqrt{\epsilon_r}} \quad (2.14)$$

By substituting Equation 2.14 into Equation 2.10, the reflection coefficient, R , at a dielectric boundary can be expressed simply by the relative dielectric constants, ϵ_{r1} and, ϵ_{r2} of the two materials. Equation 2.15 shows this simple relationship.

$$R = \frac{\sqrt{\epsilon_{r1}} - \sqrt{\epsilon_{r2}}}{\sqrt{\epsilon_{r1}} + \sqrt{\epsilon_{r2}}} \quad (2.15)$$

Therefore, the relative dielectric constants of the two materials at an interface determine the amount of energy reflected by the interface and transmitted by the interface when a microwave is incident. Suppose that the relative dielectric constant of material one, ϵ_{r1} , is less than the relative dielectric constant of material two, ϵ_{r2} . The reflection coefficient, R , will be negative. This implies that the reflected electromagnetic wave will have a polarity opposite that of the original incident wave. If the relative dielectric constant of material one, ϵ_{r1} , is greater than the relative dielectric constant of material two, ϵ_{r2} , then the reflection coefficient, R , will be positive, and the reflected wave will have the same polarity as the original incident wave. This concept is very important when using ground penetrating radar to inspect bridge decks. The strength and polarity of a reflected wave can determine if the wave is reflecting off of the asphalt/concrete interface, an air void between the asphalt overlay and the concrete, or an air filled delamination in the concrete itself.

2.2.2 Ground Penetrating Radar and Bridge Decks

The use of ground penetrating radar to inspect bridge decks involves sending electromagnetic waves through three primary materials: air, asphalt concrete, and portland cement concrete. To accurately inspect a concrete bridge deck with an asphalt overlay and determine flaw depths, the velocity of electromagnetic propagation in the bridge deck materials must be firmly determined. The velocity with which an electromagnetic wave propagates through a medium, V , is related to the speed of electromagnetic propagation in a vacuum, c , and the material's relative dielectric constant, ϵ_r . This relationship is given by Equation 2.16.

$$V = \frac{c}{\sqrt{\epsilon_r}} \quad (2.16)$$

Equation 2.16 shows that the velocity of propagation, V , is on the order of the speed of electromagnetic propagation in a vacuum (the speed of light, 3×10^8 meters/second). To accurately determine the depth at which a microwave is being reflected, D , an accurate estimation of the relative dielectric constant, ϵ_r , and the two-way time, t , of the radar pulse is required. Equation 2.17 shows the relationship.

$$D = \frac{Vt}{2} = \frac{ct}{2\sqrt{\epsilon_r}} \quad (2.17)$$

Table 2.1 shows relative dielectric constants, ϵ_r , for air, water, and concrete as well as reflection coefficients, R , for the interfaces between the three materials. Note that the signs of the reflection coefficients, R , can be either positive or negative corresponding to the polarity of the reflected signal.

Table 2.1 Relative dielectric constants, ϵ_r , and reflection coefficients, R , of the three primary materials found in bridge decks^{33,34,44}.

Materials	Relative Dielectric Constant, ϵ_r	Interface	Reflection Coefficient, R
Air	1	Air/Asphalt	-0.3
Asphalt	3-4	Asphalt/Concrete	-0.2 to 0.3
Concrete	8-12	Concrete/Air	+0.5 to +0.6
Water	81		

Figure 2.7 shows a schematic diagram of a ground penetrating radar inspection system. The initial impulse, I , is sent from the antenna and directed into the bridge deck. When the electromagnetic impulse reaches the surface of the asphalt, the dielectric boundary partially reflects some of the energy and partially transmits some of the energy according to Equation 2.15. Because the relative dielectric constant of air is less than that of asphalt, the reflected electromagnetic wave, R_1 , will have a polarity opposite of the original incident wave. As the transmitted portion of the incident wave proceeds through the depth of the pavement, it encounters another dielectric boundary between the asphalt overlay and the concrete bridge deck. Again, a portion of the energy is reflected, R_2 , and a portion is transmitted. The reflected wave may or may not have an opposite polarization due to the variability in the dielectric properties of asphalt concrete and portland cement concrete. When the original incident wave reaches an air filled flaw, the reflected wave, R_3 , will have the same polarization as the incident wave because the dielectric constant of concrete is greater than the dielectric constant of air. As the electromagnetic pulse reaches the bottom of the concrete, a final reflection, R_4 , is generated. Again, the polarity will be the same due to the concrete/air dielectric interface.

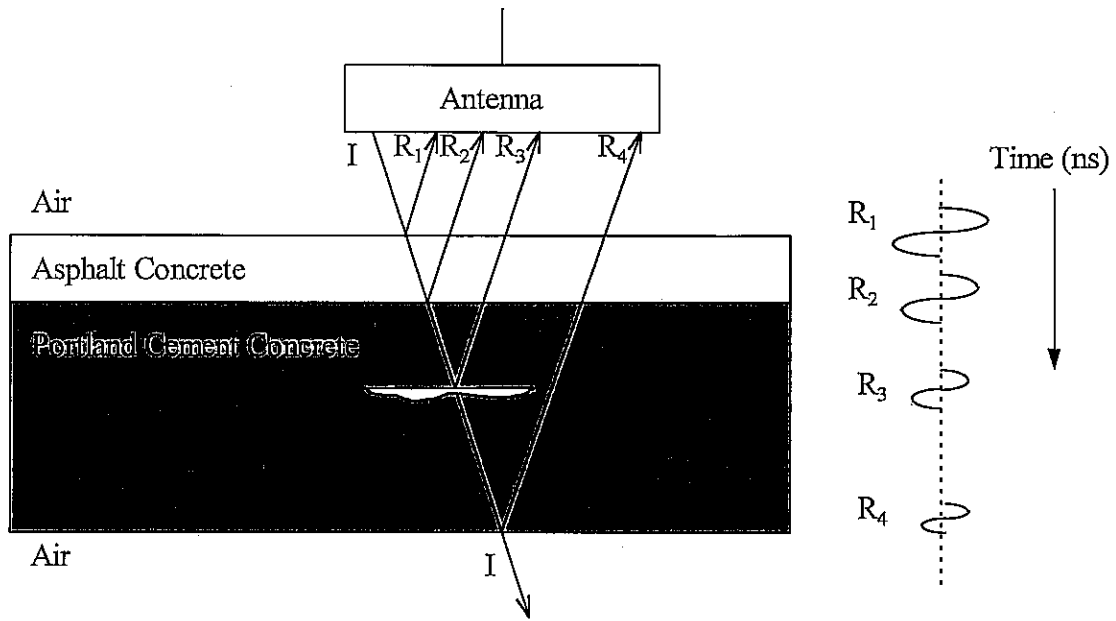


Figure 2.7 Transmission and reflection of radar pulses through a bridge deck³³.

Along the right side of Figure 2.7 is the reflected pulse train seen by the antenna. This waveform is seen by the antenna and recorded during inspection. Each of the four dielectric boundaries produces a reflection. A reflected pulse is recorded between the arrival of the asphalt/concrete reflection and the bottom concrete/air reflection where flaws are located. Typical data analysis of ground penetrating radar signals involves displaying the multiple pulse trains acquired along the length of the bridge deck next to each other. Flaws are located by observing reflections between the asphalt/concrete reflections and the bottom concrete/air reflections. If a reflection is observed between these two dielectric boundaries, it may be a flaw.

2.3 Theory of Infrared Thermography

This section presents a concise description of the theory behind the infrared thermography inspection method. For a more detailed mathematical development of this theory, consult the references at the end of this report⁵⁴⁻⁷³. Much of this discussion follows from Maldague⁵⁷ and is credited as such.

2.3.1 Principles of Infrared Radiation

The guiding principle behind infrared thermography is the electromagnetic radiation emitted by an emissive body. All bodies at a given temperature, T , radiate a spectrum of electromagnetic radiation. The standard by which all bodies are measured is called the black body. The ideal black body absorbs all incident radiation at all wavelengths and emits this radiation uniformly in all directions. Planck's Law describes this spectrum, and is represented by Equation 2.18. The spectral radiance, $N_{\lambda,b}$, of a black body at a given wavelength is a function of the temperature, T , of the body; all other terms are constants.

$$N_{\lambda,b} = \frac{2hc^2}{\lambda^5 e^{\left(\frac{hc}{\lambda T}\right)}} \quad (2.18)$$

Equation 2.18 describes the electromagnetic spectrum radiated by a black body where h is Planck's constant, c is the speed of light, k is Boltzmann's constant, and, λ is the wavelength of interest. As the temperature, T , of a body increases, the spectral radiance increases and the maximum energy wavelength emitted decreases. The maximum energy wavelength is determined by Wien's Law, described by Equation 2.19

$$\lambda_m = \frac{2898}{T} \quad (2.19)$$

Wein's Law relates the temperature of the body, T , in Kelvin to the wavelength of radiation with the highest energy, λ_m , in μm . For example, a body at room temperature of 27°C (300 K) emits its peak radiation at a wavelength of approximately $10\ \mu\text{m}$. A hot piece of steel at 2227°C (2500 K) emits its peak radiation at a wavelength close to $1\ \mu\text{m}$. These wavelengths are out of the visible range of the electromagnetic spectrum, which is approximately between $0.43\ \mu\text{m}$ to $0.69\ \mu\text{m}$, depending on the observer.

Colored bodies do not emit absorbed radiation according to that of an ideal black body. For most bodies, the emissivity, E_m (the ratio of incident radiation to re-emitted radiation) is less than 1 and dependent upon the wavelength, λ , of the radiation of interest and temperature, T , of the body. Therefore, the spectral radiance, N_λ , of a colored body can be expressed as Equation 2.20.

$$N_\lambda = E_m(\lambda, T) N_{\lambda, b}(\lambda, T) \quad (2.20)$$

Equation 2.20 describes the amount of electromagnetic radiation emitted by a body with temperature, T , for the spectrum of wavelengths; therefore, if the spectral radiance and emissivity of a body is known, the temperature can be determined. Suppose now that a camera which detects light in the infrared range of wavelengths takes a picture of a hot body. That picture would not show color, but temperature at each point of that body. Infrared bridge deck inspection is performed in this manner.

2.3.2 Infrared Radiation and Bridge Decks

The infrared thermographic inspection of bridge decks uses the principles of electromagnetic absorption and radiation, and heat transfer to ascertain the presence of voids in a portland cement concrete bridge deck overlaid with asphalt concrete. Figure 2.8 is a schematic representation of the phenomena involved in infrared thermography.

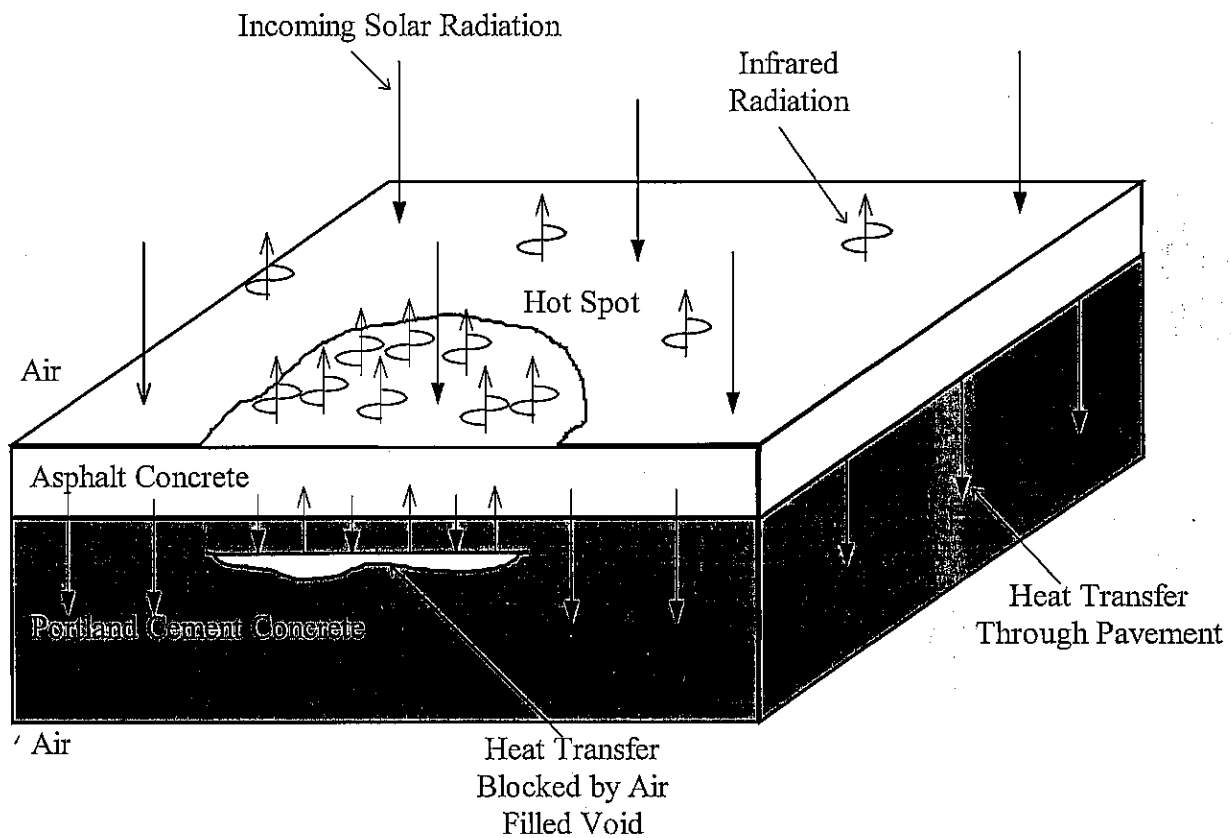


Figure 2.8 Schematic diagram showing formation of a hot spot in overlaid bridge deck.

First, solar radiation penetrates the Earth's atmosphere and strikes the asphalt overlaid surface of the bridge deck. Some of the energy of the incident radiation is absorbed by the asphalt and some is reflected according to Equation 2.20. The absorbed radiation excites the atoms in the overlay and increases its temperature. The heat transfer of the energy from the

surface into the depth, D , at time, t , of the pavement is governed by the one-dimensional Fourier diffusion equation, Equation 2.21.

$$\frac{\partial^2}{\partial D^2} T(D,t) = \frac{\rho C_h}{K} \frac{\partial T(D,t)}{\partial t} \quad (2.21)$$

The density, ρ , thermal conductivity, K , and specific heat, C_h , are the material properties which determine the rate of heat transfer within the pavement layers. As heat proceeds through the depth of the pavement, a thermal gradient is established; the top of the pavement is “warm” and the bottom of the pavement is “cool”. If there is an air void at any location within the pavement, the heat transfer from the surface of the pavement to its depths is interrupted. Air is a good insulator of heat. The air in a void insulates the pavement above the void from the pavement below the void, isolating the above pavement. A buildup of heat energy occurs. An area of relatively higher temperature, compared to the surrounding pavement, forms above the air void. At the pavement surface, this void manifests itself as a hot spot compared to the surrounding pavement surface. This hot spot emits more radiation in the infrared spectrum than the surrounding pavement and can be detected with an infrared camera.

For the formation of a hot spot to occur, a thermal gradient must be established through the thickness of the pavement. If no thermal gradient is established and the pavement is uniformly heated through its thickness, no heat transfer occurs and the air void has no visible surface effect. Figure 2.9 shows temperature curves for the bridge deck over the course of a day. There is a fairly consistent gap between the temperature of solid concrete and the temperature within an air filled void. It is this temperature differential, manifesting itself on the surface of a pavement, that provides the basis for infrared thermography of bridge decks. This temperature

differential can be so little as to be undetectable, or as great as 2 °C, depending upon the size and depth of the void. Note that absolute temperatures are irrelevant; only the relative temperature between the delaminated concrete and the sound concrete is relevant.

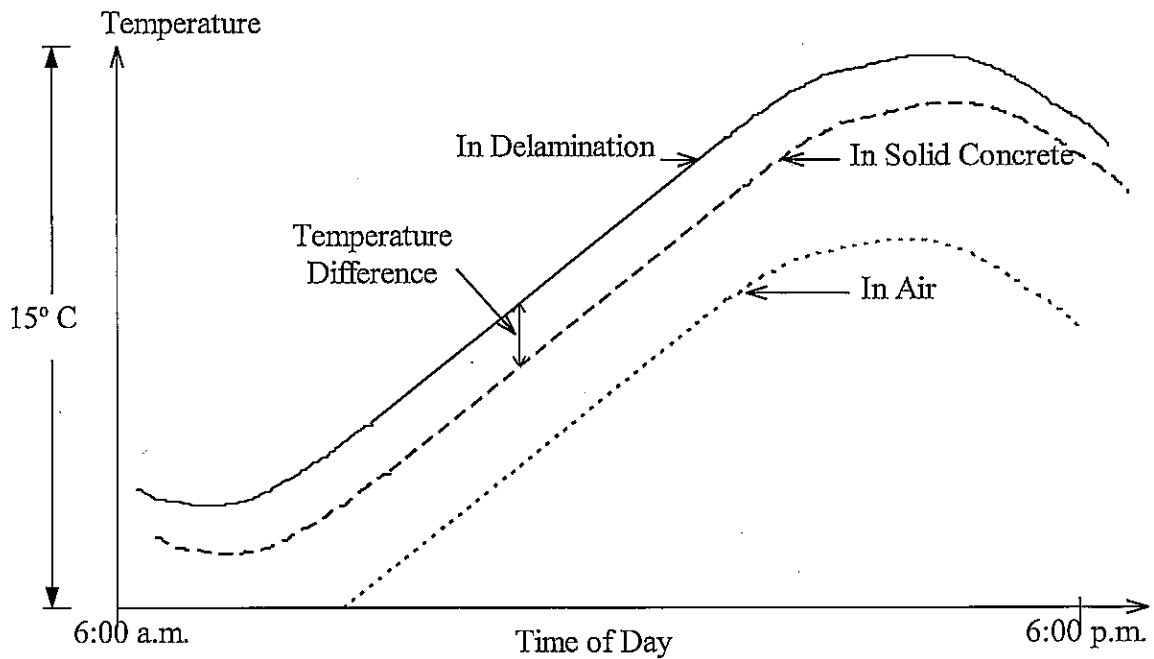


Figure 2.9 Relationship between temperature of air, solid concrete, and delaminations to time of day^{55,56}.

An important consideration of the infrared thermographic inspection technique is the effect that flaw size and flaw depth have on the ability to detect an air filled void. As flaw size decreases, the heat transfer rate approaches that of the rest of the pavement, and the temperature contrast at the surface decreases. An empirical rule states that the diameter of the smallest detectable flaw should be greater than four times its depth⁵⁷ as shown in Equation 2.22

$$d_{small} \geq 4D \quad (2.22)$$

For example, if a delamination in a bridge deck is 6 inches (152.4 mm) deep, the diameter of the flaw must be at least 24 inches (610 mm) wide to be detectable. Another useful relationship is that the loss of contrast, C , on the surface of the pavement is inversely proportional to the cube of the depth, D , of the air filled void, Equation 2.23.

$$C \propto \frac{1}{D^3} \quad (2.23)$$

Equation 2.23 shows the dramatic loss of contrast with an increase in depth. An air filled void at a depth of 6 inches (152.4 mm) will have 1/8 the contrast of an equal sized void at a depth of 3 inches (76.2 mm). Most newer infrared cameras have a temperature resolution of about 0.1 °C. This resolution limit will determine the combination of detectable flaw sizes and flaw depths.

2.4 Theory of Spectral Analysis of Surface Waves

This section presents a concise description of the theory behind the spectral analysis of surface waves inspection method. For a more detailed mathematical development of this theory, consult the references cited at the end of this report⁷⁴⁻⁸⁶. Much of this discussion follows from S. Nazarian and K. Stokoe⁷⁴⁻⁸³ and is credited as such.

The spectral analysis of surface waves (SASW) method is used to determine layer properties such as thicknesses, and stiffness profiles of soil deposits and pavement systems. The SASW method makes use of surface waves, also called Rayleigh waves or R-waves, to inspect the depth of the pavement. It is not intended to be a method for flaw detection, although the presence of flaws will affect the results of the SASW inspection.

Unlike the longitudinal and shear waves mentioned in Chapter 2.1, surface waves propagate along the surface of the pavement system. Figure 2.10 depicts a schematic diagram of

the test setup for the SASW method. A hammer is used to strike the pavement surface and generate stress waves in the pavement. A broad range of frequencies is generated as well as three main types of stress waves: longitudinal, shear, and surface. Two sensors placed along the pavement surface measure the response of the surface. Because the sensors are placed at a distance from the impact and because the surface wave displacements are very large compared to the longitudinal and shear waves at the surface of the pavement, the measured response is dominated by the surface waves.

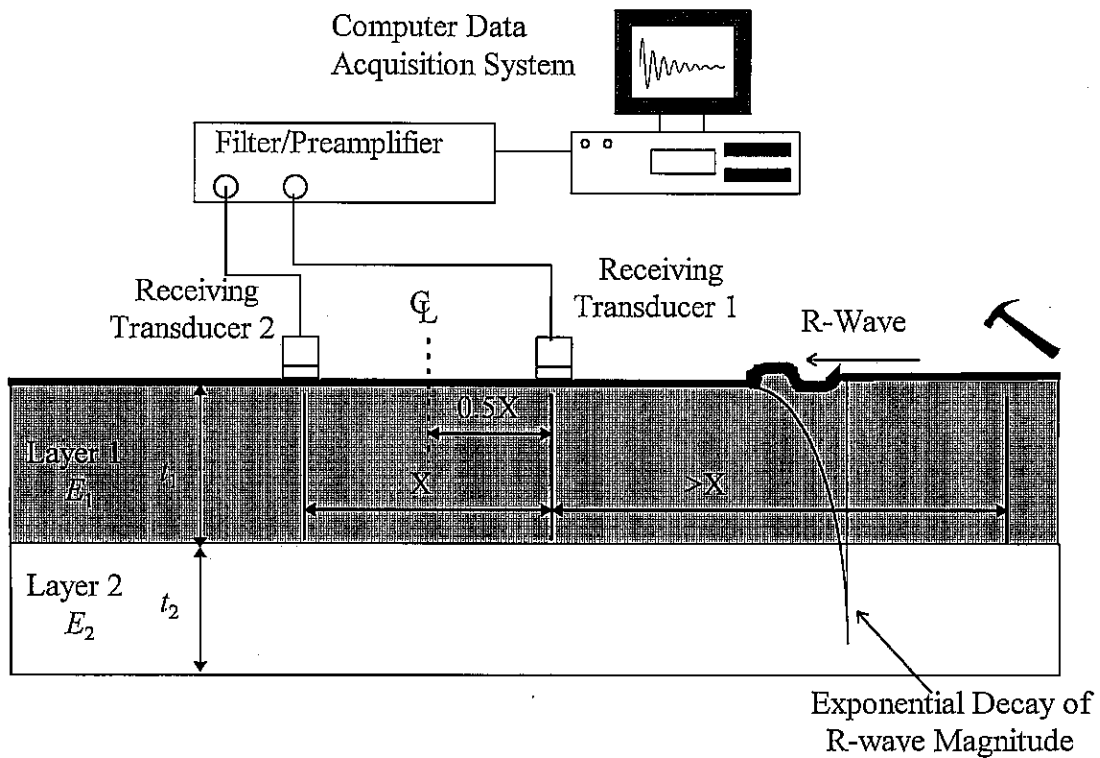


Figure 2.10 Schematic diagram of spectral analysis of surface wave test method.

The magnitude of surface waves decreases exponentially with depth in the pavement. Longer wavelengths penetrate deeper than shorter wavelengths; therefore, the longer wavelengths give information about the deeper layers and shorter wavelengths give information about the surface layer in a pavement system. To adequately inspect the entire pavement system, the impact, or combination of impacts, must contain an adequate range of high and low frequencies. The propagation of the surface waves along the pavement depend upon which pavement layers the waves propagate through. High frequency waves, with short wavelengths, will propagate only through the surface layer of the pavement; thus its propagation will depend upon the properties of the surface layer. Low frequency waves, with long wavelengths, will propagate through the surface layer and deeper layers of the pavement, depending upon wavelength, making its propagation dependent upon the properties of both the surface and deeper layers within the pavement. The velocity with which surface waves propagate depends upon the shear modulus of elasticity and the density of the layers. Therefore, the different frequencies contained within the stress wave pulse generated by the impact will propagate at different velocities depending upon which layers the frequencies travel through. Because the velocity of individual frequency components vary, surface waves are said to be dispersive. The velocities of the stress waves having different wavelengths are referred to as phase velocities.

The phase velocity of each frequency component can be calculated using the response data from the two receivers and some signal processing techniques. The phase data from each transducer is used to determine the time delay between the arrival of a particular frequency at receiver 2 from receiver 1. Once the time delay for each frequency is known, the phase velocities can be calculated because the distance between the two receivers is known. The plot of all phase velocities versus frequency is called a dispersion curve.

2.5 Theory of Chain Drag

The chain drag method of bridge inspection has been used for many decades by field inspectors for quickly determining the size and location of delaminations within a concrete bridge deck. Chain dragging along with other sounding methods, such as hammering with a small hammer or steel rod, is as much an art as a science. The accurate detection of voids in concrete bridge decks is highly dependent upon the skill of the inspector. It is suggested in the ASTM standard⁷³ that the chain drag method not be used on bridge decks with asphalt overlays because the overlay tends to dampen the sound in the deck. Although the method is subjective in nature, there are some simple, fundamental physical principles upon which the method is based:

The chain drag method makes use of the difference in sonic characteristics between solid and delaminated concrete. A typical inspection uses a short length, 1 to 3 feet (0.30 to 0.91 m), of medium weight iron chain attached to a handle. The length of chain is dragged across the bridge deck and the resulting sound produced by the concrete is evaluated by the operator, making the inspection operator dependent. The delaminated concrete produces a different sound than the surrounding solid concrete. The sonic differences between the quality and damaged concrete is a result of the dynamic vibrations induced in the concrete by the chain. Figure 2.11 illustrates the chain drag principle. Figure 2.12 shows a schematic diagram of a typical debond between the asphalt overlay and the concrete deck leading to false readings.

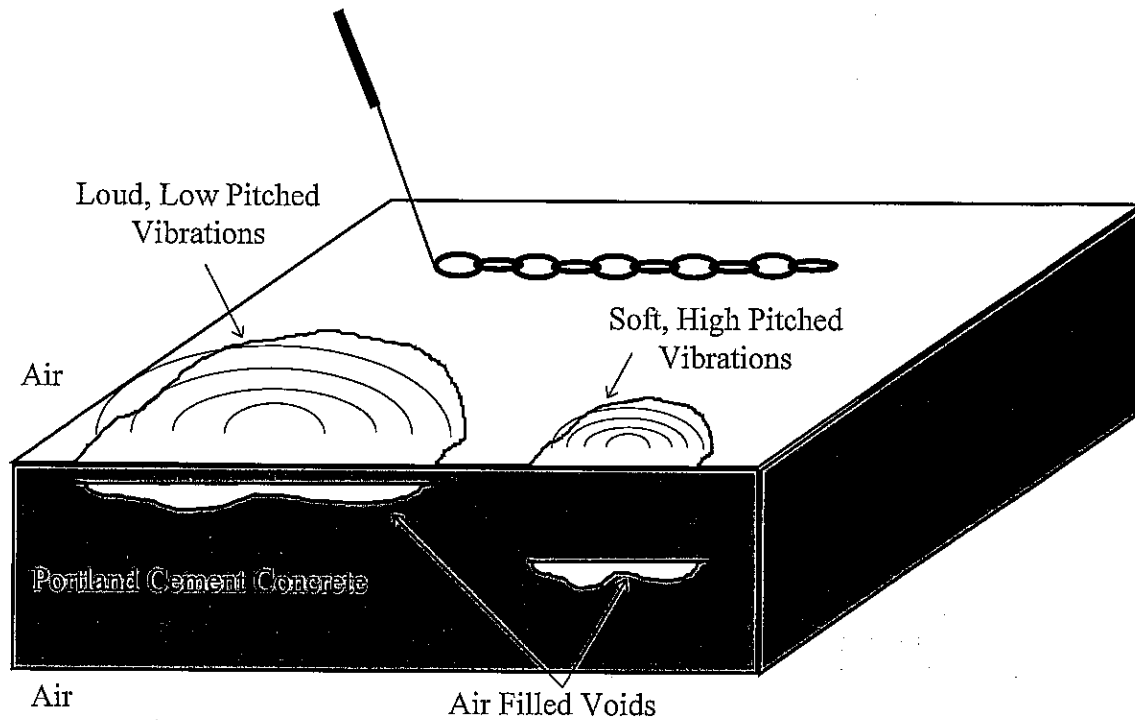


Figure 2.11 Illustration of the chain drag principle.

When the chain is dragged across a delaminated region, flexural waves are excited in the loose concrete above the flaw. Flexural waves are the bending vibrations induced in large, thin plate-like structures. The concrete above the void acts like a large speaker sending out vibrations at its fundamental frequency. There are two primary factors which determine the type of sound heard from the pavement, flaw size and flaw depth. As the flaw size increases, the frequency of vibration will decrease. A decrease in flaw size will increase the frequency. Larger flaws produce larger amplitude vibrations; they are louder and easier to detect. The depth of the flaw will also effect the frequency. A shallow flaw will have a lower frequency and a deeper flaw will have a higher frequency. Shallow flaws produce larger vibrations and deeper flaws produce smaller vibrations. The combination of flaw size and flaw depth will therefore determine the

vibration magnitude and frequency. The range of human hearing is roughly between 20 Hz and 20 KHz. While the lower end of the range is not often encountered in the field, the high frequencies of small, deep flaws combined with their soft sound is a definite limiting factor in detecting flaws using chain dragging. Generally, errors associated with chain dragging do not consist of falsely reporting delaminations which do not exist; rather, the errors usually consist of not detecting small, deep flaws which do exist. Therefore, the chain drag method is more accurate with large, shallow flaws than with small, deep flaws.

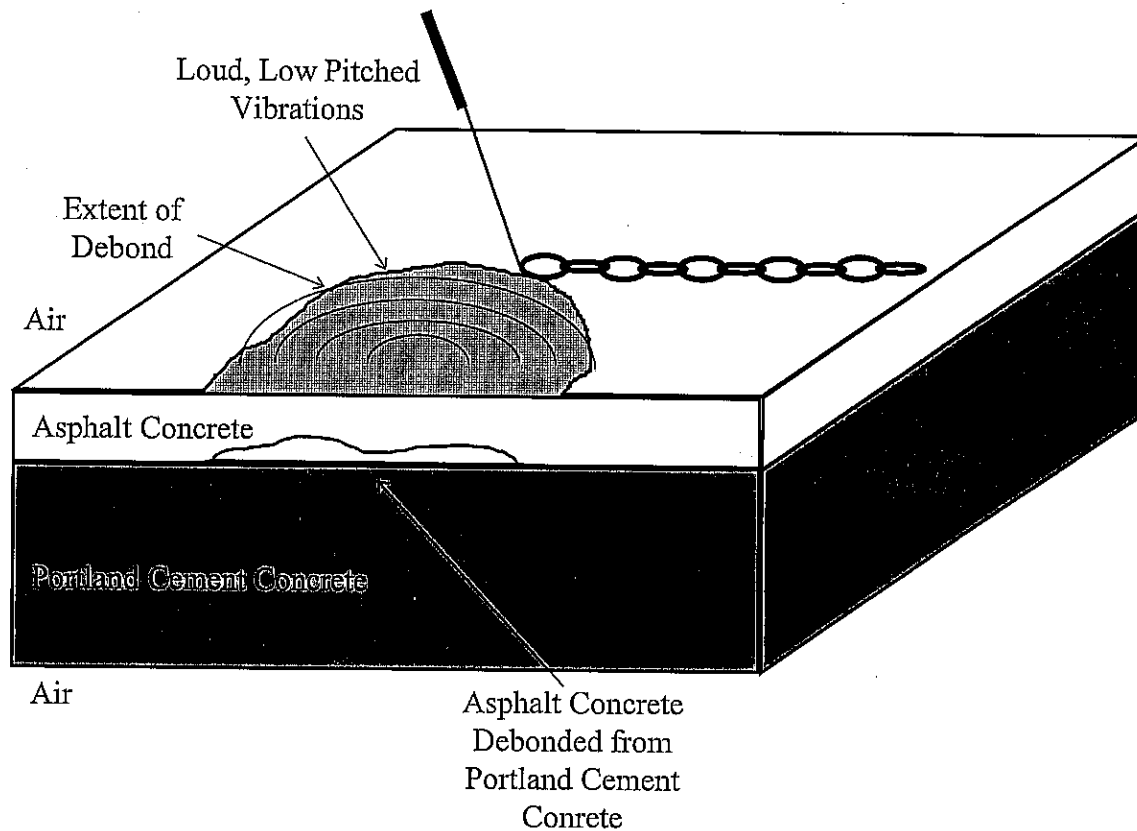


Figure 2.12 Schematic diagram a typical debond leading to false readings during chain drag.

3.0 NONDESTRUCTIVE FIELD INSPECTION OF BRIDGES

The purpose of this chapter is to provide a description of the nondestructive field inspection of the nine bridges which occurred during the summer of 1997. The chapter focuses on the individual testing methods and provides insight into field advantages and disadvantages which became evident during the field testing. The majority of information contained within this chapter was obtained from three sources: observation and participation in the testing, discussions with the testing personnel, and the final reports issued by the testing companies. The opinions expressed in this section are solely those of the author.

3.1 Impact-Echo Field Inspection

This section details the nondestructive inspection of the Marion, Illinois bridge by Olson Engineering. Participating in the inspection were Mr. Larry Olson of Olson Engineering, Mr. Amin Habboub of the University of Illinois, and Mr. Matt Baright of the University of Illinois. Due to the high cost of inspection and time consuming nature of the impact-echo method, only one bridge was chosen for inspection by this method. The bridge chosen was in Marion, Illinois, Structure Number 100-0005.

3.1.1 Impact-Echo Field Inspection Equipment

The impact-echo inspection of the bridge decks was performed with a manual, broom-like testing apparatus, Figure 3.1 and Figure 3.2. The testing apparatus was a prototype model designed and built by Olson Engineering. The apparatus consisted of four rolling transducers mounted along an aluminum shaft evenly spaced approximately 1 foot (0.30 m) apart. Small

solenoids were mounted directly behind the rolling transducers to provide the impact source. A vertical aluminum handle was used to push the rolling transducers along the surface of the pavement. A distance wheel was also mounted along the shaft to provide distance measurements, Figure 3.3. The entire apparatus was connected to a main computer, housed within a van, via a 100 foot (30.5 m) long cable. The computer controlled the triggering of the solenoid impactors, and the collection of the data.

Each rolling transducer consisted of six piezoelectric sensor elements encased in a soft polymer, Figure 3.4 through Figure 3.6. As the transducer rolled, one of the six piezoelectric sensor elements would roll into a parallel position with the pavement. Sensing this occurrence, the computer triggered the solenoid and a waveform was captured and digitized. A check was then performed on the waveform to insure its quality. If the waveform passed the quality check, the next transducer along the aluminum bar would be activated and the process would repeat. If the waveform did not pass the quality test, the computer waited until another sensor element rotated into position, triggered the solenoid, and digitized another waveform.

It is necessary to trigger only one solenoid at a time because the stress wave generated from one solenoid could be received by a different transducer. Good passes with the testing apparatus consisted of solenoids being fired in rapid succession down the aluminum shaft. Poor data collection passes consisted of multiple firings of one solenoid since the data did not pass the quality check. During good data collection passes, a waveform was digitized and collected approximately once every 3 inches (76.2 mm).

The transducers were coupled to the pavement surface with water. A thin jet of water was shot down onto the pavement surface immediately ahead of the approaching transducer. The water insured adequate contact between the transducers and pavement surface.



Figure 3.1 Use of the impact-echo testing apparatus.

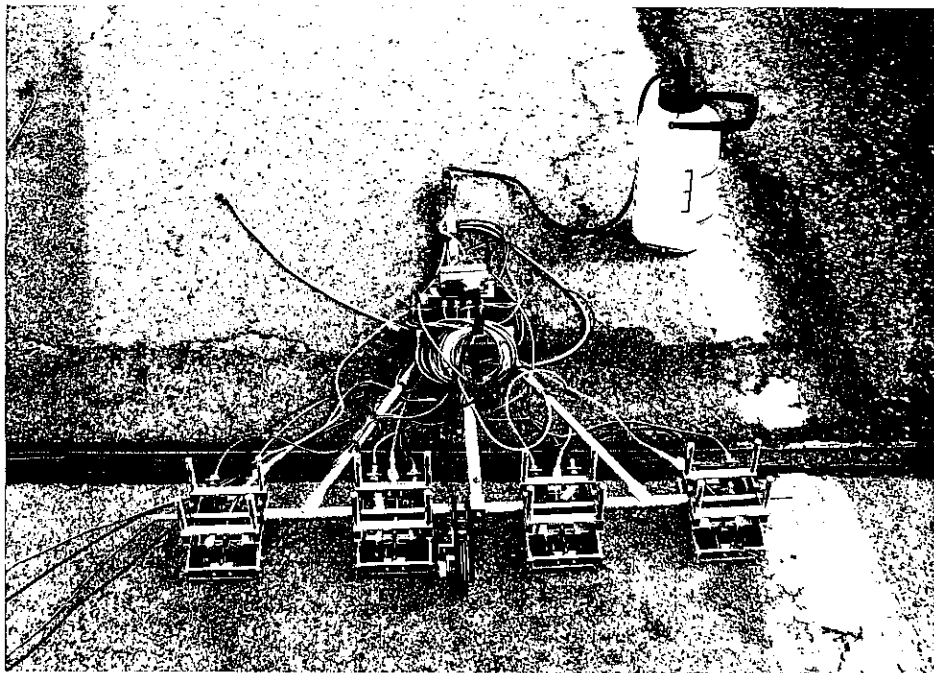


Figure 3.2 Closeup of the impact-echo testing apparatus.

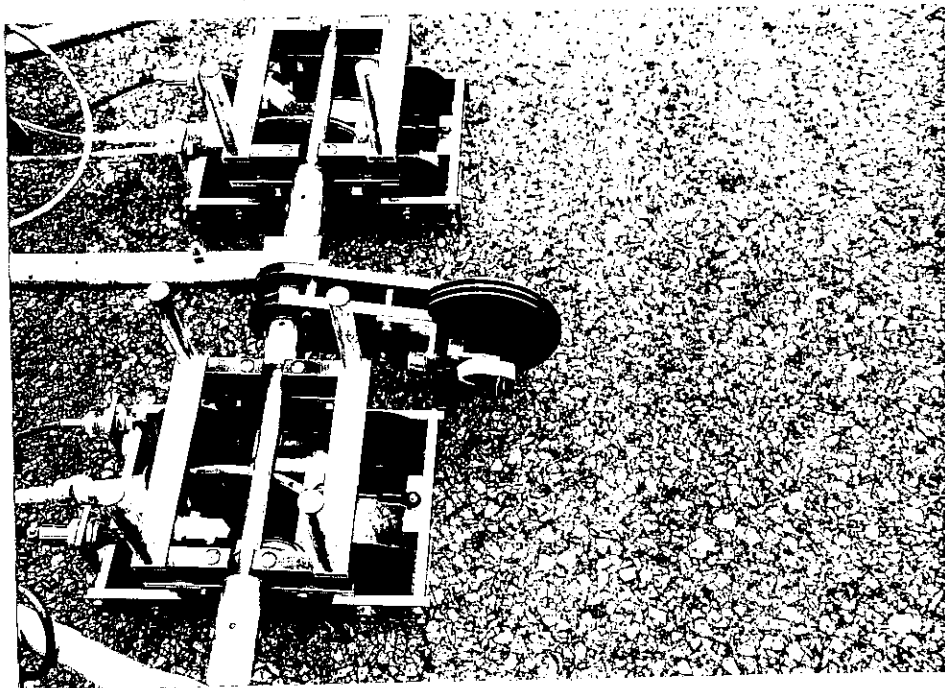


Figure 3.3 Front of the impact-echo testing apparatus showing distance wheel mounted ahead of transducer carts.

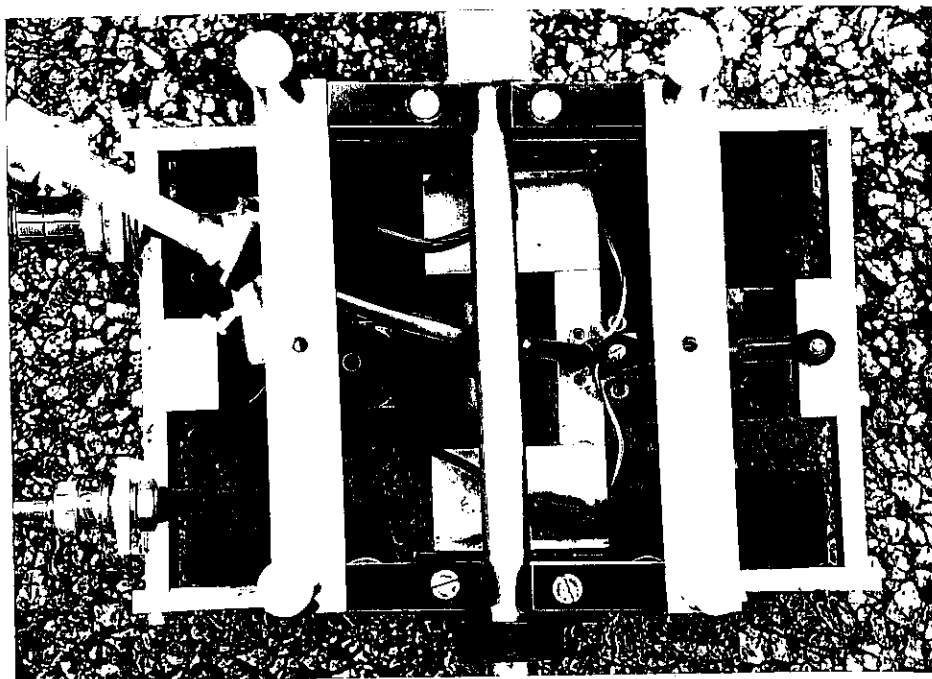


Figure 3.4 Top view of a transducer cart with the rolling transducer mounted in the center.

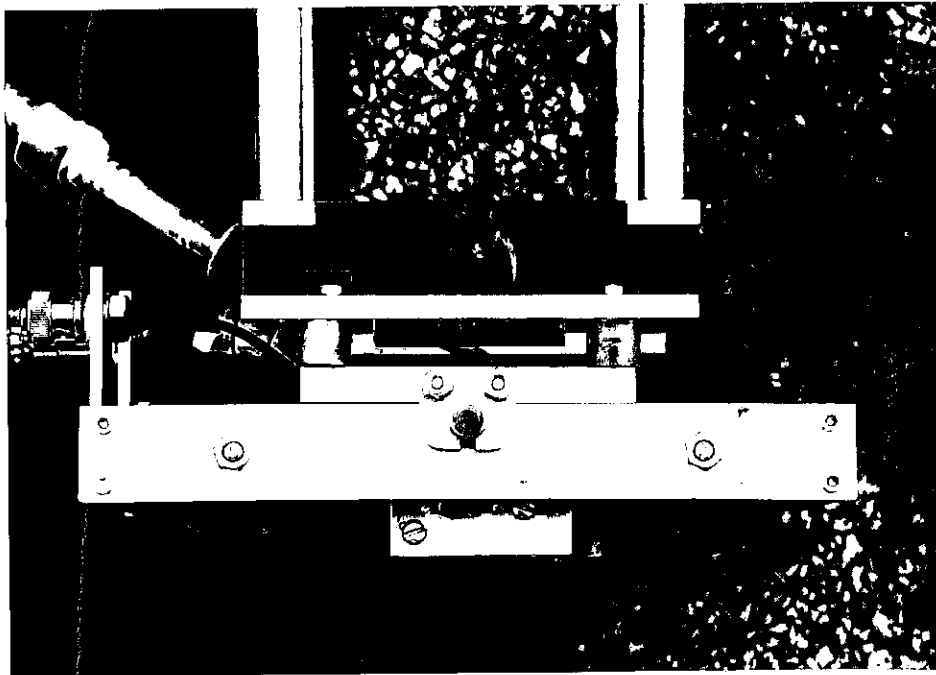


Figure 3.5 Side view of a transducer cart with the rolling emerging from the bottom.

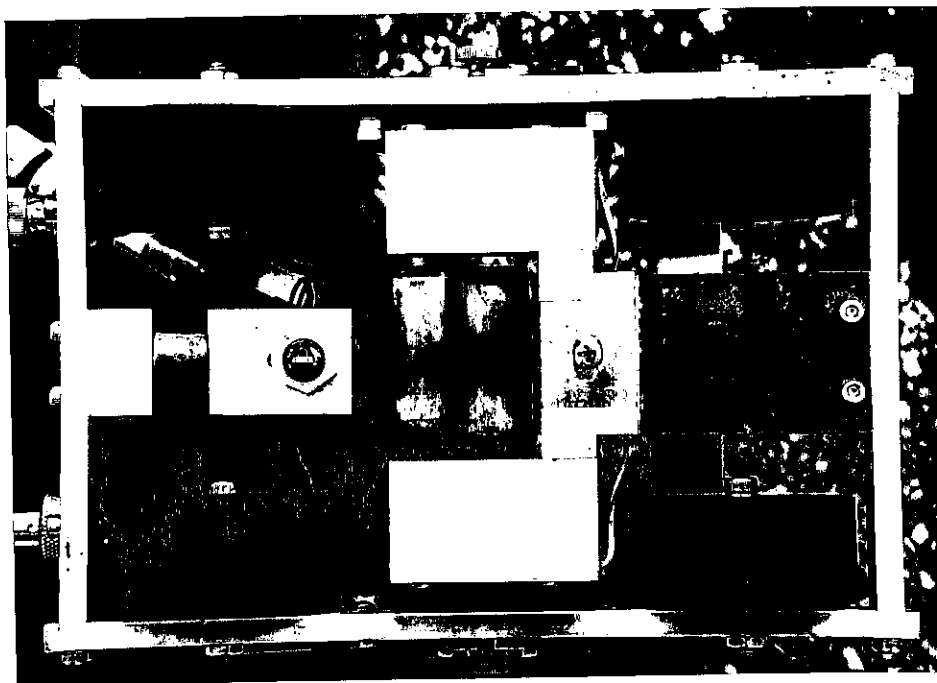


Figure 3.6 Bottom view of a transducer cart with the rolling transducer mounted in the center.

3.1.2 Impact-Echo Field Inspection Testing Method

The testing procedure required two persons, one to push the testing apparatus down the pavement, and another to operate the computer equipment in the van. Testing of the pavement was relatively slow, with speeds no greater than one foot per second (0.30 m/s). Preliminary testing was performed to judge the maximum possible speed the broom apparatus could be pushed without sacrificing data quality. Three passes were required for each lane as the testing apparatus covered only 4 horizontal feet (1.22 m). Although the testing was tedious, the operation of the equipment was not difficult. Total testing time for the Marion bridge was approximately one and a half days. As the equipment was experimental in nature, problems occasionally surfaced which required a testing pass be redone. One problem was minute particulate matter within the water supply clogging the water jets. This required the jets to be disassembled, cleaned, and reassembled—a 15 to 30 minute process. Another problem was navigating the small diameter transducer wheels over cracks or rocks greater than approximately 1 inch (25.4 mm) high.

3.1.3 Impact-Echo Hand Held Testing Equipment

Besides the automated testing equipment described in Section 3.1.1, Larry Olson also brought a hand held testing unit to the bridge deck, Figure 3.7 through Figure 3.9. This unit was used for spot checking the deck at locations of interest. The unit was completely operated by one person. A cable attached the testing unit to the main computer located in the testing van. The sensing transducer was coupled to the pavement by a silicone mat and water if needed. A solenoid similar to those on the automated testing apparatus was mounted behind the transducer

to provide the impact. The unit was triggered by a button pressed with the index finger; the data was collected automatically via computer. Real time feedback by the computer provided data quality checks and results.

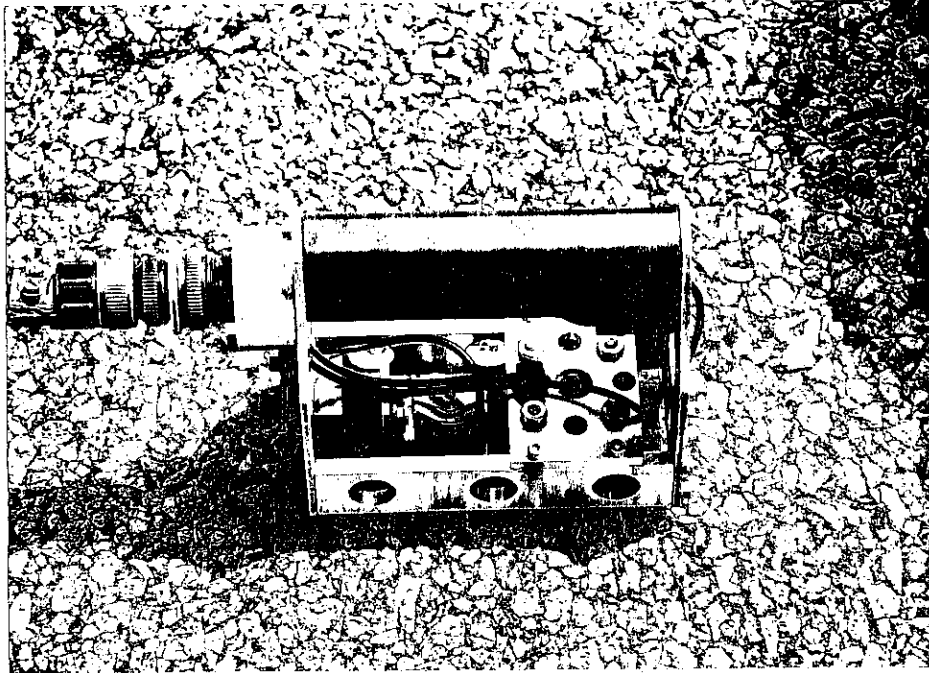


Figure 3.7 Hand held impact-echo testing apparatus.

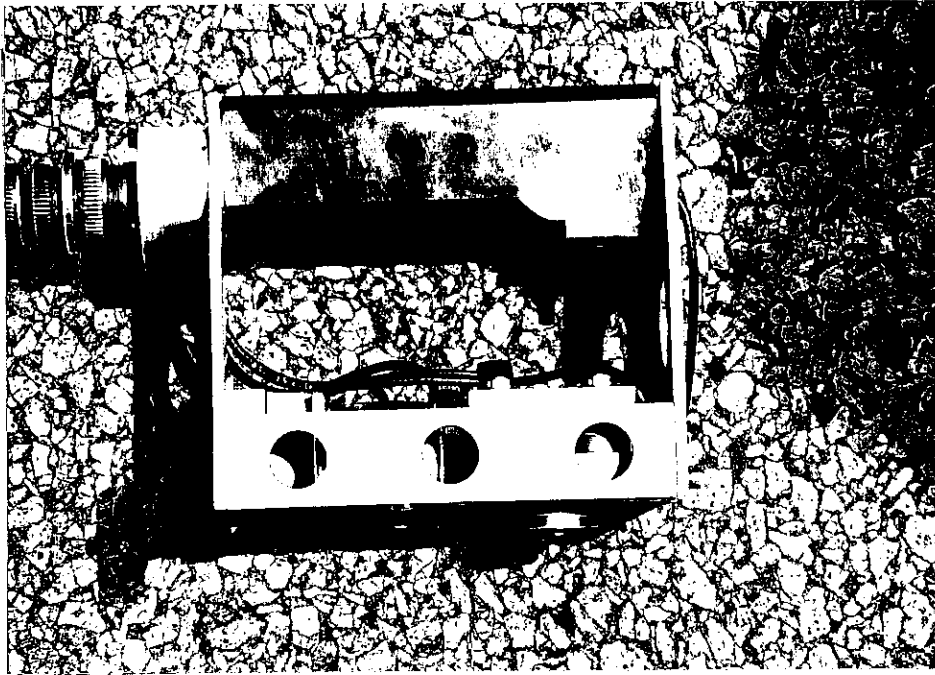


Figure 3.8 Hand held impact-echo testing apparatus showing transducer pad at bottom.

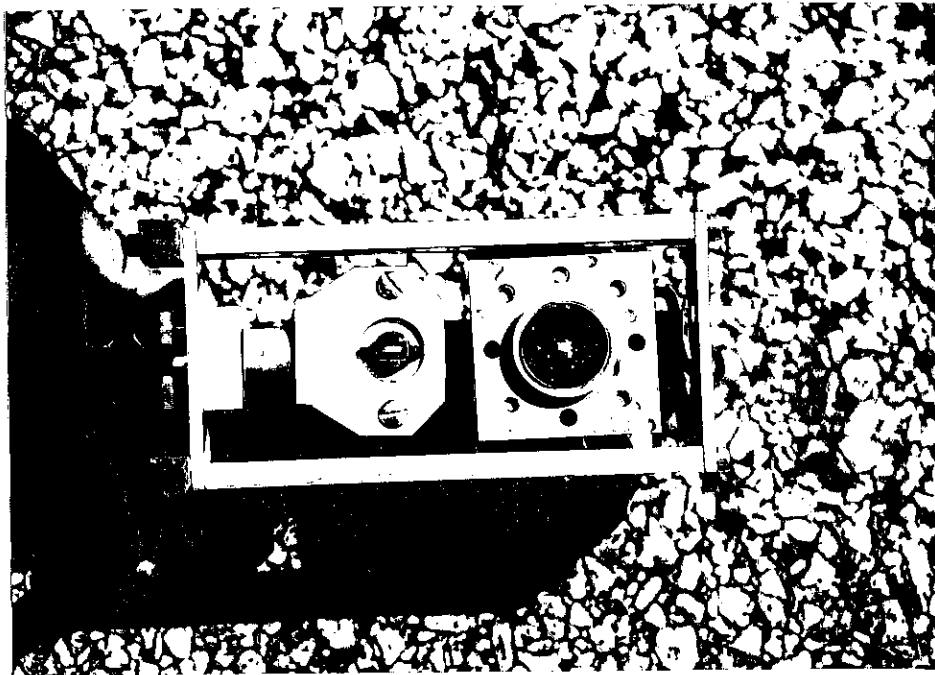


Figure 3.9 Hand held impact-echo testing apparatus showing transducer pad at right and solenoid impactor at left.

3.1.4 Impact-Echo Field Inspection and Debonding vs. Delamination

Impact-Echo testing can theoretically distinguish a debond and a delamination. Because the depth of the returning echo is determined by the main frequency, it becomes easy to distinguish the depth of the detected flaw. If the flaw depth coincides with the depth of the asphalt overlay, the flaw is a debond. If the flaw depth is deeper than the asphalt overlay, the flaw is located in the concrete deck. A fully debonded portion of the pavement prevents inspection of the underlying concrete, as the stress wave is fully reflected back into the asphalt.

One complication arises in the determination of flaw type. The dominant vibration mode in a debonded area is commonly flexural vibration, not the echo off of the bottom of the asphalt layer. Movement of the entire debonded asphalt region is much like the beating of a drum. The low frequency may be misconstrued for a deep flaw. This low frequency, however, is very often lower than the echo frequency of the entire slab and thus is easily distinguishable. Shallow delaminations also exhibit flexural vibration and are difficult to distinguish from a debond.

3.1.5 Impact-Echo Field Inspection and Test Conditions

Ideal pavement conditions for impact-echo inspection consist of a smooth, homogenous surface free of debris. Testing can be performed at any time during the day, although large swings in temperature may affect depth measurements as the stress wave velocity in asphalt is dependent upon stiffness. Two crucial factors affecting impact-echo data are the coupling between the transducer and the bridge deck, and the quality of the impact. The transducer must be coupled to the deck to receive the wide range of frequencies necessary for adequate inspection, and the impact must be of short duration to generate the high frequencies necessary to

inspect thin pavement layers. The following paragraphs detail the most common surface conditions which may lead to a reduction in data quality.

Large, smooth areas of asphalt patching do not pose a significant problem to impact-echo data quality. Smaller, uneven patches with raised or lowered edges prevent adequate coupling between the transducer and pavement surface. If an asphalt patch is composed of softer material than the surrounding pavement, this will affect the stress wave velocity and the quality of impact. Sometimes asphalt patches are improperly bonded to the underlying pavement, preventing the stress wave from penetrating the depth of the pavement, similar to a debond.

Oil on the bridge deck does not pose a significant problem to impact echo inspection. Provided that the oil is not pooled, preventing an adequate impact, the impact-echo transducers can tolerate some pickup of oil. If the oil builds up on the transducers, they need to be wiped to free debris from clinging to the surface.

All debris should be removed from the bridge deck prior to impact-echo inspection. Debris such as small rocks and sticks prevent free rotation of the transducer wheels and could potentially jam the rollers. A small rock lifts the transducer wheel off of the pavement and destroys coupling. If the impactor hits even a very small rock, adequate frequencies are not excited in the pavement and data is compromised.

Wearing of the asphalt overlay in the tire path actually aids impact-echo inspection by the removal of asphalt binder. This exposes a greater area of aggregate and improves the possibility of a quality impact. In addition, the smooth surface provides good coupling to the transducers.

Rutting of the asphalt overlay may prevent good transducer contact depending on the severity. If the ruts are too deep, the transducers will be separated from the pavement surface as

the transducer cart wheels ride along the depression. This will also affect the impact quality since the impactor is calibrated to deliver an impact at a set distance.

Mild cracking of the asphalt overlay does not pose a significant problem to impact-echo inspection provided that the edges of the cracks are not raised. Severe alligator cracking of the asphalt overlay may prevent adequate transducer contact and impacts.

Crack sealant poses a significant problem to impact-echo inspection. The soft crack sealant absorbs much of the impact energy, particularly on a hot day. If the sealant is too soft, it may adhere to the transducer wheels. Minor crack sealing on the bridge deck is avoidable, but if a significant portion of the bridge deck is covered with cracked sealant, in the case of alligator cracking, accurate impact-echo inspection may be impeded.

Lane markings and other painted surfaces do not affect impact-echo inspection since the area they cover is relatively small. In addition, the paint is generally quite hard and provides a smooth surface for impacting as well as transducer adherence.

Impact-echo inspection is not significantly hampered by most weather conditions, and testing can be performed day or night at any temperature. If depth measurements are taken, the temperature at the time of testing should be accounted for because the stress wave velocity in the material is a function of temperature. Rain aids coupling of the transducer to the surface of the asphalt, though large puddles will impede adequate impacting. Snow and ice on the deck prevent impact-echo inspection.

3.2 Ground Penetrating Radar Field Inspection

This section details the nondestructive ground penetrating radar inspection of the nine bridge decks. Participating in the inspection were Mr. Kevin J. Stephanski of Penetradar

Corporation and his assistant. Mr. Matthew Baright of the University of Illinois observed the testing.

3.2.1 Ground Penetrating Radar Field Inspection Equipment

Inspection of bridge decks with ground penetrating radar was performed with a conversion van in which all of the necessary equipment was mounted. The antennas were mounted on the front of the van, Figure 3.10 through Figure 3.14. The interior of the inspection vehicle contained a workstation for a single operator. A personal computer controlled the majority of data acquisition. A magnetic strip recorder stored the data collected. Control units for each antenna controlled the power output and other characteristics of the antenna system. An oscilloscope was present to allow the operator to monitor each radar signal in real time and verify quality data acquisition. The entire system was powered by an AC inverter powered by the vehicle. The integrated system had all of the data analysis software necessary to perform on site data reduction and generate results. The software had an intuitive windows interface.

There were three horn antennas mounted on the front of the inspection van spaced at approximately 3 foot (0.91 m) intervals. These antennas were designed and built by Penetradar Corporation. They are low power, all solid state, high resolution antennas, covered with foam and rigid epoxy for protection. Mr. Kevin Stephanski said the antennas were state of the art and was reluctant to provide details on their manufacture, as it is proprietary information.

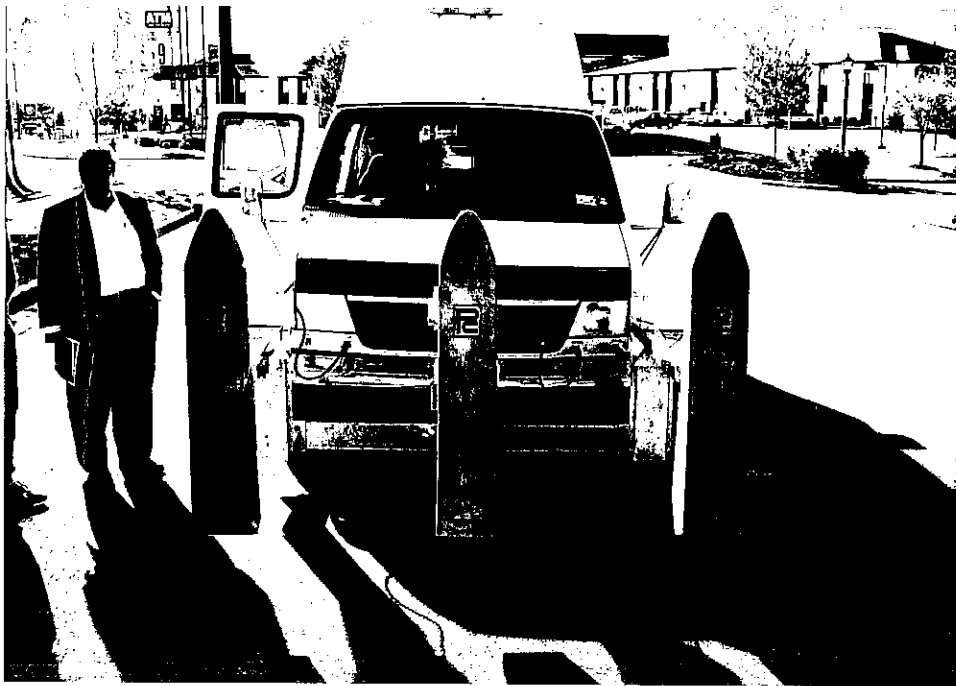


Figure 3.10 Front view of the ground penetrating radar inspection van showing antennas in deployed position.

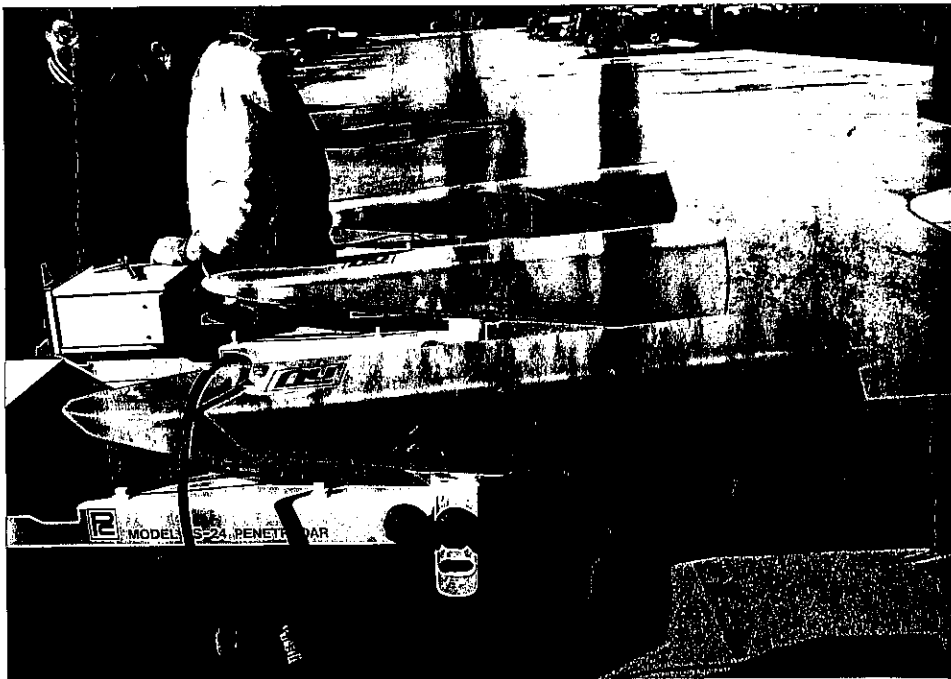


Figure 3.11 Front view of the ground penetrating radar inspection van showing antennas in stowed position.

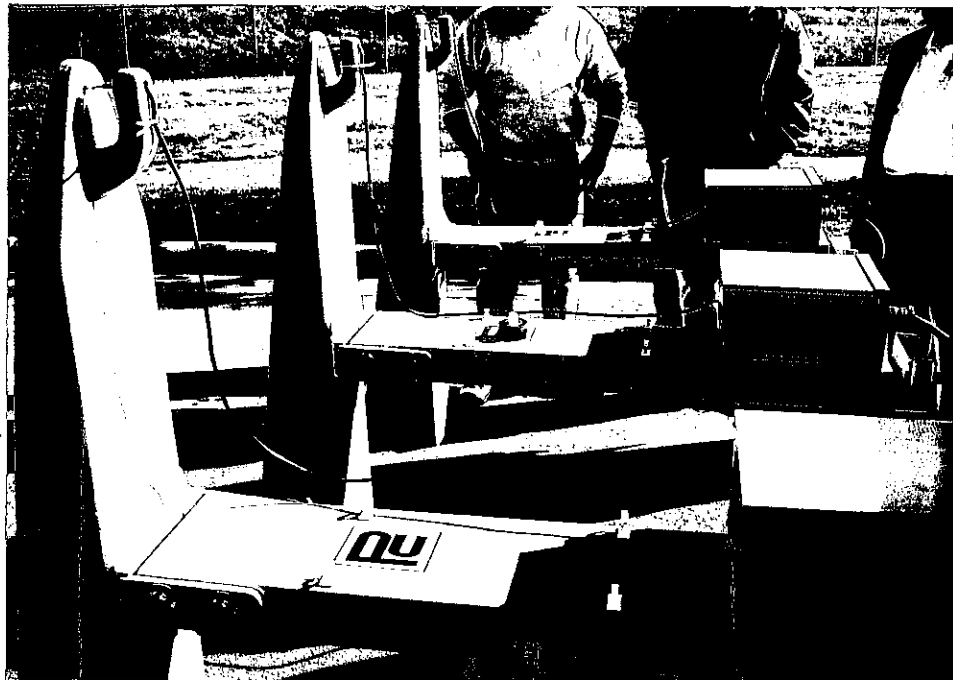


Figure 3.12 Close up of the ground penetrating radar inspection antennas in deployed position.



Figure 3.13 Interior of the ground penetrating radar inspection van showing system power controls and data recorder.

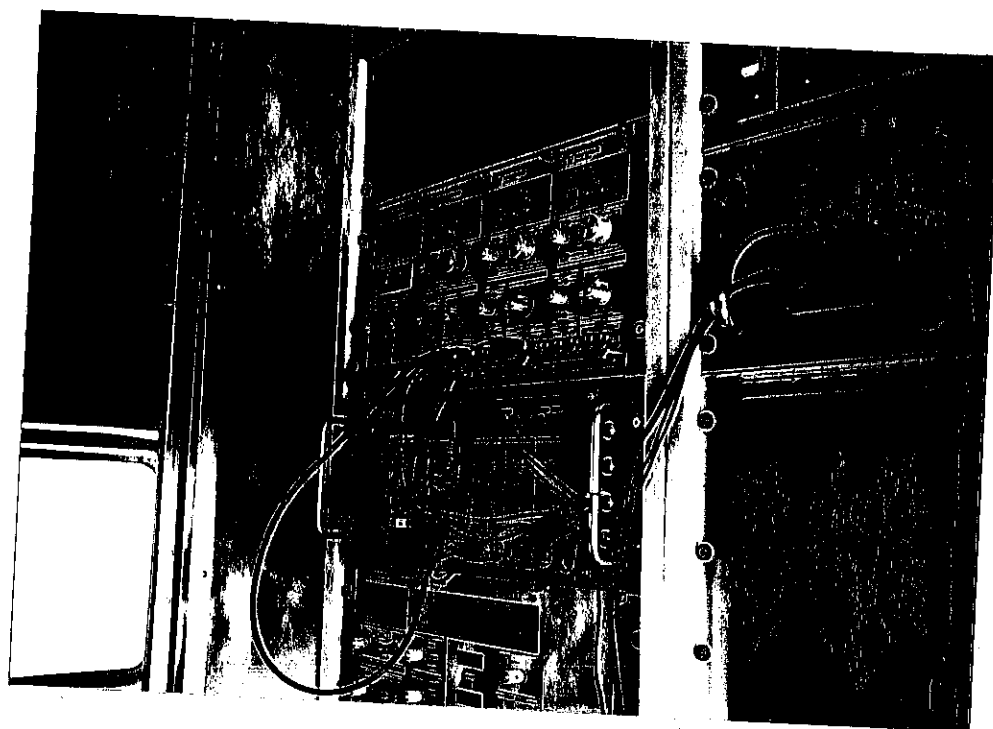


Figure 3.14 Interior of the ground penetrating radar inspection van showing antenna power controls and oscilloscope.

3.2.2 Ground Penetrating Radar Field Inspection Testing Method

The inspection procedure required two persons, one person to operate the radar and data acquisition equipment and the other to drive the van. Prior to testing, calibration of the antennas was performed by pointing them into clear air, and by aiming them at a large metal plate.

Testing of the pavement was performed at approximately 5 miles per hour (8.05 kph). At that speed, longitudinal resolution was one waveform collected every 3 inches (76.2 mm). The spacing of the antennas was approximately three feet (0.91 m) between each antenna. Two passes were required for each lane. The radar inspection was quicker than the other nondestructive tests, able to cover a 300 foot (91.44 m) lane in just a few minutes. To compensate for skewed abutment joints, the testing area was squared off with yellow paint and

data collection began before the abutments. All the operator was required to do was initiate the data collection sequence and monitor the quality of the radar signal on the oscilloscope. The data recorder recorded distance from the drive train of the van.

3.2.3 Ground Penetrating Radar Field Inspection and Debonding vs. Delamination

Ground penetrating radar testing easily distinguishes between a debond and a delamination. Because ground penetrating radar is a full depth inspection method, it is able to determine the depth at which the flaw occurs. If the void is at the surface of the concrete deck, it is a debond. If the radar reflection is deeper, the void is a delamination. The nature of electromagnetic microwaves allows ground penetrating radar to detect delaminations even if they are located under a debonded region. Because of the ability of ground penetrating radar to determine depth, it also distinguishes between delamination and scaling. Delaminations generally occur at or slightly above the reinforcing bar in the concrete deck, caused by the corrosion and subsequent expansion of the reinforcing steel. Scaling typically occurs within the top 1 inch (25.4 mm) of concrete. Its cause is generally attributed to a weak surface layer as a result of poor workmanship or deicing salts. For the purposes of this study, no distinction was made between delamination and scaling.

3.2.4 Ground Penetrating Radar Inspection and Test Conditions

Ideal pavement conditions for ground penetrating radar inspection consist of a dry surface free of debris. Because the testing method is non-contact, ground penetrating radar can be used under a wide variety of testing conditions. Testing can be performed at any time during the day or night; temperature has little effect on the accuracy of the results. The most prevalent

detriment to accurate ground penetrating radar inspection is moisture in the bridge deck.

Microwaves are attenuated by the salts dissolved in water, and the wave velocity of microwaves increases with moisture content in the bridge deck. Too much moisture on or in the bridge deck can distort the radar signal and decrease accuracy. The following paragraphs detail the most common surface conditions that may lead to a reduction in data quality.

Large, smooth areas of asphalt patching do not pose a significant problem to ground penetrating radar data quality. Although the dielectric properties of the asphalt patch may be different than the surrounding asphalt, the radar signal being reflected from the surface of the concrete and points below will not be significantly affected.

Small oil spots on the surface of the bridge deck will not have a significant impact on the quality of radar data. Larger spots and pools of oil may change the dielectric properties of the asphalt layer and increase signal attenuation as well as change wave velocity.

Small rocks and other debris on the deck will have no impact on ground penetrating radar inspection. Furthermore, wearing and rutting of the asphalt overlay does not also affect radar inspection.

Cracking of the asphalt overlay in and of itself poses little problems to ground penetrating radar inspection. But areas of cracked overlay are prone to moisture accumulation. The moisture accumulated below the overlay in cracks and debonds will have a significant impact on inspection of the underlying concrete.

Small areas of crack sealant do not significantly hamper radar inspection of the deck. If large areas of the deck are covered, particularly if the sealant is thickly applied, the dielectric properties of the asphalt layer may be changed.

Lane markings and other painted surfaces do not affect ground penetrating radar inspection since the area they cover is relatively small. In addition, the paint is usually thin and does not significantly alter dielectric properties.

To summarize, most weather conditions do not significantly hamper ground penetrating radar inspection. Testing can be performed day or night and at any temperature. The one exception is the presence of moisture in or on the bridge deck. All testing must be stopped during rain or while the surface of the deck is wet. A period of drying after rain should be allowed before inspection resumes. Moisture will increase the attenuation in the radar signal and increase propagation velocity thereby distorting depth measurements.

3.3 Infrared Thermography Field Inspection

This section details the nondestructive testing of the bridge decks using infrared thermography. Participating in the inspection were Mr. Timothy J. Crowley of RUST Environment & Infrastructure and Mr. Matthew D. Baright of the University of Illinois.

3.3.1 Infrared Thermography Field Inspection Equipment

The infrared thermography inspection of the bridge decks was performed with a conversion van in which all of the necessary equipment was mounted, Figure 3.14. The infrared camera was a late model Inframetrics system. The newer camera model used a solid state cooling system rather than the liquid nitrogen systems of earlier models. The infrared system had a temperature resolution of 0.1 degrees Celsius. The control box had many features which aided the user. Frame averaging of two or four frames was often used during the inspection to "smooth" the image and filter out grainy noise. Crosshairs were also used to compare the

temperatures at particular pixel locations. This feature was useful in determining if a sufficient temperature gradient existed for an area to be considered defective. The emissivity of the material could also be input into the system so that accurate temperatures would be displayed. For the entirety of the testing, an emissivity of 1.0 was used, which may have been slightly high for asphalt and concrete. This does not adversely effect the testing result because temperature differentials are the focus of the testing, not absolute temperatures.

The infrared camera and a visual camera were mounted side by side in an aluminum box and hoisted approximately 20 feet (6.10 m) above the surface of the pavement atop a pneumatic telescoping boom, Figure 3.15 and Figure 3.16. The boom was mounted in the center of the front bumper of the van and powered by a small air compressor in the rear of the van. Air flow controls mounted on the dashboard allowed the driver to control the height of the boom. Two steel cables tied to the top of the boom and the hood of the van were used to stabilize the boom during operation. Control and data cables ran from the two cameras into the back of the van through a porthole in the top of the van.

The operation of the thermographic imaging van requires two people, one person to drive the van and another in the back operating the data acquisition equipment. The data acquisition equipment consisted of two monitors (one per camera), two Video Cassette Recorders (VCRs), and two linear location devices, Figure 3.17. It is essential in thermographic inspection that a visual surface record be taken in addition to the infrared image. There are several surface conditions which will distort the infrared image making accurate interpretation nearly impossible. These conditions will be described later. During the inspection of the bridge deck, both VCRs were running in slow play mode to record both camera images. The position in feet was continuously updated on both screens by linear location devices. These devices measured

the distance the van traveled by recording the revolutions directly from the drive shaft of the van.

All equipment was powered by a portable gas generator mounted in the rear of the van.

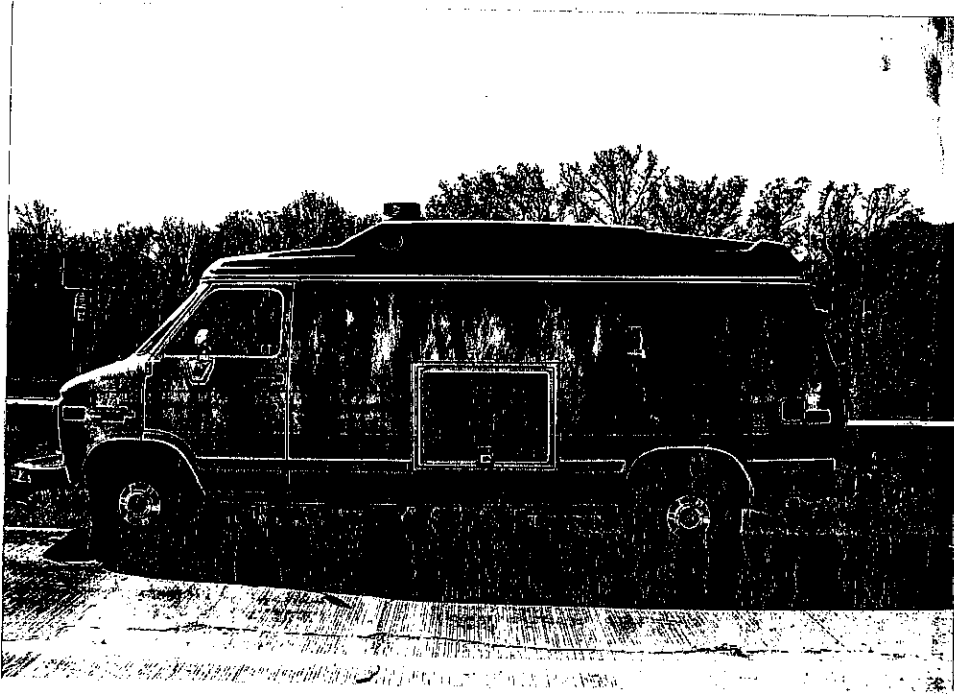


Figure 3.15 The infrared inspection van with camera mount on front of van in stowed position.

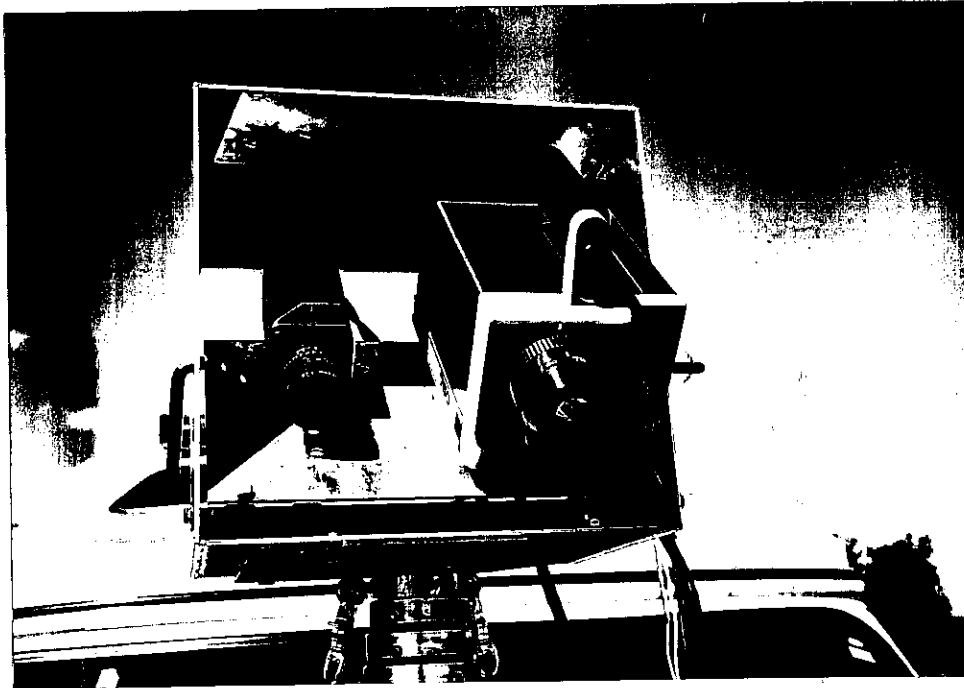


Figure 3.16 The camera mount with infrared camera at right and visual camera at left.

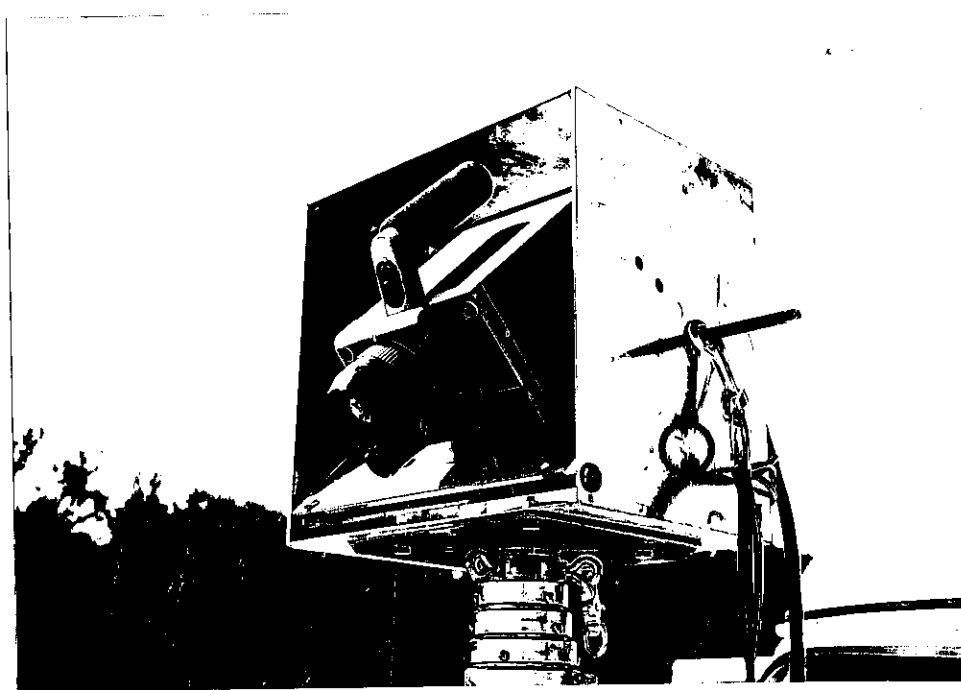


Figure 3.17 Side view of camera mount with infrared camera.

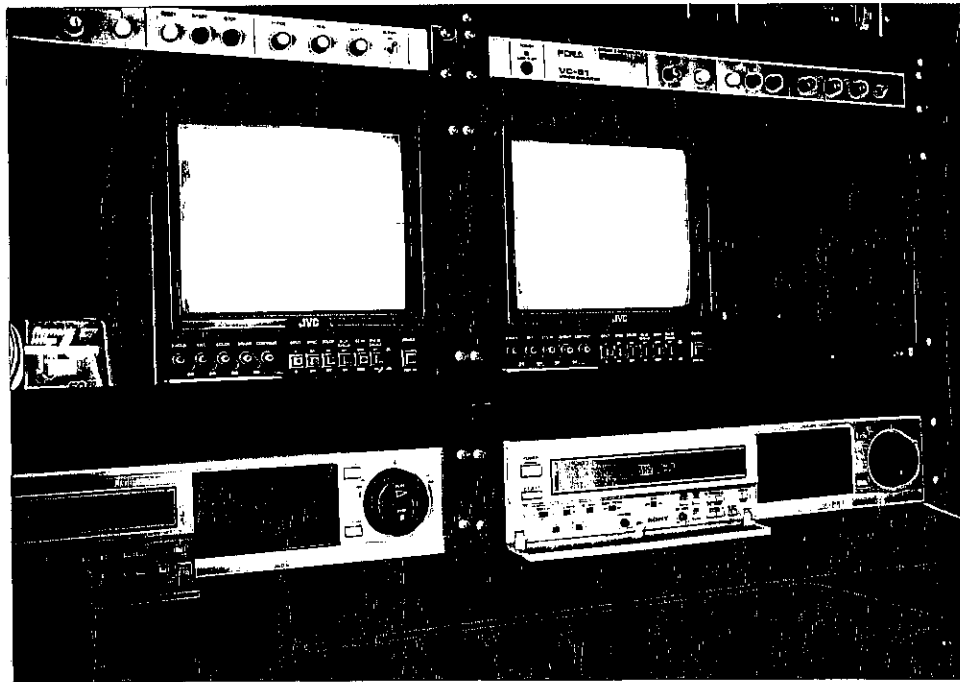


Figure 3.18 Interior of infrared inspection vehicle showing two monitors and two VCRs for the visual and infrared images, respectively.

3.3.2 Infrared Thermography Field Inspection Testing Method

The testing of each bridge deck consisted of slowly driving the van back and forth across the length of the bridge deck while the real time images were recorded with the VCRs. The velocity at which the van moves across the deck depends upon the accuracy desired in the inspection. For this testing, the speed of the van was kept very slow at 1 to 2 mph (1.61 to 3.22 kph). Mr. Timothy J. Crowley, infrared inspector for RUST, reports he has inspected bridges at speeds up to 30 mph (48.3 kph). The limiting factor of the scanning velocity is the speed at which the instrumentation can digitize the images and the number of frames that are being averaged. The higher the number of frames being averaged, the slower the scanning velocity must be.

Scanning usually begins flush to the right wall of the bridge to include inspection of the shoulders of the roadway. The camera's fields of view were approximately one 12 foot (3.66 m) lane width, but generally 3-4 passes for two lanes due to the shoulder areas were made. Although the VCRs were constantly running, accurate positioning was obtainable only during the forward inspection, as the linear location devices measured only positive forward movement. Therefore, the van was positioned such that the first abutment of the bridge was just out of view of the cameras and a pass would then be recorded for the length of the bridge. Then, the van would back up to the start of the bridge, the position recorders would be reset, and another pass would be recorded further to the left of the initial pass.

3.3.3 Infrared Thermography Field Inspection and Debonding vs. Delamination

Distinguishing between debonding of the asphalt layer and delamination of concrete is of significant importance in infrared testing. Most of the bridge decks inspected contained a waterproofing system. This system usually consisted of a fine sand based asphalt concrete layer (called "coal tar interlayer" in the plans) approximately 0.5 to 1.0 inch (12.7 to 25.4 mm) thick atop a thin fabric mesh. This waterproofing system lay upon the concrete deck and the main course of asphalt concrete lay atop the waterproofing system. While taking core samples from the bridge deck it was found that debonding was occurring in various layers. In some locations there was separation between the fabric mesh and the concrete deck. At other locations, the fabric mesh and concrete deck were bonded tightly, but the fabric mesh was separated from the sandy asphalt concrete. In some locations the sandy asphalt layer was separated from itself halfway through its thickness. Finally, instances of the surface asphalt layer separated from the sandy interlayer were noted.

Although debonding is a defect of the bridge deck, it is not of primary concern during bridge deck inspections as the surface overlay is easily replaced during normal rehabilitation operations. Detection of delamination, on the other hand, is extremely important, as these voids affect the integrity of the concrete deck. A delamination is a horizontal void or separation of concrete from itself, usually occurring at the top layer of reinforcing steel or above. At some bridges, core samples located typical delaminations just above the top layer of reinforcing steel, showing signs of considerable corrosion. The reinforcing steel was generally located at least 2 inches (50.8 mm) below the top of the concrete. Other bridges contained shallow delaminations, sometimes referred to as scaling. These delaminations occurred within 0.5 inches (50.8 mm) of the top of the concrete slab.

The delaminations discovered varied from very thin, hairline separations of concrete to voids 0.118 to 0.157 inches (3 to 4 mm) thick. The delaminations often went through large aggregate pieces.

3.3.4 Infrared Imaging of Debonds and Delaminations

Being able to distinguish between debonding and delamination is crucial to the bridge inspection process. Although an experienced infrared inspector often can make this determination, complete accuracy is not always guaranteed. Both debonded and delaminated regions appear as hot spots on the infrared image. These hot regions are suspect since a layer of air in the debond or delamination insulates the region from the body of the deck, and prevents the area from the uniform heating experienced by the surrounding pavement. Often the regions are as much as 1.1 to 1.6 degrees Celsius warmer than the surrounding pavement.

During the field inspection of the bridge decks, it was determined that the size, shape, location and temperature differential of a suspect area were important indicators in separating debonds from delaminations. On average, debonds tended to be smaller in size than delaminations. Usually debonded asphalt is no more than 2 to 3 feet (0.61 to 0.91 m) across, while delaminated areas range between 1 and 30 feet (0.30 and 9.14 m) in length. Mr. Timothy Crowley indicated that these sizes vary from bridge to bridge and represent the average for the bridges in this project.

The shape of a suspect area can be correlated to debonding or delamination. Debonded regions often were more uniformly round than delaminated regions on the bridges tested. Smaller delaminated regions seemed to favor oval or elongated shapes oriented across the width of the bridge deck. Small delaminated regions were often irregular in shape, while very few if any debonded regions exhibited irregularity. Larger delaminated regions sometimes followed a wheelpath down the length of the bridge, hinting at extensive corrosion of a particular reinforcing bar. Debonds often initiated at the edge of the bridge deck where moisture was more likely to penetrate, and the debond would take on a triangular shape. However, these observations do not apply to all bridge decks.

Location and surrounding pavement condition is important in determining whether a suspect area is a debond or delamination. Delaminations often occurred at the edges of the bridge decks and at areas where the asphalt layer was cracked. These areas allow moisture to penetrate the surface layers and get into the concrete deck. Small, round, debonded areas were often found in clusters along the length of construction joints in the asphalt overlay.

The temperature differential of suspect regions relative to the surrounding pavement is also an indication of the type of defect encountered. Debonded areas tended to be slightly hotter

than delaminated areas due to their proximity to the surface and smaller size. Debonded areas, particularly deep ones, showed up as slightly darker on the infrared image due to their depth in the pavement.

3.3.5 Taking Cores During Infrared Inspection

During the scanning process, Mr. Timothy J. Crowley often exited the van and marked suspect and/or interesting areas to be cored. The cores were taken with an electric Milwaukee drill fitted with a 2 inch (50.8 mm) diameter diamond tipped steel coring tube, Figure 3.18. The coring bit was lubricated and cooled throughout the coring process with water from a pressurized plastic hand pump container. The cores were taken to an average depth of 5 to 7 inches (127 to 177.8 mm). Each core took an average of 10 minutes to drill, extract and patch, though this time would be extended if there were difficulty in drilling through the "sticky" waterproofing fabric or if steel reinforcing bar was hit. Reinforcing bar was encountered approximately 25% of the time, requiring an additional 5 minutes of drilling time.

The primary purpose of coring was to determine if the suspect area contained a delamination or debond. Three to four cores were usually taken from each bridge with an emphasis on obtaining cores from both debonded and delaminated regions. In this manner, Mr. Crowley could correlate similar areas on the thermographic image with the results of the core tests. It is important to note that without these core tests certain suspect areas would be very difficult to classify as debond or delamination because thermographic imaging provides no method for determining depth of the flaw. While delaminated regions frequently have similarities across individual bridges, they may vary from bridge to bridge. Therefore, it is necessary to verify at least one potential delaminated area as being delaminated by extracting a

core; this will facilitate similar areas being classified as delaminated. This same verification procedure must also be applied to debonded regions.

During the coring process a number of interesting observations were noted. As the core bit bore through the top layers of asphalt pavement, debonded regions were immediately recognized as the asphalt plug released from the top of the concrete bridge deck and began to spin within the inside of the bit. Delaminated regions were immediately detectable by a pronounced change in the color of water being pumped to the surface during drilling, becoming significantly darker in color as particulate matter from corrosion of steel or deterioration of the concrete rose to the surface.

The holes left in the deck were patched with "Set 45". Set 45 is a quick setting portland cement concrete which gains rigidity in approximately 45 minutes.

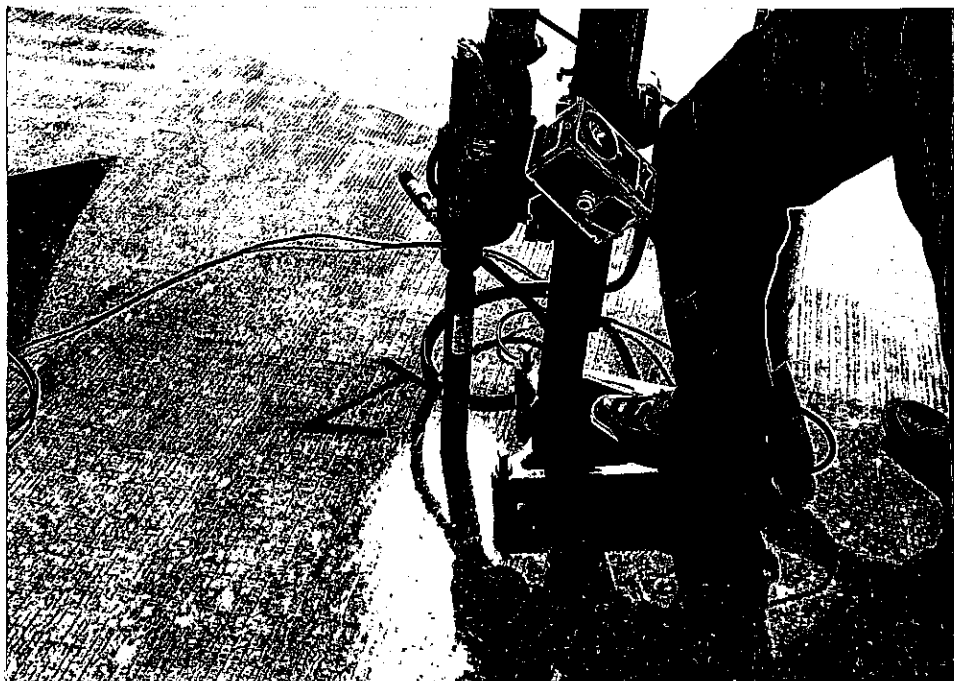


Figure 3.19 Coring of bridge deck during infrared inspection.

3.3.6 Sounding During Infrared Inspection

Sounding of the bridge deck was the other verification technique employed on site during infrared inspection. This method has been used extensively to detect delaminated concrete and debonded overlay before the advent of more sophisticated methods. During the scanning process, Mr. Crowley would repeatedly hit the surface of the bridge deck with a 2 pound (0.91 kg) handheld sledge hammer. A sound area of the bridge deck has a short, clean, high-pitched ring. Defected areas of the deck have a low, hollow, almost drum-like sound to them. The distinction between good regions and large defects is readily distinguishable. Smaller defected regions were harder to detect, but after a few days of experience even the smallest defected regions were detected easily.

Another process used in sounding the deck was to observe the behavior of small pebbles and particulate matter on the surface of the pavement. In solid regions of the deck there was no detectable movement of particles as the deck was struck with the hammer. In defected areas of the deck, the small pebbles and particles jumped off of the deck, sometimes many feet away from the impact. Similarly, Mr. Crowley often placed his hand on the deck to feel the vibrations produced by the impact and thus distinguished the high frequencies and small displacements produced by sound regions from the low frequencies and large displacements produced by defected regions.

A more difficult judgment was trying to distinguish between delaminated and debonded regions by sounding. Mr. Crowley claimed delaminated regions sound "deeper" than debonded regions. Delaminated regions tended to deteriorate (become more hollow sounding) with each

successive blow of the hammer while debonded regions did not. It may be hypothesized that the pounding actually enlarged the delaminated region.

3.3.7 Infrared Thermography Field Inspection and Test Conditions

Ideal pavement conditions for infrared thermographic inspection consist of a smooth, homogenous, evenly lit surface free of debris and markings. Unfortunately, these ideals are impossible to obtain in the field. It is critical during thermographic inspection that a corresponding visual record be kept of the surface condition of the pavement. There are many surface conditions which could be misinterpreted as a defected area or could prevent the detection of a defect. By constantly monitoring the visual record during the scanning process and later during data interpretation, the majority of misleading effects of the surface condition can be quickly and easily discounted. The following paragraphs detail the most common misleading surface conditions encountered during testing.

Asphalt patches generally show up as hot areas on the bridge deck, due to newer patching that contains a higher asphalt concentration at the surface than the surrounding bridge deck. Asphalt patches do not lead to false delamination indications because they are easy to spot on the surface of the deck. Asphalt patches do prevent delamination detection of the underlying concrete deck if the patch is of irregular thickness or of insufficient size to adequately establish a contrast between good and delaminated concrete. Asphalt patches can be particularly misleading if the patch has been used to fill a void in the concrete deck.

Oil on the bridge deck shows up as a hot area. An oil puddle completely prevents infrared inspection of the underlying concrete deck. An area of diffuse oil, such as down the

center of a lane, inhibits inspection but does not prevent the detection of delaminations, provided the oil streak is relatively uniform.

All debris should be removed from the bridge deck in the early morning hours prior to infrared inspection to allow the deck to be uniformly heated. Debris covering the entirety of the bridge deck prevents adequate solar heating of the surface, inhibiting infrared inspection. Debris such as small rocks and sticks do not pose a significant problem to infrared inspection.

Wearing of the asphalt overlay in the tire path produces slightly cooler strips due to the removal of asphalt binder. This does not pose a significant problem to infrared inspection because the phenomenon is easily detectable with the eye and uniform throughout the length of the deck.

Rutting of the asphalt overlay decreases its thickness. This has a tendency to produce an area of slightly warmer material in the wheelpath. This does not pose a significant problem to infrared inspection because the phenomenon is easily detectable with the eye and is uniform throughout the length of the deck.

Mild cracking of the asphalt overlay does not pose a problem to infrared inspection. If water penetrates the crack and spreads between the asphalt overlay and the concrete bridge deck, an area slightly cooler is noted during the infrared inspection. This is due to the higher thermal inertia of water. Severe alligator cracking of the asphalt overlay may prevent even heating of the deck.

Crack sealant poses a significant problem to infrared inspection. The crack sealant absorbs significantly more solar energy than the asphalt overlay. A single crack with sealant along lane joints is tolerable, but if a significant portion of the bridge deck is covered with

cracked sealant, especially in the case of alligator cracking, accurate infrared inspection is prevented.

The presence of subsurface patching is easily detectable using thermographic inspection. The patches show as warmer areas on the thermal scan. It is difficult to determine the integrity of subsurface patches as their small size prevents the determination of contrast.

Lane markings and other painted surfaces show up as cool regions on the infrared scan because they reflect incoming solar radiation. These markings generally do not affect infrared inspection since the area covered is small.

The weather conditions prior to and during infrared inspection are vitally important in obtaining accurate results. There must be a minimum of three hours of direct sunlight on the pavement surface before testing; otherwise, adequate thermal gradients between the sound concrete and the delaminated concrete do not develop. Ideal weather conditions consist of cool nights followed by warm, sunny days. Testing should begin no earlier than 10 a.m. By three or four p.m., the thermal contrast between sound and delaminated concrete may begin to slowly decrease, making defect detection more difficult. On a partly cloudy day, testing may have to be delayed until later in the morning allowing adequate contrast to develop. Testing cannot be performed on a completely overcast day. If clouds develop during testing, the operators have approximately 30 minutes before contrast is lost. If rain develops, all contrast is lost. Testing during the winter may be performed if the pavement is free of ice and snow.

3.4. Chain Drag Field Inspection

After the three nondestructive testing methods were performed on the bridges, the asphalt overlays were removed by the contractor. There were some difficulties removing the asphalt

overlay. The waterproofing membrane which lay between the concrete bridge deck and the asphalt overlay was extremely well bonded to the top of the concrete deck. Once this waterproofing membrane was removed the chain drag survey of the concrete deck commenced.

The chain drag survey was performed by Mr. Eugene Smania of IDOT District 4. Mr. Smania has years of experience performing chain drag surveys. Mr. Smania and Mr. Matthew D. Baright performed all chain drag surveys for this project in an effort to preserve consistency of the data. The chain drag survey consists of dragging a length of chain across the surface of the concrete deck and listening to the chain/deck response in an effort to locate areas of delaminated concrete. The equipment Mr. Smania used consisted of a length of medium weight chain approximately 18 inches (457.2 mm) long, Figure 3.20 and Figure 3.21. The chain was attached to a steel rod approximately three feet (0.91 m) long that served as a handle. Mr. Smania dragged the chain across the entire surface of the bridge deck sweeping back and forth, listening for suspect areas. Once a suspect area was located Mr. Smania outlined the area with white paint. Sometimes Mr. Smania verified a suspect area by tapping on it with a hammer and listening for the response. Having many years of experience with chain drag testing, Mr. Smania could typically complete a 300 foot (91.4 m) bridge lane in 15 to 30 minutes depending upon the number of defects found.

After the survey was performed, coordinates of the delaminated regions were measured with a tape measure. Measurements were taken from the abutment joint along the wall of the bridge deck, and from the wall of the bridge to the defect to determine the transverse distance. By measuring the starting and ending coordinates of the length of the delamination and the starting and ending coordinates of the width of the delamination, a complete area map of the defects could be generated.

The key to successfully detecting delaminated concrete regions with chain dragging is being able to distinguish the subtle differences in sound produced by the chain. When the chain passes over delaminated regions there is a "scratching" quality associated with the hollowness of the delamination. It takes many hours of experience to be accurate with this subtlety in sound. After a few days, Mr. Baright was able to detect the majority of suspect areas determined by Mr. Smania. It became quite apparent that the ability Mr. Smania had in defect detection was acquired only through many years of experience.



Figure 3.20 Apparatus used for chain drag survey.



Figure 3.21 Close up of apparatus used for chain drag survey.

4.0 RESULTS

This chapter presents the results of all of the field testing done by the three primary nondestructive tests. The results are presented by individual bridge allowing comparison between testing methods. Two primary methods of comparison are used: total area and individual delaminations. The total area proposed for rehabilitation is defined as the area of concrete to be removed during rehabilitation operations. This area includes the delaminated concrete and some surrounding concrete which squares off the rehabilitation area. Squaring off the area is necessary because the concrete saws cut in a straight line.

Individual delaminations are also compared. The rehabilitation area for each delamination as determined by the chain drag method is given a number, Appendix A. Each delamination is compared with results from the other nondestructive tests to verify whether the delamination exists. The nondestructive tests are given some latitude in the comparison. The delaminated areas do not need be the same shape or size, but do need to exist in the same location as the chain drag survey. The number of major delaminations is also presented. A major delamination is defined as having a minimum area of 10 ft² (0.93 m²). The bridge decks of Bloomington Structure Number 057-0088 and Marion Structure Number 100-0005 are not included in the individual delamination comparison because the large, continuous areas of delaminated concrete prevent individual delamination identification. Section 4.10 presents a summary of results for the nondestructive tests combined for all bridges.

4.1 Results from Bloomington Structure Number 057-0088

The Bloomington Structure Number 057-0088 bridge deck was found to be in relatively poor condition with numerous asphalt and concrete surface patches. Large portions of the deck

were delaminated, Figure 4.1 through Figure 4.3. The underside shows signs of deterioration of the support structures, Figure 4.4. Removal of the overlay revealed previous rehabilitation patches, many of which were also deteriorated, Figure 4.5. Because of the large areas of delamination and inability to identify individual delaminations, only the total area delaminated as determined by each of the testing methods will be used for comparison; Appendix A, Figure A-1 and Figure A-2 shows chain drag results. Table 4.1 and Table 4.2 summarizes the results of each test. Section 4.1.1 through Section 4.1.3 detail the results of each nondestructive test for this bridge.

Table 4.1 Areas of proposed rehabilitation for Bloomington Structure Number 057-0088 (eastbound).

Test Method	Rehabilitation Area (ft ²) (m ²)	$\frac{\text{Rehabilitation Area}}{\text{Total Bridge Deck Area}} \times 100$
Chain Drag	3869.0 (359.4)	32.6%
Infrared Thermography	2502.6 (232.5)	21.1%
Ground Penetrating Radar	3377.6 (313.8)	28.5%

Table 4.2 Areas of proposed rehabilitation for Bloomington Structure Number 057-0088 (westbound).

Test Method	Rehabilitation Area (ft ²) (m ²)	$\frac{\text{Rehabilitation Area}}{\text{Total Bridge Deck Area}} \times 100$
Chain Drag	4463.0 (414.6)	37.7%
Infrared Thermography	3844.8 (357.2)	32.4%
Ground Penetrating Radar	2808.7 (260.9)	23.7%

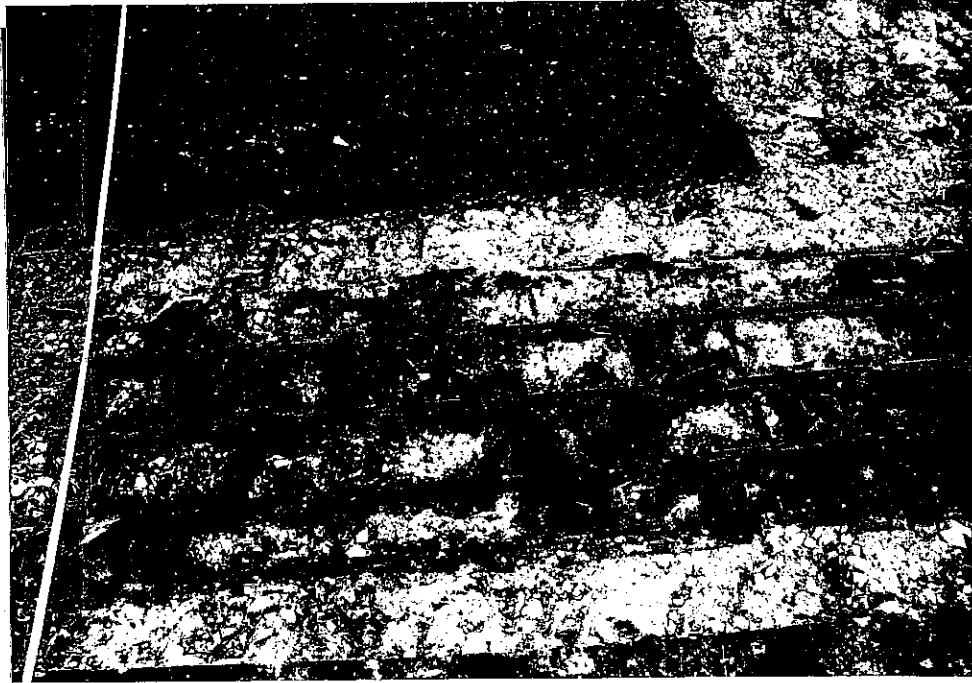


Figure 4.1 Delaminated area on Blooming 057-0088 after removal of concrete showing corroded reinforcing bars.



Figure 4.2 Corroded and broken reinforcing bars on Bloomington Structure Number 057-0088 deck.



Figure 4.3 Close up of corroded and broken reinforcing bars on Bloomington Structure Number 057-0088 deck.



Figure 4.4 Underside of Bloomington Structure Number 057-0088 deck showing corrosion of the superstructure.

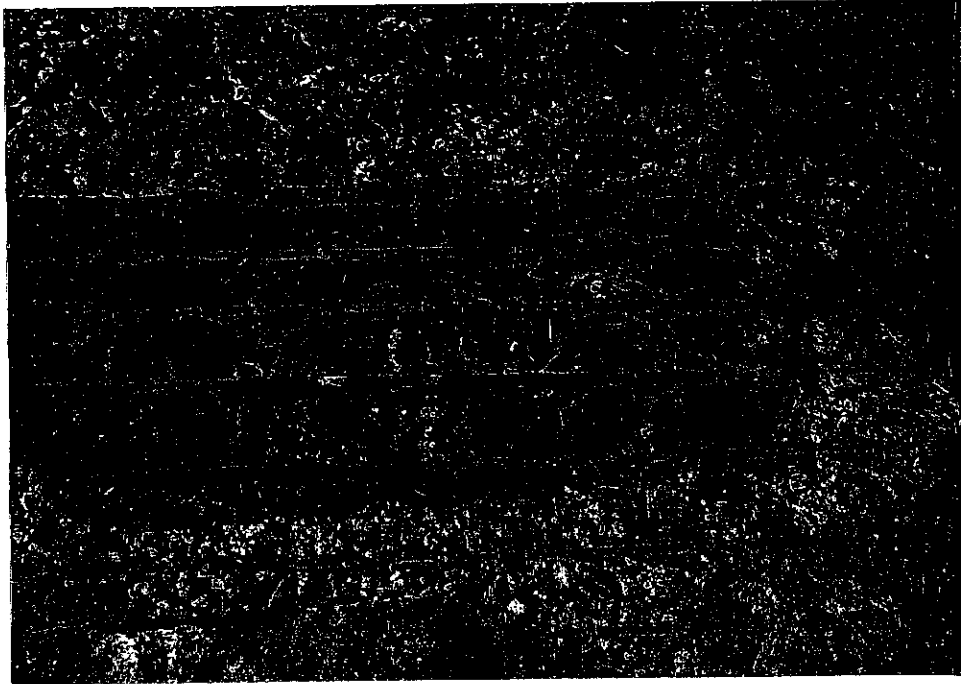


Figure 4.5 Deterioration of previous rehabilitation patch on Bloomington Structure Number 057-0088 deck.

4.1.1 Chain Drag Results from Bloomington Structure Number 057-0088

The results of the chain drag survey of the Bloomington Structure Number 057-0088 bridge deck can be seen in Appendix A; Figure A-1 is the Eastbound lanes, and Figure A-2 the westbound lanes. The delamination maps show areas found to be delaminated by chain dragging after removal of the asphalt overlay. The presence of delaminations was verified during the removal of the delaminated concrete. Figure A-1 and Figure A-2 show extensive areas of delamination in both the eastbound and westbound lanes. The greatest concentration of delaminated areas was along the outer edges of the pavement, corresponding to the low edges of the superstructure. Because of the extensive nature of the delaminated areas, only the total area delaminated is used for comparing the other nondestructive testing methods as individual delaminations could not be identified. The total area delaminated found by chain dragging and

verified during concrete removal is 3869.0 ft² (359.4 m²) for the eastbound lanes and 4463.0 ft² (414.6 m²) for the westbound lanes.

4.1.2 Infrared Thermography Results from Bloomington Structure Number 057-0088

The results of the infrared inspection of the Bloomington Structure Number 057-0088 bridge deck can be seen in Appendix B, Figure B-1. The total proposed rehabilitation area due to delamination for the eastbound lanes is 2502.6 ft² (232.5 m²) as compared with 3869.0 ft² (359.4 m²) determined by chain drag. The total proposed rehabilitation area due to delamination for the westbound lanes is 3844.8 ft² (357.2 m²) as compared with 4463.0 ft² (414.6 m²) determined by chain drag. 4.5% of the eastbound lanes and 7.6% of the westbound lanes are reported as debonded; the debonded regions are concentrated in the extreme edges of the deck. 2.1% of the eastbound lanes and 1.7% of the westbound lanes are reportedly covered with concrete patches. In addition, 5.2% of the eastbound lanes and 9.0% of the westbound lanes are reportedly covered with subsurface concrete patches below the overlay. Three cores (Core #20, Core #21, and Core #22) were taken from various points in the deck. Core #20 was found to be delaminated. Core #21 was found to be solid. Core #22 was found to have rubblized concrete from a previous rehabilitation area.

4.1.3 Ground Penetrating Radar Results from Bloomington Structure Number 057-0088

The results of the ground penetrating radar inspection of the Bloomington Structure Number 057-0088 bridge deck can be seen in Appendix C, Figure C-1 through C-4. Figure C-1 and Figure C-3 show areas of delamination in the eastbound and westbound lanes, respectively. Figure C-2 through Figure C-4 show areas of scaling in the eastbound and westbound lanes,

respectively. In the eastbound lanes, 0.5% of the total area is scaled only, 27.0% of the total area is delaminated only, and 1.0% of the total area is both scaled and delaminated. In the westbound lanes, 0.4% of the total area is scaled only, 22.1% of the total area is delaminated only, and 1.2% of the total area is both scaled and delaminated. For purposes of comparison to the other testing methods, delamination and scaling is not distinguished and total defected area is reported. The total proposed rehabilitation area due to defect for the eastbound lanes is 3377.6 ft² (313.8.4 m²) as compared with 3869.0 ft² (359.4 m²) determined by chain drag. The total proposed rehabilitation area due to defect for the westbound lanes is 2808.7 ft² (260.9 m²) as compared with 4463.0 ft² (414.6 m²) determined by chain drag.

4.2 Results from Peoria Structure Number 090-0118

The Peoria Structure Number 090-0118 bridge deck was found to be in excellent condition. This bridge deck did not have an asphalt overlay and the concrete surface was in excellent condition, Figure 4.6. The underside showed no signs of deterioration. Only one delaminated area was found by chain dragging, Appendix A, Figure A-3. Table 4.3 and Table 4.4 summarizes the results of each test. Section 4.2.1 through Section 4.2.3 detail the results of each nondestructive test.

Table 4.3 Areas of proposed rehabilitation for Peoria Structure Number 090-0118.

Test Method	Rehabilitation Area (ft ²) (m ²)	$\frac{\text{Rehabilitation Area}}{\text{Total Bridge Deck Area}} \times 100$
Chain Drag	9.0 (0.84)	0.07%
Infrared Thermography	0.0	0%
Ground Penetrating Radar	494.4 (45.9)	4.2%

Table 4.4 Individual delaminations for Peoria Structure Number 090-0118.

Chain Drag Delamination #	Area (ft ²) (m ²)	Detected By Infrared?	Detected By Radar?
1	9.0 (0.84)	no	yes

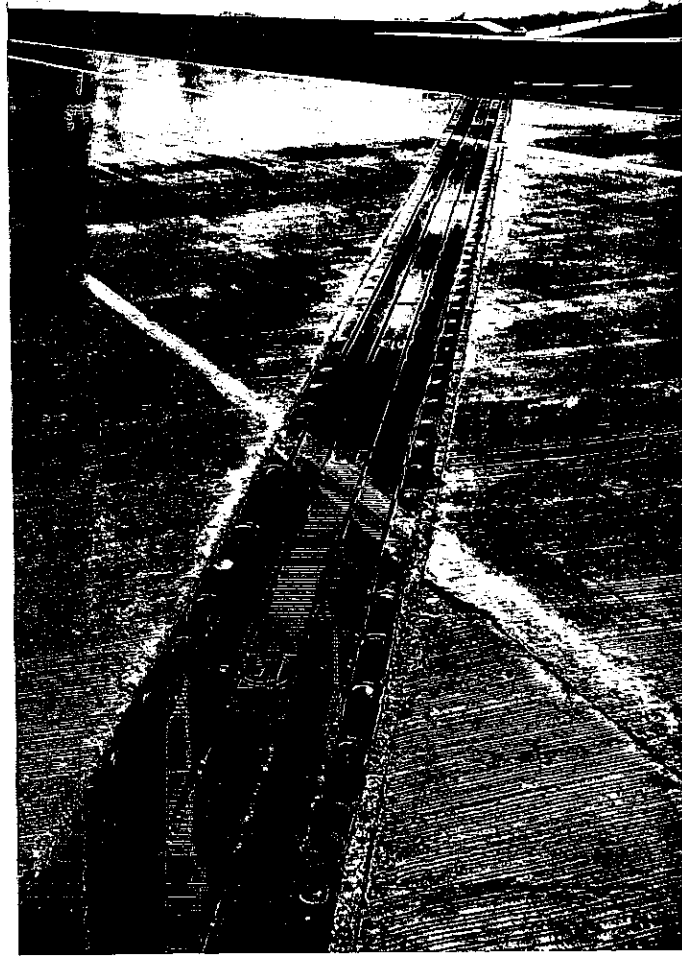


Figure 4.6 Peoria Structure Number 090-0118 deck showing excellent condition of pavement surface and abutment joint.

4.2.1 Chain Drag Results from Peoria Structure Number 090-0118

The results of the chain drag survey of the Peoria Structure Number 090-0118 bridge deck can be seen in Appendix A, Figure A-3. The delamination map shows areas that were found to be delaminated using the chain drag method. The presence of delaminations was verified during the removal of the damaged concrete. Figure A-3 shows one small area of delamination over the entire bridge deck. The total area delaminated found by chain dragging and verified during concrete removal is 9 ft² (0.84 m²). Both the locations of the individual

delaminated areas as well as the total delaminated area are used as a basis of comparison for the other nondestructive testing methods.

4.2.2 Infrared Thermography Results from Peoria Structure Number 090-0118

The results of the infrared inspection of the Peoria Structure Number 090-0118 bridge deck can be seen in Appendix B, Figure B-2. The infrared inspection of the bridge deck found no delaminations as compared with one delamination found by the chain drag inspection. The total proposed rehabilitation area due to delamination is 0 ft² as compared with 9 ft² (0.84 m²) determined by chain drag. The southern edge of the bridge deck could not be inspected due to shading by the south wall, an area amounting to 6.5% of the total area of the deck. One core (core #1) was taken at the western end of the bridge and found to be solid.

4.2.3 Ground Penetrating Radar Results from Peoria Structure Number 090-0118

The results of the ground penetrating radar inspection of the Peoria Structure Number 090-0118 bridge deck can be seen in Appendix C, Figure C-5. Figure C-5 shows areas of delamination. Over the entire deck, 4.2% of the total area is delaminated. No areas of scaling were found. The ground penetrating radar inspection of the bridge deck found the one delamination found by chain drag. The total proposed rehabilitation area due to defect is 494.4 ft² (45.9 m²) as compared with 9.0 ft² (0.84 m²) determined by chain drag.

4.3 Results from Peoria Structure Number 072-0106

The Peoria Structure Number 072-0106 bridge deck was found to be in good condition. This bridge deck had only minor asphalt patching along its longitudinal construction joints. The

underside showed no signs of deterioration. There were 15 delaminated areas found by chain dragging, Appendix A, Figure A-4. Table 4.4 and Table 4.5 summarizes the results of each test. Section 4.3.1 through Section 4.3.3 detail the results of each nondestructive test.

Table 4.5 Areas of proposed rehabilitation for Peoria Structure Number 072-0106.

Test Method	Rehabilitation Area (ft ²) (m ²)	$\frac{\text{Rehabilitation Area}}{\text{Total Bridge Deck Area}} \times 100$
Chain Drag	77.0 (7.2)	0.9%
Infrared Thermography	5.4 (0.50)	0.06%
Ground Penetrating Radar	479.8 (44.6)	5.4%

Table 4.6 Individual delaminations for Peoria Structure Number 072-0106.

Chain Drag Delamination #	Area (ft ²) (m ²)	Detected By Infrared	Detected By Radar
1	4.0 (0.37)	no	no
2	12.0 (1.1)	yes	yes
3	4.0 (0.37)	no	no
4	6.0 (0.56)	no	no
5	1.0 (0.09)	no	no
6	6.0 (0.56)	no	no
7	6.0 (0.56)	no	no
8	8.0 (0.74)	no	yes
9	6.0 (0.56)	no	no
10	6.0 (0.56)	no	no
11	2.0 (0.19)	no	no
12	6.0 (0.56)	no	no
13	4.0 (0.37)	no	no
14	4.0 (0.37)	no	no
15	2.0 (0.19)	no	no

4.3.1 Chain Drag Results from Peoria Structure Number 072-0106

The results of the chain drag survey of the Peoria Structure Number 072-0106 bridge deck can be seen in Appendix A, Figure A-4. The delamination maps show areas found to be delaminated by chain dragging after the asphalt overlay was removed. The presence of delaminations was verified during the removal of the damaged concrete. Figure A-4 shows the highest concentration of delaminated areas were in the center of the bridge deck. There were a total of fifteen distinct delaminated areas. Individual delaminated areas were relatively small, with only one, number 2, exceeding 10 ft² (0.93 m²) in areal extent. The total delaminated area found by chain dragging and verified during concrete removal is 77 ft² (7.15 m²). Both the locations of the individual and total delaminated areas are used as a basis of comparison for the other nondestructive testing methods.

4.3.2 Infrared Thermography Results from Peoria Structure Number 072-0106

The results of the infrared inspection of the Peoria Structure Number 072-0106 bridge deck can be seen in Appendix B, Figure B-3. The infrared inspection of the bridge deck found one distinct delamination as compared with 15 found by the chain drag inspection. The total proposed rehabilitation area due to delamination is 5.4 ft² (0.50 m²) as compared with 9 ft² (0.84 m²) determined by chain drag. 13.1% of the bridge deck is reported debonded, concentrated along the east and west edges of the deck. Two cores (Core #6 and Core #7) were taken in the center of the bridge. Core #6 was found to be delaminated and Core #7 to be debonded.

4.3.3 Ground Penetrating Radar Results from Peoria Structure Number 072-0106

The results of the ground penetrating radar inspection of the Peoria Structure Number 072-0106 bridge deck can be seen in Appendix C, Figure C-6 and Figure C-7. Figure C-6 shows areas of delamination while Figure C-7 shows areas of scaling. Over the entire deck, 0.9% of the total area is scaled only, 4.1% of the total area is delaminated only, and 0.4% of the total area is both scaled and delaminated. For purposes of comparison to the other testing methods, delamination and scaling is not distinguished and total defected area is reported. The ground penetrating radar inspection of the bridge deck located 2 of the 15 distinct defects found by the chain drag inspection. The total proposed rehabilitation area due to defects is 479.8 ft² (44.6 m²) as compared with 77 ft² (7.15 m²) determined by chain drag.

4.4 Results from Peoria Structure Number 072-0107

The Peoria Structure Number 072-0107 bridge deck was found to be in fair condition, Figure 4.7. This bridge deck had minor asphalt patching along its longitudinal construction joints and some asphalt patches over previous rehabilitation work. The underside showed no signs of deterioration. There were 46 delaminated areas found by chain dragging, Appendix A, Figure A-5. Table 4.6 and Table 4.7 summarize the results of each test. Section 4.4.1 through Section 4.4.3 detail the results of each nondestructive test.

Table 4.7 Areas of proposed rehabilitation for Peoria Structure Number 072-0107.

Test Method	Rehabilitation Area (ft ²) (m ²)	$\frac{\text{Rehabilitation Area}}{\text{Total Bridge Deck Area}} \times 100$
Chain Drag	230.0 (21.4)	3.1%
Infrared Thermography	199.1 (18.5)	2.7%
Ground Penetrating Radar	724.6 (67.3)	9.7%

Table 4.8 Individual delaminations for Peoria Structure Number 072-0107.

Chain Drag Delamination #	Area (ft ²) (m ²)	Detected By Infrared	Detected By Radar
1	2.0 (0.19)	no	yes
2	3.0 (0.28)	no	yes
3	6.0 (0.56)	no	yes
4	3.0 (0.28)	no	no
5	6.0 (0.56)	no	yes
6	6.0 (0.56)	no	no
7	6.0 (0.56)	no	yes
8	1.0 (0.90)	no	no
9	6.0 (0.56)	yes	no
10	1.0 (0.90)	no	no
11	2.0 (0.19)	no	no
12	4.0 (0.37)	no	no
13	8.0 (0.74)	yes	no
14	4.0 (0.37)	yes	no
15	4.0 (0.37)	no	no
16	9.0 (0.84)	yes	no
17	8.0 (0.74)	no	yes
18	4.0 (0.37)	no	yes
19	4.0 (0.37)	yes	no
20	4.0 (0.37)	no	no
21	6.0 (0.56)	yes	yes
22	4.0 (0.37)	yes	yes
23	4.0 (0.37)	yes	no
24	4.0 (0.37)	no	no
25	4.0 (0.37)	no	no
26	4.0 (0.37)	no	no
27	3.0 (0.28)	no	no
28	4.0 (0.37)	no	no
29	2.0 (0.19)	no	no
30	15.0 (1.4)	yes	yes
31	4.0 (0.37)	no	no
32	6.0 (0.56)	yes	no
33	6.0 (0.56)	yes	no
34	1.0 (0.09)	yes	no

Table 4.8 Individual delaminations for Peoria Structure Number 072-0107 (Continued).

35	9.0 (0.84)	yes	no
36	4.0 (0.37)	yes	yes
37	9.0 (0.84)	yes	yes
38	12.0 (1.1)	yes	no
39	9.0 (0.84)	yes	no
40	6.0 (0.56)	yes	no
41	4.0 (0.37)	no	no
42	9.0 (0.84)	yes	yes
43	4.0 (0.37)	yes	yes
44	2.0 (0.19)	no	yes
45	1.0 (0.09)	no	yes
46	3.0 (0.28)	no	yes



Figure 4.7 Peoria Structure Number 072-0107 after removal of west lane asphalt overlay.

4.4.1 Chain Drag Results from Peoria Structure Number 072-0107

The results of the chain drag survey of the Peoria Structure Number 072-0107 bridge deck can be seen in Appendix A, Figure A-5. The delamination maps show areas that were found to be delaminated by chain dragging after the asphalt overlay was removed. The presence

of delaminations was verified during the removal of the damaged concrete. Figure A-4 shows the greatest concentration of delaminated areas in the center two-thirds of the bridge deck. There were a total of 46 distinct delaminated areas. Most of the individual delaminated areas were relatively small. Only two delaminations, numbers 30 and 38, exceeded 10 ft² (0.93 m²) in areal extent. The total area delaminated found by chain dragging and verified during concrete removal is 230 ft² (21.4 m²). Both the locations of the individual and total delaminated areas were used as a basis of comparison for the other nondestructive testing methods.

4.4.2 Infrared Thermography Results from Peoria Structure Number 072-0107

The results of the infrared inspection of the Peoria Structure Number 072-0107 bridge deck can be seen in Appendix B, Figure B-4. The infrared inspection of the bridge deck found 20 of the 46 distinct delaminations found by the chain drag inspection. The total proposed rehabilitation area due to delamination is 199.1 ft² (18.5 m²) as compared with 230 ft² (21.4 m²) determined by chain drag. 2.6% of the bridge deck is reported debonded, concentrated along the east and west edges of the deck. Three cores (Core #3, Core #4, and Core #5) were taken in the center of the bridge. Core #3 was found to be delaminated and debonded. Core #4 was found to be debonded. Core #5 was found to be delaminated and debonded.

4.4.3 Ground Penetrating Radar Results from Peoria Structure Number 072-0107

The results of the ground penetrating radar inspection of the Peoria Structure Number 072-0107 bridge deck can be seen in Appendix C, Figure C-8 and Figure C-9. Figure C-8 shows areas of delamination while Figure C-9 shows areas of scaling. Over the entire deck, 0.1% of the total area is scaled only, 9.0% of the total area is delaminated only, and 0.6% of the total area is

both scaled and delaminated. For purposes of comparison to the other testing methods, delamination and scaling is not distinguished and total defected area is reported. The ground penetrating radar inspection of the bridge deck found 17 of the 46 distinct defects found by the chain drag inspection. The total proposed rehabilitation area due to defects is 724.6 ft² (67.3 m²) as compared with 230 ft² (21.4 m²) determined by chain drag.

4.5 Results from Peoria Structure Number 072-0108

The Peoria Structure Number 072-0108 bridge deck was found to be in good condition. This bridge deck had only minor asphalt patching along its longitudinal construction joints. The underside showed no signs of deterioration. There were only 3 delaminated areas found by chain dragging, Appendix A, Figure A-6. Table 4.8 and Table 4.9 summarizes the results of each test. Section 4.5.1 through Section 4.5.3 detail the results of each nondestructive test.

Table 4.9 Areas of proposed rehabilitation for Peoria Structure Number 072-0108.

Test Method	Rehabilitation Area (ft ²) (m ²)	$\frac{\text{Rehabilitation Area}}{\text{Total Bridge Deck Area}} \times 100$
Chain Drag	33.0 (3.1)	0.4%
Infrared Thermography	5.4 (0.50)	0.07%
Ground Penetrating Radar	626.7 (58.2)	7.7%

Table 4.10 Individual delaminations for Peoria Structure Number 072-0108.

Chain Drag Delamination #	Area (ft ²) (m ²)	Detected By Infrared	Detected By Radar
1	4.0 (0.37)	no	no
2	14.0 (1.3)	no	yes
3	15.0 (1.4)	yes	yes

4.5.1 Chain Drag Results from Peoria Structure Number 072-0108

The results of the chain drag survey of the Peoria Structure Number 072-0108 bridge deck can be seen in Appendix A, Figure A-6. The delamination maps show areas that were found to be delaminated by chain dragging after the asphalt overlay was removed. The presence of delaminations was verified during the removal of the damaged concrete. Figure A-6 shows a total of 3 distinct delaminated areas concentrated at the south end of the deck. Two of the three delaminations, numbers 2 and 3, exceed 10 ft² (0.93 m²) in areal extent. The total area delaminated found by chain dragging and verified during concrete removal is 33 ft² (3.1 m²). Both the locations of the individual and total delaminated areas are used as a basis of comparison for the other nondestructive testing methods.

4.5.2 Infrared Thermography Results from Peoria Structure Number 072-0108

The results of the infrared inspection of the Peoria Structure Number 072-0108 bridge deck can be seen in Appendix B, Figure B-5. The infrared inspection of the bridge deck found one of the 3 distinct delaminations found by the chain drag inspection. The total proposed rehabilitation area due to delamination is 5.4 ft² (0.50 m²) as compared with 33 ft² (3.1 m²) determined by chain drag. 14.6% of the bridge deck is reported debonded, concentrated along

the east and west edges of the deck, with large areas in the middle of the deck. Four cores (Core #8, Core #9, Core #10, and Core #10A) were taken in the center of the bridge. Core #8 was found to be debonded. Core #9 was found to be delaminated and debonded. Core #10 and Core #10A were found to be debonded.

4.5.3 Ground Penetrating Radar Results from Peoria Structure Number 072-0108

The results of the ground penetrating radar inspection of the Peoria Structure Number 072-0108 bridge deck can be seen in Appendix C, Figure C-10 and Figure C-11. Figure C-10 shows areas of delamination while Figure C-11 shows areas of scaling. Over the entire deck, 0.2% of the total area is scaled only, 6.4% of the total area is delaminated only, and 0.7% of the total area is both scaled and delaminated. For purposes of comparison to the other testing methods, delamination and scaling is not distinguished and total defect area is reported. The ground penetrating radar inspection of the bridge deck found 2 of the 3 distinct defects found by the chain drag inspection. The total proposed rehabilitation area due to defects is 626.7 ft² (58.2 m²) as compared with 33 ft² (3.1 m²) determined by chain drag.

4.6 Results from Peoria Structure Number 072-0109

The Peoria Structure Number 072-0109 bridge deck was found to be in good condition, Figure 4.7. This bridge deck had minor asphalt patching along its longitudinal construction joints and a large asphalt patch at its north end. The underside showed no signs of deterioration. There were 15 delaminated areas found by chain dragging, Appendix A, Figure A-7. Six of these areas were minor spalling along the transverse joints in the deck. In addition, the deck had unusual potholes in the surface of the concrete, Figure 4.8 and Figure 4.9. Table 4.10 and Table

4.11 summarizes the results of each test. Section 4.6.1 through Section 4.6.3 detail the results of each nondestructive test.

Table 4.11 Areas of proposed rehabilitation for Peoria Structure Number 072-0109.

Test Method	Rehabilitation Area (ft ²) (m ²)	$\frac{\text{Rehabilitation Area}}{\text{Total Bridge Deck Area}} \times 100$
Chain Drag	64.0 (5.9)	0.8%
Infrared Thermography	0.0	0%
Ground Penetrating Radar	379.3 (35.2)	4.6%

Table 4.12 Individual delaminations for Peoria Structure Number 072-0109.

Chain Drag Delamination #	Area (ft ²) (m ²)	Detected By Infrared	Detected By Radar
1	4.0 (0.37)	no	yes
2	2.0 (0.19)	no	yes
3	4.0 (0.37)	no	yes
4	2.0 (0.19)	no	yes
5	4.0 (0.37)	no	no
6	1.0 (0.09)	no	no
7	8.0 (0.74)	no	no
8	4.0 (0.37)	no	no
9	4.0 (0.37)	no	yes
10	27.0 (2.5)	no	yes
11	2.0 (0.19)	no	yes
12	2.0 (0.19)	no	yes



Figure 4.8 Peoria Structure Number 072-0109 after removal of west lane asphalt overlay.

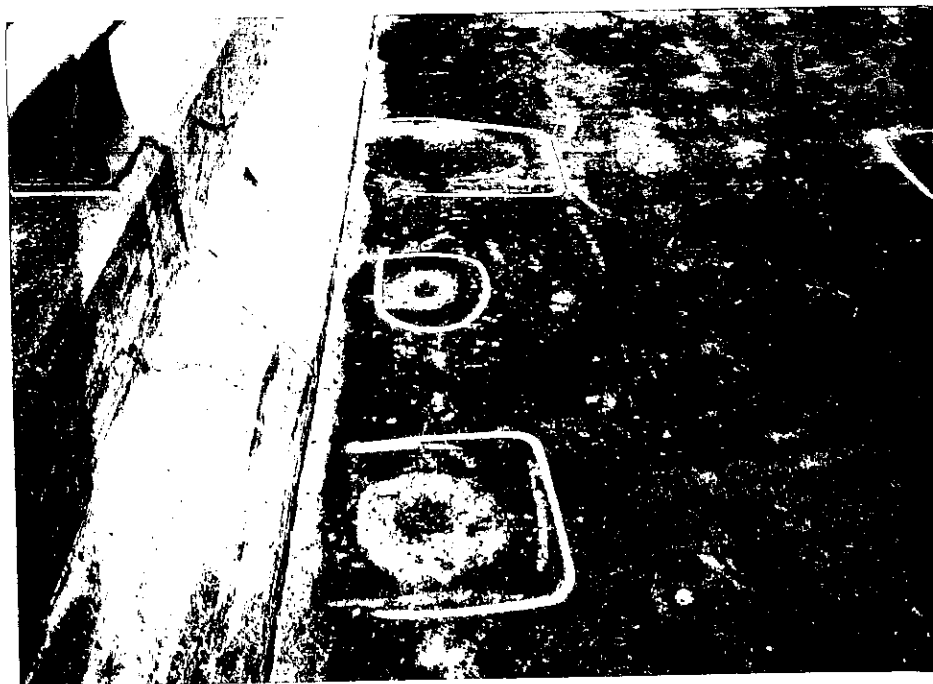


Figure 4.9 Peoria Structure Number 072-0109 potholes in concrete.

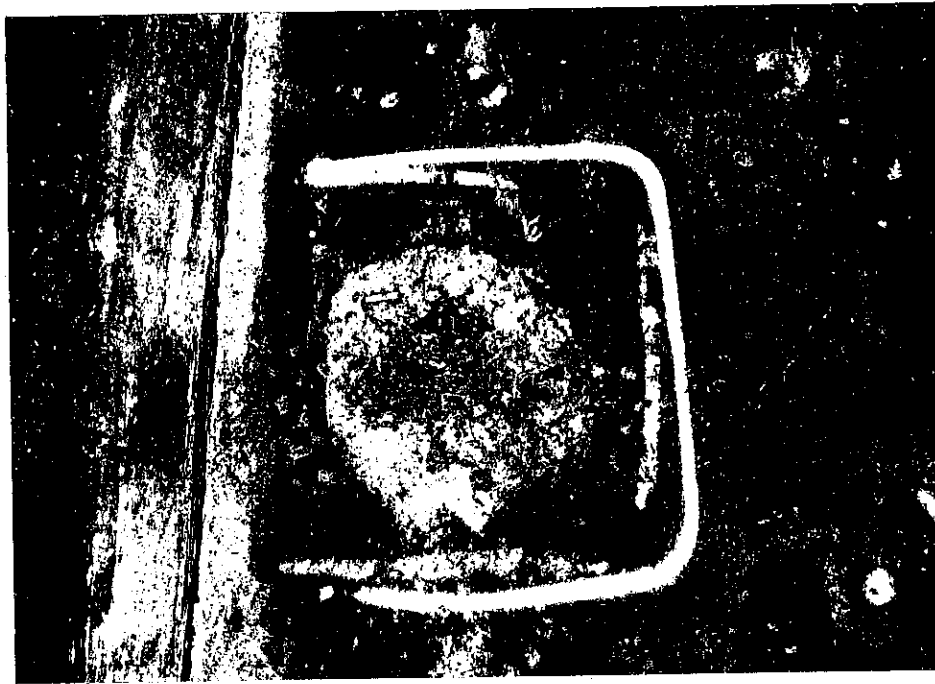


Figure 4.10 Peoria Structure Number 072-0109 close up of pothole in concrete.

4.6.1 Chain Drag Results from Peoria Structure Number 072-0109

The results of the chain drag survey of the Peoria Structure Number 072-0109 bridge deck can be seen in Appendix A, Figure A-7. The delamination maps show areas that were found to be delaminated by chain dragging after the asphalt overlay was removed. The presence of delaminations was verified during the removal of the damaged concrete. Figure A-7 shows a total of 12 distinct delaminated areas scattered about the deck. Only one delamination, number 10, exceeds 10 ft² (0.93 m²) in areal extent. It should be noted that delamination numbers 2, 3, 4, 11, and 12 are minor spalling along the steel bay joints in the deck. Also, delamination numbers 1, 5, 6, and 8 are unusual potholes found in the concrete surface. These defects exist at the low end of the superstructure. The total area delaminated found by chain dragging and verified during concrete removal is 64 ft² (5.9 m²). Both the locations of the individual delaminated areas

as well as the total delaminated area are used as a basis of comparison for the other nondestructive testing methods.

4.6.2 Infrared Thermography Results from Peoria Structure Number 072-0109

The results of the infrared inspection of the Peoria Structure Number 072-0109 bridge deck can be seen in Appendix B, Figure B-6. The infrared inspection of the bridge deck found 0 of the 12 distinct delaminations found by the chain drag inspection. The total proposed rehabilitation area due to delamination is 0 ft² as compared with 64 ft² (5.9 m²) determined by chain drag. 10.8% of the bridge deck is reported debonded, concentrated along the west edge of the deck. One core (Core #2) was taken at the north end of the bridge. Core #2 was found to be debonded.

4.6.3 Ground Penetrating Radar Results from Peoria Structure Number 072-0109

The results of the ground penetrating radar inspection of the Peoria Structure Number 072-0109 bridge deck can be seen in Appendix C, Figure C-12 and Figure C-13. Figure C-12 shows areas of delamination while Figure C-13 shows areas of scaling. Over the entire deck, 0.5% of the total area is scaled only, 3.7% of the total area is delaminated only, and 0.5% of the total area is both scaled and delaminated. For purposes of comparison to the other testing methods, delamination and scaling is not distinguished and total defected area is reported. The ground penetrating radar inspection of the bridge deck found 8 of the 12 distinct defects found by the chain drag inspection. The total proposed rehabilitation area due to defects is 379.3 ft² (35.2 m²) as compared with 64 ft² (5.9 m²) determined by chain drag.

4.7 Results From Peoria Structure Number 072-0110

The Peoria Structure Number 072-0110 bridge deck was found to be in fair condition, Figure 4.11. This bridge deck had no areas of asphalt patching. The underside showed no signs of deterioration. Upon removal of the asphalt overlay, milling gouges across most of the surface of the deck were observed, Figure 4.12. Some of the gouges were 1 inch (25.4 mm) deep, Figure 4.13. There were 34 delaminated areas found by chain dragging, Appendix A, Figure A-8. Table 4.12 and Table 4.13 summarizes the results of each test. Section 4.7.1 through Section 4.7.3 detail the results of each nondestructive test.

Table 4.13 Areas of proposed rehabilitation for Peoria Structure Number 072-0110.

Test Method	Rehabilitation Area (ft ²) (m ²)	$\frac{\text{Rehabilitation Area}}{\text{Total Bridge Deck Area}} \times 100$
Chain Drag	169.0 (15.7)	1.9%
Infrared Thermography	127.0 (11.8)	1.5%
Ground Penetrating Radar	394.0 (36.6)	4.5%

Table 4.14 Individual delaminations for Peoria Structure Number 072-0110.

Chain Drag Delamination #	Area (ft ²) (m ²)	Detected By Infrared	Detected By Radar
1	4.0 (0.37)	no	yes
2	1.0 (0.09)	no	no
3	6.0 (0.56)	no	yes
4	9.0 (0.84)	yes	yes
5	6.0 (0.56)	no	yes
6	1.0 (0.09)	yes	no
7	2.0 (0.19)	yes	no
8	9.0 (0.84)	yes	no
9	8.0 (0.74)	no	no
10	8.0 (0.74)	yes	no
11	4.0 (0.37)	yes	yes
12	4.0 (0.37)	yes	no
13	8.0 (0.74)	yes	no
14	4.0 (0.37)	yes	no
15	19.0 (1.8)	yes	yes
16	6.0 (0.56)	yes	yes
17	1.0 (0.09)	no	no
18	5.0 (0.46)	yes	no
19	5.0 (0.46)	yes	no
20	2.0 (0.19)	yes	no
21	2.0 (0.19)	no	yes
22	8.0 (0.74)	yes	yes
23	6.0 (0.56)	yes	no
24	1.0 (0.09)	no	no
25	2.0 (0.19)	no	no
26	4.0 (0.37)	yes	no
27	4.0 (0.37)	yes	yes
28	4.0 (0.37)	yes	yes
29	4.0 (0.37)	yes	no
30	2.0 (0.19)	yes	yes
31	6.0 (0.56)	no	no
32	1.0 (0.09)	yes	yes
33	2.0 (0.19)	yes	yes
34	1.0 (0.09)	no	yes



Figure 4.11 Peoria Structure Number 072-0110 after removal of left lane overlay revealing milling gouges.

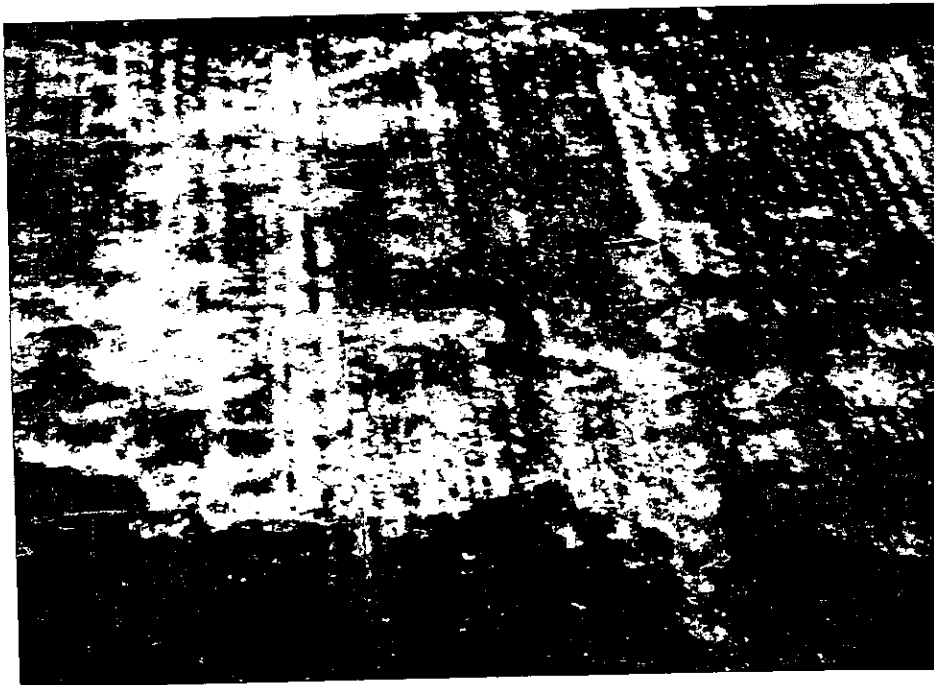


Figure 4.12 Peoria Structure Number 072-0110 close up of milling gouges.

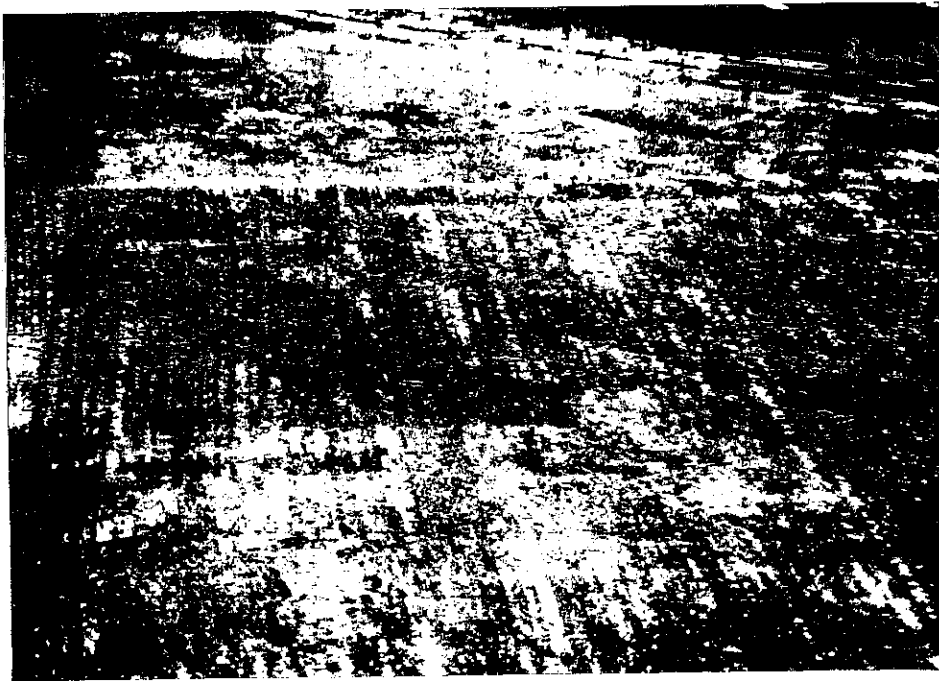


Figure 4.13 Peoria Structure Number 072-0110 close up of milling gouges showing 1 inch (25.4 mm) depth.

4.7.1 Chain Drag Results From Peoria Structure Number 072-0110

The results of the chain drag survey of the Peoria Structure Number 072-0110 bridge deck can be seen in Appendix A, Figure A-8. The delamination maps show areas that were found to be delaminated by chain dragging after the asphalt overlay was removed. The presence of delaminations was verified during the removal of the damaged concrete. Figure A-8 shows a total of 34 distinct delaminated areas concentrated at the center and south end of the deck, but only one of the delaminations, number 15, exceed 10 ft² (0.93 m²) in areal extent. The total area delaminated found by chain dragging and verified during concrete removal is 169 ft² (15.7 m²). Both the locations of the individual and total delaminated areas are used as a basis of comparison for the other nondestructive testing methods.

4.7.2 Infrared Thermography Results From Peoria Structure Number 072-0110

The results of the infrared inspection of the Peoria Structure Number 072-0110 bridge deck can be seen in Appendix B, Figure B-7. The infrared inspection of the bridge deck found 23 of the 34 distinct delaminations found by the chain drag inspection. The total proposed rehabilitation area due to delamination is 127.0 ft² (11.8 m²) as compared with 169 ft² (15.7 m²) determined by chain drag. 2.1% of the bridge deck is reported debonded, concentrated in the right lane of the deck. The western edge of the bridge deck could not be inspected due to shading by the west wall, an area amounting to 3.7% of the total area of the deck. Two cores (Core #14 and Core #15) were taken at the south and north end of the bridge, respectively. Core #14 and Core #15 were found to be delaminated.

4.7.3 Ground Penetrating Radar Results From Peoria Structure Number 072-0110

The results of the ground penetrating radar inspection of the Peoria Structure Number 072-0110 bridge deck can be seen in Appendix C, Figure C-14 and Figure C-15. Figure C-14 shows areas of delamination while Figure C-15 shows areas of scaling. Over the entire deck, 0.2% of the total area is scaled only, 4.2% of the total area is delaminated only, and 0.1% of the total area is both scaled and delaminated. For purposes of comparison to the other testing methods, delamination and scaling is not distinguished and total defected area is reported. The ground penetrating radar inspection of the bridge deck found 15 of the 34 distinct defects found by the chain drag inspection. The total proposed rehabilitation area due to defects is 394.0 ft² (36.6 m²) as compared with 169.0 ft² (15.7 m²) determined by chain drag.

4.8 Results from Peoria Structure Number 072-0111

The Peoria Structure Number 072-0111 bridge deck was found to be in fair to poor condition. This bridge deck had one small area of asphalt patching. The underside showed no signs of deterioration. There were 68 delaminated areas found by chain dragging, Appendix A, Figure A-9. Table 4.14 and Table 4.15 summarizes the results of each test. Section 4.8.1 through Section 4.8.3 detail the results of each nondestructive test.

Table 4.15 Areas of proposed rehabilitation for Peoria Structure Number 072-0111.

Test Method	Rehabilitation Area (ft ²) (m ²)	$\frac{\text{Rehabilitation Area}}{\text{Total Bridge Deck Area}} \times 100$
Chain Drag	485.0 (45.1)	4.4%
Infrared Thermography	415.5 (38.6)	3.7%
Ground Penetrating Radar	1578.5 (146.6)	14.2%

Table 4.16 Individual delaminations for Peoria Structure Number 072-0111.

Chain Drag Delamination #	Area (ft ²) (m ²)	Detected By Infrared	Detected By Radar
1	1.0 (0.09)	no	yes
2	15.0 (1.4)	no	yes
3	6.0 (0.56)	no	yes
4	6.0 (0.56)	no	yes
5	4.0 (0.37)	no	yes
6	1.0 (0.09)	no	yes
7	4.0 (0.37)	no	no
8	6.0 (0.56)	no	yes
9	5.0 (0.46)	no	yes
10	2.0 (0.19)	no	yes
11	4.0 (0.37)	no	yes
12	8.0 (0.74)	no	no
13	1.0 (0.09)	no	no
14	6.0 (0.56)	no	yes
15	4.0 (0.37)	no	yes
16	4.0 (0.37)	no	yes
17	1.0 (0.09)	no	yes
18	6.0 (0.56)	yes	yes
19	4.0 (0.37)	no	yes
20	1.0 (0.09)	no	no
21	27.0 (2.5)	no	no
22	4.0 (0.37)	no	yes
23	2.0 (0.19)	no	no
24	21.0 (2.0)	yes	yes
25	2.0 (0.19)	no	no
26	2.0 (0.19)	no	no
27	18.0 (1.7)	yes	yes
28	2.0 (0.19)	no	no
29	10.0 (0.93)	no	yes
30	24.0 (2.2)	yes	no
31	20.0 (1.9)	yes	yes
32	1.0 (0.09)	no	yes
33	2.0 (0.19)	yes	yes
34	4.0 (0.37)	yes	no
35	27.0 (2.5)	yes	no
36	36.0 (3.3)	yes	yes
37	1.0 (0.09)	yes	no
38	2.0 (0.19)	no	no
39	2.0 (0.19)	no	yes
40	15.0 (1.4)	yes	yes
41	6.0 (0.56)	yes	no
42	6.0 (0.56)	no	yes

Table 4.16 Individual delaminations for Peoria Structure Number 072-0111 (Continued).

43	2.0 (0.19)	no	yes
44	2.0 (0.19)	no	no
45	6.0 (0.56)	no	yes
46	2.0 (0.19)	no	no
47	6.0 (0.56)	yes	yes
48	4.0 (0.37)	no	yes
49	4.0 (0.37)	no	yes
50	27.0 (2.5)	no	yes
51	21.0 (2.0)	yes	yes
52	4.0 (0.37)	yes	yes
53	12.0 (1.1)	yes	yes
54	4.0 (0.37)	yes	yes
55	12.0 (1.1)	yes	yes
56	2.0 (0.19)	no	yes
57	3.0 (0.28)	no	no
58	4.0 (0.37)	no	yes
59	4.0 (0.37)	no	yes
60	4.0 (0.37)	no	no
61	3.0 (0.28)	no	yes
62	6.0 (0.56)	yes	no
63	8.0 (0.74)	yes	yes
64	8.0 (0.74)	yes	yes
65	4.0 (0.37)	no	yes
66	6.0 (0.56)	no	no
67	2.0 (0.19)	no	no
68	2.0 (0.19)	no	yes

4.8.1 Chain Drag Results from Peoria Structure Number 072-0111

The results of the chain drag survey of the Peoria Structure Number 072-0111 bridge deck can be seen in Appendix A, Figure A-9. The delamination maps show areas that were found to be delaminated by chain dragging after the asphalt overlay was removed. The presence of delaminations was verified during the removal of the damaged concrete. Figure A-9 shows a total of 68 distinct delaminated areas concentrated across the entire deck. Fourteen individual delaminations exceed 10 ft² (0.93 m²) in areal extent. The total area delaminated found by chain

dragging and verified during concrete removal is 485 ft² (45.1 m²). Both the locations of the individual and total delaminated areas are used as a basis of comparison for the other nondestructive testing methods.

4.8.2 Infrared Thermography Results from Peoria Structure Number 072-0111

The results of the infrared inspection of the Peoria Structure Number 072-0111 bridge deck can be seen in Appendix B, Figure B-8. The infrared inspection of the bridge deck found 21 of the 68 distinct delaminations found by the chain drag inspection. The total proposed rehabilitation area due to delamination is 415.5 ft² (38.6 m²) as compared with 485 ft² (45.1 m²) determined by chain drag. 3.2% of the bridge deck is reported debonded, concentrated in the east edge of the deck. Three cores (Core #11, Core #12, and Core #13) were taken from the middle of the deck. Core #11 was found to be delaminated. Core #12 was found to be debonded and Core #13 was found to be delaminated.

4.8.3 Ground Penetrating Radar Results from Peoria Structure Number 072-0111

The results of the ground penetrating radar inspection of the Peoria Structure Number 072-0111 bridge deck can be seen in Appendix C, Figure C-16 and Figure C-17. Figure C-16 shows areas of delamination while Figure C-17 shows areas of scaling. Over the entire deck, 0.2% of the total area is scaled only, 13.8% of the total area is delaminated only, and 0.2% of the total area is both scaled and delaminated. For purposes of comparison to the other testing methods, delamination and scaling is not distinguished and total defected area is reported. The ground penetrating radar inspection of the bridge deck found 47 of the 68 distinct defects found

by the chain drag inspection. The total proposed rehabilitation area due to defects is 1578.5 ft² (146.6 m²) as compared with 485.0 ft² (45.1 m²) determined by chain drag.

4.9 Results from Marion Structure Number 100-0005

The Marion Structure Number 100-0005 bridge deck was found to be in relatively poor condition with numerous asphalt and concrete surface patches. Large portions of the deck were delaminated; Appendix A, Figure A-10 shows chain drag results. The underside shows signs of deterioration of the support structures. After all testing was performed on this bridge deck, the Illinois Department of Transportation decided not to remove the overlay. Because of the large areas of delamination and inability to identify individual delaminations, only the total area delaminated as determined by each of the testing methods will be used for comparison. Table 4.17 summarizes the results of each test. Section 4.9.1 through Section 4.9.5 detail the results of each nondestructive test.

Table 4.17 Areas of proposed rehabilitation for Marion Structure Number 100-0005.

Test Method	Rehabilitation Area (ft ²) (m ²)	$\frac{\text{Rehabilitation Area}}{\text{Total Bridge Deck Area}} \times 100$
Chain Drag	2984.0 (277.2)	41.6%
Infrared Thermography	1649.0 (153.2)	23.5%
Ground Penetrating Radar	3129.8 (290.8)	43.6%

4.9.1 Chain Drag Results from Marion Structure Number 100-0005

The results of the chain drag survey of the Marion Structure Number 100-0005 bridge deck can be seen in Appendix A, Figure A-10. The delamination map shows areas that were found to be delaminated by chain dragging while the overlay remained on the bridge deck. The presence of delaminations was not able to be verified as the overlay was never removed. Figure A-10 shows extensive areas of delamination. The greatest concentration of delaminated areas were along the east and south edges of the pavement. Because of the extensive nature of the delaminated areas, only the total area delaminated is used for comparing the other nondestructive testing methods as individual delaminations could not be identified. The total area delaminated found by chain dragging is 2984 ft² (277.2 m²).

4.9.2 Infrared Thermography Results from Marion Structure Number 100-0005

The results of the infrared inspection of the Marion Structure Number 100-0005 bridge deck can be seen in Appendix B, Figure B-9. The total proposed rehabilitation area due to delamination is 1649.0 ft² (153.2 m²) as compared with 2984 ft² (277.2 m²) determined by chain drag. 2.9% of the bridge deck is reported debonded, concentrated in the west edge of the deck. The eastern edge of the bridge deck was unable to be inspected due to shading by the east wall, an area amounting to 2.4% of the total area of the deck. 6.9% of the bridge deck was reportedly covered with concrete patches. Four cores (Core #16, Core #17, Core #18, and Core #19) were taken from various locations in the deck. Core #16 was found to be delaminated. Core #17 was found to be solid. Core #18 was found to be debonded, and Core 19 was found to be delaminated.

4.9.3 Ground Penetrating Radar Results from Marion Structure Number 100-0005

The results of the ground penetrating radar inspection of the Marion Structure Number 100-0005 bridge deck can be seen in Appendix C, Figure C-18 and Figure C-19. Figure C-18 shows areas of delamination, while Figure C-19 shows areas of scaling. Over the entire deck, 0.2% of the total area is scaled only, 41.4% of the total area is delaminated only, and 2.0% of the total area is both scaled and delaminated. For purposes of comparison to the other testing methods, delamination and scaling is not distinguished and total defected area is reported. The total proposed rehabilitation area due to defects is 3129.8 ft² (290.8 m²) as compared with 2984.0 ft² (277.2 m²) determined by chain drag.

4.9.4 Impact-Echo Results from Marion Structure Number 100-0005

Example impact-echo records from handheld tests at coreholes with good asphalt overlay bonding and visually sound conditions are presented in Appendix D, Figure D-2 and Figure D-3. Analysis of the spectral echo peak frequency data indicate an average velocity of approximately 11,700 feet per second (3566 m/s) for the deck section consisting of 1.75 inches (44.45 mm) of asphalt covering 0.25 inches (6.35 mm) of grout sand layered over an 8 inch (203 mm) thick concrete deck. This velocity was used to analyze the impact-echo scanner results. The handheld impact-echo-1 scan line was performed along east scan line 1, channel 2 of the impact-echo scanner test line (see Appendix D, Figure D-1 for location). The results of the handheld impact-echo testing echo depths, and energy versus distance, along the 80 foot (24.4 m) long scan line are presented in Appendix D, Figure D-4 and Figure D-5. Review of these results reveals several areas of apparent thicknesses much greater than 10 inches (254 mm); these are most likely low

frequency flexural responses indicative of debonded conditions at the asphalt-concrete interface, or a shallow delamination in the concrete deck. Many areas showed full thickness echoes of 10 inches (254 mm) in these figures.

The impact-echo scanner results ranged from good--nominally 10 inches (254 mm) deep--to inconsistent thickness echoes. A qualitative summary of the data obtained from each of the 88 scanner test lines is presented in Table 4.18. Review of Table 4.18 shows 7 scanner lines had good results indicative of the expected 10 inch (254 mm) deck thickness echoes, 10 lines had fair quality data with fairly consistent 10 inch (254 mm) thickness echoes, 41 lines had poor quality data with inconsistent 10 inch (254 mm) thickness echoes, and 30 lines had erratic data and no consistent 10 inch (254 mm) thickness echoes. Better results were commonly obtained from portions of the center lane where the surface seemed to be less rough.

Examples of good and poor impact-echo scanner records are presented in Appendix D, Figure D-6 and Figure D-7. Typical thickness echo plots of good and poor 10 inch (254 mm) thickness echo data are presented in Appendix D, Figure D-8 and Figure D-9, respectively. The plot in Figure D-9 is from east scan line 1, transducer channel 2, the same line for the handheld impact-echo 1 thickness plots presented in Figure D-4 and Figure D-5. Unfortunately, the data quality is very poor for the impact-echo scanner on this line, offering no direct comparison of the impact-echo 1 and impact-echo scanner results. The handheld impact-echo 1 thickness plots of Figure D-4 and Figure D-5 can be qualitatively compared against impact-echo scanner lines with good quality data, Figure D-8. These comparisons show similar, consistent 10 inch (254 mm) thickness echo results. An estimated total area delaminated on the bridge deck can not be determined due to the difficulty in obtaining quality data.

Table 4.18 Impact-echo scanner consistency with 10 inch (254 mm) depth for Marion Structure Number 100-0005.

Scan Line (Tests)	Transducer Channel 1	Transducer Channel 2	Transducer Channel 3	Transducer Channel 4	Comments
C1 (536)	Poor	Poor	Poor	Poor	Faster scanning walk
C2 (803)	Poor	Poor	Good	Fair	Fast walk, slow after 30 feet (9.11 m)
C3 (936)	Fair	Good	Good	Poor	
C4 (817)	Poor	Poor	Poor	No	Channel 4 on patches, cracks
C5 (634)	Poor	Poor	Poor	Poor	
C6 (798)	Poor	Fair	Fair	Poor	Cleaned #2, #1 water jets after scan
C7 (1201)	Poor	Poor	Poor	Poor	Jets clogged during scan
C8 (900)	Poor	Poor	Poor	Poor	
C9 (827)	Poor	Poor	Poor	Poor	Good data at 45 to 47 feet (13.7 to 14.3 m)
C10 (756)	Fair	Fair	Fair	Fair	Scan C10- Channel 1 same line as Scan C9- Channel 4 and similar results
W1 (936)	Poor	Poor	Poor	No	
W2 (809)	No	No	No	No	
W3 (718)	Good	Good	Good	Fair	Cleaned jets after scan

Table 4.18 Impact-echo scanner consistency with 10 inch (254 mm) depth for Marion Structure Number 100-0005 (Continued).

W4 (841)	No	No	No	No	
W5 (618)	No	No	No	No	
W6 (144)	No	No	No	No	Jets clogged, minimal coupling water for scan. Channel 3 and 4 were driest.
E1 (1139)	Poor	Poor	Poor	Poor	Weak spring - tiebacks broken Channel 4
E2 (1163)	Fair	No	No	Fair	
E3 (898)	No	No	No	No	Scan E3-Ch4 is same line as E2-Channel 1, but data is dissimilar
E4 (1160)	No	No	No	No	
E5 (1056)	Poor	Poor	No	No	
E6 (848)	No	No	No	No	
TOTALS	Channel 1	Channel 2	Channel 3	Channel 4	
Good - 7	1	2	4	0	
Fair - 10	3	2	1	4	
Poor - 41	12	11	9	9	
No - 30	6	7	8	9	
Lines - 88	22	22	22	22	

4.9.5 Spectral Analysis of Surface Waves Results from Marion Structure Number 100-0005

The theoretical and experimental dispersion curves determined by the spectral analysis of surface waves testing is shown in Appendix D, Figure D-10. Spectral analysis of surface waves (SASW) tests were performed in a line by corehole 2. The SASW results indicate surface wave velocities of 2,250 to 4,000 feet per second (686 to 1219 m/s) for the asphalt overlay and 6,700 feet per second (2070 m/s) for the concrete deck. These velocities correspond to impact-echo compression wave velocities of 4,000 to 7,200 feet per second (1219 to 2195 m/s) for asphalt and 13,000 feet per second (3962 m/s) for the concrete. Weighting the SASW compression wave velocities for 2 inch (50.8 mm) asphalt and 8 inch (203.2 mm) concrete thicknesses produces an average deck velocity of approximately 11,300 feet per second (3444 m/s), relatively comparable to the measured, average impact-echo compression wave velocity of 11,700 feet per second (3566 m/s) at the two coreholes. The good phase data of the SASW tests confirms good asphalt/concrete bonding to form a solid section near corehole 2.

4.10 Summary of All Results

This section presents the combined results of all test methods for each bridge. Table 4.19 summarizes the total area of delaminations for all bridge decks. The chain drag survey found 12383.0 ft² (1150.4 m²) of rehabilitation area, 13.0% of the total area of all the decks. The infrared thermography survey found 8748.9 ft² (812.8 m²) of rehabilitation area, 9.2% of the total area of all the decks. The ground penetrating radar survey found 13993.4 ft² (1300.0 m²) of rehabilitation area, 14.7% of the total area of all the decks.

Table 4.20 summarizes the total number of individual delaminations found for all bridge decks, excepting Bloomington Structure Number 057-0088 and Marion Structure Number 100-0005. The chain drag survey found 179 total individual delaminations. The infrared thermography survey found 66 total individual delaminations, 36.9% of the number found by chain drag. The ground penetrating radar survey found 91 total individual delaminations, 50.8% of the number found by chain drag.

Table 4.21 summarizes the total number of major delaminations found for all bridge decks, excepting Bloomington Structure Number 057-0088 and Marion Structure Number 100-0005. Major delaminations are those of at least 10 ft² (0.93 m²). The chain drag survey found 22 major individual delaminations. The infrared thermography survey found 15 major individual delaminations, 68.2% of the number found by chain drag. The ground penetrating radar survey found 15 major individual delaminations, 77.3% of the number found by chain drag.

Table 4.19 Areas of proposed rehabilitation for all bridge decks.

Test Method	Rehabilitation Area (ft ²) (m ²)	$\frac{\text{Rehabilitation Area}}{\text{Total Bridge Deck Area}} \times 100$
Chain Drag	12383.0 (1150.4)	13.0%
Infrared Thermography	8748.9 (812.8)	9.2%
Ground Penetrating Radar	13993.4 (1300.0)	14.7%

Table 4.20 Number of individual delaminations for all bridge decks except Bloomington Structure Number 057-0088 and Marion Structure Number 100-0005.

Test Method	Number of Individual Delaminations Found	Percent of Delaminations Found by Chain Drag
Chain Drag	179	100%
Infrared Thermography	66	36.9%
Ground Penetrating Radar	91	50.8%

Table 4.21 Number of major delaminations (minimum 10 ft²) for all bridge decks, excepting Bloomington Structure Number 057-0088 and Marion Structure Number 100-0005.

Test Method	Number of Individual Delaminations Found	Percent of Delaminations Found by Chain Drag
Chain Drag	22	100%
Infrared Thermography	15	68.2%
Ground Penetrating Radar	17	77.3%

5.0 DISCUSSION OF RESULTS

This chapter presents a discussion of the results given in the previous chapter. The section begins with an overview of results of each nondestructive test for bridge, and concludes with a discussion of the main issues involved with each testing method.

5.1 Discussion of Results from Bloomington Structure Number 057-0088

The chain drag survey of Bloomington Structure Number 057-0088 eastbound, Appendix A, Figure A-1, reveals the bridge deck to be in poor condition with numerous areas of delamination. Because of the extensive nature of the delaminations, individual delaminations are not marked and will not be used for comparison. A visual comparison between the results of the infrared thermography survey, Appendix B, Figure B-1, and the ground penetrating radar survey, Appendix C, Figure C-1 and Figure C-2, reveal both nondestructive testing methods found large areas of delamination and deterioration in the same vicinity as the chain drag survey. For example, the southern edge of the bridge is highly delaminated, determined by both thermography and radar.

Infrared thermography could not adequately inspect the longitudinal and transverse joints of the bridge due to the extensive asphalt patching. Areas of small, subsurface concrete patches could not be effectively inspected as the area did not provide sufficient contrast with the surrounding pavement. Ground penetrating radar was unaffected by surface or subsurface patching, but did miss some delaminations on the north edges of the deck, particularly in the northwest corner. The radar survey indicates there is some scaling along the steel joints in the deck. Infrared thermography proposes 21.1% of the bridge deck needs rehabilitation and ground penetrating radar proposes 28.5% of the bridge deck needs rehabilitation. The chain drag survey

found 32.6% of the deck needs rehabilitation, the amount actually removed. The low estimates by the nondestructive testing methods are probably caused by their closer boundary delineations for the delaminated areas than the chain drag survey. Additionally, portions of the deck could not be adequately inspected by the infrared inspection due to patching.

The chain drag survey of Bloomington Structure Number 057-0088 westbound, Appendix A, Figure A-2, reveals the bridge deck to be in poorer condition than the eastbound side with numerous areas of delamination. Because of the extensive nature of the delaminations, individual delaminations are not marked and will not be used for comparison. A visual comparison between the results of the infrared thermography survey, Appendix B, Figure B-1, and the ground penetrating radar survey, Appendix C, Figure C-3 and Figure C-4, reveal both nondestructive testing methods found large areas of delamination and deterioration in the same vicinity at the chain drag survey. For example, the northern edge of the bridge is highly delaminated, determined by both thermography and radar.

Infrared thermography could not adequately inspect the longitudinal and transverse joints of the bridge due to extensive asphalt patching. Areas of small, subsurface concrete patches could not be effectively inspected as the area did not provide sufficient contrast with the surrounding pavement. Ground penetrating radar was unaffected by the surface or subsurface patching, but did miss some rather large regions of delamination on the north edges of the deck, particularly in the center. Infrared thermography proposes 32.4% of the bridge deck needs rehabilitation and ground penetrating radar proposes 23.7% of the bridge deck needs rehabilitation. The chain drag survey found 37.7% of the deck needs rehabilitation, the amount actually removed. The low estimates by the nondestructive testing methods are probably caused by their closer boundary delineations for the delaminated areas than the chain drag survey.

Additionally, portions of the deck could not be adequately inspected by the infrared inspection due to patching.

5.2 Discussion of Results from Peoria Structure Number 090-0118

The chain drag survey of Peoria Structure Number 090-0118, Appendix A, Figure A-3, reveals the bridge deck to be in excellent condition, with only one area of delamination. This bridge deck did not have an asphalt overlay on it; it was bare concrete. The infrared thermography survey, Appendix B, Figure B-2, reveals no areas of delamination. The ground penetrating radar survey, Appendix C, Figure C-5, shows numerous areas of delamination, including the one found by chain dragging, indicating the radar survey falsely identified a large number of delaminated areas. The radar results suggest 4.2% of the deck is delaminated, a high figure compared to the chain drag and infrared results. This is unusual, particularly for a deck without an overlay. One possible explanation is the grooving in the surface of the deck (which provides better traction) which possibly scattered the radar signal.

5.3 Discussion of Results from Peoria Structure Number 072-0106

The chain drag survey of Peoria Structure Number 072-0106, Appendix A, Figure A-4, reveals the bridge deck to be in good condition, with 15 areas of delamination. A visual comparison between the results of the infrared thermography survey, Appendix B, Figure B-3, and the ground penetrating radar survey, Appendix C, Figure C-6 and Figure C-7, indicates both nondestructive testing methods missed a majority of the delaminated regions. Infrared thermography found one of 15 individual delaminations, while ground penetrating radar found 2 of 15. The radar survey has falsely identified regions of delamination and scaling mainly along

the steel joints in the deck, suggesting that the presence of the steel joint has adversely effected the radar signal. The one delamination found by both tests was the largest on the deck at 12 ft² (1.1 m²). The radar may have missed the other delaminations if they were small enough to pass between the antennas. Thermography may have missed the other delaminations if the temperature contrast was too small to detect, or thermography may have misidentified the delaminations as debonds.

5.4 Discussion of Results from Peoria Structure Number 072-0107

The chain drag survey of Peoria Structure Number 072-0107, Appendix A, Figure A-5, reveals the bridge deck to be in fair condition, with 46 areas of delamination. A visual comparison between the results of the infrared thermography survey, Appendix B, Figure B-4, and the ground penetrating radar survey, Appendix C, Figure C-8 and Figure C-9, indicate both nondestructive testing methods missed a majority of the delaminated regions. Infrared thermography found 20 of 46 individual delaminations, while ground penetrating radar found 17 of 46 delaminated regions. Infrared thermography found both delaminations which were greater than 10 ft² (0.93 m²), while ground penetrating radar found one of two. The radar survey falsely identified regions of delamination and scaling, primarily along the steel joints in the deck, suggesting that the presence of the steel joint has adversely affected the radar signal. The radar may have missed the other delaminations if they were small enough to pass between the antennas. Thermography may have missed the other delaminations if the temperature contrast was too small to detect, or thermography may have misidentified the delaminations as debonds. Infrared thermography could not adequately inspect the asphalt patching on the deck, identifying some areas to be rehabilitated where the chain drag survey found nothing. Chain drag and

infrared were in close agreement concerning the total area to be rehabilitated, 3.1% and 2.7%, respectively. Radar was quite high, proposing 9.7% of the area as delaminated, mainly due to the misidentification of areas around steel joints.

5.5 Discussion of Results from Peoria Structure Number 072-0108

The chain drag survey of Peoria Structure Number 072-0108, Appendix A, Figure A-6, reveals the bridge deck to be in good condition with 3 areas of delamination. A visual comparison between the results of the infrared thermography survey, Appendix B, Figure B-5, and the ground penetrating radar survey, Appendix C, Figure C-10 and Figure C-11, indicate the infrared diagnosis was the better of the two. Infrared thermography found one of 3 individual delaminations, while ground penetrating radar found 2 of 3. However, ground penetrating radar misidentified large areas as being delaminated which were in good condition. Infrared thermography found one of 2 delaminations greater than 10 ft² (0.93 m²), while ground penetrating radar found both. The radar survey falsely identified regions of delamination and scaling, primarily along the steel joints in the deck, suggesting that the presence of the steel joint has adversely affected the radar signal. Thermography may have misidentified the delaminations as debonds. Chain drag and infrared were in close agreement concerning the total area to be rehabilitated, 0.4% and 0.07%, respectively. Radar was quite high, proposing 7.7% of the area as delaminated, mainly due primarily to the misidentification of areas around the steel joints.

5.6 Discussion of Results from Peoria Structure Number 072-0109

The chain drag survey of Peoria Structure Number 072-0109, Appendix A, Figure A-7, reveals the bridge deck to be in good condition, with 12 areas of delamination. A visual

comparison between the results of the infrared thermography survey, Appendix B, Figure B-6, and the ground penetrating radar survey, Appendix C, Figure C-12 and Figure C-13, indicate that radar had the better diagnosis. Infrared thermography found 0 of 12 individual delaminations, while ground penetrating radar found 8 of 12. Ground penetrating radar located the one delamination greater than 10 ft² (0.93 m²). The radar survey falsely identified regions of delamination and scaling primarily along the steel joints in the deck, suggesting the presence of the steel joint adversely affected the radar signal. The radar may have missed the other delaminations if they were small enough to pass between the antennas. Thermography may have missed the delaminations if the temperature contrast was too small to detect, or thermography may have misidentified the delaminations as debonds. Chain drag and infrared were not in close agreement concerning the total area to be rehabilitated, 0.8% and 0%, respectively. Radar was quite high, proposing 4.6% of the area was delaminated, primarily due to the misidentification of areas around the steel joints.

5.7 Discussion of Results from Peoria Structure Number 072-0110

The chain drag survey of Peoria Structure Number 072-0110, Appendix A, Figure A-8, reveals the bridge deck to be in fair condition with 46 areas of delamination. A visual comparison between the results of the infrared thermography survey, Appendix B, Figure B-7, and the ground penetrating radar survey, Appendix C, Figure C-14 and Figure C-15, indicates infrared had the better diagnosis of the bridge deck. Infrared thermography found 23 of 34 individual delaminations, while ground penetrating radar found 15 of 34 delaminated regions. Infrared thermography and ground penetrating radar found the one delamination greater than 10 ft² (0.93 m²). The radar survey falsely identified regions of delamination and scaling, primarily

along the steel joints in the deck, suggesting that the presence of the steel joint adversely affected the radar signal. The radar may have missed the other delaminations if they were small enough to pass between the antennas. Thermography may have missed the other delaminations if the temperature contrast was too small to detect, or thermography may have misidentified the delaminations as debonds. Chain drag and infrared were in close agreement concerning the total area to be rehabilitated, 1.9% and 1.5%, respectively. Radar was quite high, proposing 4.5% of the area as being delaminated, mainly due to the misidentification of areas around the steel joints.

5.8 Discussion of Results from Peoria Structure Number 072-0111

The chain drag survey of Peoria Structure Number 072-0111, Appendix A, Figure A-9, reveals the bridge deck to be in poor condition, with 68 areas of delamination. A visual comparison between the results of the infrared thermography survey, Appendix B, Figure B-8, and the ground penetrating radar survey, Appendix C, Figure C-16 and Figure C-17, indicates radar had the better diagnosis of the bridge deck. Infrared thermography found 21 of 68 individual delaminations, while ground penetrating radar found 46 of 68 delaminated regions. Infrared thermography found 9 of 14 of the delaminations greater than 10 ft² (0.93 m²), and radar found 10 of 14. The radar survey falsely identified regions of delamination and scaling, primarily along the steel joints in the deck, suggesting that the presence of the steel joint adversely affected the radar signal. The radar may have missed the other delaminations if they were small enough to pass between the antennas. Thermography may have missed the other delaminations if the temperature contrast was too small to detect, or thermography may have misidentified the delaminations as debonds. Chain drag and infrared were in close agreement concerning the total area to be rehabilitated, 4.4% and 3.7% respectively. Radar was quite high,

proposing 14.2% of the area as being delaminated, mainly due to the misidentification of areas around the steel joints.

5.9 Discussion of Results from Marion Structure Number 100-0005

The chain drag survey of Marion Structure Number 100-0005, Appendix A, Figure A-10, reveals the bridge deck to be in poor condition with numerous areas of delamination. These results may not be completely accurate as the asphalt overlay was never removed from the deck. Due to the extensive nature of the delaminations, individual delaminations are not marked and will not be used for comparison. A visual comparison between the results of the infrared thermography survey, Appendix B, Figure B-9, and the ground penetrating radar survey, Appendix C, Figure C-18 and Figure C-19, indicates both nondestructive testing methods located large areas of delamination and deterioration in the same vicinity as the chain drag survey. For example, the southern end of the bridge is highly delaminated, shown by thermography and radar.

Infrared thermography could not adequately inspect the concrete surface patches as the small area did not provide sufficient contrast with the surrounding pavement. Ground penetrating radar was unaffected by the surface patching, but did miss some delaminations along the extreme eastern and western edges of the deck. The radar survey indicates there is some scaling in the southwest corner of the deck. Infrared thermography proposes 23.5% of the bridge deck needs rehabilitation and ground penetrating radar proposes 43.6% of the bridge deck needs rehabilitation. The chain drag survey determined 41.6% of the deck needs rehabilitation, in close agreement with the radar results. The low estimates by the nondestructive testing methods are probably caused by their closer boundary delineations for the delaminated areas than the chain

drag survey. Additionally, portions of the deck could not be adequately inspected by the infrared inspection due to patching.

The following discussion paragraphs are provided by the Olson final report⁸⁹. Examples handheld impact-echo records are presented for coreholes 1 and 2 in Figure D-2 and Figure D-3 (see Figure D-1 for approximate locations of coreholes). Review of these records reveal similar time domain responses (top traces of each figure), individual displacement spectra (center traces), and averaged spectra (bottom traces). The thickness echo frequency peaks are 7031 Hz each, corresponding to an average impact-echo compression wave velocity of 11,700 feet per second (3566 m/s) for the nominally 10 inch (254 mm) thick deck, as shown for the spectral calculations in the figures. No higher frequencies are present to indicate shallow cracking or potential debonding of the overlay, nor are low frequency echo peaks present to indicate overlay debonding or shallow concrete delamination. Results indicate the deck sections are sound for tests around the coreholes, agreeing with visual inspection, infrared thermography, and ground penetrating radar. The velocity of 11,700 feet per second (3566 m/s) is an average deck velocity reflecting the slower velocity of 2 inches (50.8 mm) of hot asphalt on 8 inches (203.2 mm) of faster velocity concrete.

The handheld impact-echo unit was used to perform 2 tests every foot (0.30 m) along east scan line 1, transducer channel 2 of the impact-echo scanner test line as shown in Figure D-1. The dominant frequency echo thickness (0 to 40 inches [1016 mm] on the horizontal scale) versus distance plots (in feet on the vertical scale) are presented in Figure D-4 for 0 to 31.5 feet (9.6 m) and in Figure D-5 for 32 to 80 ft (9.75 to 24.3 m). Review of Figure D-4 indicates that approximately half of the points show corresponding to the nominal thickness of 10 inches (254 mm), indicating sound deck conditions and bonded asphalt/concrete. Other areas of significantly

greater thickness are indicative of either debonded overlay conditions or shallow delaminations within the concrete deck. The area of greatest low frequency, large thickness, and high spectral energy (see bottom scale in volt-microseconds, $V\mu S$) occurred between 24 and 28 feet (7.32 and 8.53 m) suggesting severe debonding or delamination conditions. Review of Figure D-5 reveals that approximately 80% of the tests performed along the 32 to 80 feet (9.75 to 24.4 m) distance found solid, 10 inch (254 mm) thick concrete. There are 5 areas of apparently greater thickness, indicating potential debonding or delamination conditions. The results agree with infrared thermography and ground penetrating radar inspections. In both figures the variation from the nominal 10 inch (254 mm) thickness (based on an average impact-echo compression wave velocity of 11,700 feet per second [3566 m/s]) is typically less than 1 inch (25.4 mm).

The impact-echo scanner test line locations and labels are shown in Figure D-1. The impact-echo scanner was originally developed for scanning smooth, pre-stressed, concrete cylinder pipe on a U.S. Bureau of Reclamation research project. It was later adapted as a prototype floor slab scanner for smooth concrete surfaces. One of the objectives of this feasibility research was to gain data on the effects of rough to very rough asphalt on impact-echo scanner data quality. It was expected that the data quality may be severely degraded if good contact could not be maintained between the water-coupled rolling transducer wheel and the test surface.

An example of a good quality displacement spectra record from a rolling transducer scan is presented in Figure D-6. The record shows a dominant echo peak at 7610 Hz, corresponding to a thickness echo of 9.23 inches (234 mm) using the average compression wave velocity of 11,700 feet per second (3566 m/s). This record provides a clearly identifiable thickness echo

corresponding to sound deck conditions at this location. However, significant portions of the records were of poor quality, and Figure D-7 has no clearly identifiable echo peak. The transducer appears to have bounced, as there is considerable energy at frequencies above 12.5 kHz, compared to Figure D-6, with almost no energy above 12.5 kHz. The current impact-echo analysis software chooses the three largest amplitude echo peaks, and the largest is selected to calculate the thickness (or depth) of the echo. Depth significantly exceeding the actual thickness indicates high amplitude, lower frequency, flexural resonance that typically corresponds to debonded overlay or delaminated concrete. Echo depths between 5 and 9 inches (127 and 229 mm) indicate a crack in the deck. A thickness echo may be present if the crack is closed, but not a low frequency echo peak indicative of the flexural response of a debond or delamination.

Representative good and poor impact-echo scanner plots of thickness and energy vs. depth are presented in Figure D-8 and Figure D-9, respectively. Review of the good thickness plot in Figure D-8 shows an average thickness of 10 inches (254 mm), with some thinner areas due to potentially deeper cracking and thicker areas of potential debonding or delamination. However, the poor consistency thickness plot in Figure D-9 shows significant scatter, and few consistent thicknesses of 10 inches (254 mm). Review of displacement spectra records indicate some of poor quality, Figure D-9, and some of comparatively good quality, Figure D-8. The plot in Figure D-9 is for the same scan line because Figure D-4 and Figure D-5 for the handheld impact-echo unit. Unfortunately, no data comparison was possible with the handheld unit results as the scanner data in Figure D-9 is of poor quality.

The 88 impact-echo scanner test lines were qualitatively evaluated for consistency of nominal 10 inch (254 mm) thickness as "good", "fair", "poor" and "no" consistency with respect to the expected 10 inch (254 mm) thickness echoes. The results are summarized in Table 4.18.

Of 88 scan lines tested, 7 lines had good results representative of the 10 inch (254 mm) deck thickness. Fair results, with a significant percentage of 10 inch (254 mm) thickness echoes, were obtained from 10 scan lines. Poor results with minimum percentage of 10 inch (254 mm) thickness echoes were obtained from 41 scan lines. No consistent 10 inch (254 mm) thicknesses were obtained from 30 of the scan lines.

It is impractical to review all of the data without the use of software programs because over 18,000 impact-echo tests were performed with the impact-echo scanner system. The majority of data was scanned for the dominant echo peaks between 0 and 25,000 Hz. A few plots were scanned from 2,000 Hz to 25,000 Hz where low frequency noise corrupted the data. Consequently, noise due to poor coupling of the rolling transducers at the time of measurement may have resulted in many false, misleading, high amplitude spectral frequency echo peaks. It is believed that rough to very rough surfaces caused the poor to no consistent 10-inch (254 mm) thickness echo data. Where good to fair 10-inch (254 mm) thickness echo results were obtained, the deck appeared to have a comparatively smoother, but still somewhat rough asphalt overlay surface, Figure D-1. Enough inconsistencies remain in the thicknesses of good and fair impact-echo scanner lines that it is not possible to predict debonding and delamination damage in the deck with confidence.

5.10 Discussion of Results from All Bridges

Table 4.19 displays the total proposed rehabilitation area for all bridge decks as determined by chain drag, infrared thermography, and ground penetrating radar. Chain drag found 13.0% of the total area inspected for all bridge decks in need of repair. This compares

with 9.2% from infrared and 14.7% from radar. Though radar was closer numerically to chain drag than infrared, many instances of false delamination were reported.

Table 4.20 displays the number of delaminations found by each nondestructive testing method as a percentage of the number of delaminations detected by chain drag. Infrared thermography found 36.9% of the delaminations found by chain drag, radar found 50.8%. Each delamination reported by chain drag was verified when the site contractor removed the concrete with a jackhammer. The success rate for the nondestructive tests was lower than anticipated and lower than similar studies have found. A probable cause for the low success rates is the small size (less than 10 ft²) of the majority of delaminations found over the nine bridge decks. Table 4.21 lends credence to this theory. The success rate for major delaminations (minimum 10 ft²) is 68.2% for infrared and 77.3% for radar, a dramatic improvement over the detection rate for all delaminations. Infrared and radar also performed better on the Bloomington Structure Number 057-0088 and Marion Structure Number 100-0005 bridge decks. These decks have large, continuous areas of delamination.

The scanner results indicate that the impact-echo test method has potential to evaluate the state of damage in concrete bridge decks if two key problems identified during this study are overcome. First, the scanner needs to be re-designed to allow consistent impacts and coupling between the rolling transducers and the rough to very rough concrete and asphalt surfaces. This was the single largest factor which caused only 17 of 88 scan lines to have fair to good quality 10 inch (254 mm) thickness echo data. Second, based only on the impact-echo results, it is currently unclear as to whether the low frequency, high amplitude response in the data is due to concrete delamination or debonding of the asphalt overlay. The use of very high frequency impacts to inspect shallow depths of 1 to 2 inches (25.4 to 50.8 mm) would help the test. High pass filtering

of the data may be another solution. It may be necessary to perform simultaneous impact-echo and spectral analysis of surface waves scanning in order to confidently predict the existence and extent of delaminations in overlaid decks.

The amount and type of information available from impact-echo data is promising. Current research indicates that aggregate gradation curves and base support conditions can be determined from new impact-echo data processing techniques^{90,91}. Furthermore, a handheld impact-echo device could be developed which would perform the same function currently done by chain dragging, but with far greater accuracy. Impact-echo tests performed on the bridge deck without the asphalt overlay would solve the problems of coupling and repeatable impacting.

5.11 Discussion of Major Issues in Nondestructive Testing of Bridge Decks

This section presents a discussion of the most relevant issues in nondestructive testing of bridge decks. The issues presented draw upon information gained from literature, theory, expert knowledge, and field testing experience.

Repeatability of testing is the ability of each test to produce the same results over the same test area. Ground penetrating radar is very repeatable, provided the movement of moisture in the bridge deck is minimal. Infrared thermography is repeatable provided solar conditions are consistent. Testing performed during different conditions may produce different results. Impact-echo is somewhat repeatable. Individual aggregate particles lead to inconsistent impacts and inconsistent coupling of the transducers to the surface of the overlay.

Sensitivity of testing is the ability of each test to detect a delamination of a given severity. Ground penetrating radar and infrared thermography easily detect large delaminated areas having wide crack widths. Smaller, deeper, delaminated areas, less than 10 ft² (0.93 m²), are more

difficult for these methods, particularly infrared thermography. Impact-echo should theoretically detect even the smallest defect because of its characteristic of high degree location identification. The theoretical limitation of detectable crack separation width is small compared to practical requirements.

The ability of each test to detect defects of varying orientation is an important consideration in inspecting concrete bridge decks. All three tests are unable to detect defects oriented perpendicularly to the pavement surface. An angular defect may be detectable by ground penetrating radar, but there would be a limit to the detectable angle as a greater portion of the radar energy is scattered away from the receiving antenna. A similar phenomenon would occur for impact-echo, with more stress wave energy scattered away from the receiving transducer at greater defect angles. Infrared thermography can detect defects at an angle; although hotter than the surrounding pavement, they would appear to have a temperature gradient across their surface.

Another important consideration is the ability of each test to inspect layered media and determine flaw depth. Ground penetrating radar and impact-echo can easily inspect multi-layered systems and determine flaw depth as well as layer thicknesses. Infrared thermography can not determine flaw depth.

The ability of each test to detect shallow versus deep delaminations and distinguish debonding of the asphalt overlay from shallow delaminations is another important consideration. Ground penetrating radar detects shallow and deep delaminations with equal accuracy. Because depth is precisely determined, there is no confusion between shallow delaminations and debonding. Additionally, ground penetrating radar results distinguished surface scaling of the concrete deck from delaminations. Impact-echo theoretically detects shallow and deep

delaminations with equal accuracy. Practically, impact-echo is often unable to distinguish between debonding and shallow delaminations because the dominant mode of vibration is flexural. Flexural vibrations have a low frequency and dominate the response of shallow delaminations and debonds. Infrared thermography theoretically cannot distinguish a shallow delamination from a debond. Practically, the two can be distinguished by noting certain particular characteristics, such as size and shape, and by cross correlating with core samples. Only ground penetrating radar can inspect a concrete deck for delaminations with a debonded asphalt layer. Debonding of the asphalt layer prevents inspection of the underlying concrete by infrared thermography and impact-echo. Chapter 3 discusses this issue in greater depth.

Each test is susceptible to reporting false delaminations to some degree. Infrared thermography reported few false indications of delaminations. The majority of errors were on the conservative side, mis-identifying delaminations as debonds. Ground penetrating radar reported a large number of delaminations where none were found by chain drag or visual inspection. Impact-echo, having difficulty distinguishing debonding from delamination, reported many false indications.

Each test estimated the total area of repair needed for each bridge deck. On the decks where there were large areas of delamination, both ground penetrating radar and infrared thermography did well estimating total rehabilitation area. On the decks with small, individual delaminated areas, infrared thermography frequently underestimated the total area in need of repair and ground penetrating radar tended to overestimate the total area in need of repair.

The presence of reinforcing steel in the bridge decks has little effect on the tests. Reinforcing steel has no effect on infrared thermography. Ground penetrating radar can detect

the presence of reinforcing steel and determine its depth. Impact-echo can also detect and determine the depth of reinforcing steel.

Steel abutment joints effects some of the tests. Steel abutment joints have very little effect on infrared thermography and impact-echo. The results of this test indicate ground penetrating radar is affected by steel abutment joints. There is a high incidence of false indications surrounding the steel joints. As the antenna approaches the steel joints, the radar pulse may be distorted by the presence of the large amount of ferrous material.

Before testing can begin, surface preparation needs to be considered. Infrared thermography requires a surface free of dirt and large areas of debris. Wet pavement surfaces cannot be tested. Impact-echo needs a surface free of large rocks allowing the transducers to roll smoothly across the asphalt. Ground penetrating radar requires no surface preparation. Chapter 3 discusses this issue in greater depth.

Weather conditions must be evaluated prior to testing. Infrared thermography requires a clear, sunny day; rain or snow prevents infrared inspection. The best conditions for infrared inspection are cool nights followed by warm, sunny days. Impact-echo inspection requires no special weather considerations assuming heavy rain does not damage the electrical equipment. Ground penetrating radar can be performed in most conditions provided rain or snow is not collecting on the bridge deck. Chapter 3 discusses this issue in greater depth.

Each test has a different inspection speed. Impact-echo, due to the prototypical nature of the inspection equipment, usually requires a day to inspect a typical bridge deck. Infrared thermography can inspect a deck in one to two hours. Ground penetrating radar can inspect a bridge in less than an hour. These time estimates do not include the time required for data processing. During all inspections, the lanes were closed to traffic, and the inspection rate was

no greater than 5 mph (8.05 kph). The field inspectors for infrared and radar state that inspections can be performed at normal traffic speeds without lane closings. This would almost certainly result in a degradation in data quality.

Vibrations caused by traffic has little effect on any of the three tests. Impact-echo uses a simple high-pass filter to filter out the low frequency vibrations averaging 10 Hz.

The sampling resolution is the number of data points taken for a given inspection length. During impact-echo testing, a sample point was taken once approximately every 3 inches (76.2 mm). There was a one foot (0.30 m) spacing between each line of testing. For ground penetrating radar inspection, a waveform was digitized approximately once every 3 to 6 inches (76.2 to 152.4 mm), with a 3 foot (0.91 m) spacing between antennas. Infrared thermography provided a full field digitized view of the pavement with a temperature measurement of at least 0.5 inch (12.7 mm) resolution.

The ability of each test to accurately pinpoint the location of each delamination for subsequent repair is another important consideration. Both infrared thermography and ground penetrating radar measured distance from the drive train of the inspection vehicle. From comparison with the chain drag results, the distances could have been off by as much as 2 feet (0.61 m) depending upon where the zero location was marked. Skewed abutments also added to the error. Lateral distances could also be off a few feet as the driver may have chosen to follow lane markings which merged with other lanes. Impact-echo used a small distance wheel mounted on the front of the testing apparatus which may be inaccurate due to weaving during testing or going over rocks.

6.0 CONCLUSIONS AND RECOMMENDATIONS FOR FUTURE WORK

This chapter briefly lists the major findings of this study based upon information gathered from literature, theory, expert opinion, and field comparison. The field comparison results are based upon this study only and are not necessarily indicative of all situations.

Infrared thermography provides certain advantages for nondestructive inspection of concrete bridge decks. Infrared provides a full field view of the bridge deck. There is no sampling during data collection; resolution is limited only by the digitization of the camera. Infrared can provide accurate size and shape delineation of large areas of delamination. Boundaries can be determined accurately to within 1 inch (25.4 mm) or less. Infrared is relatively quick. A three lane, 300 foot (91.4 m) bridge can be inspected in less than an hour. Infrared is most accurate for large delaminations. In this study, infrared gave very few false indications of delaminated concrete.

Infrared thermography has certain disadvantages for nondestructive inspection of concrete bridge decks. Infrared cannot make a determination of flaw depth, thereby making discernment between delaminations and debonds challenging. Infrared cannot accurately inspect small surface or subsurface regions which have been patched with asphalt or concrete. Infrared has specific weather criteria in which testing is not viable during periods of adverse weather including cloudiness or precipitation. In addition, inspection can only reliably be performed between the hours of 10 a.m. and 4 p.m. Infrared is adversely affected by several surface conditions such as debris, moisture, wearing, discoloration, and crack sealant. In this study, infrared proved susceptible to underestimating the total area of the bridge deck in need of repair.

Ground penetrating radar provides certain advantages for nondestructive inspection of concrete bridge decks. Radar provides accurate depth information, allowing easy discernment

between delaminations and debonds. Radar inspection can be performed at any time during the day or night. Radar inspection is very fast. A three lane, 300 ft (91.4 m) bridge can be inspected in less than half an hour. Radar is not affected by the majority of adverse surface conditions.

Ground penetrating radar has certain disadvantages for nondestructive inspection of concrete bridge decks. Radar does not provide a full field view. It requires a discrete antenna spacing and is limited by the speed of the data collection wave digitizer. Radar is sensitive to moisture in the bridge deck, and standing pools of water prevent deck inspection. Radar has shown in this study to overestimate the amount of deterioration in bridge decks and gives false indications of damaged concrete. This is particularly evident around steel joints and abutments. However, the accuracy of ground penetrating radar can be improved by using a larger number of antennas, i.e., four or five antennas instead of three as in this study.

Impact-echo provides certain advantages for nondestructive inspection of concrete bridge decks. Impact-echo provides accurate depth information, allowing easy discernment between delaminations and debonds. Impact-echo inspection can be performed at any time during the day or night. Impact-echo is not affected by most adverse weather conditions, including standing water on the deck. Future impact-echo data analysis techniques will provide information on characteristics of the quality of the concrete such as ground support⁹⁰, gradation⁹¹, strength, and durability.

Impact-echo has certain disadvantages for nondestructive inspection of concrete bridge decks. Impact-echo is not a full field view. It requires a point by point data collection system. Impact-echo is adversely affected by debris, crack sealant, surface roughness, and other irregularities on the surface of the deck. Impact-echo equipment for pavement inspection is in

the early stages of development. Future work needs to be done on data collection systems designed for field use. Current systems are too slow for practical use.

Based upon the major points listed above, the following generalizations are made. Infrared thermography performs best on bridges with large areas of delamination. In this study, it underestimated the amount of concrete needed to be replaced for adequate rehabilitation. Ground penetrating radar is more proficient at finding smaller areas of delamination. However, radar falsely reported delaminations in this study. Infrared thermography and ground penetrating radar are widely used, proven methods for rapid delamination detection in concrete bridge decks. Impact-echo, although showing promise in determining areas in need of rehabilitation, needs further development of field inspection equipment to make bridge inspection practical. The main limitation of the impact-echo method in this application is its inability to inspect the underlying concrete for delaminations under a debonded portion of the asphalt overlay in a bridge deck. While this limitation could potentially be overcome by inspecting the bridge deck from the bottom side, it would clearly be cumbersome. Further development of the impact-echo method may provide information the other two methods do not. For example, on-going research to further develop the impact-echo test method already indicates strong potential to provide information regarding segregation of asphalt concrete as well as its dynamic material properties, i.e., complex moduli. It has also potential to provide information regarding the gradation in Portland cement concrete as well as the intimacy of contact at the interface between concrete pavements and the supporting subgrade layer. Future development of impact-echo testing equipment may provide a reliable replacement for chain dragging as an inspection technique for bridge decks with and without asphalt overlays. It is recommended that a combination of

infrared thermography and ground penetrating radar be used for the most accurate inspection of bridge decks, and impact-echo be further developed .

REFERENCES

1. Sansalone, M., and Carino, N. J., "Impact-echo: A method for flaw detection in concrete using transient stress waves," *National Bureau of Standards*, Gaithersburg, Md., Sept. 1986.
2. Sansalone, M., and Carino, N. J., "A point source-point receiver, pulse-echo technique for flaw detection in concrete," *ACI Materials Journal*, March-April 1986, pp. 199-208.
3. Sansalone, M., and Carino, N. J., "Impact-echo method," *Concrete International*, April 1988, pp. 38-46.
4. Sansalone, M., and Carino, N. J., "Stress wave propagation methods," *CRC Handbook on Nondestructive Testing of Concrete*, pp. 275-304.
5. Sansalone, M., and Carino, N. J., "Transient impact response of plates containing flaws," *Journal of Research of the National Bureau of Standards*, Vol. 92, No. 6, Nov.-Dec. 1987, pp. 369-381.
6. Sansalone, M., and Carino, N. J., "Transient impact response of thick circular plates," *Journal of Research of the National Bureau of Standards*, Vol. 92, No. 6, Nov.-Dec. 1987, pp. 355-367.
7. Sansalone, M., and Carino, N. J., "A finite element study of transient wave propagation in plates," *Journal of Research of the National Bureau of Standards*, Vol. 92, No. 4, July-Aug. 1987, pp. 267-278.
8. Sansalone, M., and Carino, N. J., "A finite element study of the interaction of transient stress waves with planar flaws," *Journal of Research of the National Bureau of Standards*, Vol. 92, No. 4, July-Aug. 1987, pp. 279-290.
9. Yiching, L., Sansalone, M., and Carino, N. J., "Finite element studies of the impact-echo response of plates containing thin layers and voids," *Journal of Nondestructive Evaluation*, Vol. 9, No. 1, 1990, pp. 27-47.
10. Sansalone, M., and Carino, N. J., "Detecting delamination in concrete slabs with and without overlays using the impact-echo method," *ACI Materials Journal*, March-April 1989, pp. 175-184.
11. Cheng, C. C., and Sansalone, M., "Effects on impact-echo signals caused by steel reinforcing bars and voids around bars," *ACI Materials Journal*, Sept.-Oct. 1993, pp. 421-434.

12. Lin, Y., and Sansalone, M., "Detecting flaws in concrete beams and columns using the impact-echo method," *ACI Materials Journal*, July-Aug. 1992, pp. 394-405.
13. Jiunn-Ming, L., and Sansalone, M., "The transverse elastic impact response of thick hollow cylinders," *Journal of Nondestructive Evaluation*, Vol. 12, No. 2, 1993, pp. 139-149.
14. Yiching, L., and Sansalone, M., "Transient response of thick circular and square bars subjected to transverse elastic impact," *Journal of the Acoustical Society of America*, Vol. 91, No. 2, Feb. 1992, pp. 885-893.
15. Jiunn-Ming, L., and Sansalone, M., "Impact-echo response of hollow cylindrical concrete structures surrounded by soil and rock: Part 1—numerical studies," *Geotechnical Testing Journal*, Vol. 17, No. 2, June 1994, pp. 207-219.
16. Jiunn-Ming, L., and Sansalone, M., "Impact-echo response of hollow cylindrical concrete structures surrounded by soil and rock: Part 2—experimental studies," *Geotechnical Testing Journal*, Vol. 17, No. 2, June 1994, pp. 220-226.
17. Cheng, C. C., and Sansalone, M., "Determining the minimum crack width that can be detected using the impact-echo method Part 1: Experimental study," *Materials and Structures*, Vol. 28, 1995, pp. 74-82.
18. Cheng, C. C., and Sansalone, M., "Determining the minimum crack width that can be detected using the impact-echo method Part 2: Numerical fracture analysis," *Materials and Structures*, Vol. 28, 1995, pp. 125-131.
19. Pessiki, S. P., and Carino, N. J., "Measurement of the setting time and strength of concrete by the impact-echo method," *National Bureau of Standards*, Gaithersburg, Md., July 1987.
20. Pessiki, S. P., and Carino, N. J., "Setting time and strength of concrete using the impact-echo method," *ACI Materials Journal*, Sept.-Oct. 1988, pp. 389-399.
21. Pessiki, S. P., and Johnson, M. R., "Nondestructive evaluation of early-age concrete strength in plate structures by the impact-echo method," *ACI Materials Journal*, May-June 1996, pp. 260-271.
22. Pessiki, S. P., and Johnson, M. R., "Nondestructive evaluation of in-place concrete strength in plate structures by the impact-echo method," *ATLSS Engineering Research Center*, Bethlehem, PA, Sept. 1993, pp. 260-271.
23. Pratt, D., and Sansalone, M., "Impact-echo signal interpretation using artificial intelligence," *ACI Materials Journal*, March-April 1992, pp. 178-187.

24. Popovics, J. S., and Rose, J. L., "A survey of developments in ultrasonic NDE of concrete," *IEEE Transactions on Ultrasonics, Ferroelectrics, and Frequency Control*, Vol. 41, No. 1, Jan. 1994, pp. 140-143.
25. Popovics, J. S., Rose, J. L., Popovics, S., Newhouse, V. L., Lewin, P., and Bilgutay, N., "Approaches for the generation of stress waves in concrete," *Experimental Mechanics*, March 1995, pp. 36-41.
26. Proctor, T. M. Jr., "An improved piezoelectric acoustic emission transducer," *Journal of the Acoustical Society of America*, Vol. 71, No. 5, May 1982, pp. 1163-1168.
27. Proctor, T. M. Jr., "Some details on the NBS conical transducer," *Journal of Acoustic Emission*, Vol. 1, No. 3, July 1982, pp. 173-178.
28. Proctor, T. M. Jr., "More recent improvements on the NBS conical transducer," *Journal of Acoustic Emission*, Vol. 5, No. 4, July 1986, pp. 134-142.
29. Greenspan, M., "The NBS conical transducer: Analysis," *Journal of the Acoustical Society of America*, Vol. 81, No. 1, Jan. 1987, pp. 173-183.
30. Sack, D. A., and Olson, L. D., "A comparison of the time and frequency domain performance of several impact echo transducers," *Olson Engineering, Inc. Technical Paper*.
31. Sack, D. A., and Olson, L. D., "Impact echo scanning of concrete slabs and pipes," *Olson Engineering, Inc. Technical Paper*.
32. Sack, D. A., and Olson, L. D., "Impact echo scanning of concrete and wood," *Olson Engineering, Inc. Technical Paper*.
33. Clemeña, G. G., "Survey of bridge decks with ground-penetrating radar -- a manual," Virginia Highway & Transportation Research Council, Charlottesville, VA, July 1985.
34. Clemeña, G. G., Sprinkel, M. M., and Long, R. R. Jr., "Use of ground-penetrating radar for detecting voids underneath a jointed concrete pavement," Virginia Highway & Transportation Research Council, Charlottesville, VA, May 1986.
35. Church, R. H., and Webb, W. E., "Evaluation of a ground penetrating radar system for detecting subsurface anomalies," U.S. Bureau of Mines, University, AL, 1986.
36. Alongi, A. J., Clemeña, G. G., and Cady, P. D., "Condition evaluation of concrete bridges relative to reinforcement corrosion," Strategic Highway Research Program, Washington, D.C., May 1992.

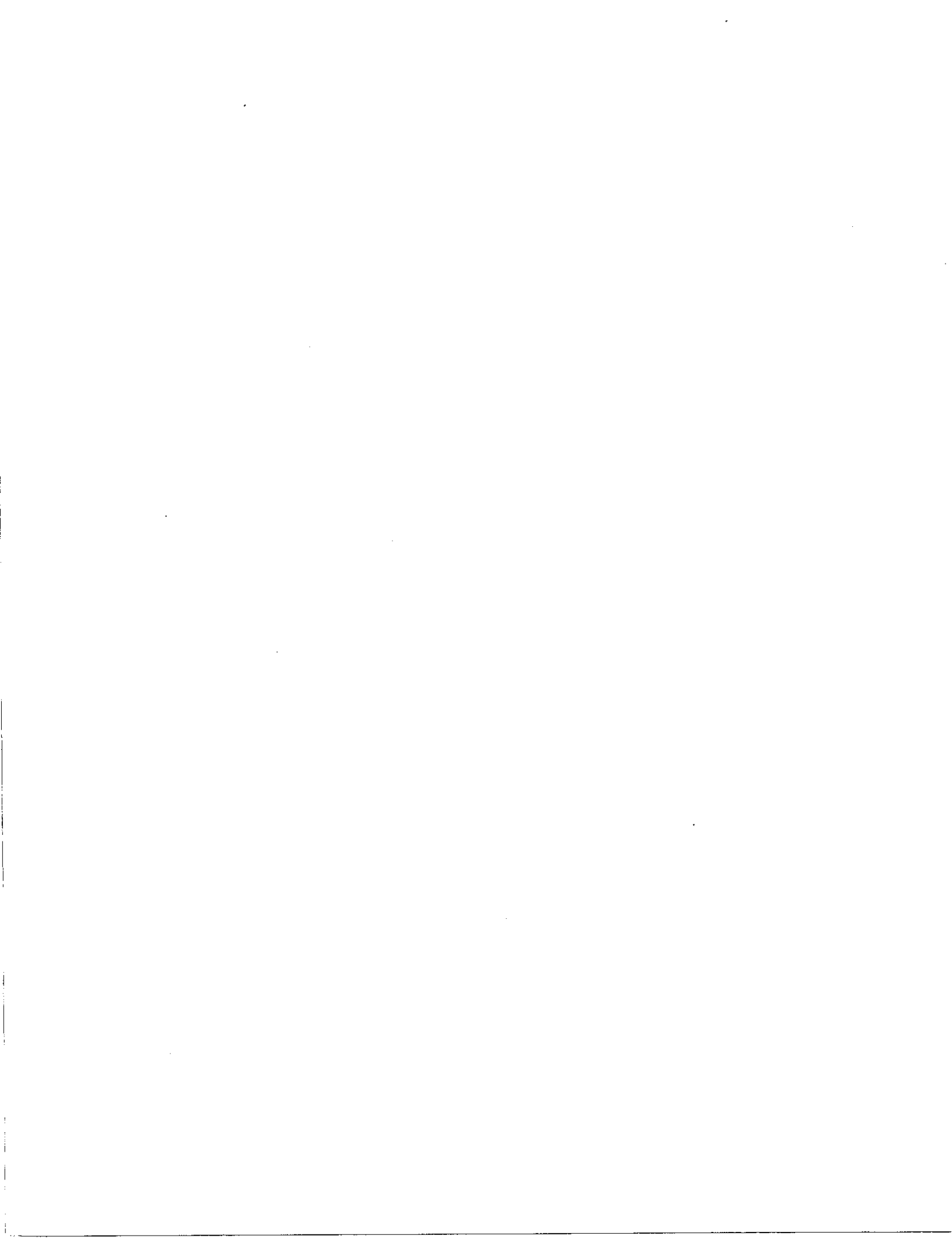
37. Warhus, J.P., Mast, J.E., Nelson, S.D., and Johansson, E.M., "Ground-penetrating radar development for bridge deck and road bed inspection" Lawrence Livermore National Laboratory, Livermore, CA, May 1993.
38. Saarenketo, T., and Sonderqvist, Miss M.K., "Ground penetrating radar applications for bridge deck evaluations in Finland," *Insight*, Vol. 36, No. 7, July 1994, pp. 496-501.
39. Holloway, A. L., and Mugford, J. C., "Fracture characterization in granite using ground probing radar," *CIM Bulletin*, Vol. 83, No. 940, Aug. 1990, pp. 61-70.
40. Holloway, A.L., Soonawala, N.M., and Collett, L.S., "Three-dimensional fracture mapping in granite excavations using ground-penetrating radar," *CIM Bulletin*, Vol. 79, No. 896, 1986, pp. 54 -59.
41. Witten, A. J., Molyneux, J. E., and Nyquist, J. E., "Ground penetrating radar tomography: algorithms and case studies," *IEEE Transactions on Geoscience and Remote Sensing*, Vol. 32, No. 2, March 1994, pp. 461-467.
42. ASTM Designation: D 4748-87, Standard test method for determining the thickness of bound pavement layers using the short-pulse radar, 1988.
43. AASHTO Provisional Standard: TP36, Standard test method for evaluating asphalt-covered concrete bridge decks using pulsed radar.
44. Halabe, Udaya B., Sotoodehnia, Arash, Maser, Kenneth R., and Kausel, Eduardo A., "Modeling the electromagnetic properties of concrete," *ACI Materials Journal*, Vol. 90, No. 6, Nov.-Dec. 1993, pp. 552-563.
45. Halabe, U. B., Maser, K. R., and Kausel, E. A., "Condition assessment of reinforced concrete structures using electromagnetic waves," *ACI Materials Journal*, Vol. 92, No. 5, Sept.-Oct. 1995, pp. 511-523.
46. Chen, H.L., Halabe, U. B., Sami, Z., and Bhandarkar, V., "Impulse radar reflection wave forms of simulated reinforced concrete bridge decks," *Materials Evaluation*, Dec. 1994, pp. 1382-1388.
47. Chung, T., Carter, C.R., Masliwec, T., and Manning, D.G., "Impulse radar evaluation of concrete, asphalt and waterproofing membrane," *IEEE Transactions on Aerospace and Electronic Systems*, Vol. 30, No. 2, April 1994, pp. 404-415.
48. Shoukry, S. N., Martinelli, D., Varadarajan, S. T., and Halabe, U. B., "Radar signal interpretation using neural network for defect detection in concrete," *Materials Evaluation*, March 1996, pp. 393-397.

49. Attoh-Okine, N.O., "Using ground penetrating radar in pavement thickness measurements—a cost comparison with the traditional coring method," *Proceedings of the Institution of Civil Engineers and Municipal Engineers*, Vol. 115, June 1996, pp. 86-89.
50. Maser, K. R., "Bridge deck survey technique using high-speed radar," Tennessee Department of Transportation, November 14, 1994.
51. Mesher, D. E., Dawley, C. B., Davis, J. L., Rossiter, J. R., "Evaluation of new ground penetrating radar technology to quantify pavement structures," The Transportation Research Board, Jan., 1995.
52. "Ground penetrating radar pavement thickness measurement performance evaluation," Penetradar Corporation, Technical Note PTN-004, Niagara Falls, New York.
53. Udpa, S. S., Hsiu, H. C., "Advanced microwave and millimeter-wave detectors." *Proceedings of The International Society for Optical Engineering*, Vol. 2275, San Diego, California, July 25-26, 1994.
54. Joyce, R. P., "Rapid non-destructive delamination detection," IIT Research Institute, Chicago, IL, April 1985.
55. Benz, C. J., Ulrikson, D. D., "Bridge evaluation through thermal infrared and ground penetrating radar" 7th Annual International Bridge Conference, Pittsburgh, PA, June 18-20, 1990.
56. Eales, J. W., "Nondestructive testing and evaluation of pavements and bridge decks using ground penetrating radar and infrared thermography," SEC Donohue, Inc., Milwaukee, WI, 1992.
57. Maldague, X. P.V., "Nondestructive evaluation of materials by infrared thermography," Springer-Verlag, New York, 1992.
58. Lucier, R. D., "Recent work in infrared thermography: history, results, and feedback," *Materials Evaluation*, July 1991, pp. 856-859.
59. Shiratori, M., Qiang, Y., Takahashi, Y., and Ogasawara, N., "Application of infrared thermography to detection of flaws in honeycomb sandwich constructions," *JSME International Journal*, Vol. 37, No. 4, 1994, pp. 396-402.
60. Shiratori, M., Takahashi, Y., and Qiang, Y., "Application of infrared thermography to detection of cracks," *JSME International Journal*, Vol. 37, No. 3, 1994, pp. 296-302.
61. Qin, Y.-W., and Bao, N.-K., "Infrared thermography and its application in the NDT of sandwich structures," *Optics and Lasers in Engineering*, Vol. 25, 1996, pp. 205-211.

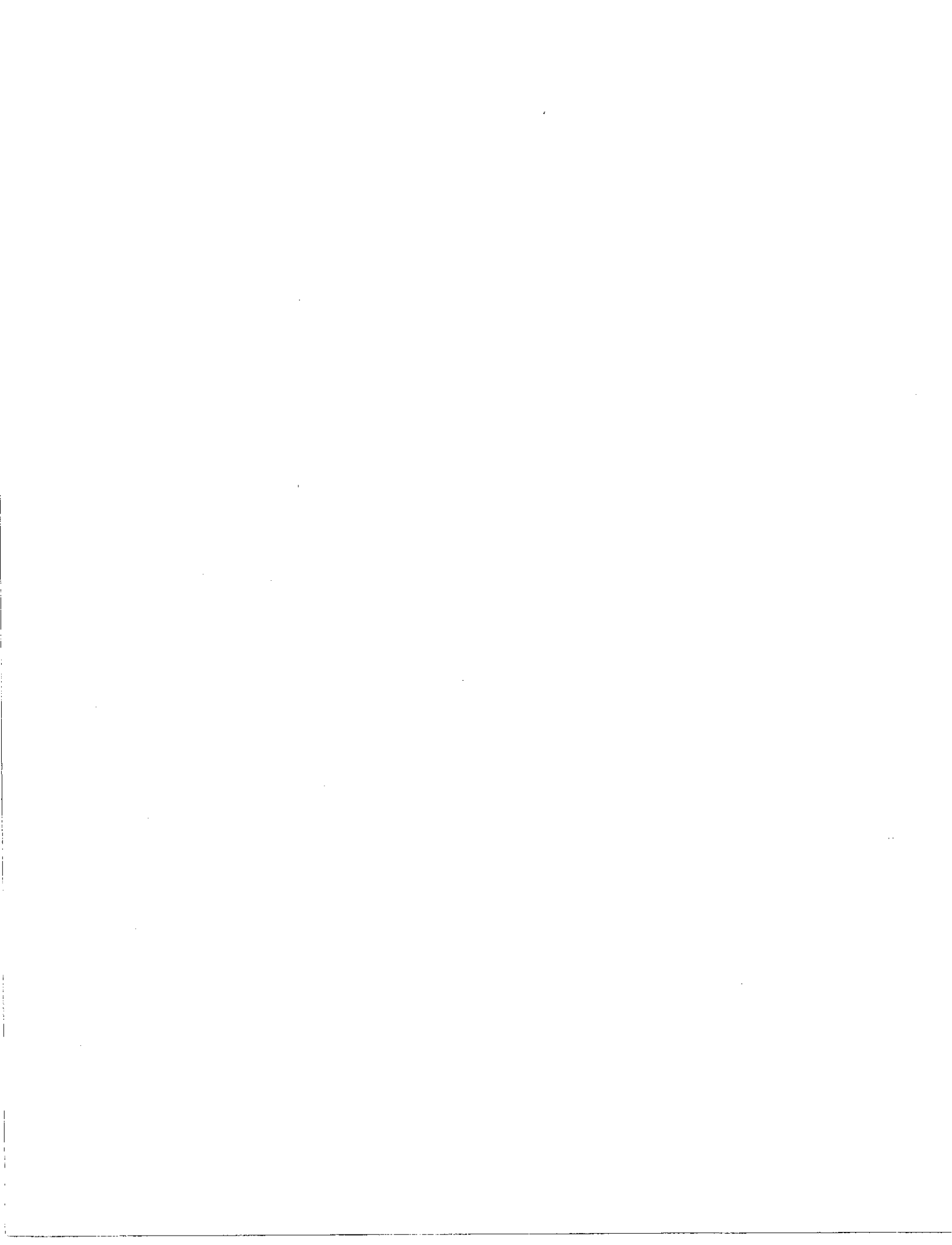
62. Sandor, B.I., Lohr, D.T., and Schmid, K.C., "Nondestructive testing using differential infrared thermography," *Materials Evaluation*, Vol. 45, April 1987, pp. 392-395.
63. Yu, T.R., Henning, J.G., and Croxall, J.E., "Loose rock detection with infrared thermography," *CIM Bulletin*, Vol. 83, No. 937, May 1990, pp. 46-52.
64. ASTM Designation: D 4788-88, Standard test method for detecting delaminations in bridge decks using infrared thermography, 1993.
65. Love, B. W., "The detection of delamination in reinforced bridge decks using infrared thermography," Indiana Department of Highways, Division of Research and Training, West Lafayette, IN, June 1986.
66. Winters, P. C., and Frascoia, R. I., "Field comparison of infrared thermography and manual survey results," Vermont Agency of Transportation, Materials & Research Division, Montpelier, VT, Sept. 1988.
67. Komiyama, T., Tanigawa, Y., and Nakano, Y., "Study on limitations of thermographic survey applied to the detection of delamination in concrete structures," Structural Materials Technology An NDT Conference, Feb. 20-23, San Diego, CA, 1996.
68. "Shortwave vs. longwave, which is best?," Inframetrics Reports, May 1992.
69. Inframetrics Model 760 Infrared Thermal Imaging Radiometer Brochure, Inframetrics, 1994.
70. Weil, G. J. "Detecting the defects," *Civil Engineering*, Sept. 1989, pp. 74-77.
71. Thomas, R. L., Favro, L. D., Kuo, P.-K., and Bruno, Robert, "Using thermal wave imaging to see below the surface," *Photonics Spectra*, Jan. 1993.
72. McMullan, P. C., "Infrared inspections increase the reliability of new masonry structures," *Reliability Magazine*, May-June 1994.
73. ASTM Designation: D 4580-86, Standard test method for measuring delaminations in concrete bridge decks by sounding, 1992.
74. Nazarian, S., "In situ determination of elastic moduli of soil deposits and pavement systems by spectral-analysis-of-surface-waves method," Ph.D. Dissertation, The University of Texas at Austin, 1984.

75. Nazarian, S., and Stokoe, K. H., "In situ determination of elastic moduli of pavement systems by spectral-analysis-of-surface-waves method (practical aspects)," Research Report No. 368-1F, Center for Transportation Research, The University of Texas at Austin, August 1985.
76. Nazarian, S., and Stokoe, K. H., "In situ determination of elastic moduli of pavement systems by spectral-analysis-of-surface-waves method (theoretical aspects)," Research Report No. 437-2, Center for Transportation Research, The University of Texas at Austin, November 1986.
77. Heisey, J.S., Stokoe, K. H., and Meyer, A.H., "Moduli of pavement systems from spectral analysis of surface waves," Research Record No. 852, Transportation Research Board, pp. 22-31.
78. Nazarian, S., Stokoe, K. H., and Hudson, W.R., "Use of spectral analysis of surface waves method for determination of moduli and thicknesses of pavement systems," Research Record No. 930, Transportation Research Board, pp. 38-45.
79. Nazarian, S., and Stokoe, K. H., "Nondestructive testing of pavements using surface waves," Research Record No. 993, Transportation Research Board, pp. 67-79.
80. Nazarian, S., and Stokoe, K. H., "Use of surface waves in pavement evaluation," Research Record No. 1070, Transportation Research Board, pp. 132-144.
81. Rix, G. J., and Stokoe, K. H., "Stiffness profiling of pavement subgrades," Research Record No. 1235, Transportation Research Board, pp. 1-9.
82. Sanchez-Salinerio, I., Roesset, J. M., Shao, K.-Y., Stokoe, K. H., and Rix, G. J., "Analytical evaluation of variables affecting surface wave testing of pavements," Research Record No. 1136, Transportation Research Board, pp. 86-95.
83. Roesset, J. M., Chang, D.-W., Stokoe, K. H., and Aouad, M., "Modulus and thickness of the pavement surface layer from SASW tests," Research Record No. 1260, Transportation Research Board, pp. 53-63.
84. Hiltunen, D. R., and Woods, R. D., "Variables affecting the surface waves method," Research Record No. 1260, Transportation Research Board, pp. 42-52.
85. Hiltunen, D. R., "Experimental evaluation of variables affecting the testing of pavements by the spectral-analysis-of-surface-waves method," Technical Report GL-88-12, U.S. Army Engineer Waterways Experiment Station, August 1988.
86. Rix, G. J., Stokoe, K. H., and, Roesset, Jose M., "Experimental study of factors affecting the spectral-analysis-of-surface-waves method," Research Report No. 1123-5, Center for Transportation Research, The University of Texas at Austin, February 1991.

87. "Infrared thermographic survey of nine structures for University of Illinois at Urbana-Champaign Department of General Engineering," Rust Environment & Infrastructure, Final Project Report, August 1997.
88. "Ground penetrating radar survey of nine structures for University of Illinois at Urbana-Champaign Department of General Engineering," Penetradar Corporation, Final Project Report, December 1997.
89. "Nondestructive testing investigation feasibility evaluation of prototype impact-echo scanner for deck delamination survey," Olson Engineering, Inc., Final Project Report, December 1997.
90. Reis, H.L.M. dos, Baright, M. D., and Habboub, A. K., "Nondestructive evaluation of ground support in airport pavements," Accepted for publication in a *Special Topics Volume on NDT&E of Infrastructure*, ASNT, 1997.
91. Reis, H.L.M. dos, Carpenter, S.H., Baright, M. D., Habboub, A. K., and Voegele, A. C., "Nondestructive evaluation of segregation in bituminous overlays," Accepted for publication in a *Special Topics Volume on NDT&E of Infrastructure*, ASNT, 1997.



APPENDIX A—CHAIN DRAG SURVEY RESULTS



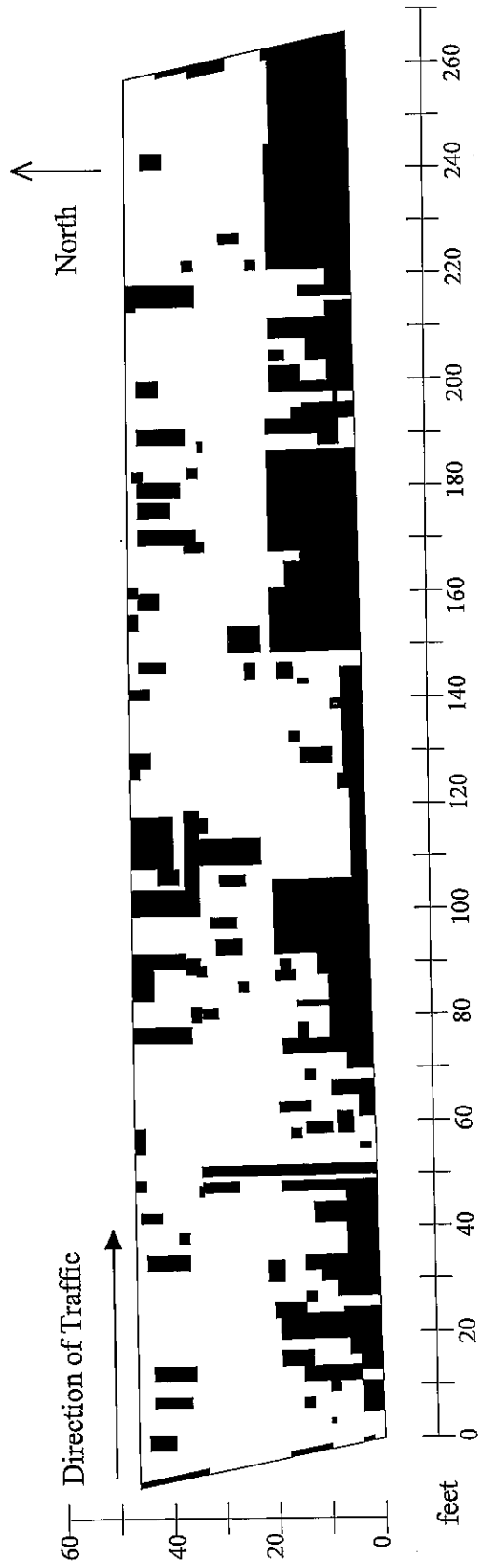


Figure A-1. Bloomington Structure Number 057-0088 eastbound chain drag survey. Dark areas indicate delaminations.

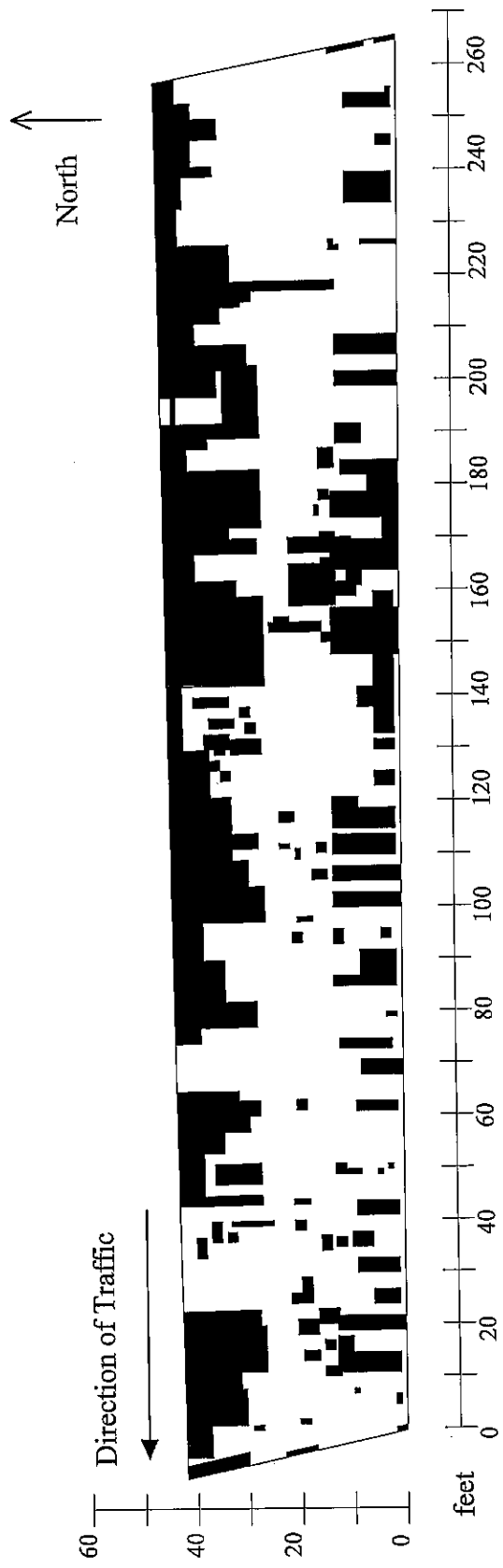


Figure A-2. Bloomington Structure Number 057-0088 westbound chain drag survey. Dark areas indicate delaminations.

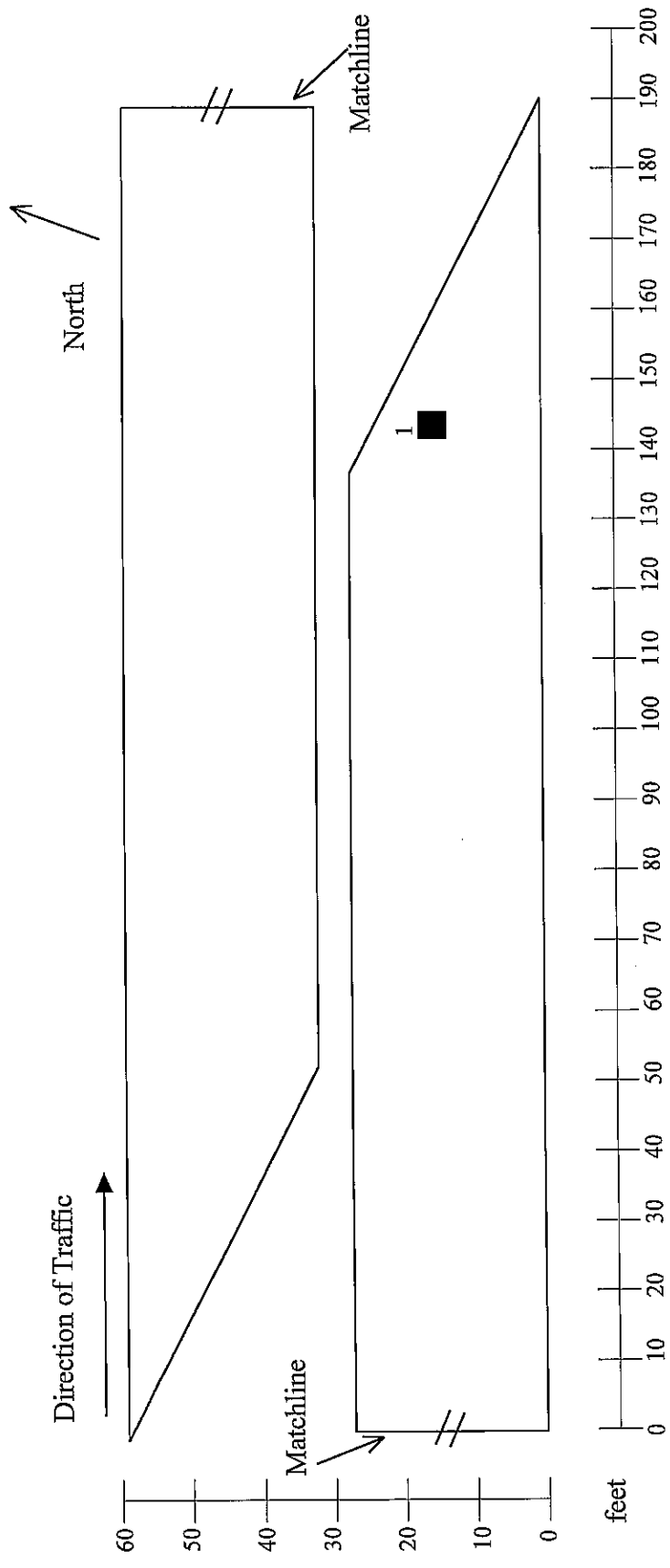


Figure A-3. Peoria Structure Number 090-0118 chain drag survey. Dark areas indicate delaminations.

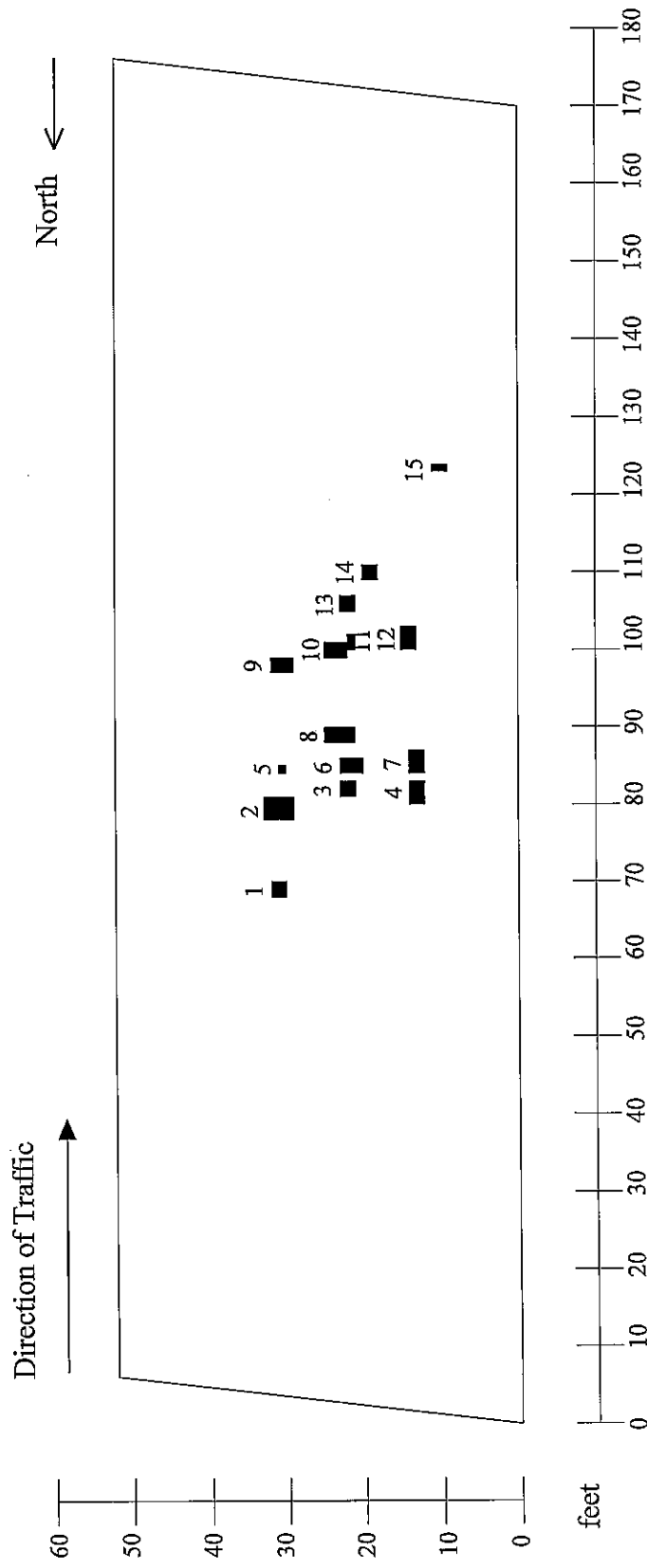


Figure A-4. Peoria Structure Number 072-0106 chain drag survey. Dark areas indicate delaminations.

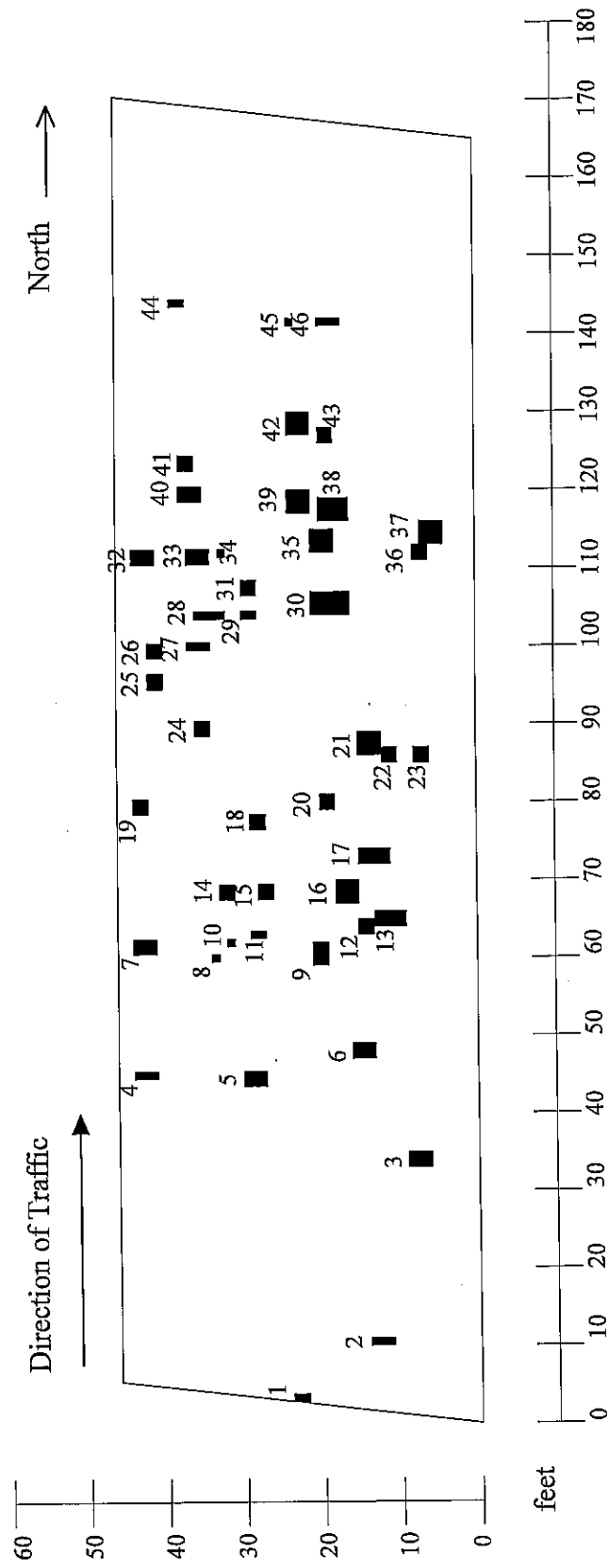


Figure A-5. Peoria Structure Number 072-0107 chain drag survey. Dark areas indicate delaminations.

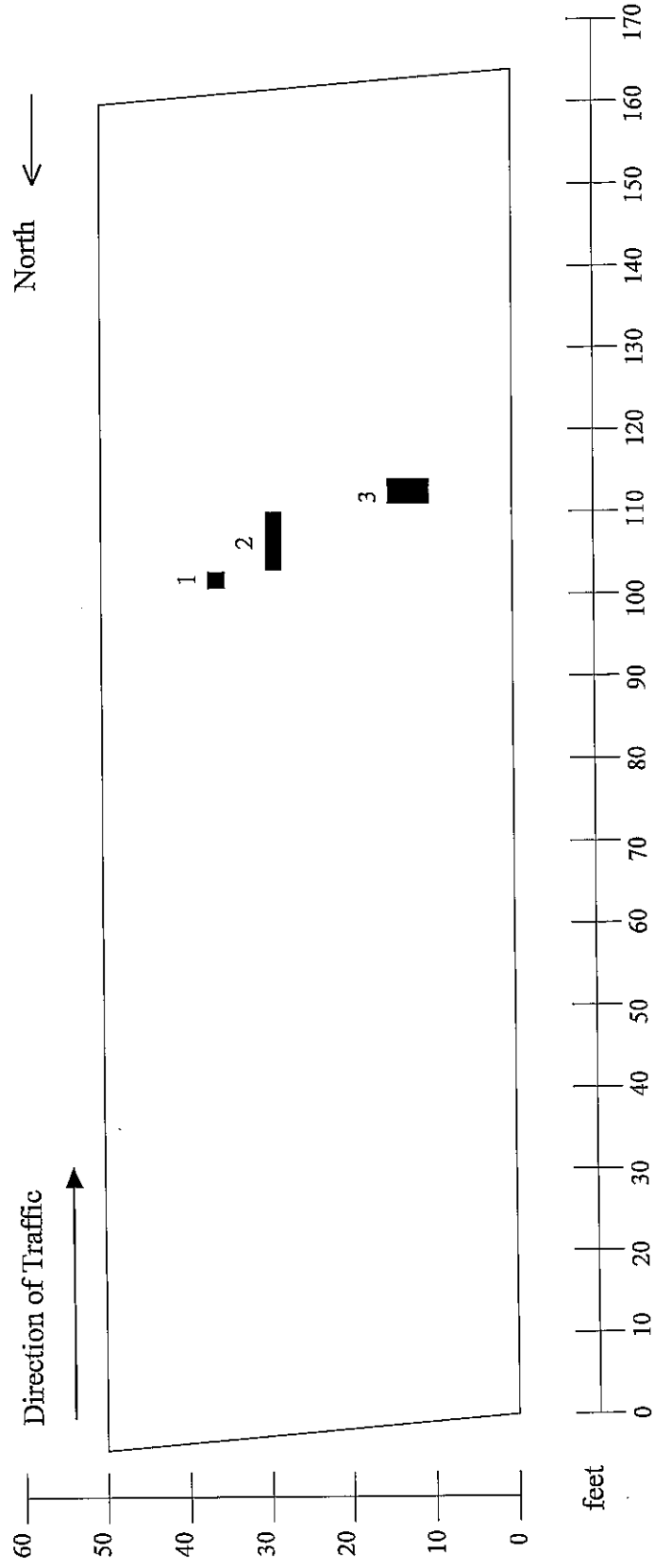


Figure A-6. Peoria Structure Number 072-0108 chain drag survey. Dark areas indicate delaminations.

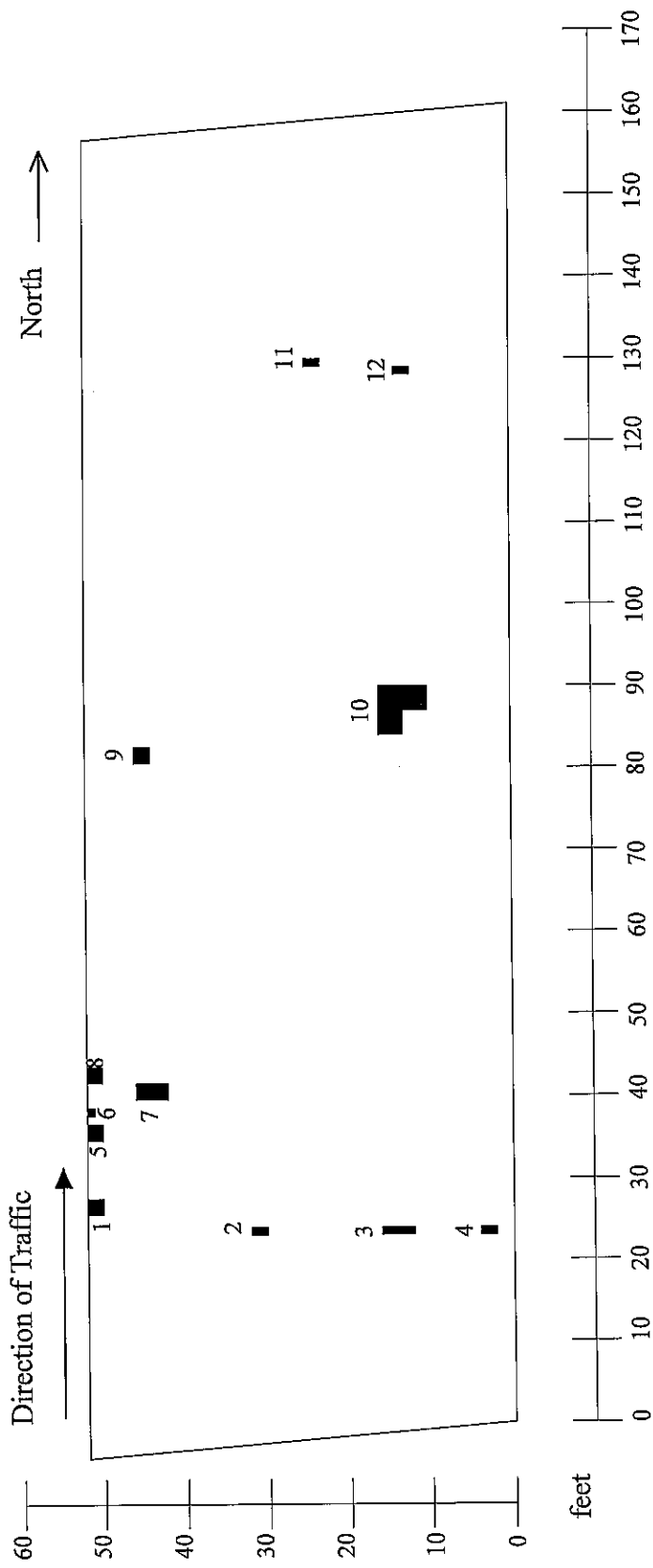


Figure A-7. Peoria Structure Number 072-0109 chain drag survey. Dark areas indicate delaminations.

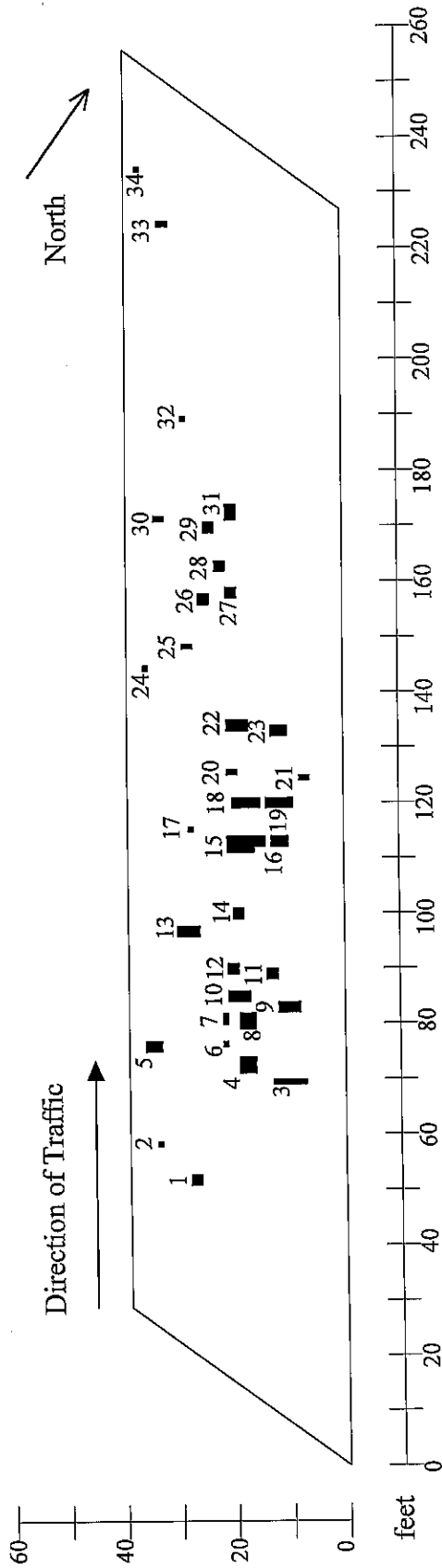


Figure A-8. Peoria Structure Number 072-0110 chain drag survey. Dark areas indicate delaminations.

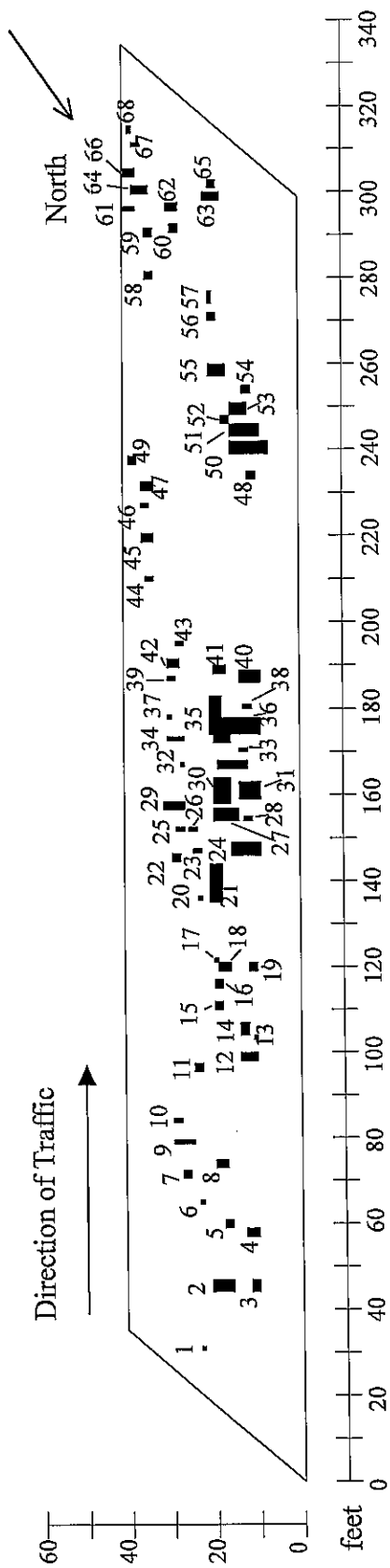


Figure A-9. Peoria Structure Number 072-0111 chain drag survey. Dark areas indicate delaminations.

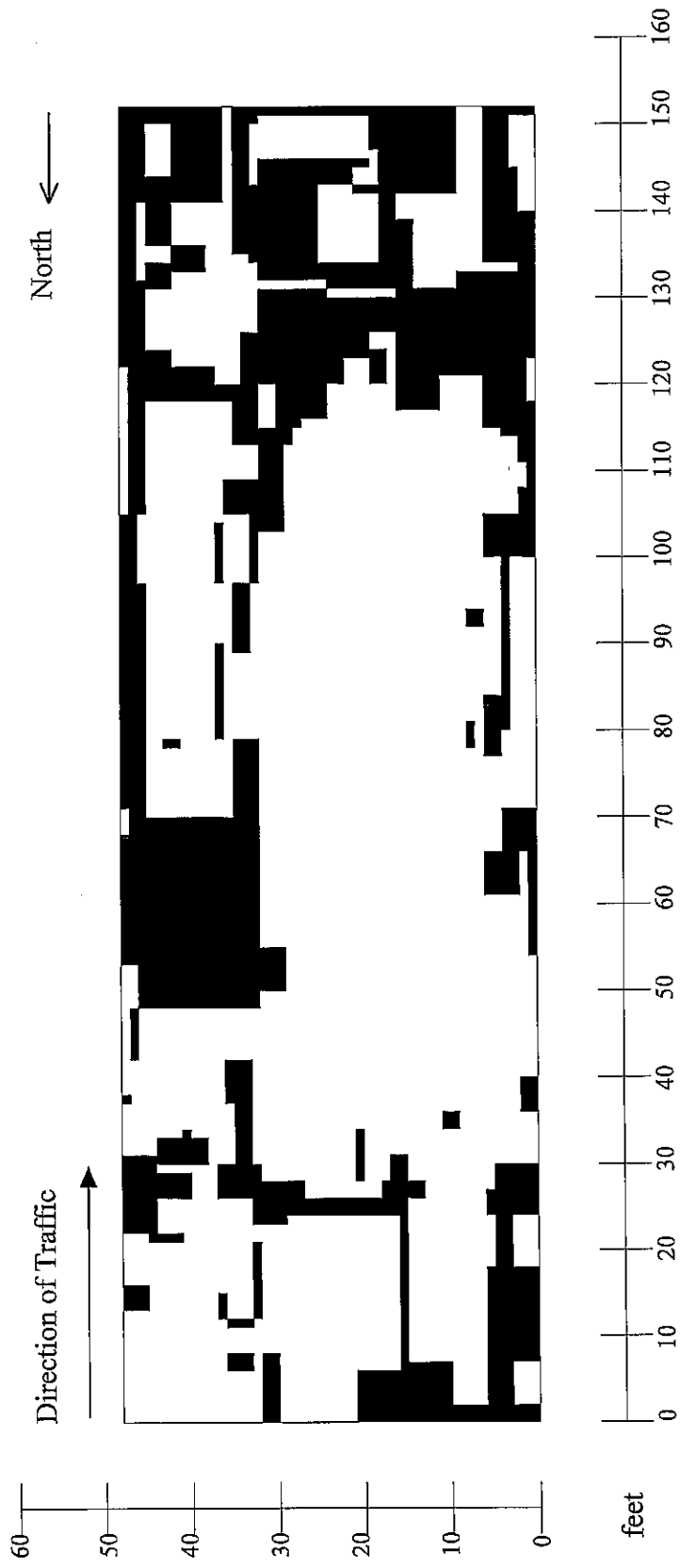


Figure A-10. Marion Structure Number 100-0005 chain drag survey. Dark areas indicate delaminations.

APPENDIX B—INFRARED THERMOGRAPHY SURVEY RESULTS

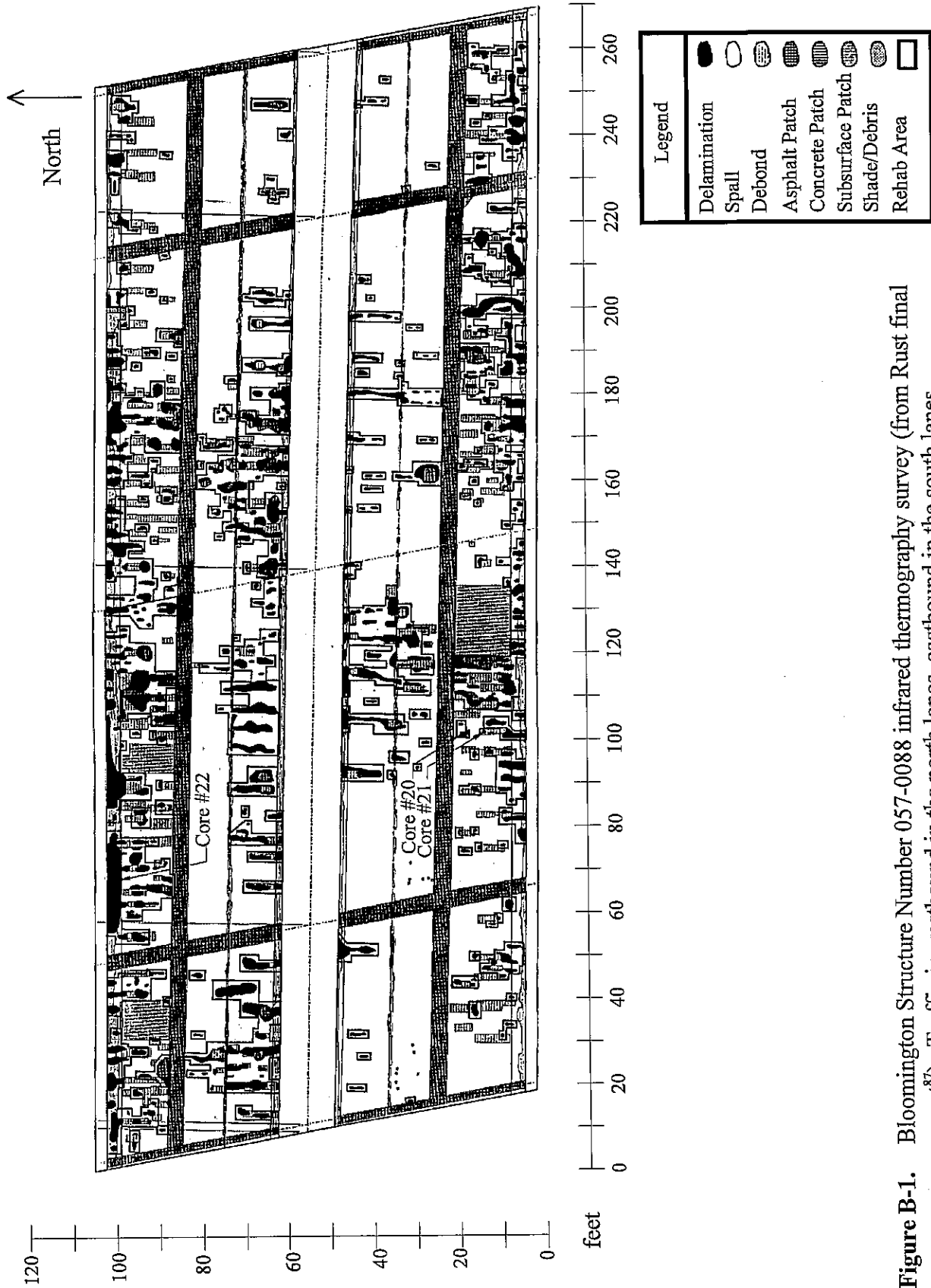


Figure B-1. Bloomington Structure Number 057-0088 infrared thermography survey (from Rust final report⁸⁷). Traffic is westbound in the north lanes, eastbound in the south lanes.

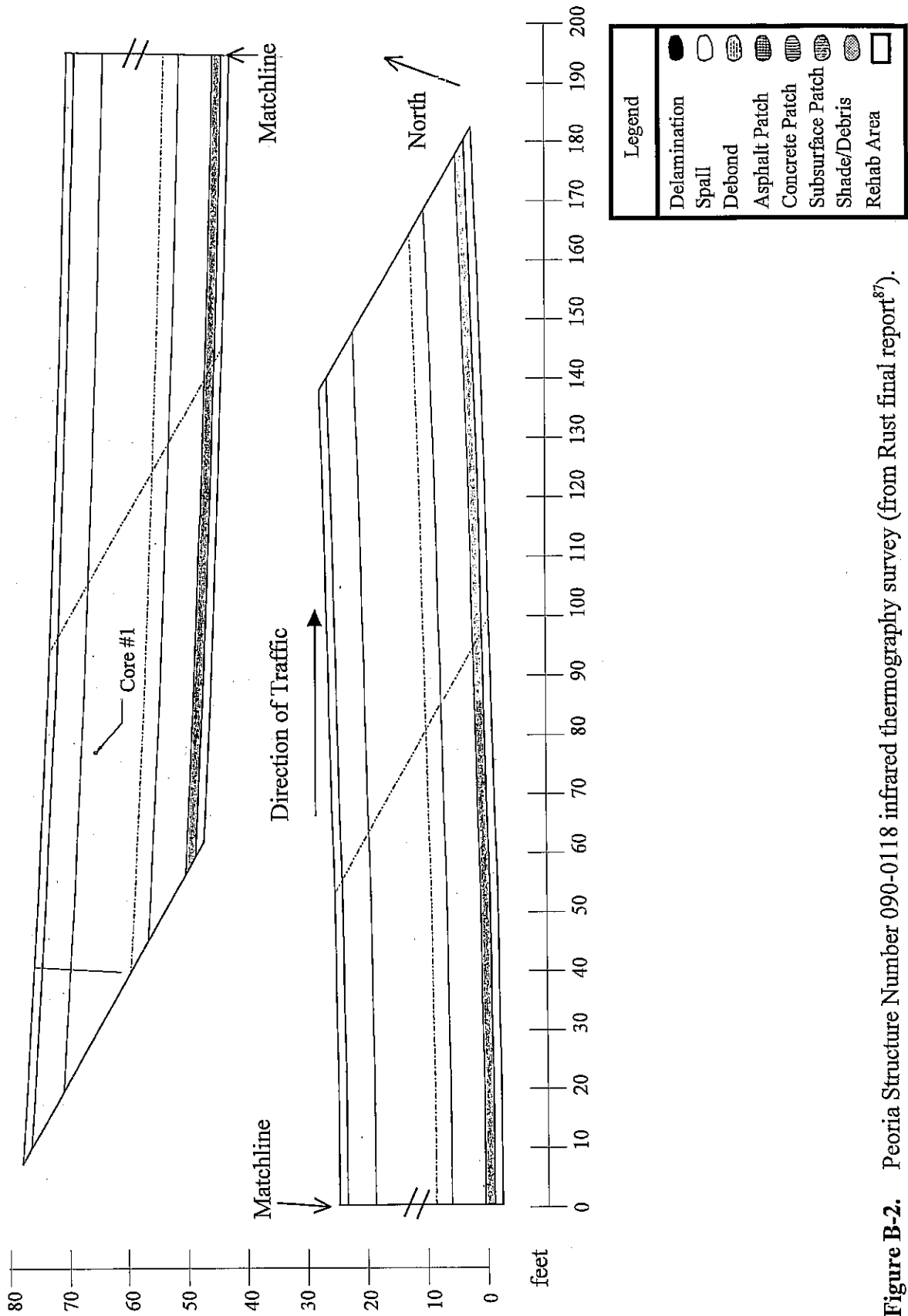


Figure B-2. Peoria Structure Number 090-0118 infrared thermography survey (from Rust final report⁸⁷).

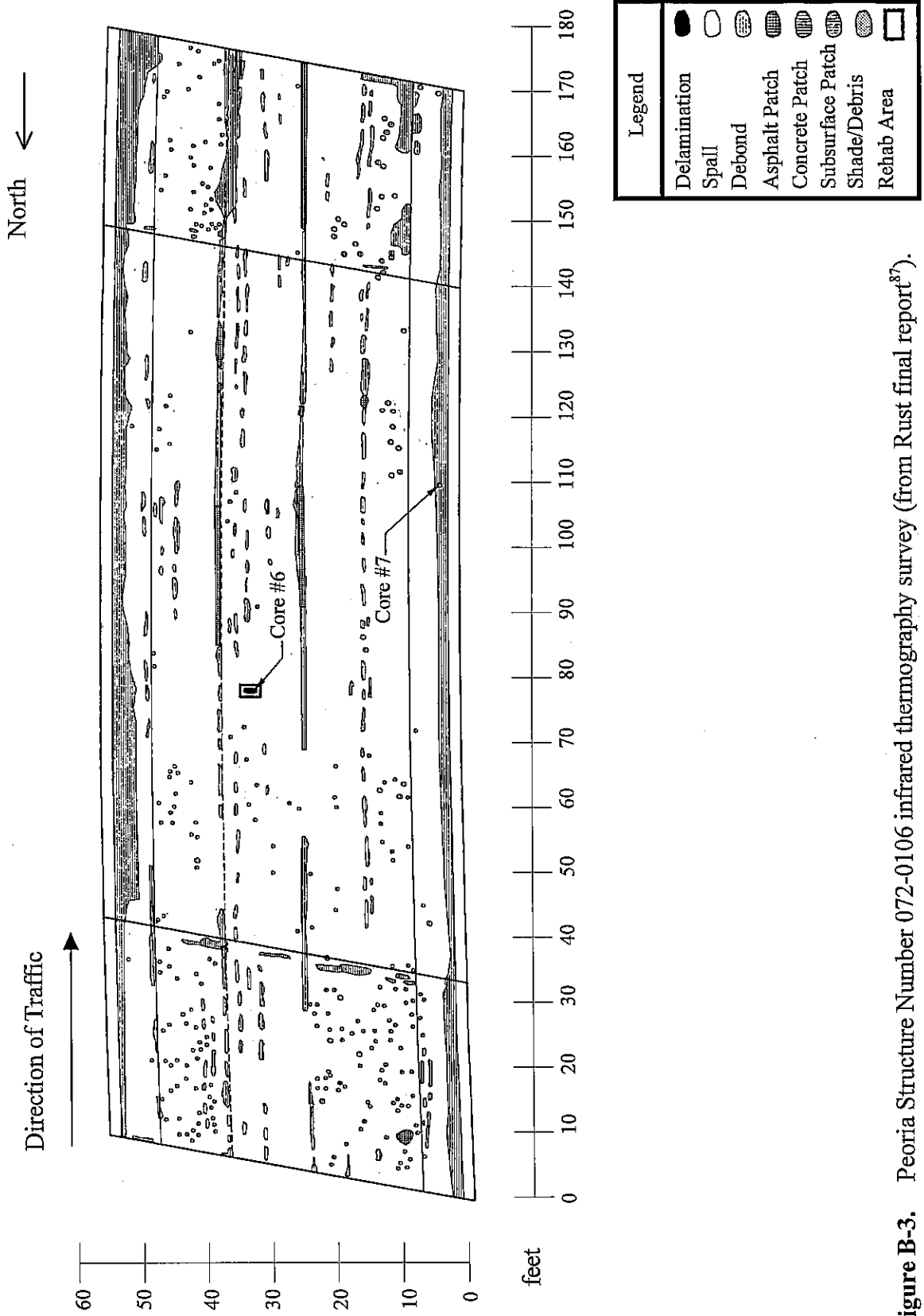


Figure B-3. Peoria Structure Number 072-0106 infrared thermography survey (from Rust final report⁸⁷).

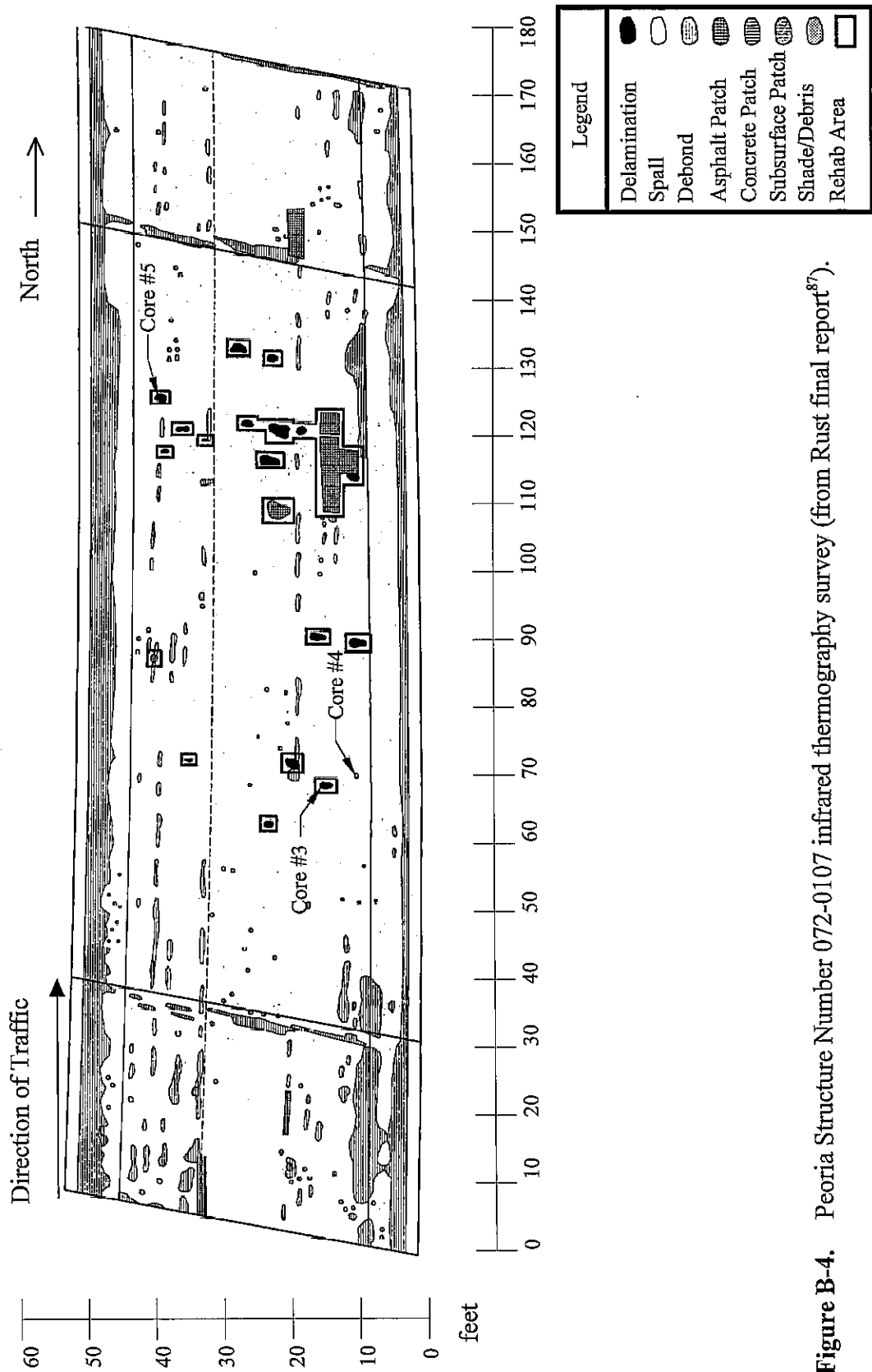


Figure B-4. Peoria Structure Number 072-0107 infrared thermography survey (from Rust final report⁸⁷).

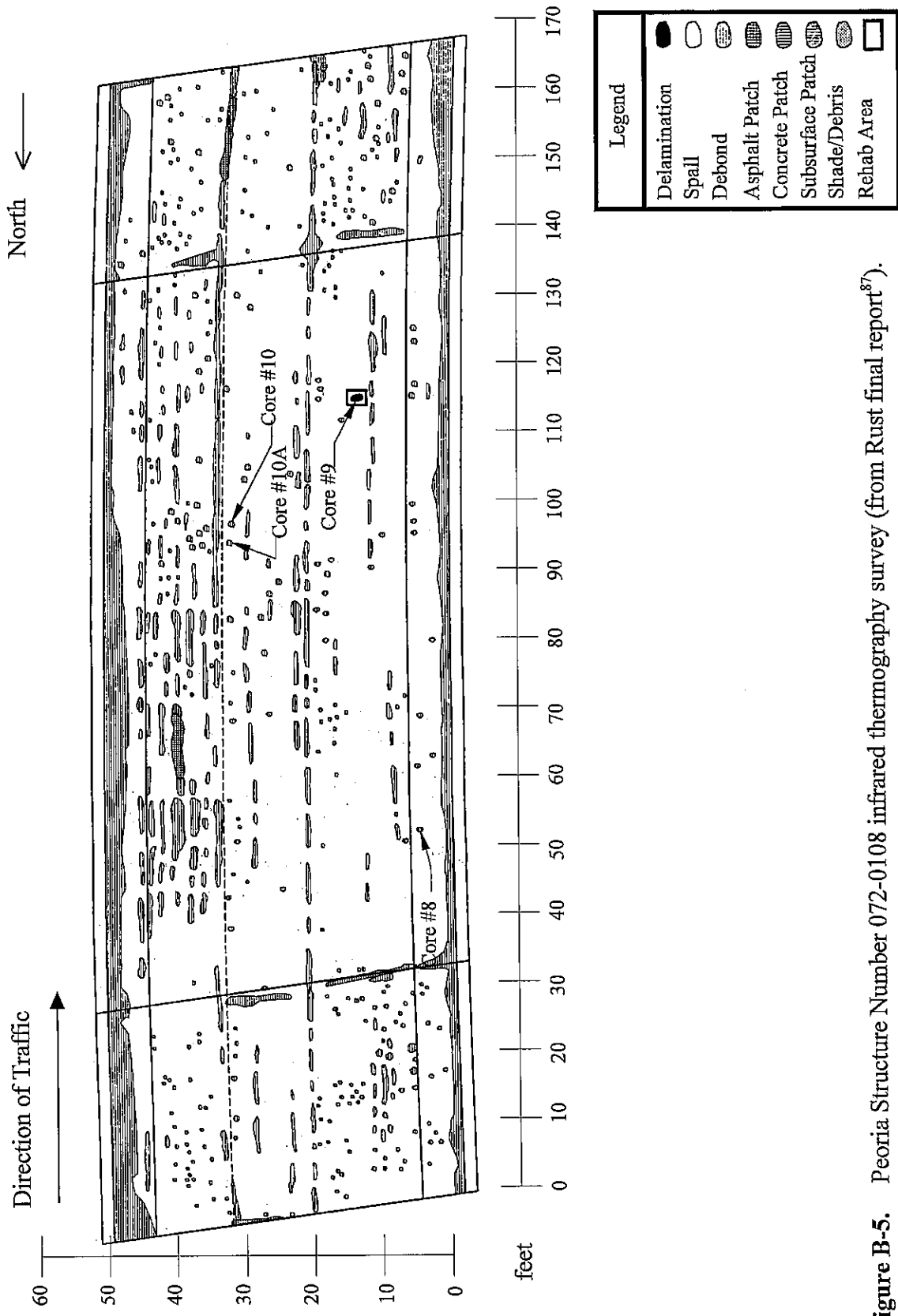


Figure B-5. Peoria Structure Number 072-0108 infrared thermography survey (from Rust final report⁸⁷).

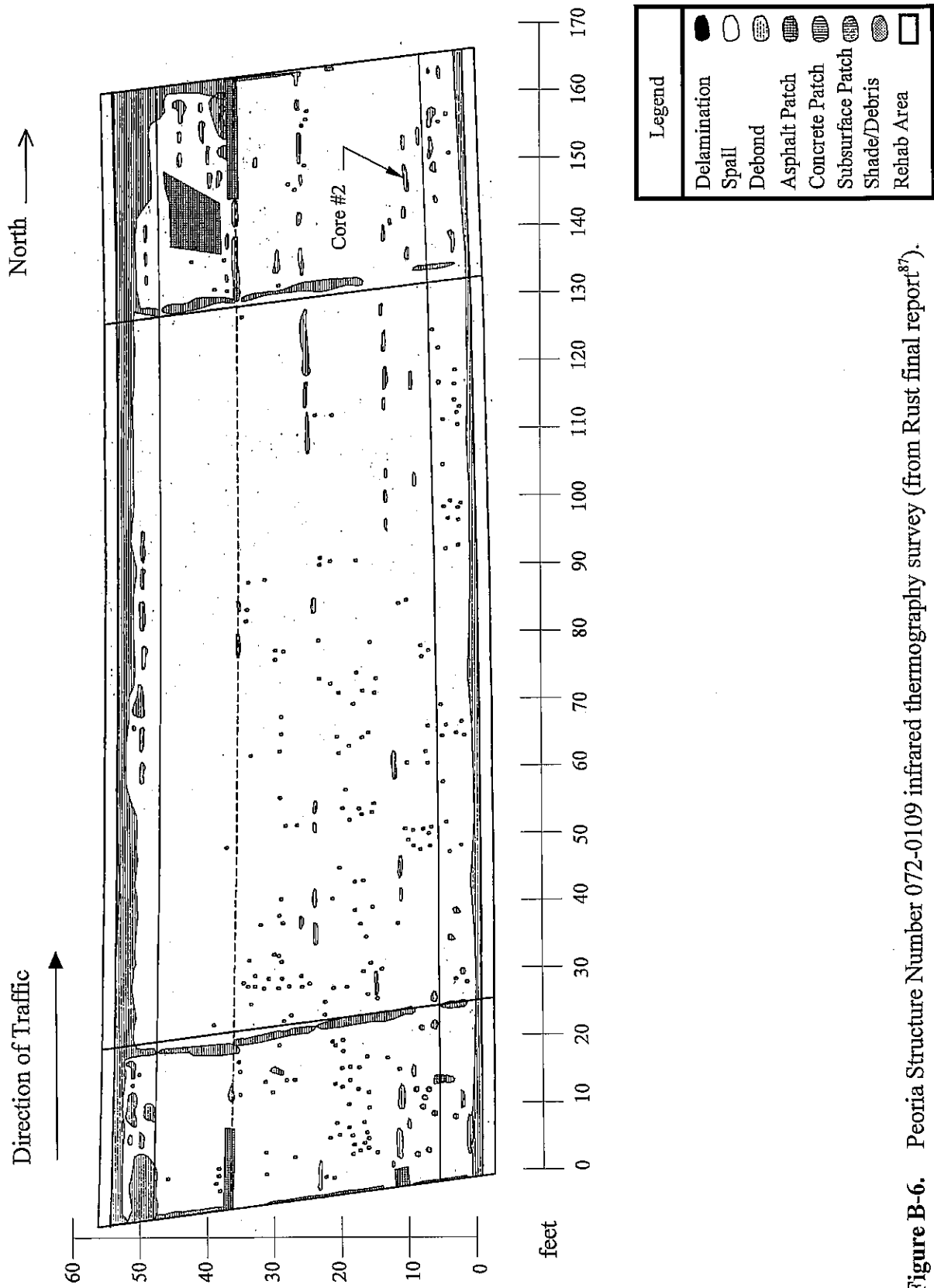


Figure B-6. Peoria Structure Number 072-0109 infrared thermography survey (from Rust final report⁸⁷).

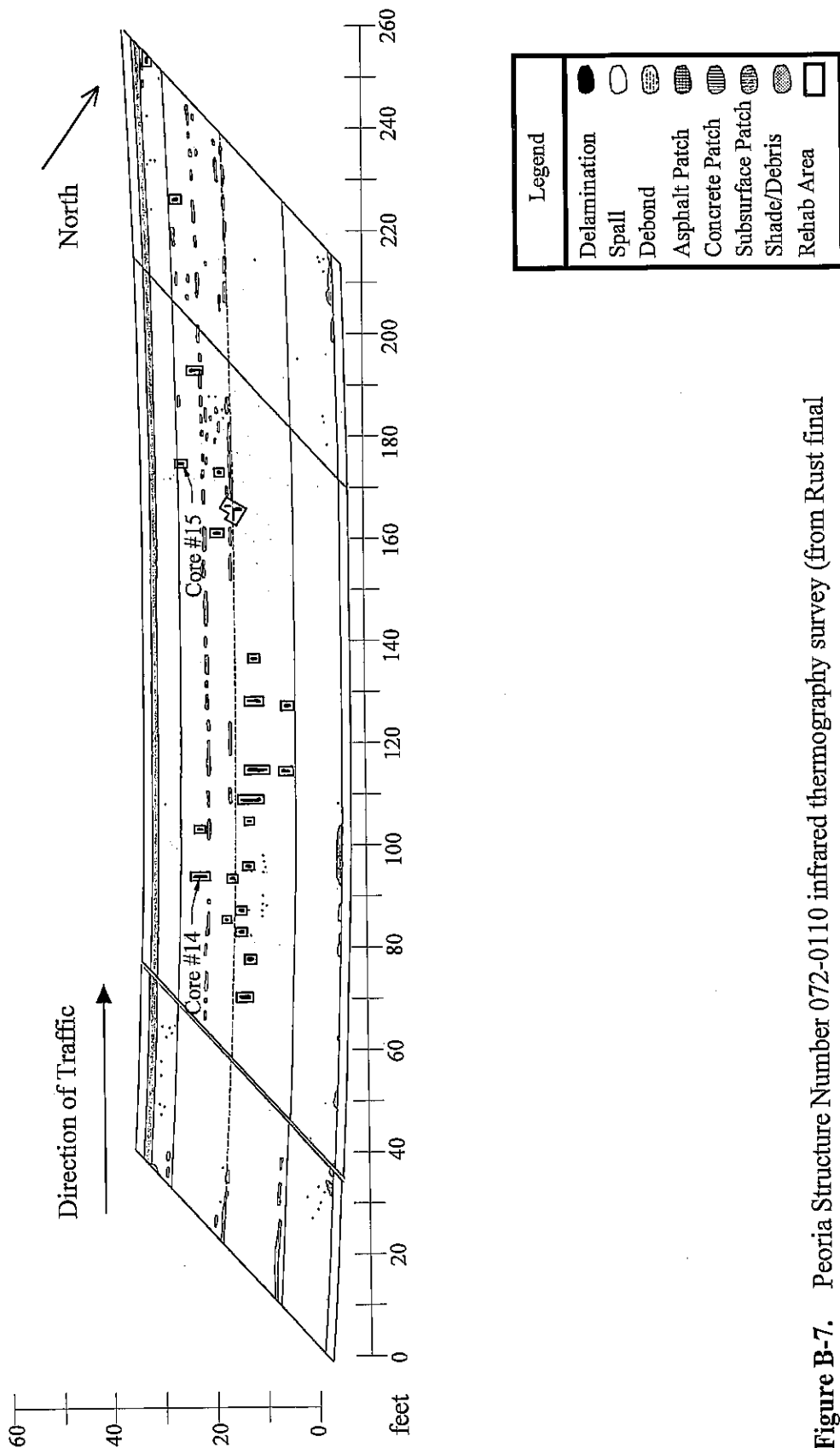


Figure B-7. Peoria Structure Number 072-0110 infrared thermography survey (from Rust final report⁸⁷).

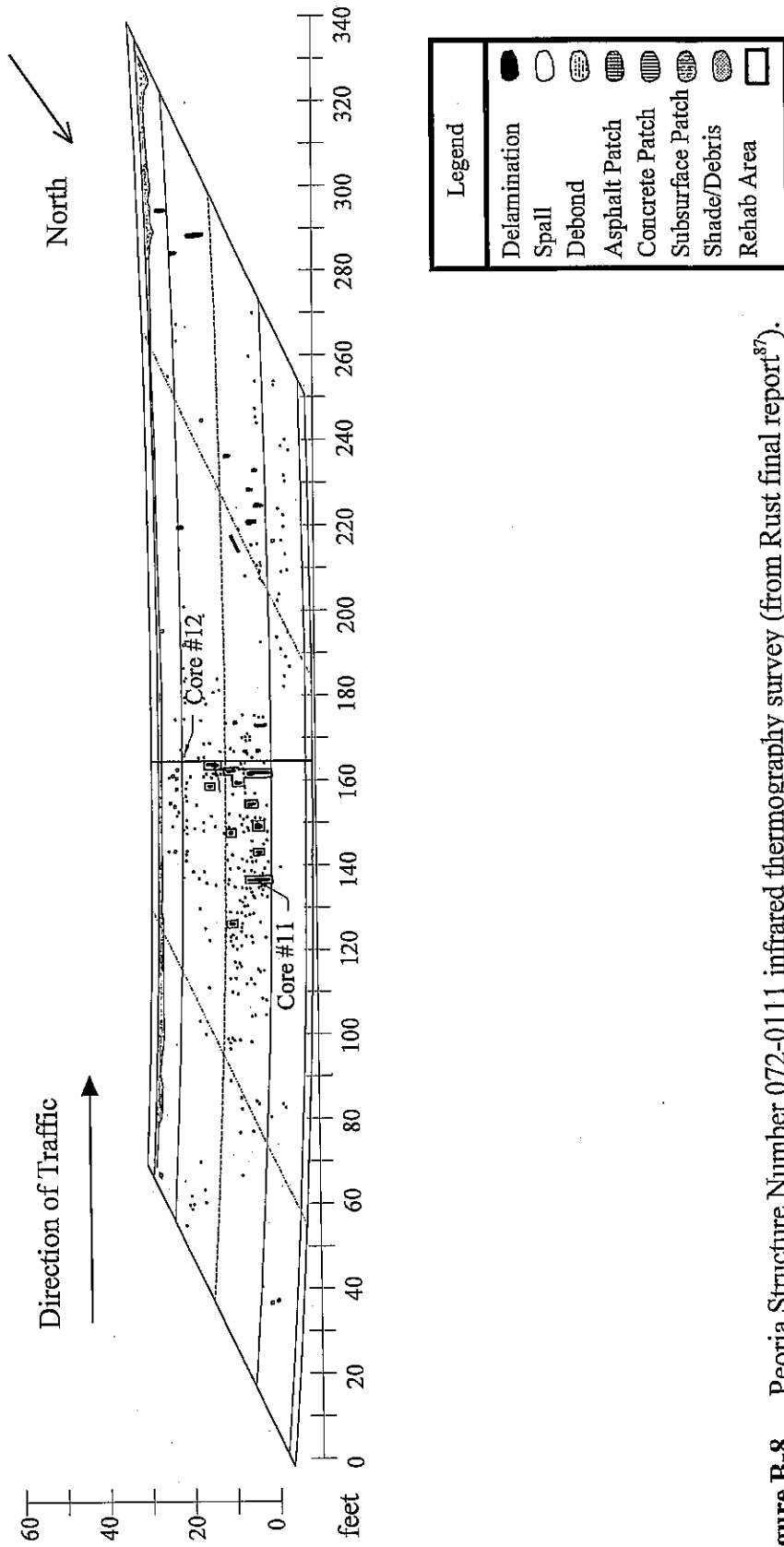


Figure B-8. Peoria Structure Number 072-0111 infrared thermography survey (from Rust final report⁸⁷).

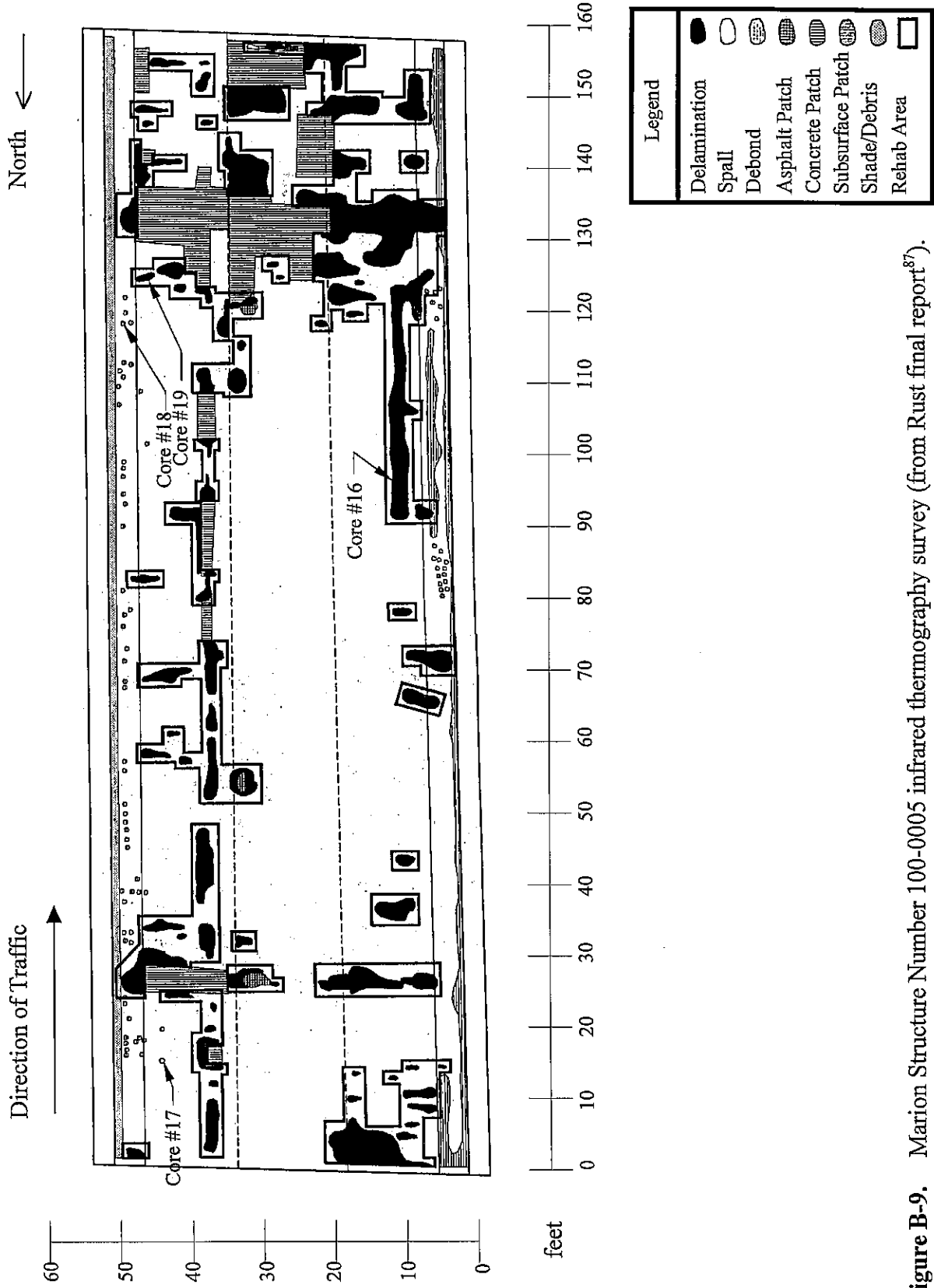


Figure B-9. Marion Structure Number 100-0005 infrared thermography survey (from Rust final report⁸⁷).

APPENDIX C—GROUND PENETRATING RADAR RESULTS

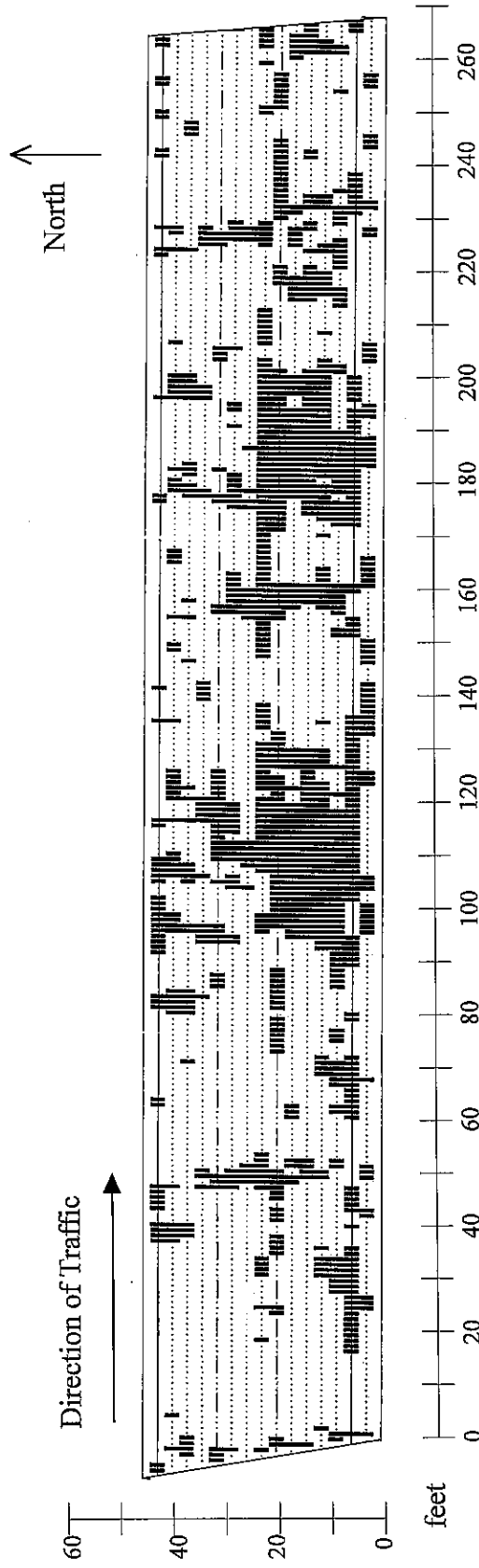


Figure C-1. Bloomington Structure Number 057-0088 eastbound ground penetrating radar delamination survey (from Penetradar final report⁸⁸). Dark areas indicate delaminations.

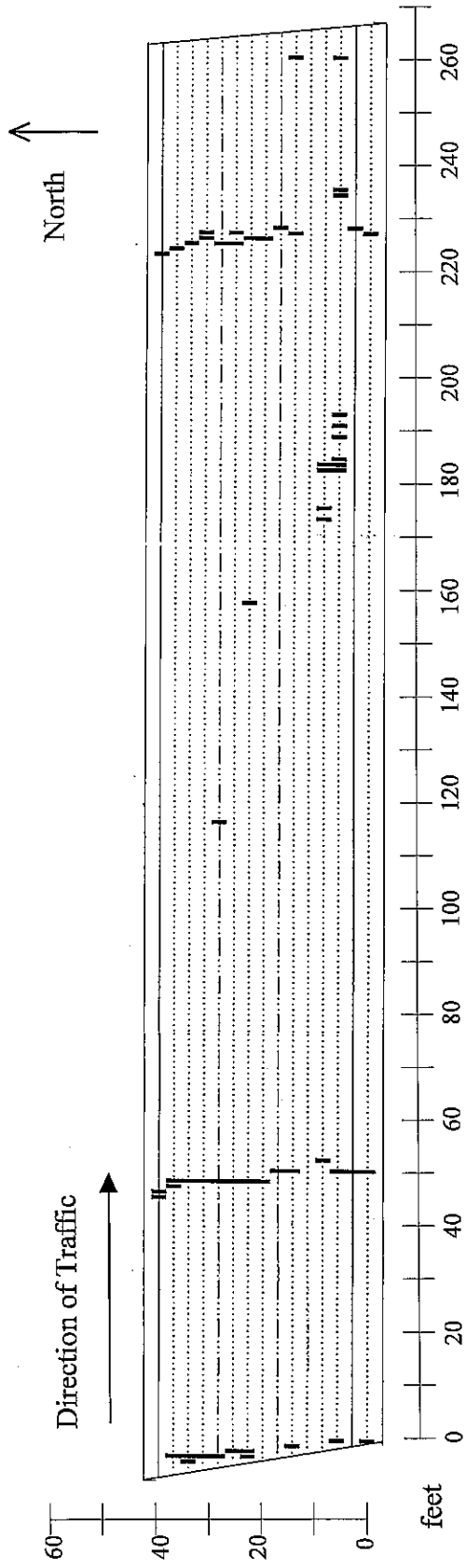


Figure C-2. Bloomington Structure Number 057-0088 eastbound ground penetrating radar scaling survey (from Penetradar final report⁸⁸). Dark areas indicate delaminations.

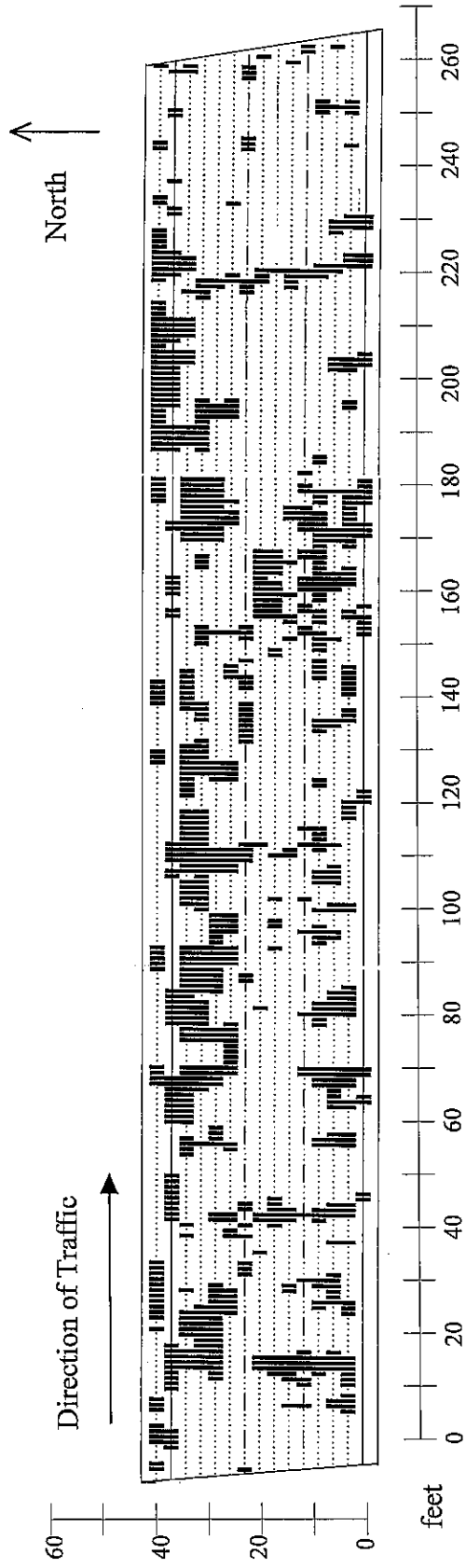


Figure C-3. Bloomington Structure Number 057-0088 westbound ground penetrating radar delamination survey (from Penetradar final report⁸⁸). Dark areas indicate delaminations.

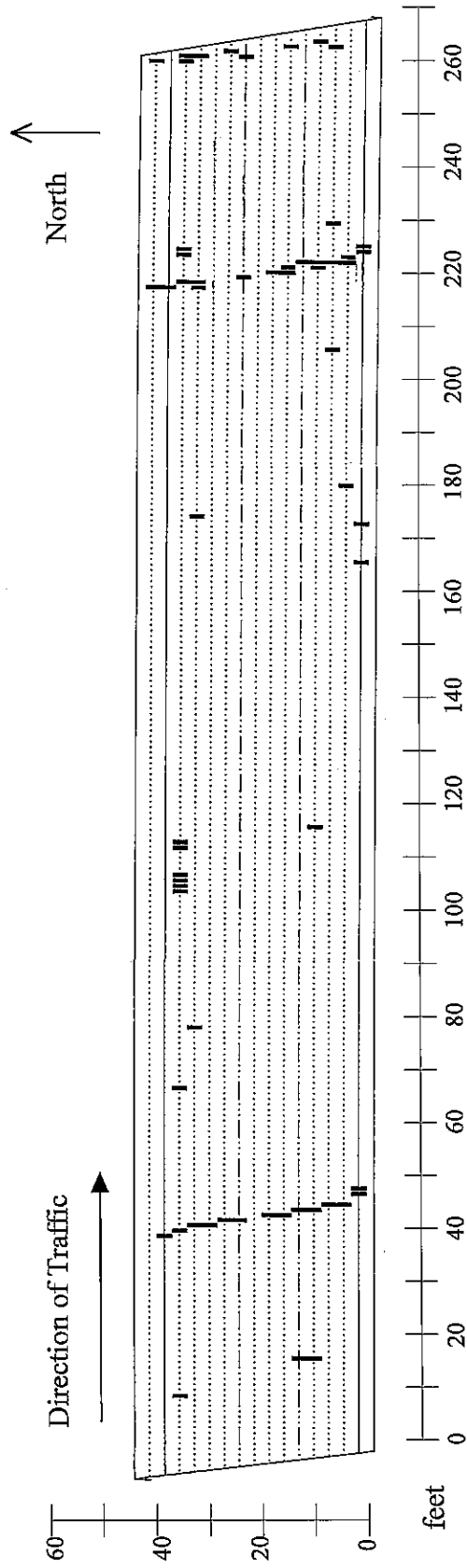


Figure C-4. Bloomington Structure Number 057-0088 westbound ground penetrating radar scaling survey (from Penetradar final report⁸⁸). Dark areas indicate delaminations.

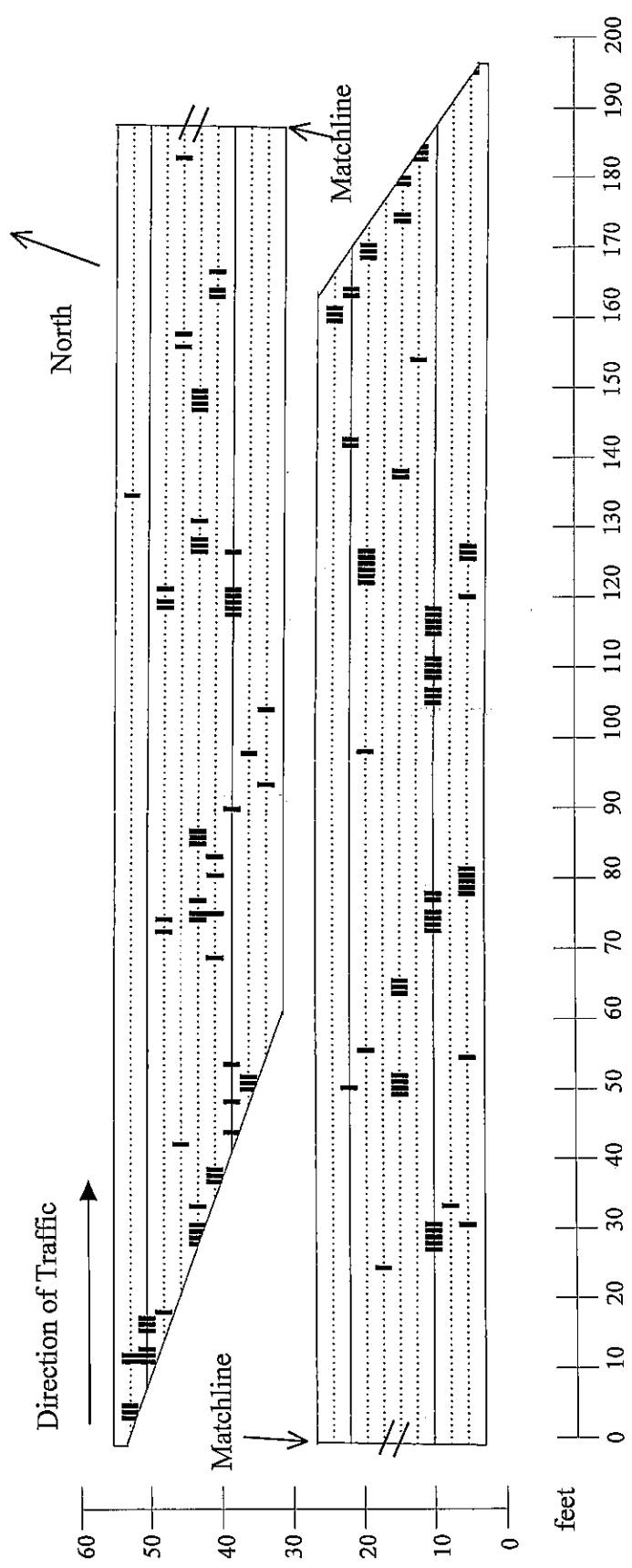


Figure C-5. Peoria Structure Number 090-0118 ground penetrating radar delamination survey (from Penetradar final report⁸⁸). Dark areas indicate delaminations.

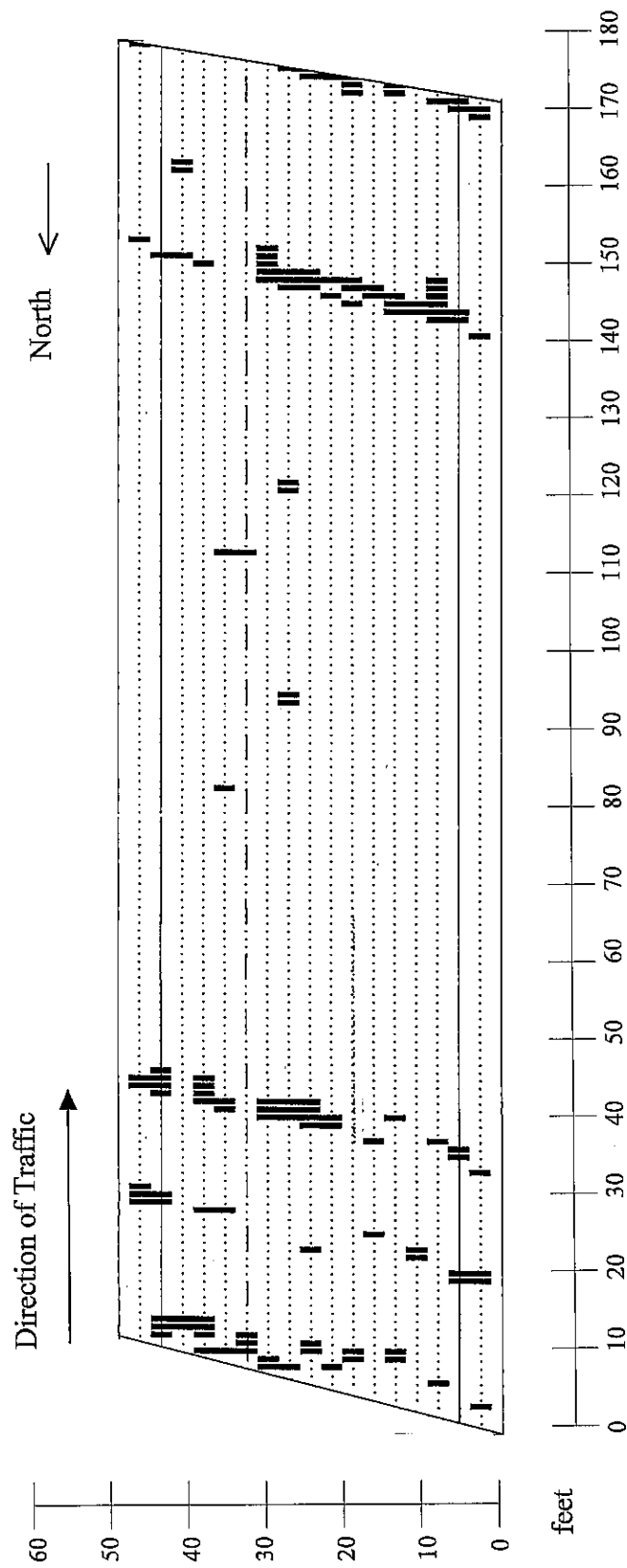


Figure C-6. Peoria Structure Number 072-0106 ground penetrating radar delamination survey (from Penetradar final report⁸⁸). Dark areas indicate delaminations.

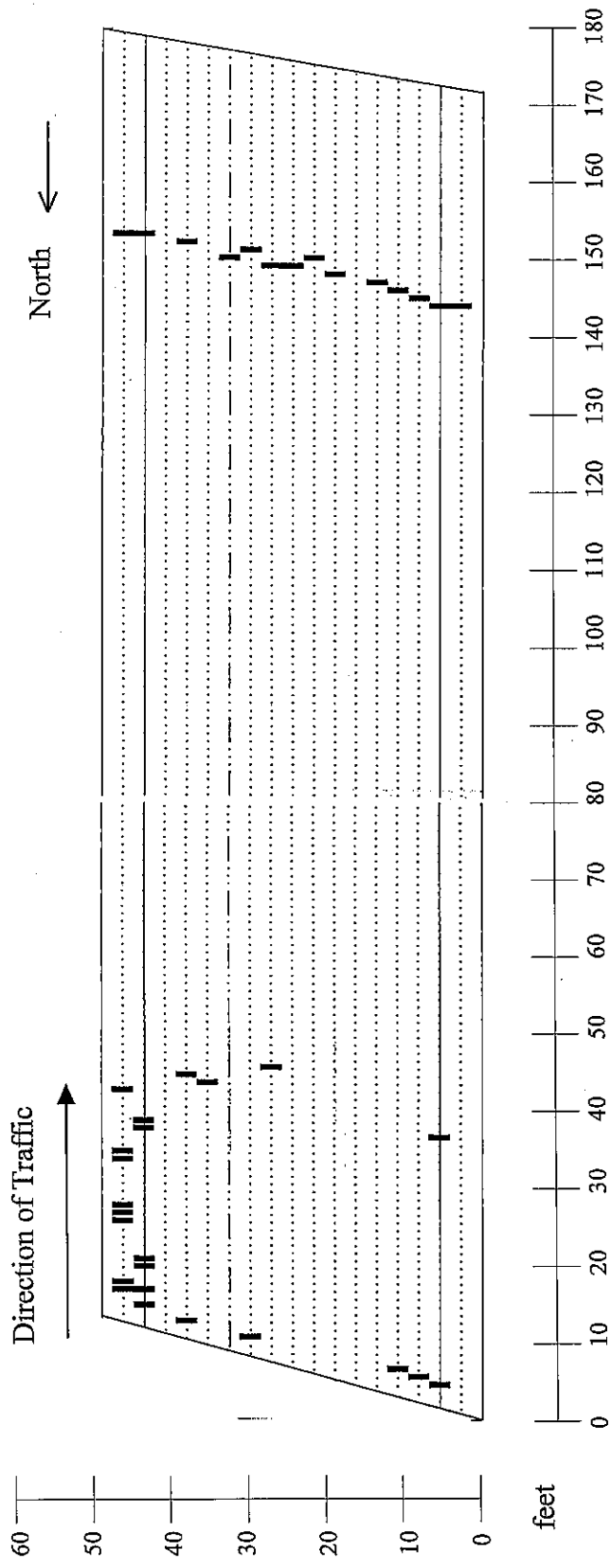


Figure C-7. Peoria Structure Number 072-0106 ground penetrating radar scaling survey (from Penetradar final report⁸⁸). Dark areas indicate delaminations.

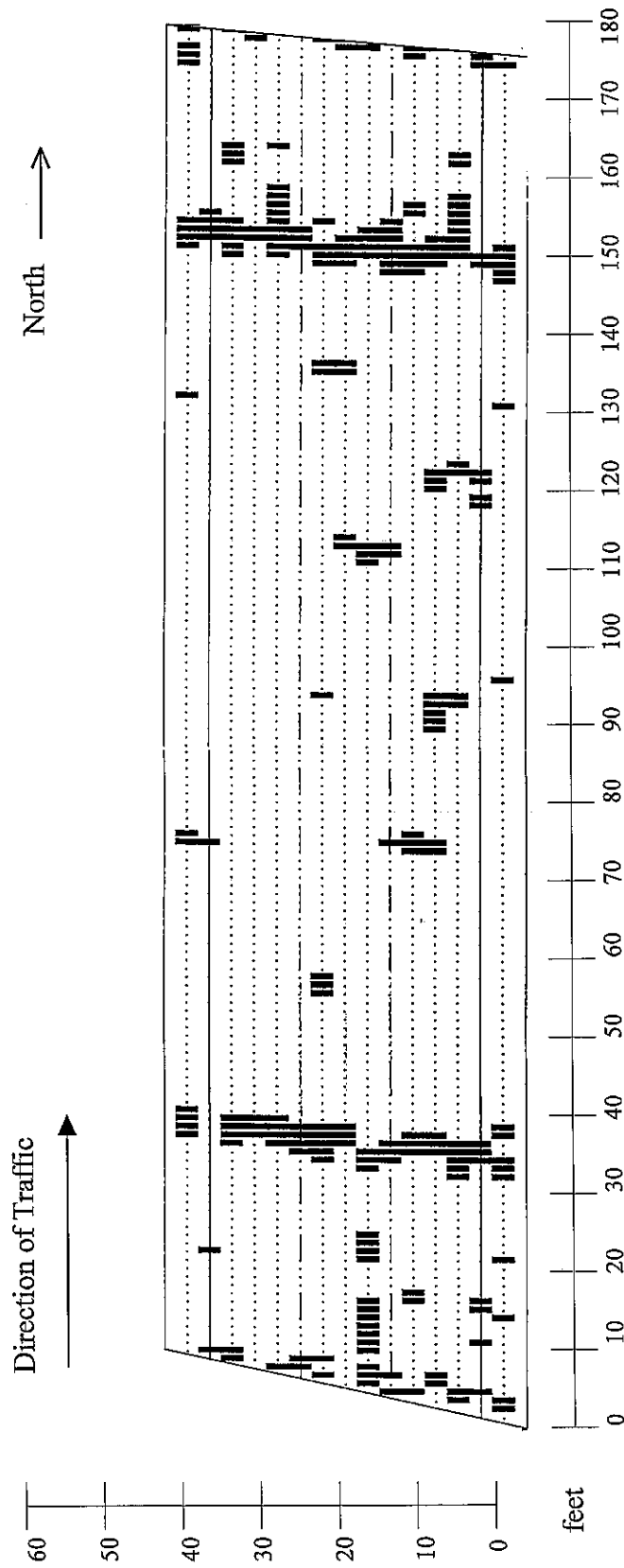


Figure C-8. Peoria Structure Number 072-0107 ground penetrating radar delamination survey (from Penetradar final report⁸⁸). Dark areas indicate delaminations.

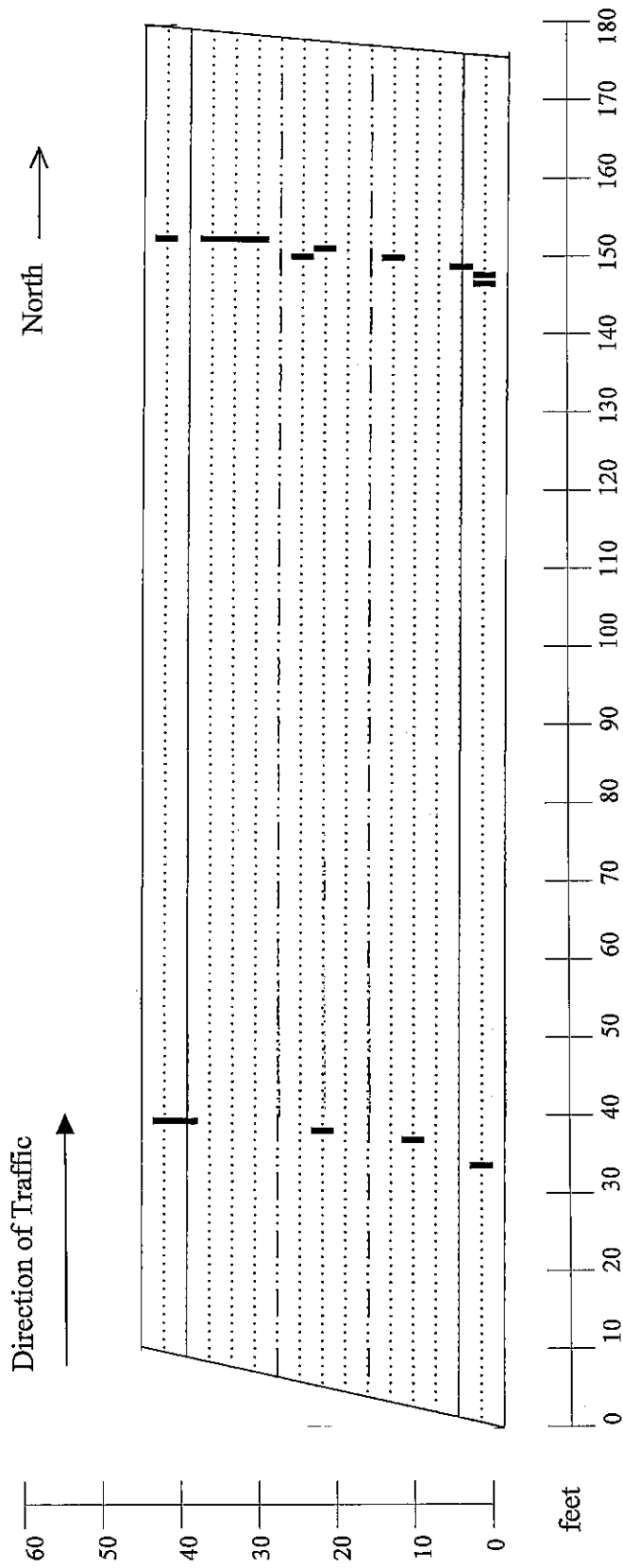


Figure C-9. Peoria Structure Number 072-0107 ground penetrating radar scaling survey (from Penetradar final report⁸⁸). Dark areas indicate delaminations.

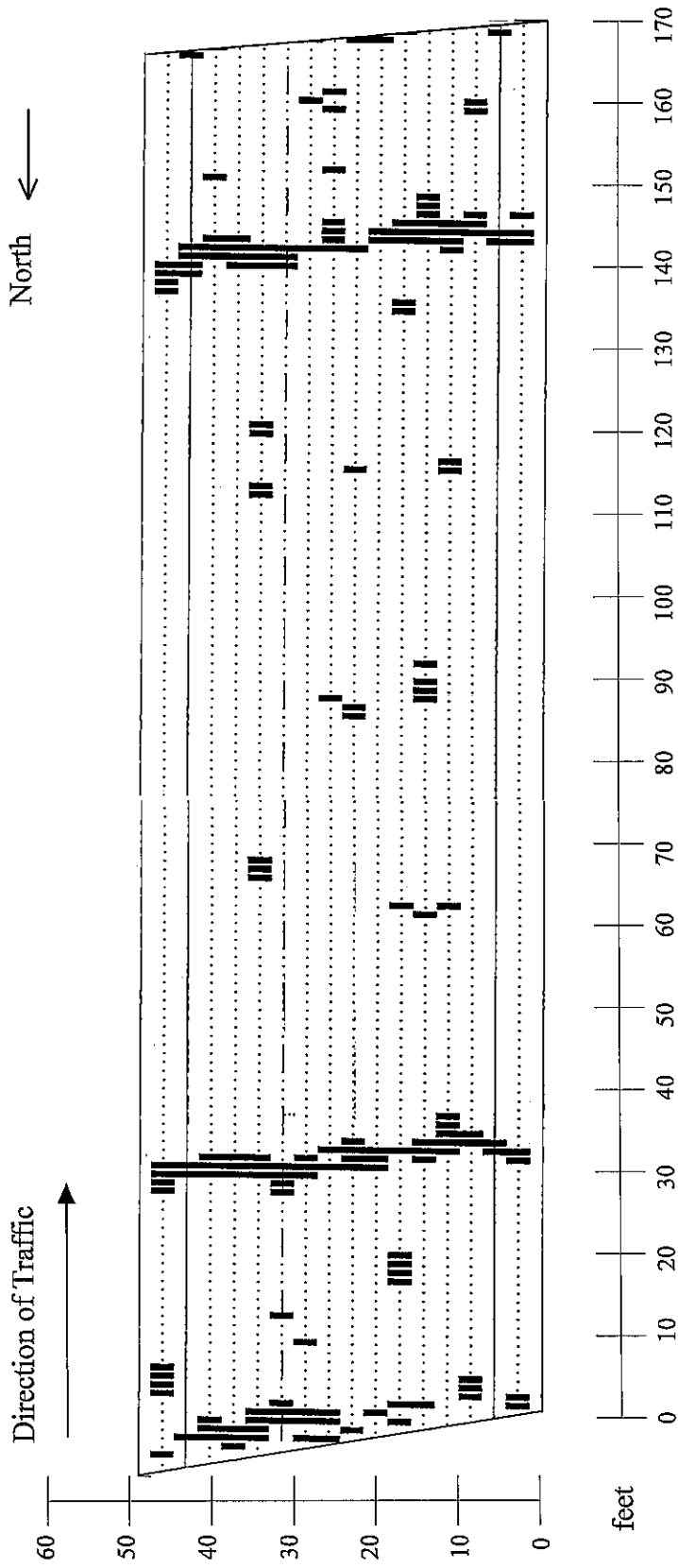


Figure C-10. Peoria Structure Number 072-0108 ground penetrating radar delamination survey (from Penetradar final report⁸⁸). Dark areas indicate delaminations.

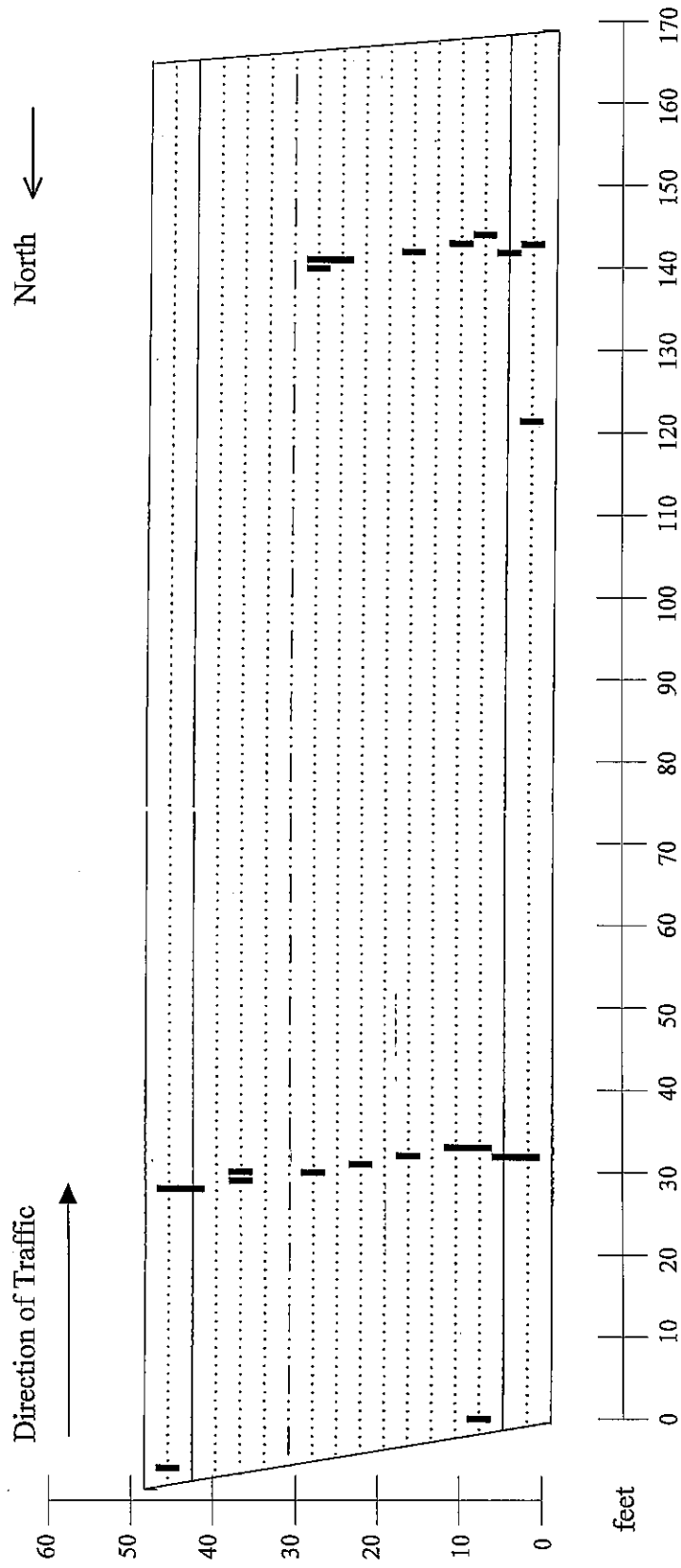


Figure C-11. Peoria Structure Number 072-0108 ground penetrating radar scaling survey (from Penetradar final report⁸⁸). Dark areas indicate delaminations.

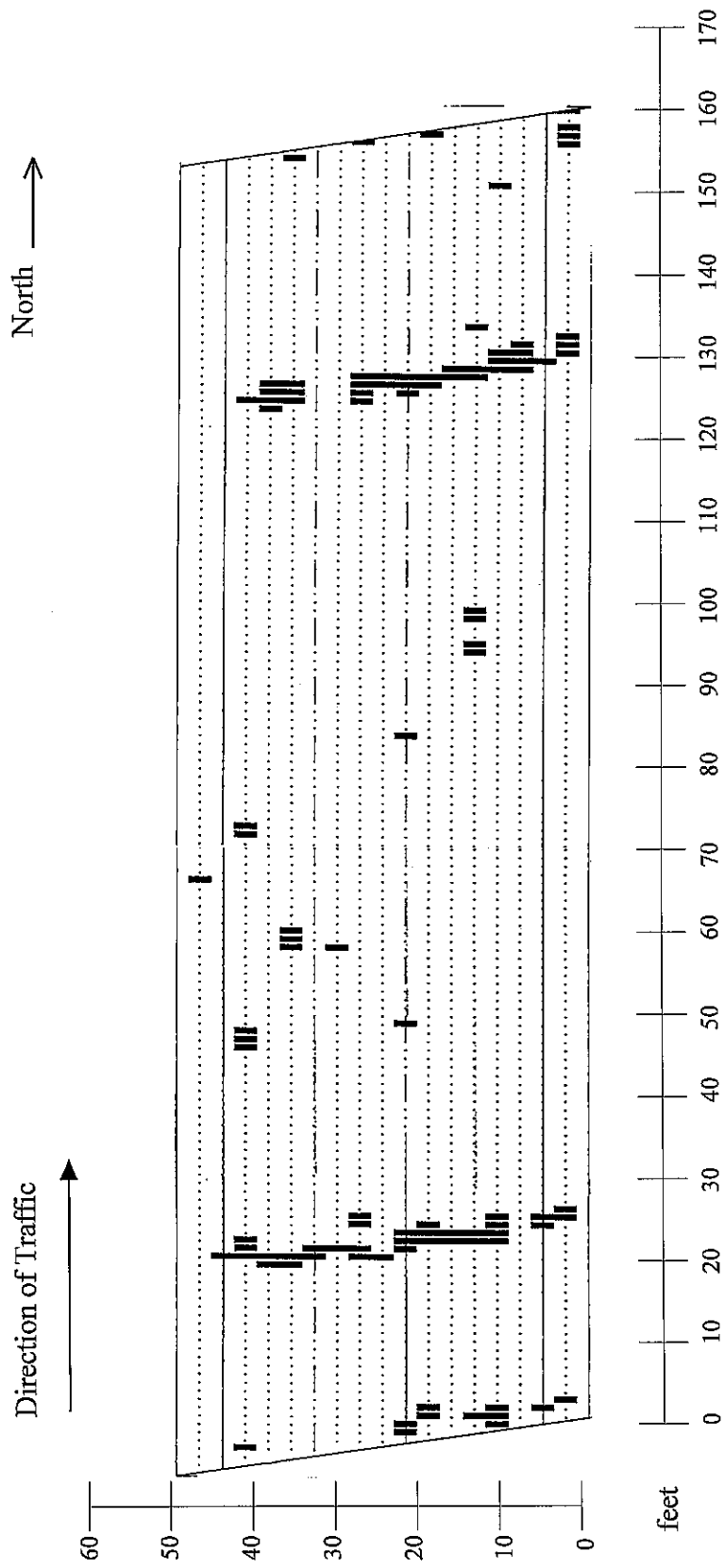


Figure C-12. Peoria Structure Number 072-0109 ground penetrating radar delamination survey (from Penetradar final report⁸⁸). Dark areas indicate delaminations.

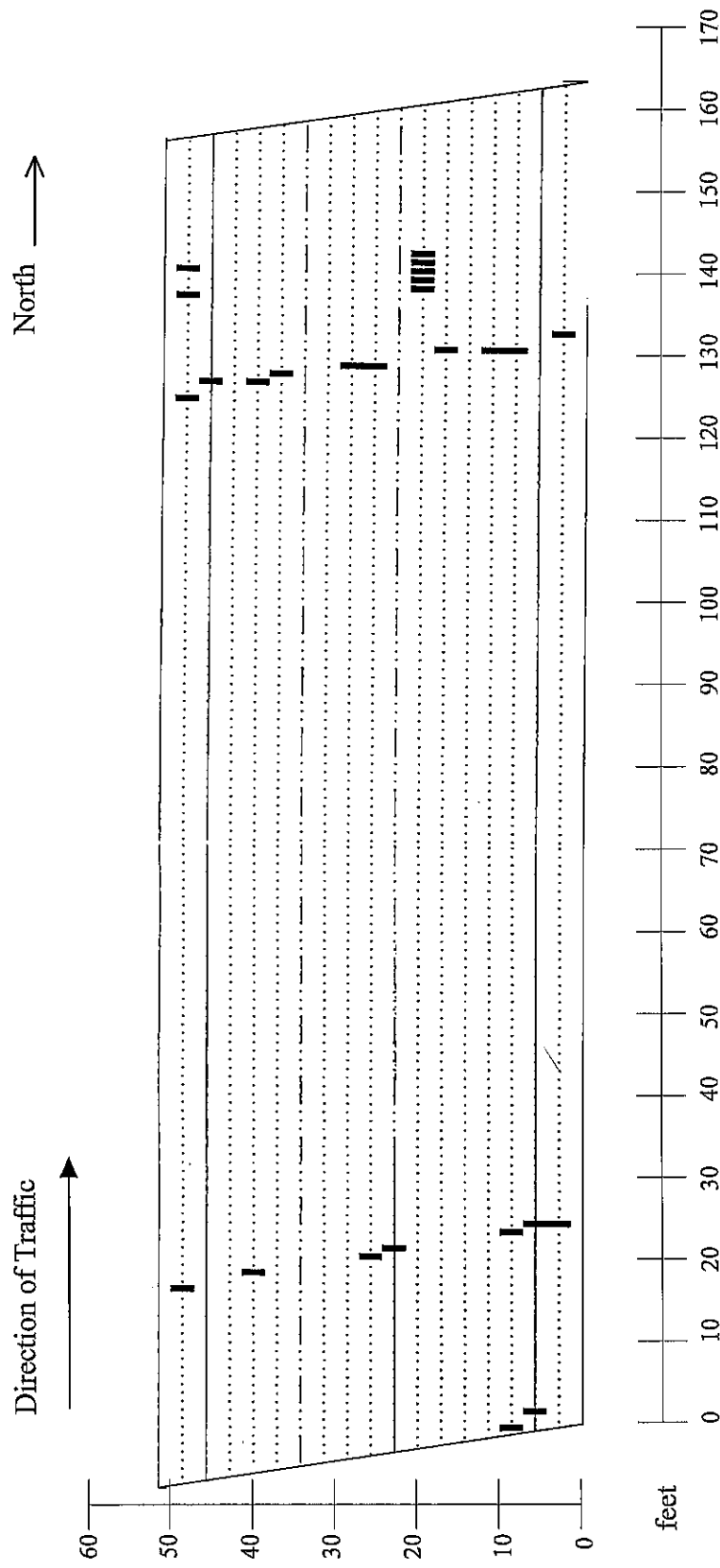


Figure C-13. Peoria Structure Number 072-0109 ground penetrating radar scaling survey (from Penetradar final report⁸⁸). Dark areas indicate delaminations.

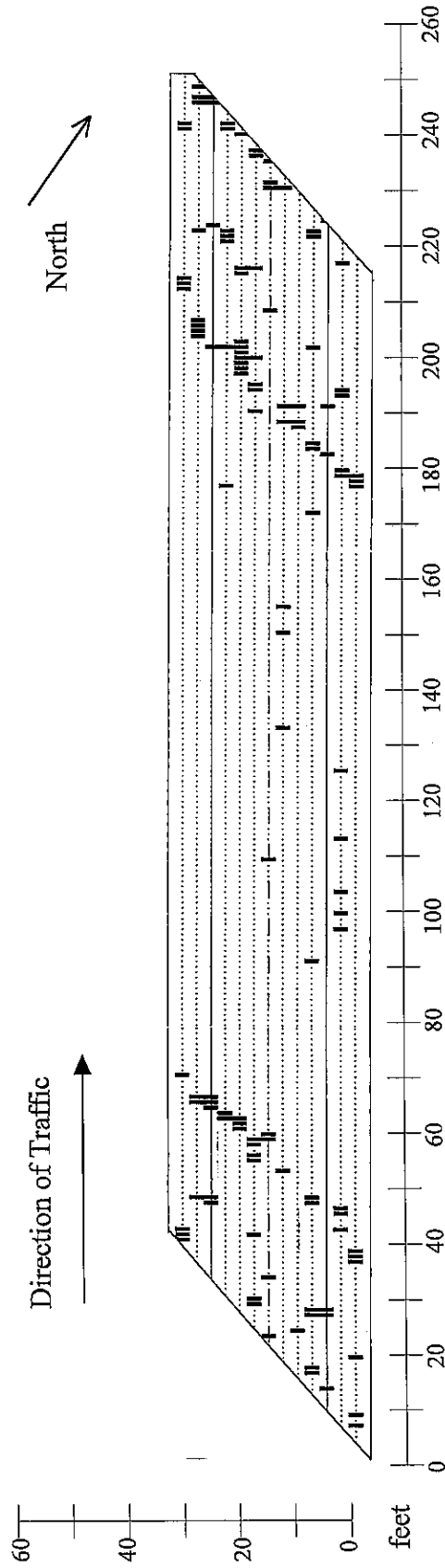


Figure C-14. Peoria Structure Number 072-0110 ground penetrating radar delamination survey (from Penetradar final report⁸⁸). Dark areas indicate delaminations.

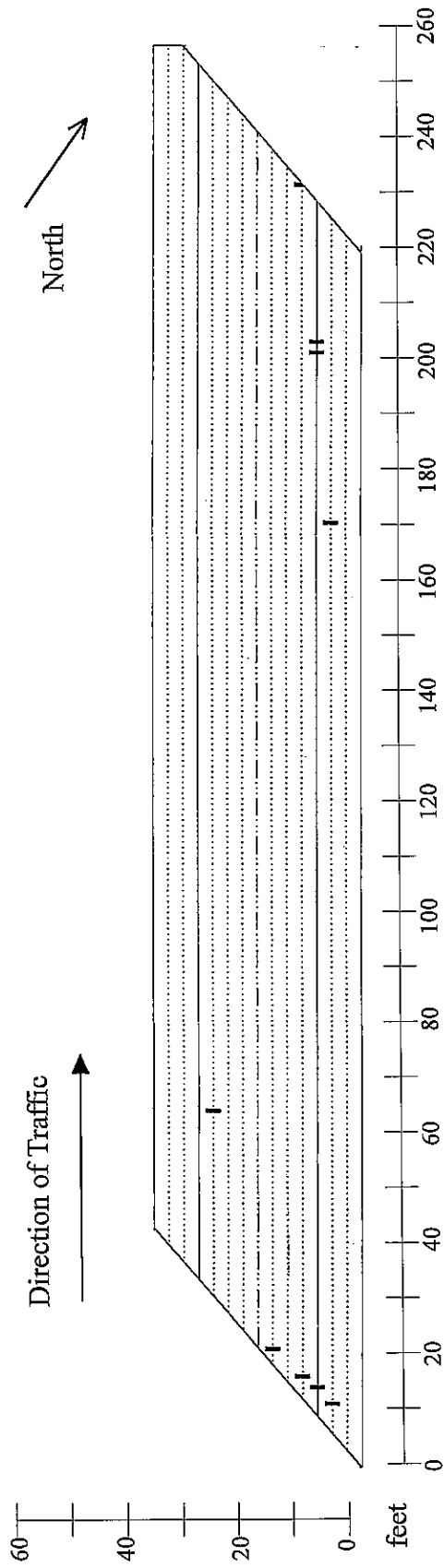


Figure C-15. Peoria Structure Number 072-0110 ground penetrating radar sealing survey (from Penetradar final report⁸⁸). Dark areas indicate delaminations.

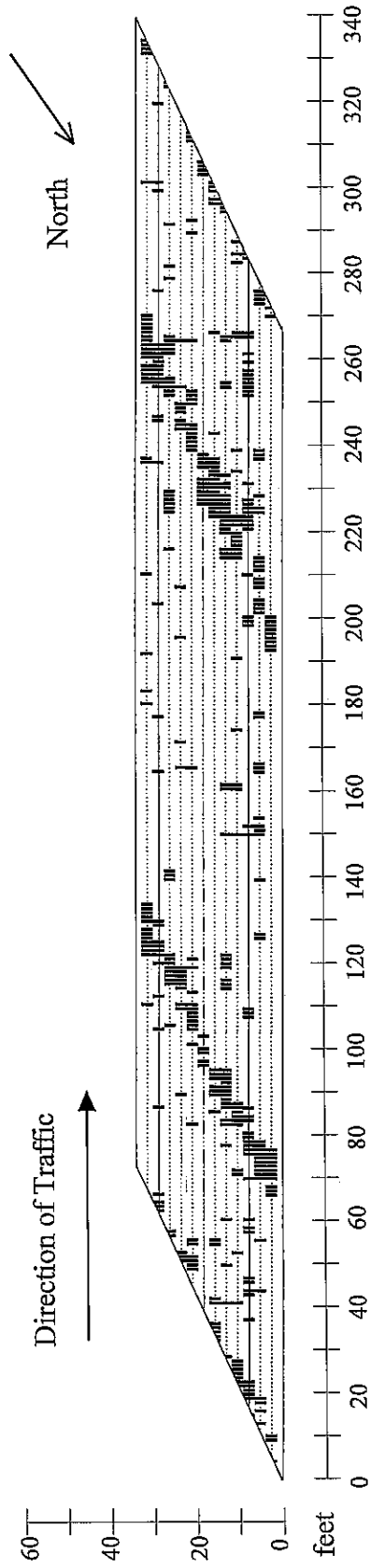


Figure C-16. Peoria Structure Number 072-0111 ground penetrating radar delamination survey (from Penetradar final report⁸⁸). Dark areas indicate delaminations.

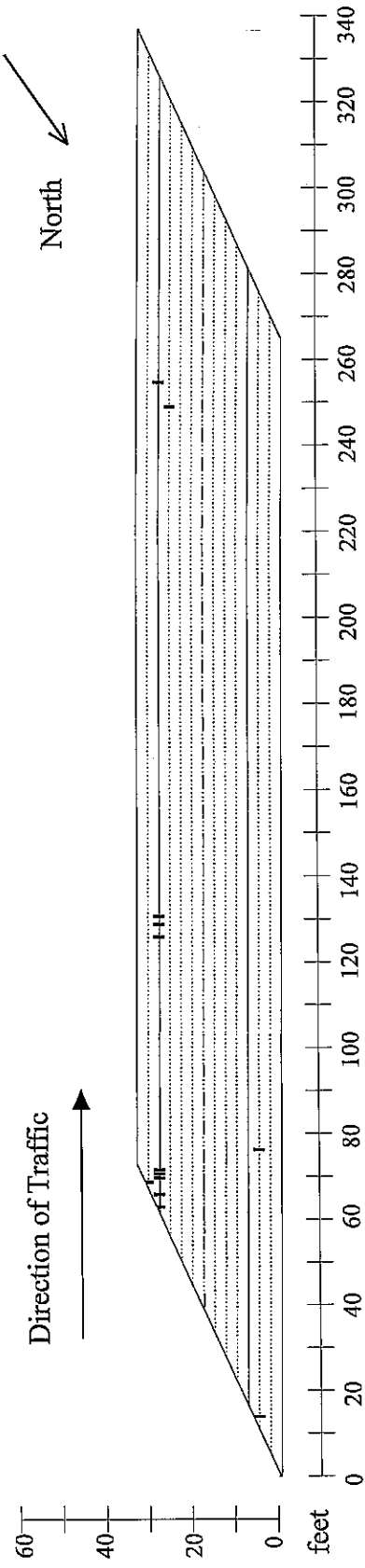


Figure C-17. Peoria Structure Number 072-0111 ground penetrating radar scaling survey (from Penetradar final report⁸⁸). Dark areas indicate delaminations.

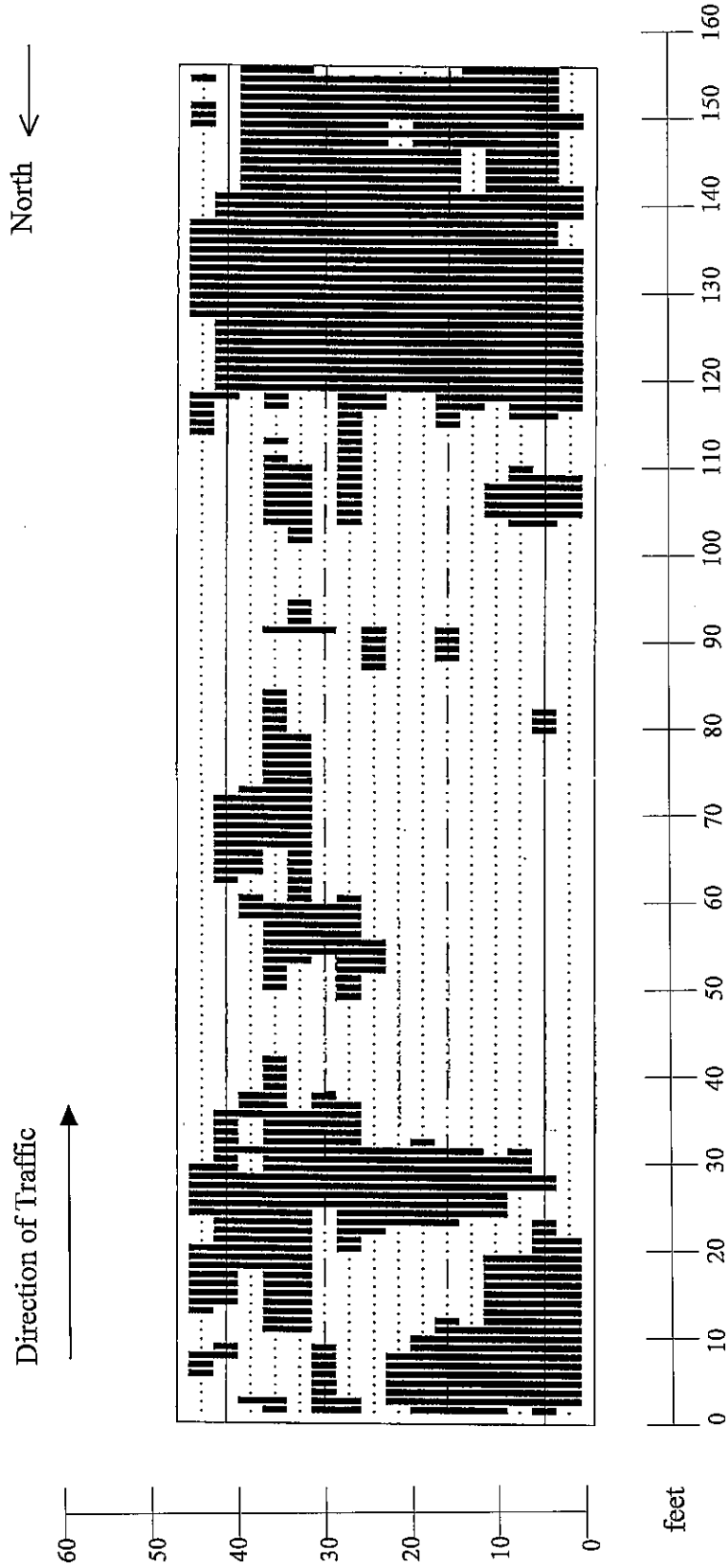


Figure C-18. Marion Structure Number 100-0005 ground penetrating radar delamination survey (from Penetradar final report⁸⁶). Dark areas indicate delaminations.

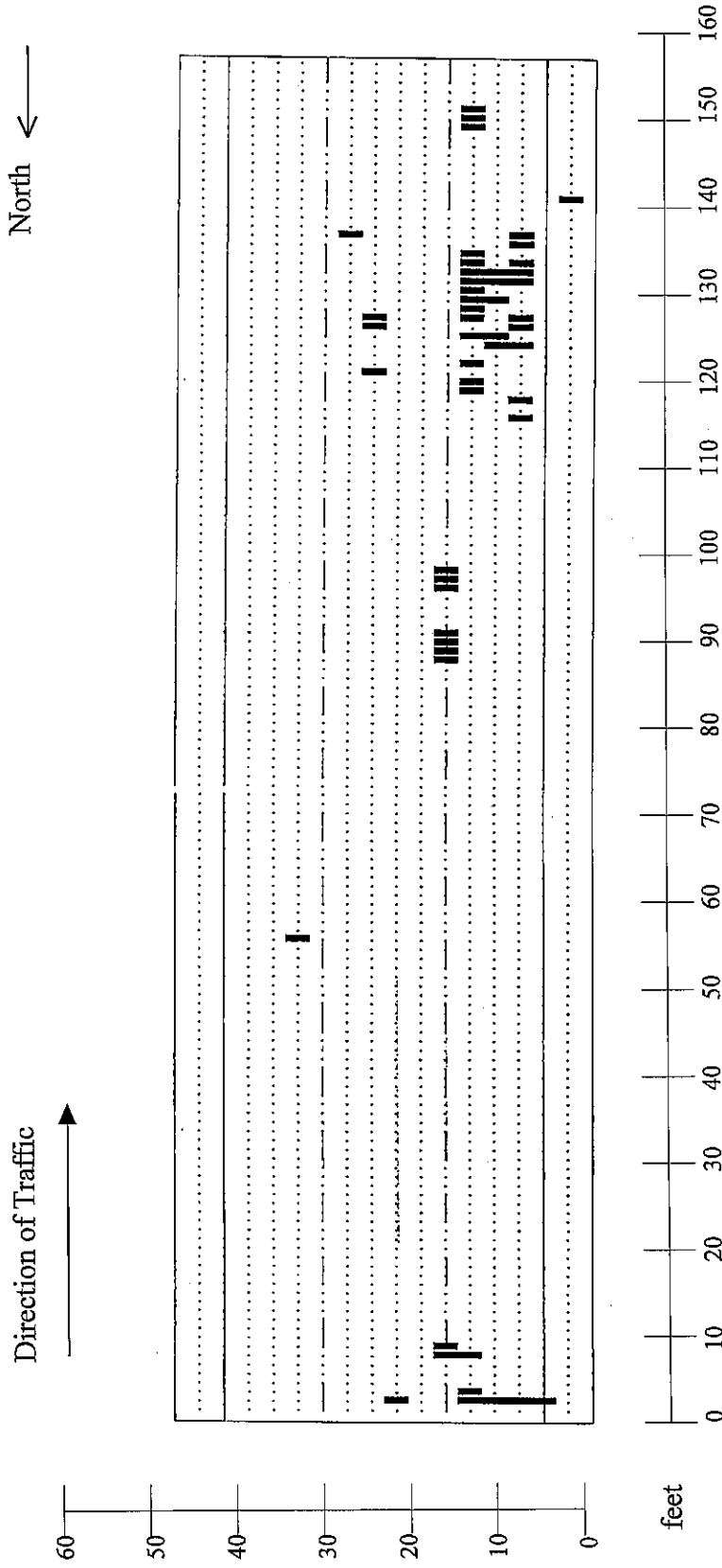


Figure C-19. Marion Structure Number 100-0005 ground penetrating radar scaling survey (from Penetradar final report⁸⁸). Dark areas indicate delaminations.

APPENDIX D—IMPACT-ECHO AND SPECTRAL ANALYSIS OF SURFACE WAVES
SURVEY RESULTS

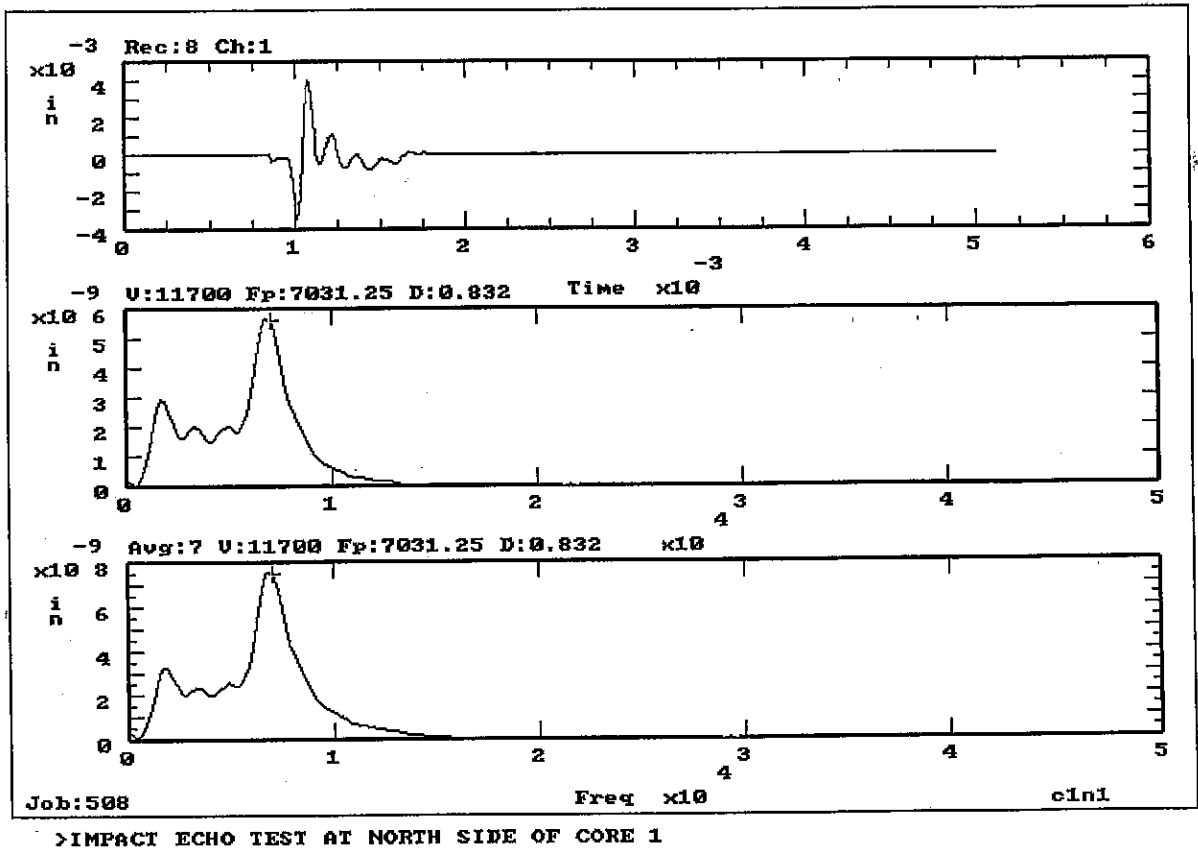


Figure D-2. Marion Structure Number 100-0005 handheld impact-echo test at north side of corehole 1 (from Olson final report⁸⁹).

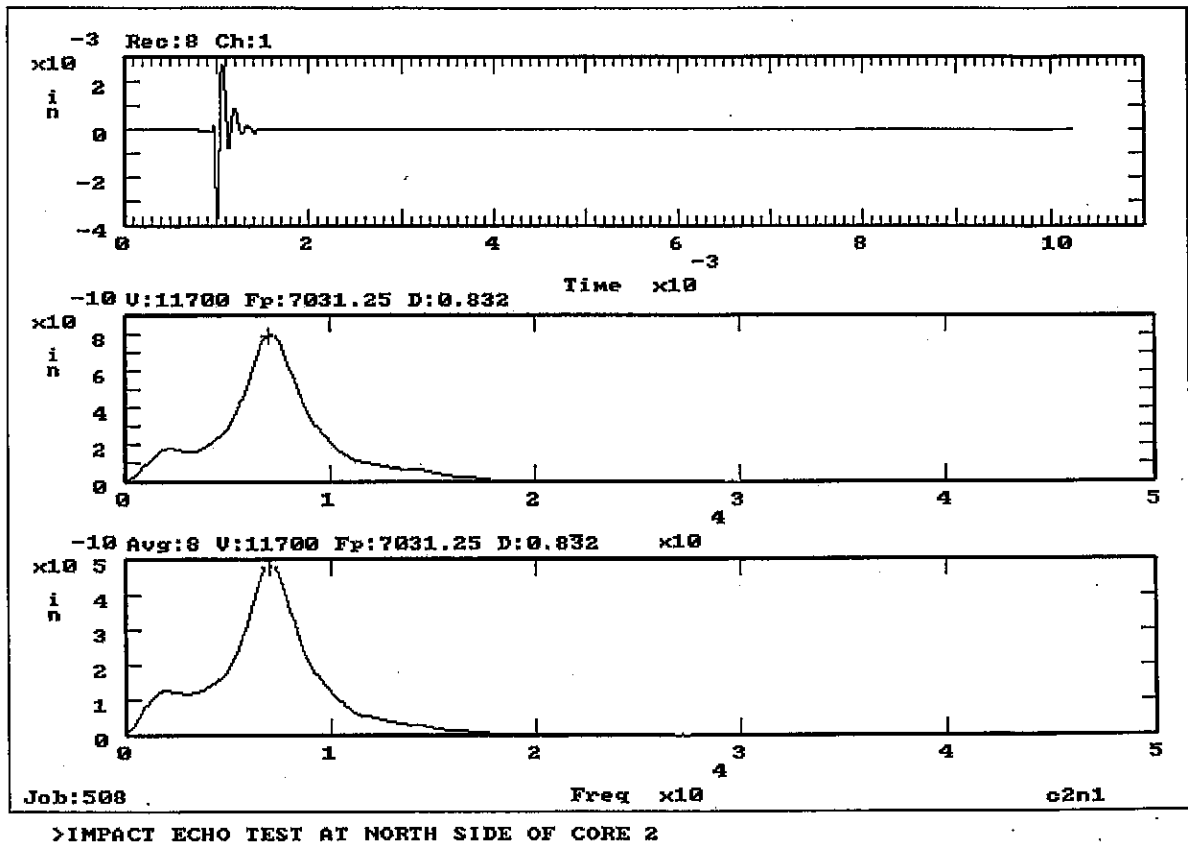


Figure D-3. Marion Structure Number 100-0005 handheld impact-echo test at north side of corehole 2 (from Olson final report⁸⁹).

JOB: E. LANE SCAN 1 LOG: IE1.PL1	CURRENT CHAN: 1
DEPTH vs. THICKNESS _____	RECORD: 5 DIST: 2.0 ft.
DEPTH vs. TOT. ENERGY	WT = 10.43 in.
	Etot = 8 VuS Ense = 0.00 VuS

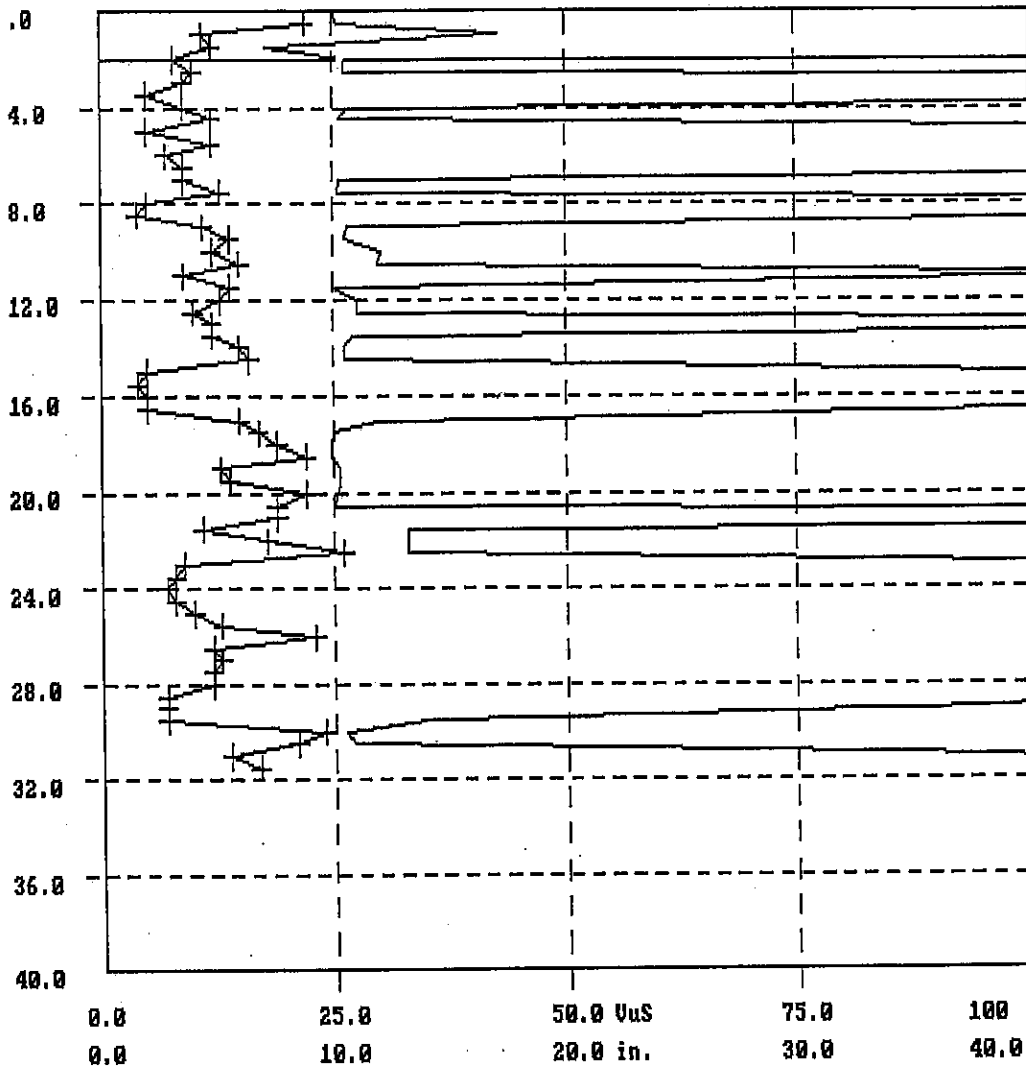


Figure D-4. Marion Structure Number 100-0005 handheld impact-echo thickness plots from 0 to 31.5 feet (9.60 m) along east scan line1-channel 2 (from Olson final report⁸⁹).

JOB: IE-1 SCAN E1 L2 LOG: IE2.PL1	CURRENT CHAN: 1
DEPTH vs. THICKNESS	RECORD: 10 DIST: 4.5 ft.
DEPTH vs. TOT. ENERGY	WT = 10.73 in.
	Etot = 13 VuS Ense = 0.00 VuS

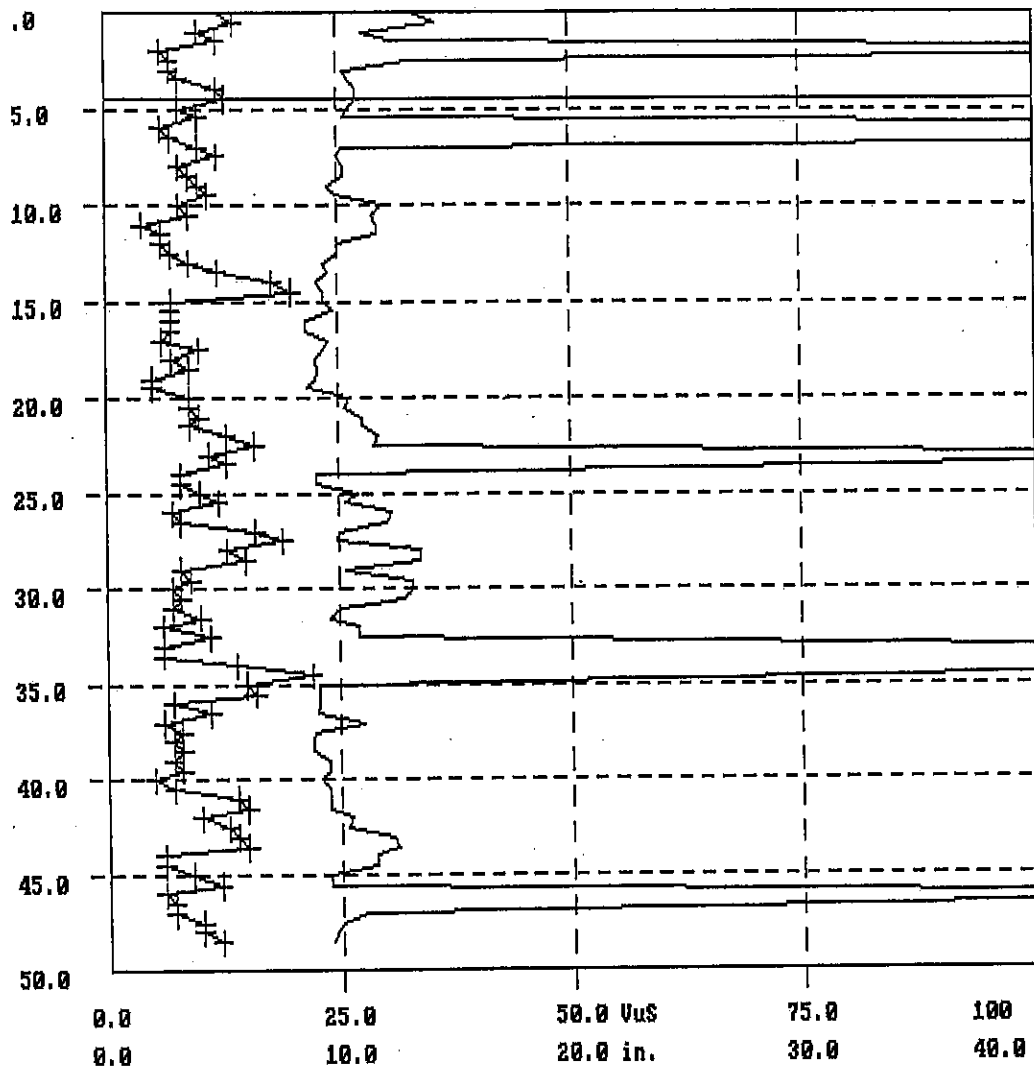


Figure D-5. Marion Structure Number 100-0005 handheld impact-echo thickness plots from 32.0 to 80.0 ft (9.75 to 24.4 m) along east scan line1-channel 2 (from Olson final report⁸⁹).

JOB: CENTER SCAN 2	LOG: C2.PL	PEAK: 7.61kHz/ 9.22 in
RECORD: 59	DEPTH: 26.0 ft.	PEAKS: 5.07 3.50 kHz Etot: 227
VOLTAGE vs. FREQ		Pk Sig: 17676 mV
PLOTTING...		Freq: 7.60 kHz, U: 3764 mV WT: 9.23 in

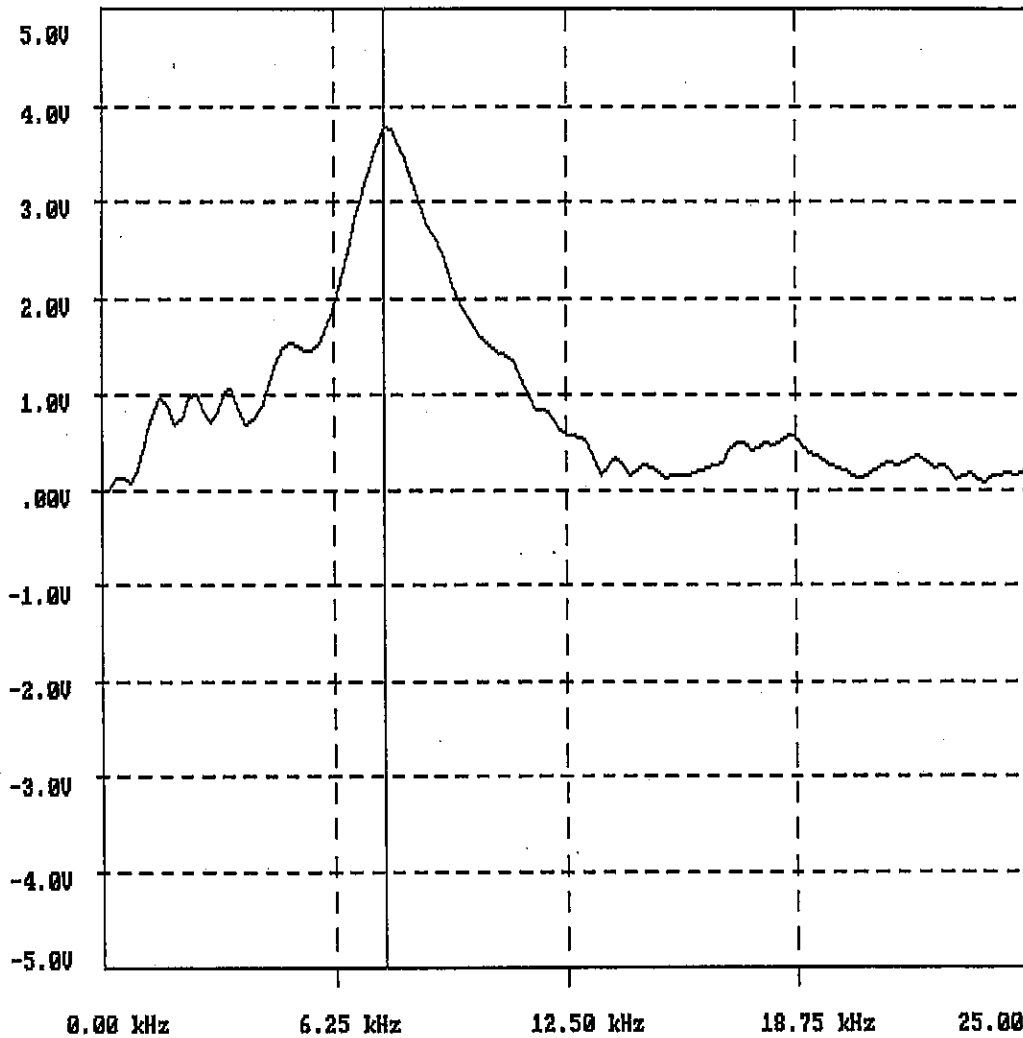


Figure D-6. Marion Structure Number 100-0005 impact-echo scanner example of good results from center scan line 2, transducer channel 3 (from Olson final report⁸⁹).

JOB: CENTER SCAN 2	LOG: C2.PL	PEAK: 1.56kHz/ 45.00 in
RECORD: 52	DEPTH: 22.8 ft.	PEAKS: 19.53 5.45 kHz Etot: 347
VOLTAGE vs. FREQ		Pk Sig: 31424 mV
PLOTTING...		Freq: 6.82 kHz, U: 1591 mV WT: 10.28 in

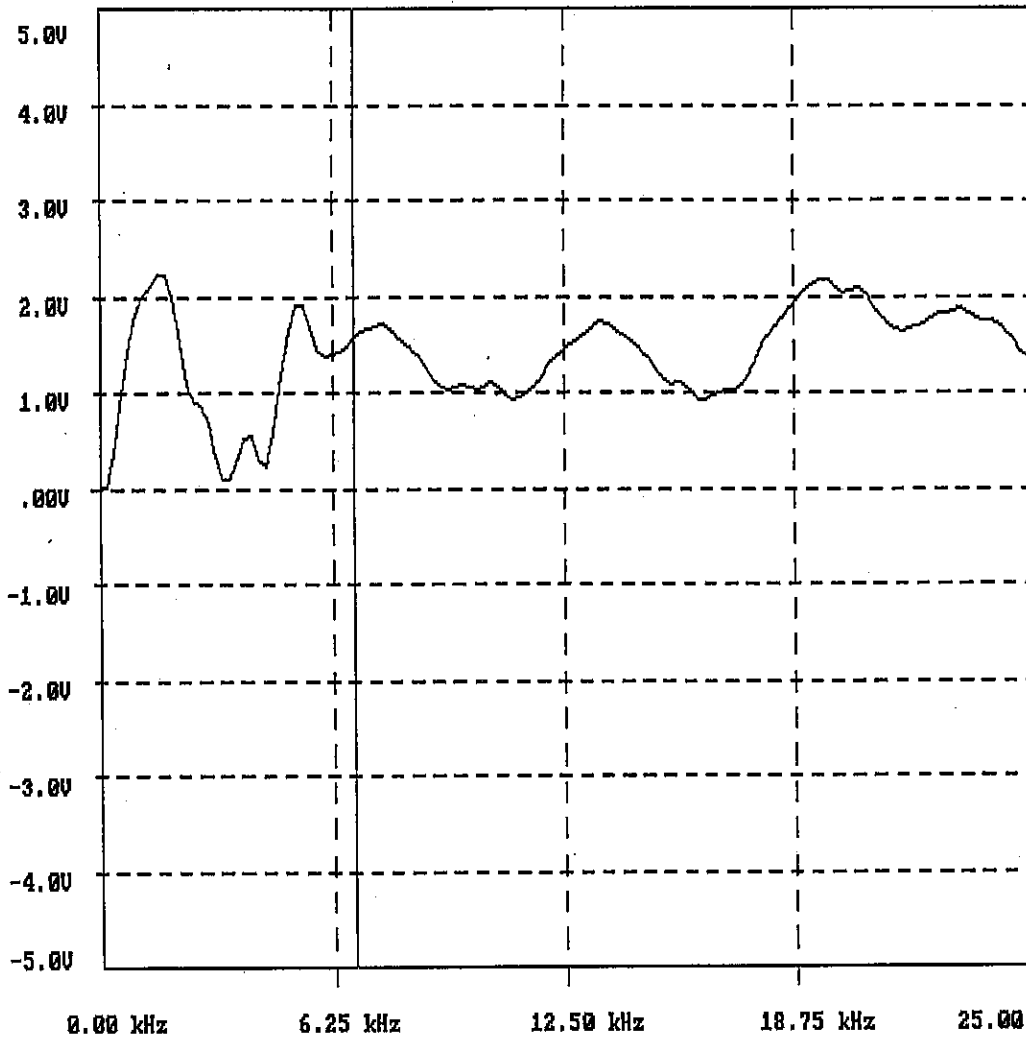


Figure D-7. Marion Structure Number 100-0005 impact-echo scanner example of poor results from center scan line 2, transducer channel 4 (from Olson final report⁸⁹).

JOB: CENTER SCAN 2	LOG: C2.PL1	CURRENT CHAN: 3
DEPTH vs. THICKNESS		RECORD: 4
DEPTH vs. TOT. ENERGY	+++++	DIST: 2.3 ft
		WT = 9.46 in
		Etot = 107 VuS
		Ense = 0.00 VuS

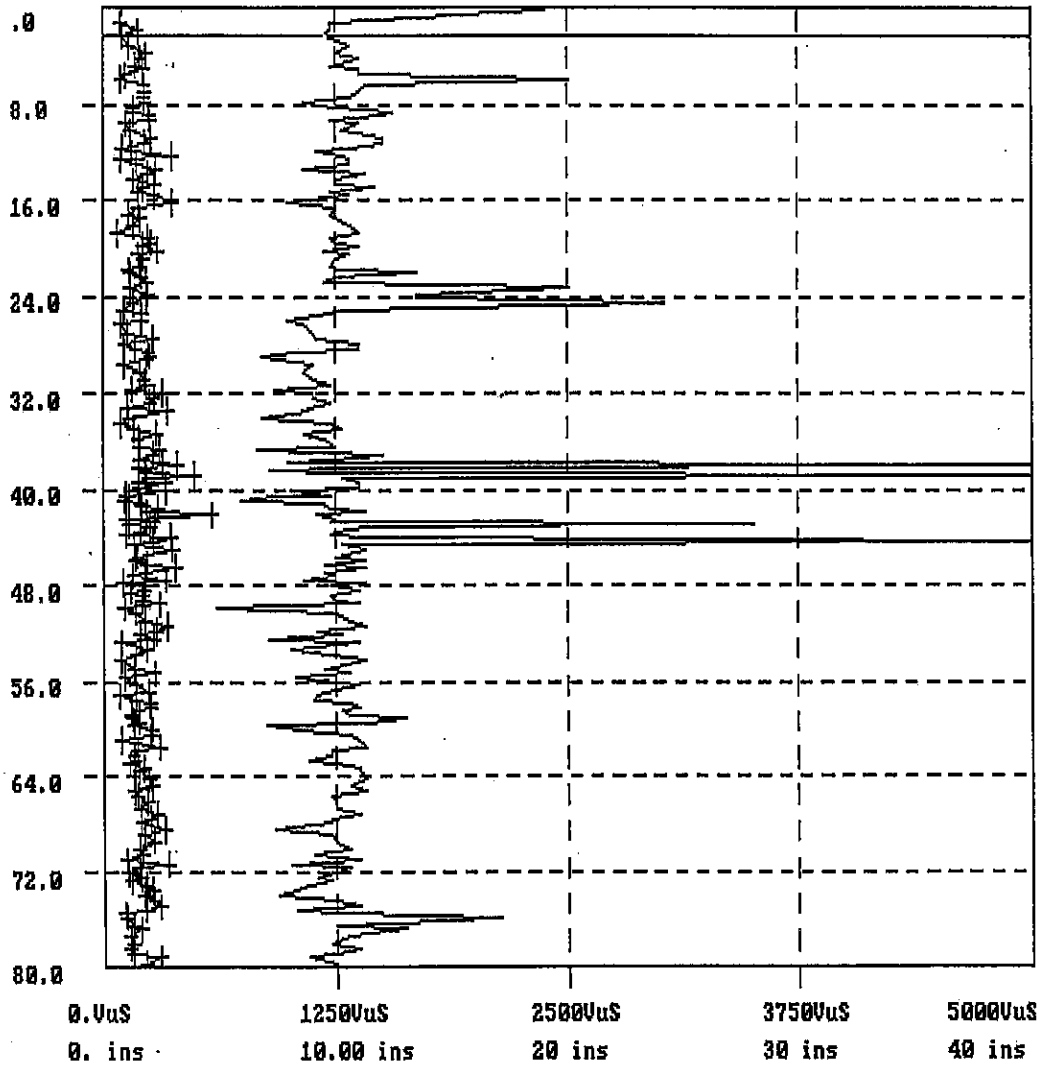


Figure D-8. Marion Structure Number 100-0005 impact-echo scanner example of good thickness results from center scan line 2, channel 3 (from Olson final report⁸⁹).

JOB: EAST SCAN 1	LOG: E1.PL1	CURRENT CHAN: 2
DEPTH vs. THICKNESS		RECORD: 17
DEPTH vs. TOT. ENERGY		DIST: 4.2 ft
		WT = 7.99 in
		Etot = 269 VuS
		Ense = 0.00 VuS

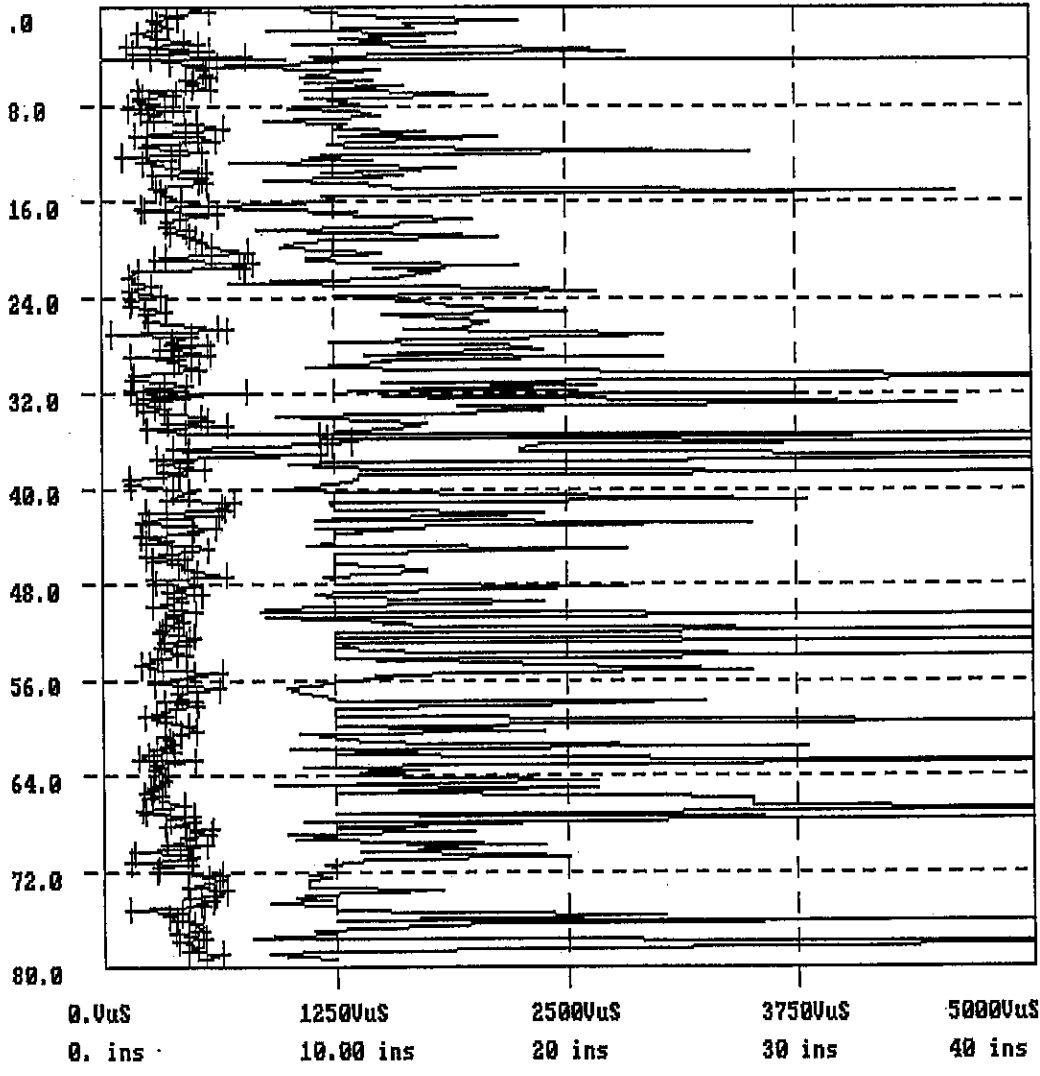


Figure D-9. Marion Structure Number 100-0005 impact-echo scanner example of poor thickness results from east scan line 1, channel 2 (from Olson final report⁸⁹).

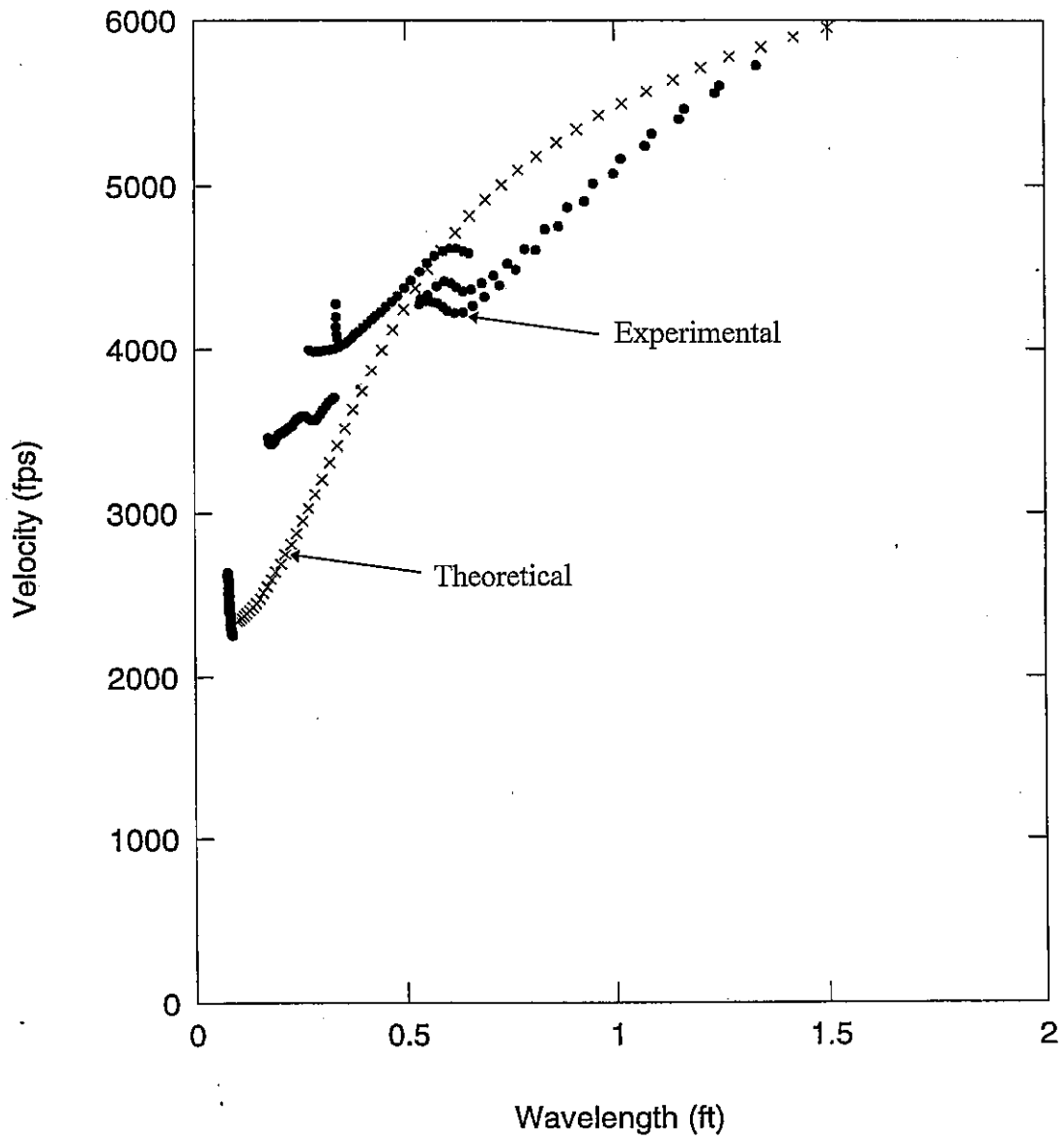
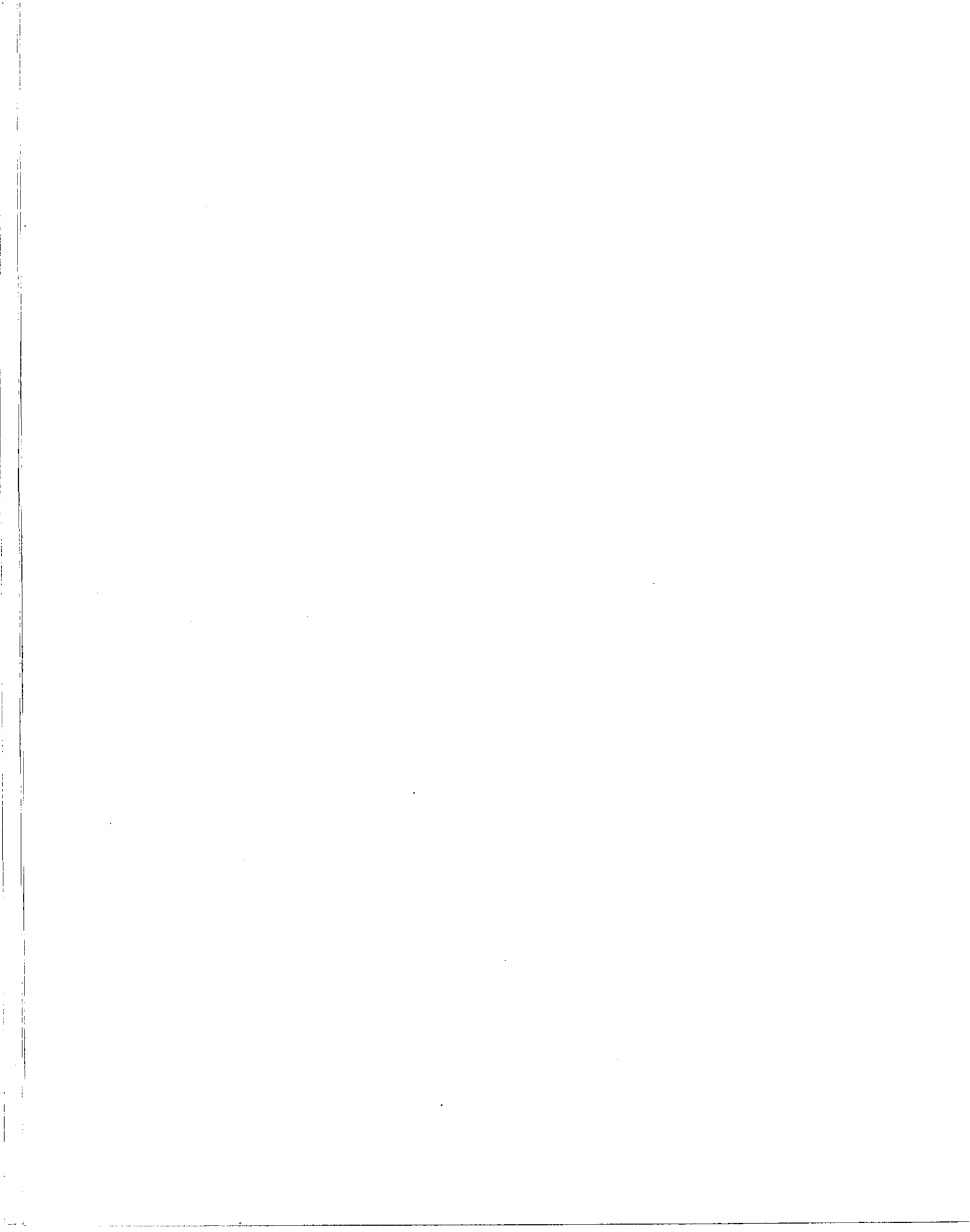


Figure D-10. Marion Structure Number 100-0005 spectral analysis of surface waves experimental and theoretical dispersion curves at core 2 (from Olson final report⁸⁹).



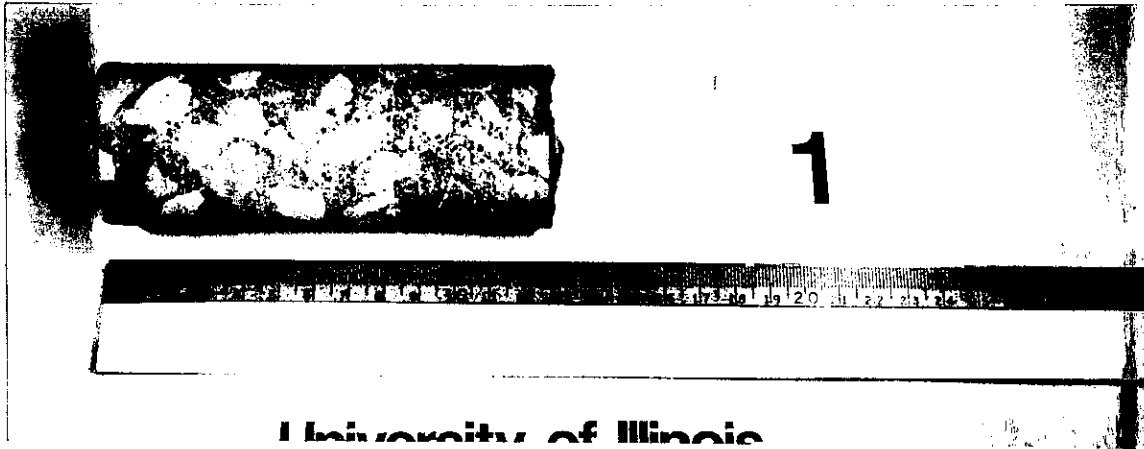


Figure E-1. Core #1 from Peoria Structure Number 090-0118—solid (from Rust final report⁸⁷).

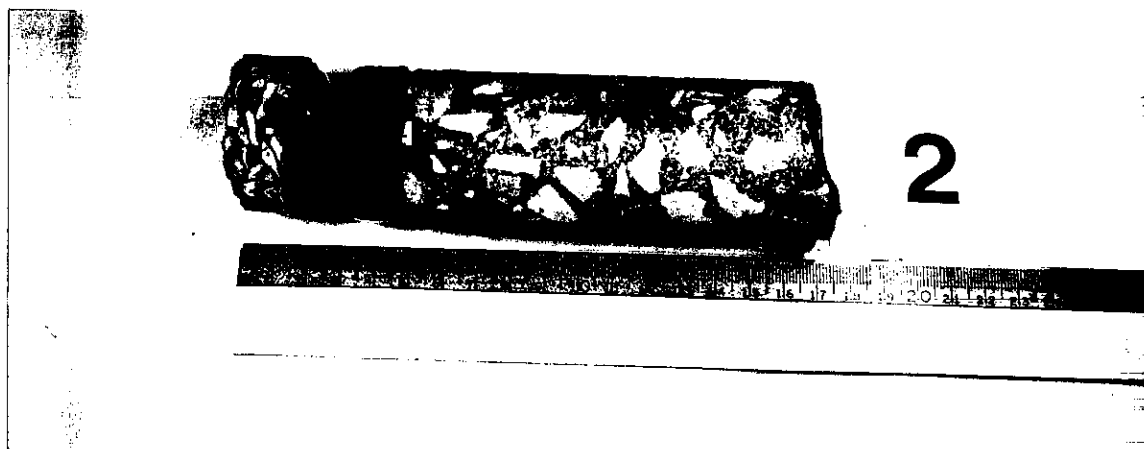


Figure E-2. Core #2 from Peoria Structure Number 072-0109—debonded (from Rust final report⁸⁷).

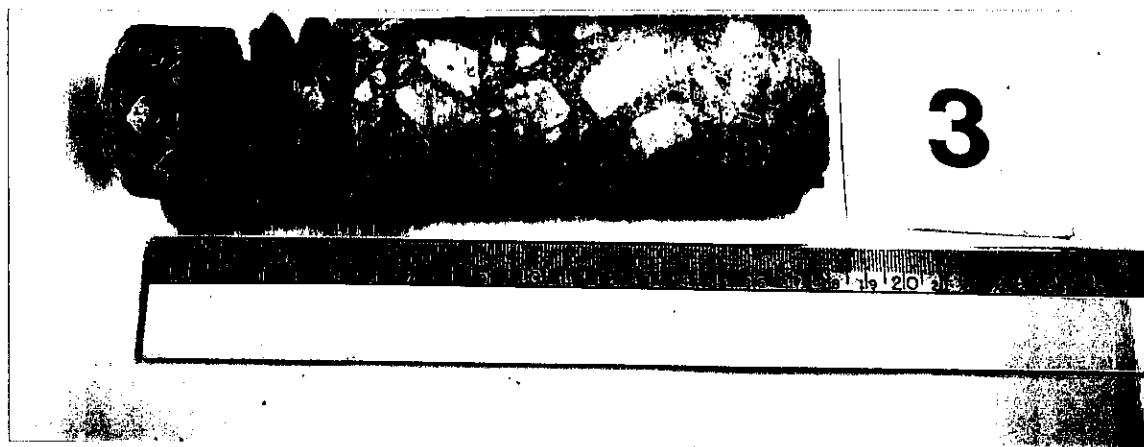


Figure E-3. Core #3 from Peoria Structure Number 072-0109—debonded and delaminated (from Rust final report⁸⁷).

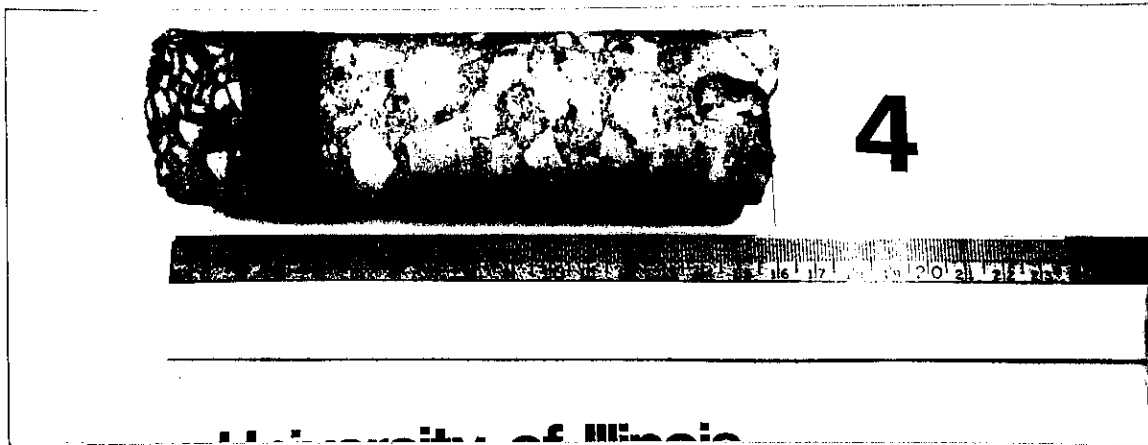


Figure E-4. Core #4 from Peoria Structure Number 072-0107—debonded (from Rust final report⁸⁷).

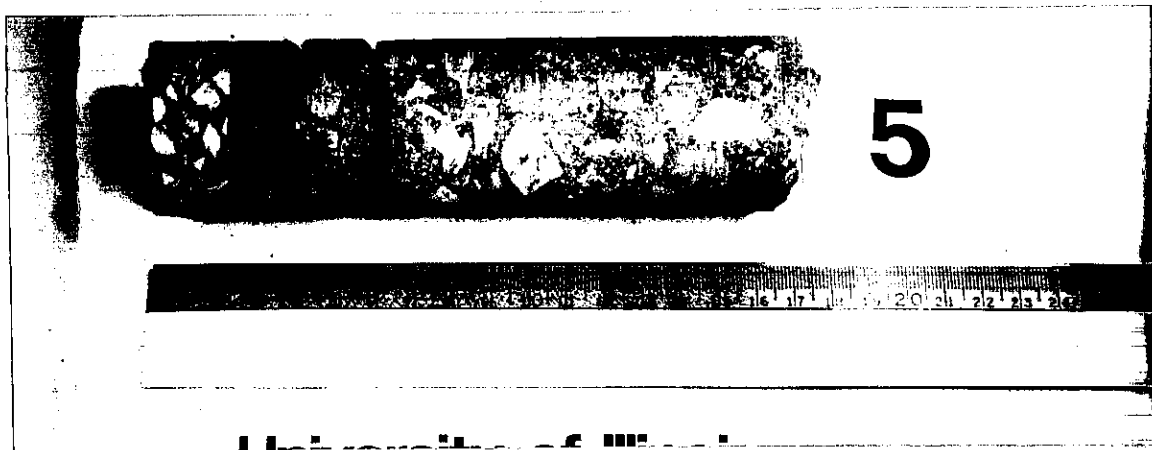


Figure E-5. Core #5 from Peoria Structure Number 072-0107—debonded and delaminated (from Rust final report⁸⁷).

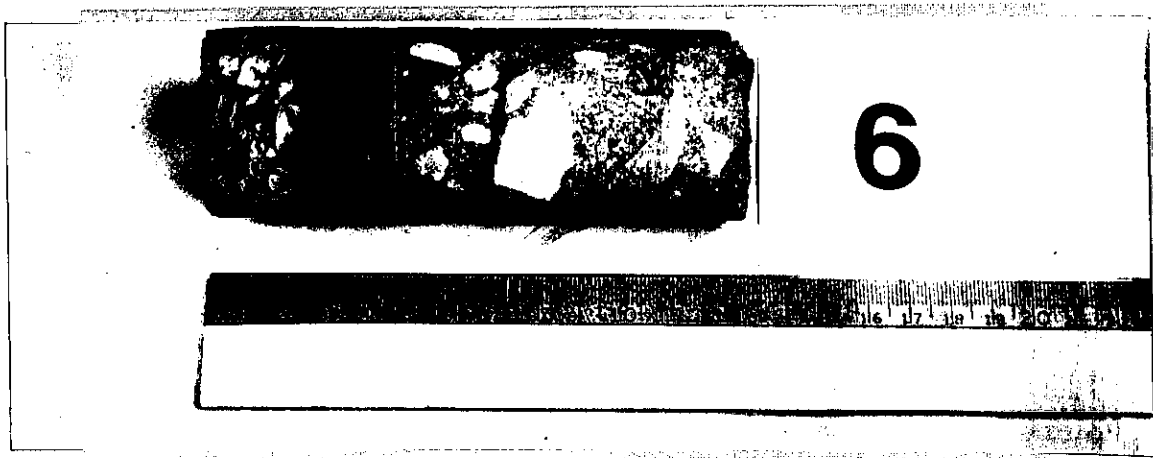


Figure E-6. Core #6 from Peoria Structure Number 072-0106—delaminated (from Rust final report⁸⁷).

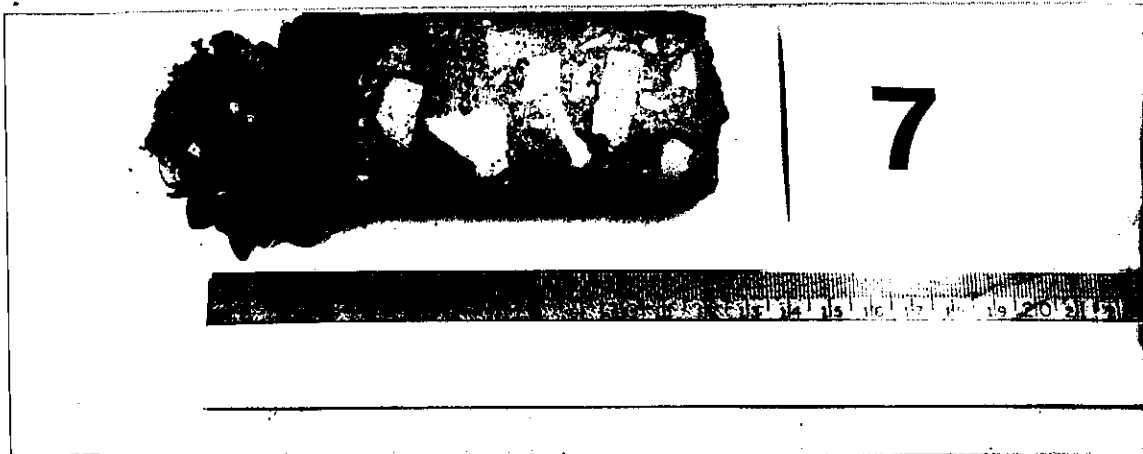


Figure E-7. Core #7 from Peoria Structure Number 072-0106—debonded (from Rust final report⁸⁷).

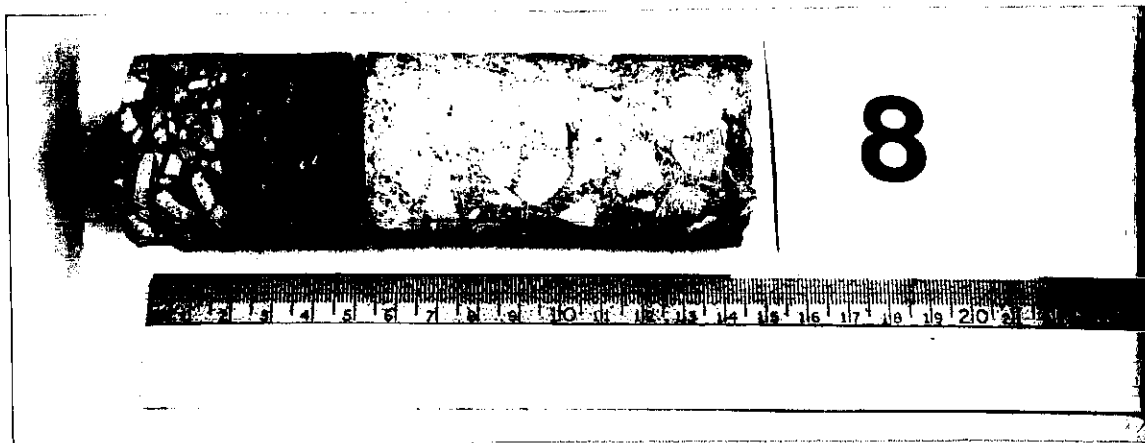


Figure E-8. Core #8 from Peoria Structure Number 072-0108—debonded (from Rust final report⁸⁷).

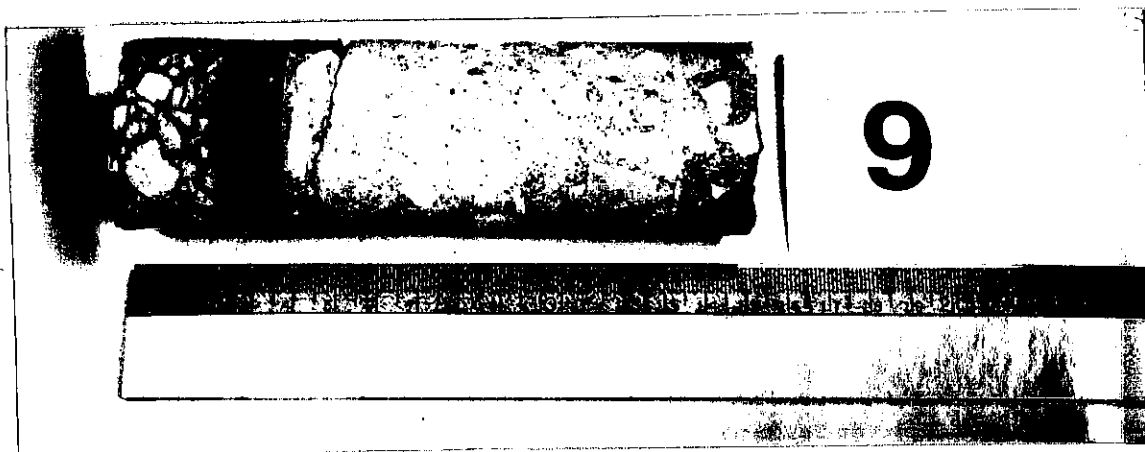


Figure E-9 Core #9 from Peoria Structure Number 072-0108—debonded and delaminated (from Rust final report⁸⁷).

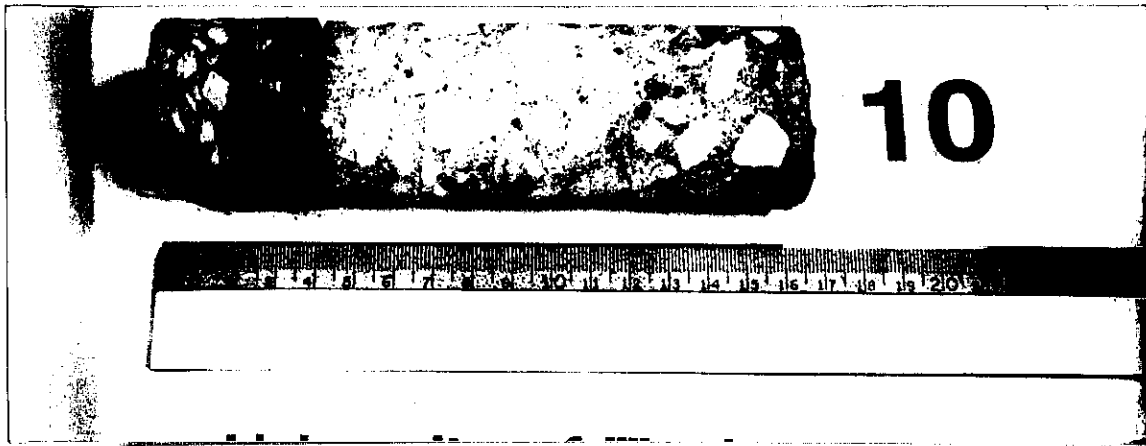


Figure E-10. Core #10 from Peoria Structure Number 072-0108—debonded (from Rust final report⁸⁷).

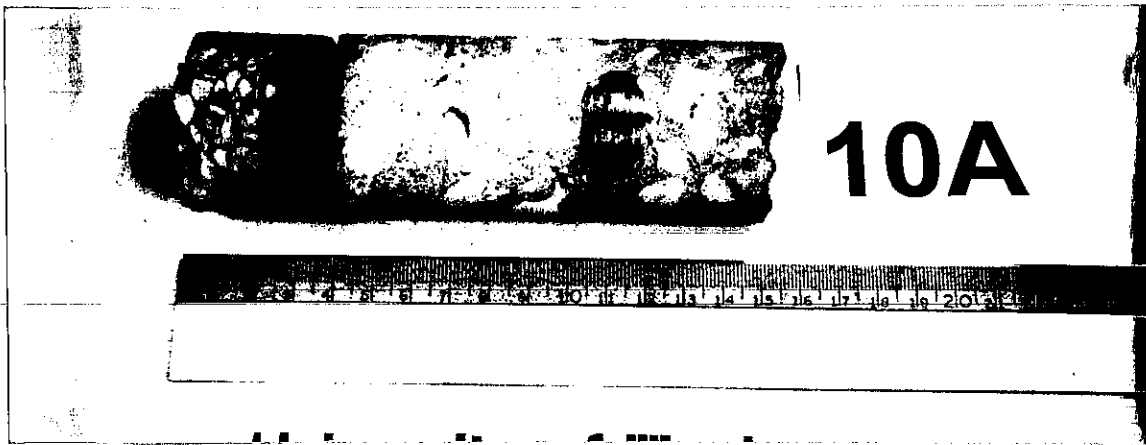


Figure E-10A. Core #10A from Peoria Structure Number 072-0108—debonded (from Rust final report⁸⁷).

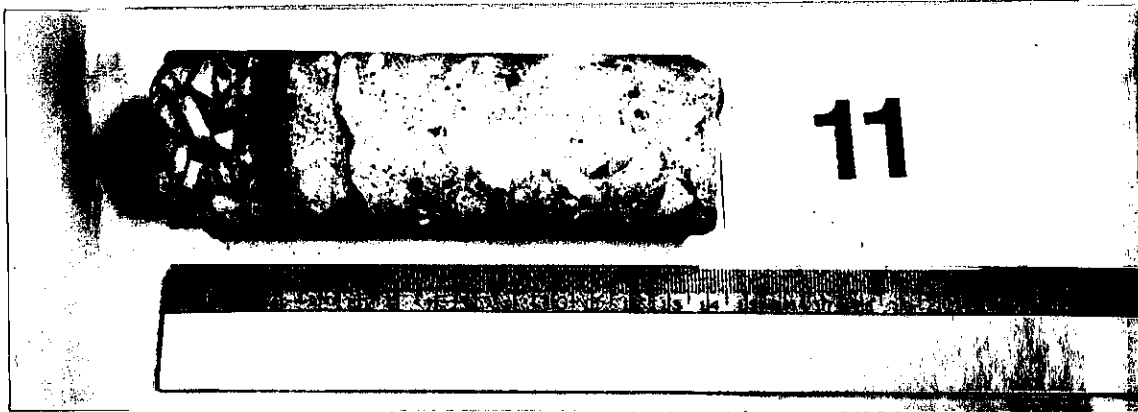


Figure E-11. Core #11 from Peoria Structure Number 072-0111—delaminated (from Rust final report⁸⁷).

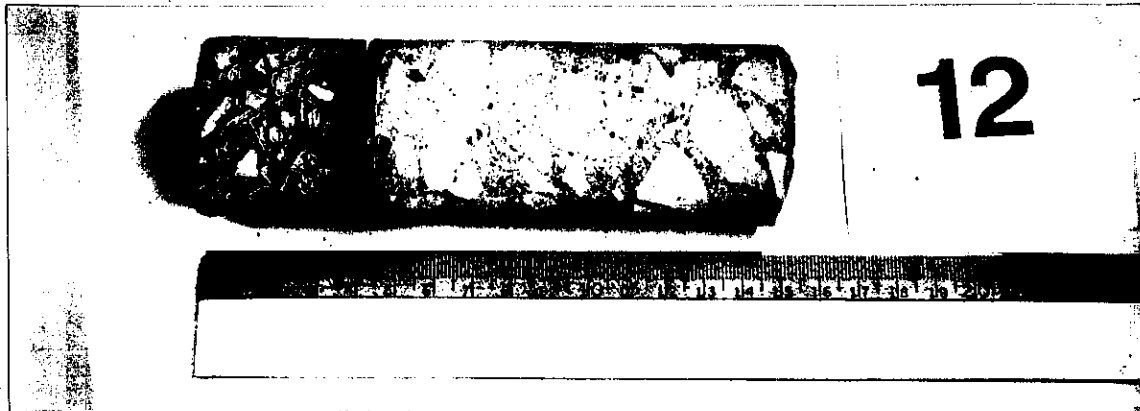


Figure E-12. Core #12 from Peoria Structure Number 072-0111—debonded (from Rust final report⁸⁷).

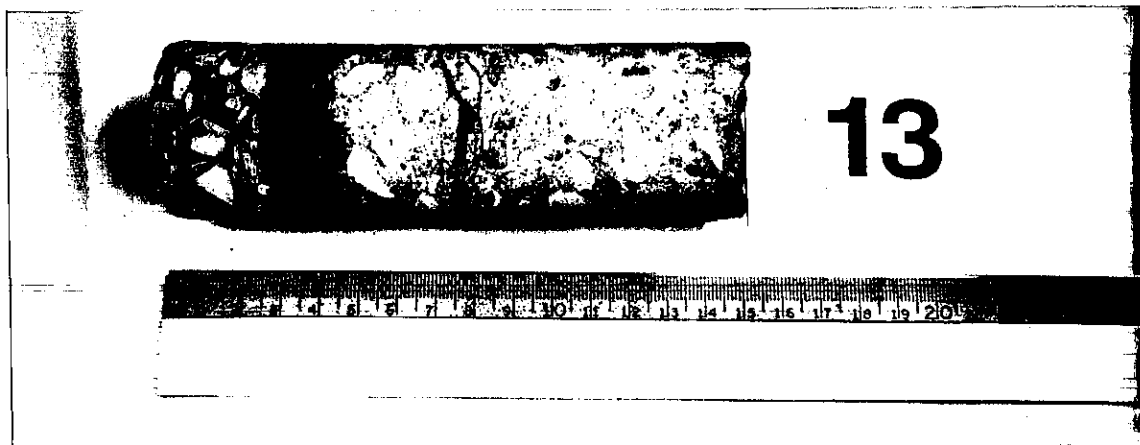


Figure E-13. Core #13 from Peoria Structure Number 072-0111—delaminated (from Rust final report⁸⁷).

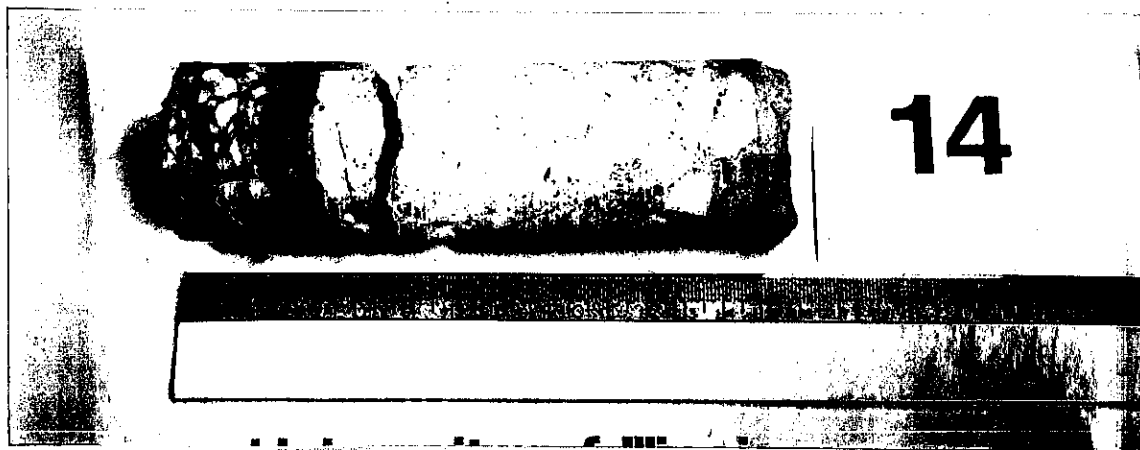


Figure E-14. Core #14 from Peoria Structure Number 072-0110—delaminated (from Rust final report⁸⁷).

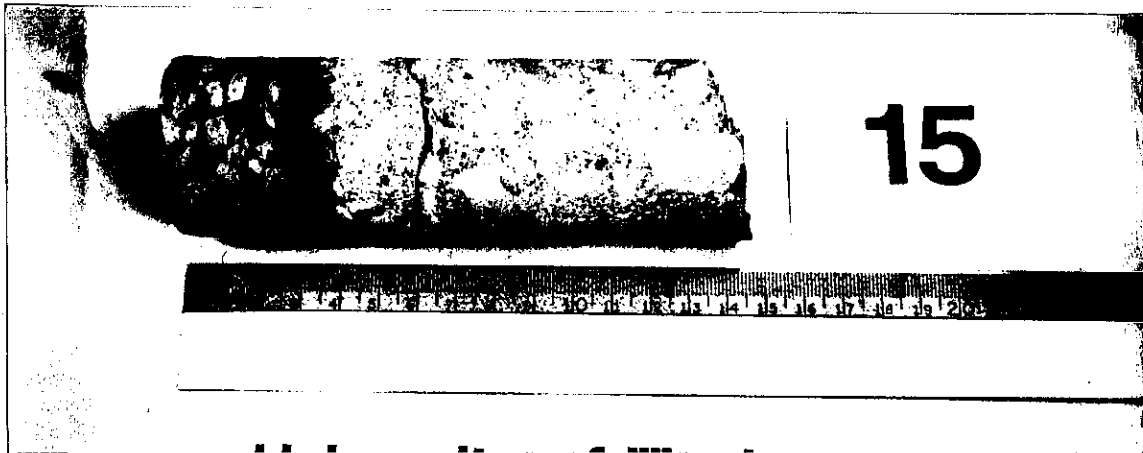


Figure E-15. Core #15 from Peoria Structure Number 072-0110—delaminated (from Rust final report⁸⁷).

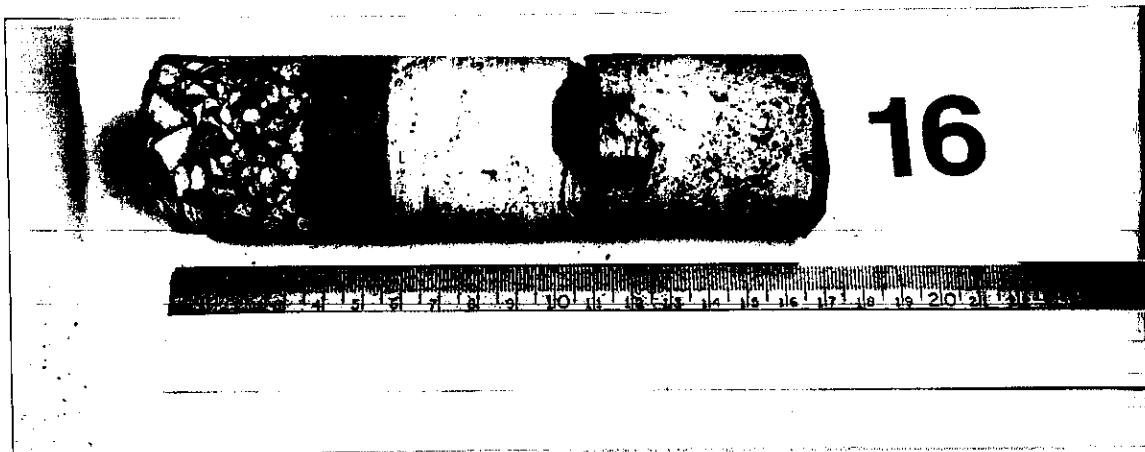


Figure E-16. Core #16 from Marion Structure Number 100-0005—delaminated (from Rust final report⁸⁷).

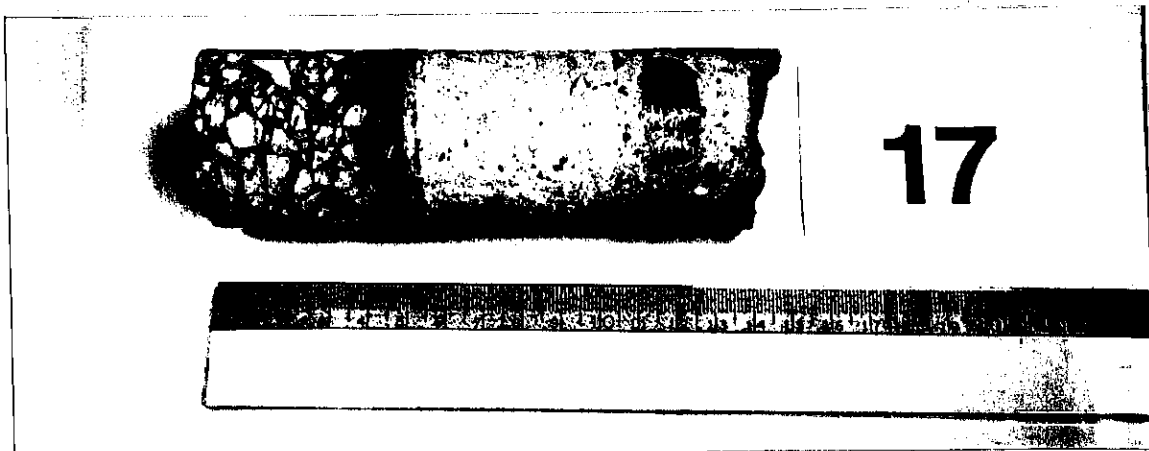


Figure E-17. Core #17 from Marion Structure Number 100-0005—solid (from Rust final report⁸⁷).

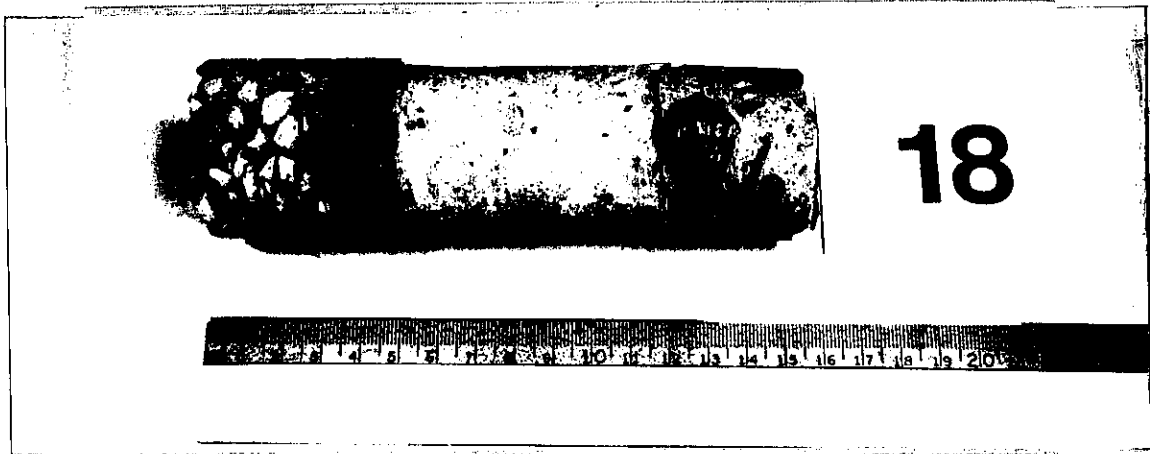


Figure E-18. Core #18 from Marion Structure Number 100-0005—debonded (from Rust final report⁸⁷).

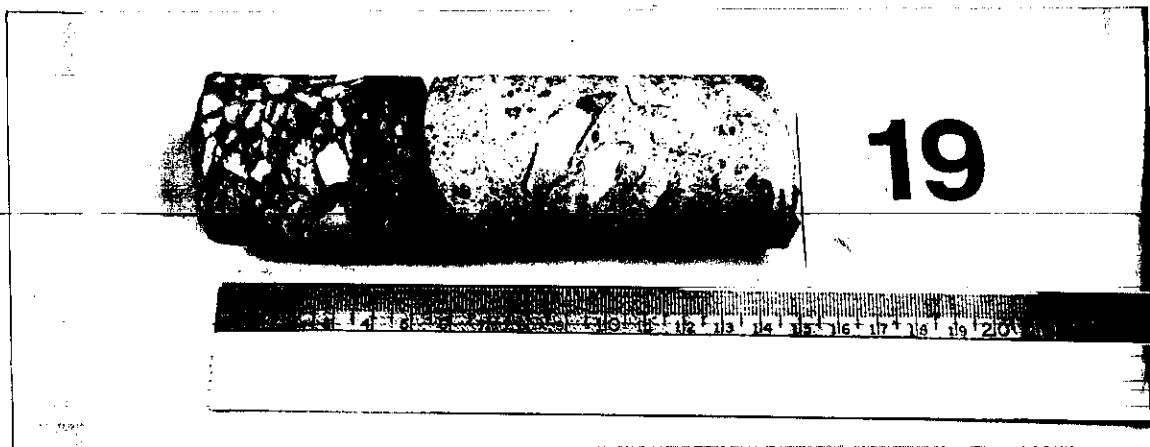


Figure E-19. Core #19 from Marion Structure Number 100-0005—delaminated (from Rust final report⁸⁷).



Figure E-20. Core #20 from Bloomington Structure Number 057-0088—delaminated (from Rust final report⁸⁷).

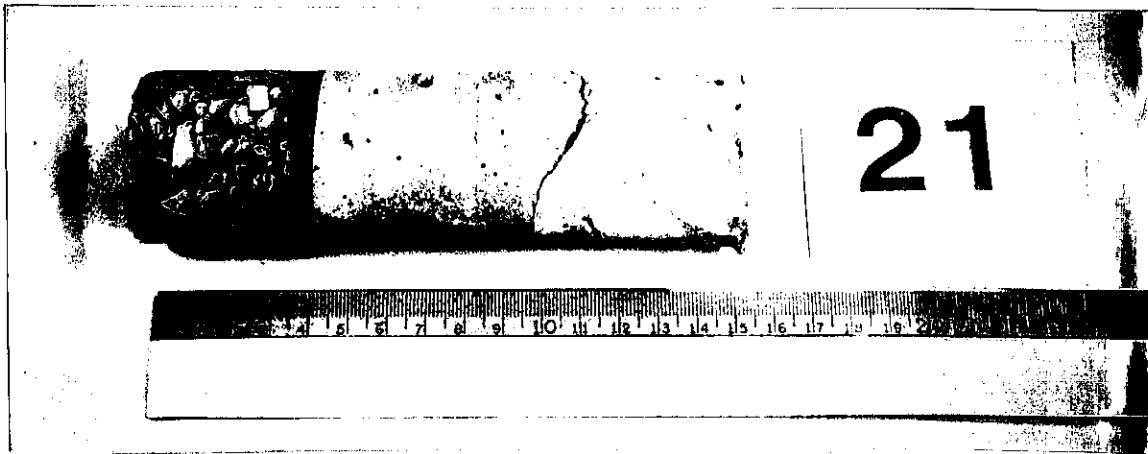


Figure E-21. Core #21 from Bloomington Structure Number 057-0088—solid (from Rust final report⁸⁷).

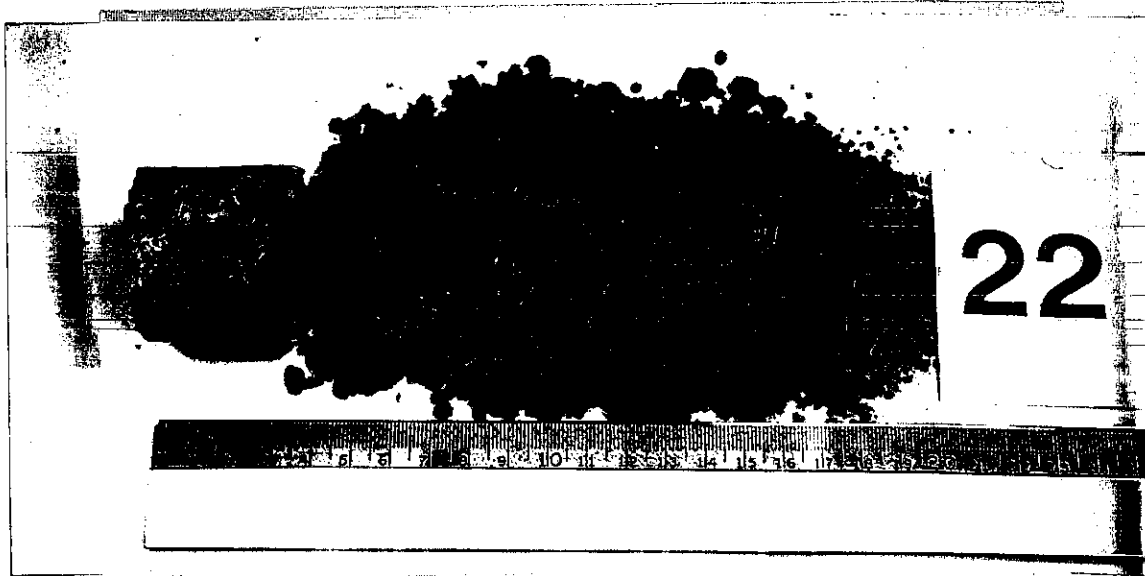


Figure E-22. Core #22 from Bloomington Structure Number 057-0088—rubble (from Rust final report⁸⁷).

APPENDIX F—CHAIN DRAG DATA

Table F-1 Chain drag survey field data for Bloomington Structure Number 057-0088 eastbound.

East Bound from Abutment About and Along Right (South) Curb in Feet			
Length Start	Length End	Width Start	Width End
0	1	2	4
0	1	10	18
3	4	9	10
6	8	13	15
5	11	0	4
9	11	8	10
11	14	4	15
14	17	13	19
13	16	0	4
16	19	0	6
19	24	0	19
23	25	0	7
23	26	14	20
26	28	12	14
27	30	0	8
30	32	0	11
32	35	0	14
30	34	18	21
36	41	0	6
41	45	0	12
35	47	0	6
47	49	0	18
47	49	26	33
50	52	0	33
55	56	1	3
58	62	4	7
58	60	8	13
57	59	14	16
62	64	12	18
61	65	0	3
65	68	0	8
68	70	11	13
70	73	0	5
73	76	0	17
76	79	12	14
76	88	0	8
82	83	8	14
87	89	14	18
85	87	23	25
80	82	29	32
88	92	0	10
87	88	14	18
88	91	15	17
88	90	31	33
92	106	0	18

Table F-1 Chain drag survey field data for Bloomington Structure Number 057-0088 eastbound (Continued).

92	95	24	29
97	99	25	30
105	107	23	28
109	114	20	33
115	118	30	33
106	123	0	3
123	126	0	5
128	131	6	12
126	146	0	4
132	134	12	14
138	140	4	6
143	144	10	12
144	147	13	16
144	147	20	22
149	154	19	25
149	161	0	17
161	166	0	14
166	168	0	11
168	187	0	17
168	170	29	33
182	184	30	32
187	189	29	30
188	190	3	7
190	193	3	17
193	195	0	12
195	196	0	10
196	198	3	4
198	200	0	16
200	209	0	5
200	203	10	16
204	208	0	9
208	212	0	16
204	206	13	16
212	215	0	5
216	218	0	10
218	221	0	5
221	223	0	16
221	223	18	20
221	223	30	32
223	245	0	16
226	228	21	25
245	248	0	6
245	263	0	15
262	264	15	16
262	264	23	30

Table F-2 Chain drag survey field data for Bloomington Structure Number 057-0088 eastbound.

East Bound from Abutment About and Along Left (North) Curb in Feet			
Length Start	Length End	Width Start	Width End
0	1	0	13
7	10	2	7
15	17	3	10
20	23	3	11
41	44	2	10
46	48	8	10
50	52	1	5
55	57	12	13
56	58	0	2
63	68	0	2
84	87	0	11
88	91	11	13
92	98	0	4
98	101	0	10
97	100	10	13
108	113	0	13
113	128	10	13
114	117	5	9
117	127	0	8
134	139	0	2
136	139	2	4
149	151	0	4
154	156	2	7
162	165	0	2
166	169	2	6
168	170	0	2
178	181	2	13
183	186	2	8
187	190	2	10
190	192	1	3
197	200	2	11
206	209	2	6
222	223	0	2
223	225	0	13
225	227	0	13
249	252	3	7
265	266	6	12

Table F-3 Chain drag survey field data for Bloomington Structure Number 057-0088 westbound.

Westbound from Abutment About and Along Right (North) Curb in Feet			
Length Start	Length End	Width Start	Width End
0	4	0	4
4	18	0	7
7	11	7	12
16	18	5	11
18	24	0	5
24	31	0	4
31	40	0	14
38	40	0	34
40	42	0	18
42	43	0	16
43	46	0	12
46	50	0	7
50	55	0	17
55	60	0	11
54	65	12	19
55	65	2	3
65	68	0	19
68	70	0	9
70	74	0	5
74	85	0	19
85	87	0	13
87	90	0	18
90	95	0	6
95	98	0	14
98	110	0	19
110	115	0	19
117	119	5	12
119	121	14	16
121	123	8	13
124	127	7	12
122	124	15	17
125	128	12	18
127	128	9	11
127	137	0	8
115	127	0	3
129	131	7	10
131	133	10	12
136	143	0	12
143	146	0	17
146	148	0	12
148	153	0	15
153	160	0	18
150	167	0	6
167	175	0	10
175	180	0	16

Table F-3 Chain drag survey field data for Bloomington Structure Number 057-0088 westbound (Continued).

180	183	0	5
192	194	0	12
194	197	0	16
194	200	0	14
200	204	5	9
200	214	0	5
206	210	7	16
212	214	5	16
217	218	10	18
217	221	6	8
219	221	9	11
220	224	3	5
213	214	22	25
217	219	22	24
220	223	27	29
228	232	23	25
231	233	21	25
234	237	26	30
236	239	22	26
240	242	27	29
242	244	23	26
245	247	27	30
255	256	22	24
261	262	19	25
234	237	0	15
237	246	0	16
246	249	0	11
249	256	0	12
256	257	13	15
263	265	0	12
256	262	0	5
194	196	23	25
162	164	23	25
159	160	24	27
150	152	27	30
146	148	24	25
139	141	21	24
145	147	28	30
145	146	21	23
102	104	21	24
103	105	20	30
105	107	30	32
92	100	24	33
91	92	30	33
87	90	24	36
86	88	30	33
81	83	29	30
78	80	30	32
70	74	30	33

Table F-4 Chain drag survey field data for Bloomington Structure Number 057-0088 westbound.

Westbound from Abutment About and Along Left (South) Curb in Feet			
Length Start	Length End	Width Start	Width End
0	1	0	4
0	1	6	13
10	11	1	2
11	14	1	10
19	21	1	4
32	36	1	10
39	40	0	7
39	40	12	13
40	41	11	13
57	61	0	12
64	67	0	12
74	78	7	12
81	84	0	11
84	87	0	6
87	92	0	13
92	96	0	3
96	102	0	13
102	105	7	10
104	107	8	13
106	109	1	5
109	118	0	13
118	124	1	5
124	128	1	8
128	133	1	5
134	136	1	5
140	143	1	5
145	147	8	13
147	151	1	13
152	156	1	13
158	161	0	13
163	166	0	13
170	172	2	4
170	173	11	13
174	179	1	8
179	181	1	13
186	187	1	3
191	193	2	12
195	198	0	8
203	205	1	9
215	216	2	3
215	216	11	13
216	217	4	5
216	217	8	13
222	225	1	9
228	231	6	10

Table F-4 Chain drag survey field data for Bloomington Structure Number 057-0088 westbound (Continued).

229	231	11	13
233	236	1	9
239	242	1	6
244	247	0	13
248	251	10	13
251	255	1	13
259	261	1	2
258	259	9	10
265	266	0	2

Table F-5 Chain drag survey field data for Peoria Structure Number 090-0118.

Eastbound from Abutment About and Along Left (North) Curb in Feet			
Length Start	Length End	Width Start	Width End
330	330	10	13

Table F-6 Chain drag survey field data for Peoria Structure Number 072-0106.

Southbound from Abutment About and Along Left (East) Curb in Feet			
Length Start	Length End	Width Start	Width End
NONE			

Table F-7 Chain drag survey field data for Peoria Structure Number 072-0106.

Southbound from Abutment About and Along Right (West) Curb in Feet			
Length Start	Length End	Width Start	Width End
80	83	12	14
68	70	30	32
78	81	29	33
81	83	21	23
84	87	12	14
84	86	20	23
84	85	30	31
88	90	21	25
100	103	13	15
100	102	21	22
99	101	22	25
97	99	29	32
105	107	21	23
109	111	18	20
123	124	9	11

Table F-8 Chain drag survey field data for Peoria Structure Number 072-0107.

Northbound from Abutment About and Along Left (West) Curb in Feet			
Length Start	Length End	Width Start	Width End
38	40	16	19
39	40	2	5
54	55	12	13
55	57	2	5
56	57	14	15
57	58	17	19
62	64	13	15
62	64	18	20
71	73	17	19
73	75	2	4
83	85	10	12
89	91	4	6
93	95	4	6
94	95	9	12
98	99	10	14
98	99	16	18
101	103	16	18
105	107	2	5
105	107	9	12
106	107	13	14
113	115	8	11
117	119	8	10
138	139	7	9

Table F-9 Chain drag survey field data for Peoria Structure Number 072-0107.

Northbound from Abutment About and Along Right (East) Curb in Feet			
Length Start	Length End	Width Start	Width End
0	1	22	24
10	11	11	14
33	35	6	9
47	49	13	16
59	62	19	21
63	65	13	15
64	66	9	13
67	70	15	18
72	74	11	15
79	81	18	20
86	89	12	15
85	87	10	12
85	87	6	8
104	107	16	21
111	113	6	8
112	115	18	21
113	116	4	7
116	119	16	20
117	120	21	24
126	128	18	20
127	130	21	24
141	142	17	20
141	142	23	24

Table F-10 Chain drag survey field data for Peoria Structure Number 072-0108.

Southbound from Abutment About and Along Left (East) Curb in Feet			
Length Start	Length End	Width Start	Width End
105	107	13	15

Table F-11 Chain drag survey field data for Peoria Structure Number 072-0108.

Southbound from Abutment About and Along Right (West) Curb in Feet			
Length Start	Length End	Width Start	Width End
110	103	28	30
111	114	10	15

Table F-12 Chain drag survey field data for Peoria Structure Number 072-0109.

Northbound from Abutment About and Along Left (West) Curb in Feet				
Length Start	Length End	Width Start	Width End	Comment
30	32	0	2	pothole/popout
39	41	0	2	pothole/popout
42	43	0	1	pothole/popout
44	46	6	10	
46	48	0	2	pothole/popout
85	87	6	8	

Table F-13 Chain drag survey field data for Peoria Structure Number 072-0109.

Northbound from Abutment About and Along Right (East) Curb in Feet				
Length Start	Length End	Width Start	Width End	Comment
84	87	13	16	
87	90	10	16	
23	24	2	4	minor spalling along joint
23	24	12	14	minor spalling along joint
23	24	14	16	minor spalling along joint
23	24	30	32	minor spalling along joint
128	129	12	14	minor spalling along joint
129	130	23	25	minor spalling along joint

Table F-14 Chain drag survey field data for Peoria Structure Number 072-0110.

Northwest Bound from Abutment About and Along Left (South West) Curb in Feet			
Length Start	Length End	Width Start	Width End
22	24	11	13
29	30	5	6
46	48	3	6
47	48	17	18
51	53	17	18
67	69	9	11
67	69	11	13
86	87	11	12
115	116	3	4
119	120	10	12
127	129	13	15
133	135	16	18
140	142	14	16
142	143	5	7
160	161	10	11
195	196	6	8
205	206	2	3

Table F-15 Chain drag survey field data for Peoria Structure Number 072-0110.

Northwest Bound from Abutment About and Along Right (NorthEast) Curb in Feet			
Length Start	Length End	Width Start	Width End
69	70	7	13
71	74	16	19
79	82	16	19
82	84	8	12
84	86	17	21
88	90	12	14
89	91	19	21
99	101	18	20
111	114	16	21
112	114	14	16
112	114	10	13
119	121	15	20
119	121	9	14
124	125	6	8
125	126	19	21
133	135	17	21
132	134	10	13
157	159	19	21
171	174	19	21

Table F-16 Chain drag survey field data for Peoria Structure Number 072-0111.

South Bound from Abutment			
Measured about and along joint of left and right lanes (left lane is positive) in feet.			
Length Start	Length End	Width Start	Width End
9	10	0	-1
43	44	0	-1
49	51	2	4
57	58	1	6
62	63	4	6
74	76	-1	1
114	115	-1	0
123	125	4	6
125	126	-1	1
130	131	0	2
130	131	3	5
135	137	3	8
145	146	3	4
151	152	3	7
156	157	6	7
165	166	5	7
168	170	4	7
173	174	3	5
188	189	10	12
197	199	10	13
205	206	11	13
209	211	10	13
215	217	14	16
258	260	10	12
268	270	10	12
269	271	4	6
274	276	4	7
274	275	14	17
278	280	11	15
282	284	14	17
289	290	13	15
292	294	15	16

Table F-17 Chain drag survey field data for Peoria Structure Number 072-0111.

South Bound from Abutment About and Along Right (West) Curb in Feet			
Length Start	Length End	Width Start	Width End
98	100	10	14
103	104	10	11
104	107	12	14
110	112	18	20
115	117	18	20
119	121	10	12
119	121	16	19
121	122	19	20
135	144	18	21
146	149	9	16
154	155	11	13
154	157	14	20
159	163	9	14
158	164	16	20
166	168	12	19
170	171	12	14
172	174	16	20
174	178	9	21
178	183	18	21
180	181	11	13
186	189	9	14
188	190	17	20
239	242	7	16
243	246	9	16
248	251	12	16
257	260	17	21
270	272	19	21
274	277	20	21
301	303	19	21
44	47	10	12
44	47	16	21
57	59	10	13
59	61	16	18
73	75	17	20
233	235	10	12
246	248	16	18
253	255	11	13
298	300	18	22

Table F-18 Chain drag survey field data for Marion Structure Number 100-0005.

South Bound from Abutment About and Along Right (West) Curb				
Length Start	Length End	Width Start	Width End	Comment
0	2	0	16	
2	7	10	16	
2	7	3	6	
7	18	0	6	
18	24	3	5	
24	27	0	6	
27	30	0	5	
24	26	15	16	
26	28	13	16	
27	30	0	4	
34	36	9	11	
36	40	0	2	
54	66	0	1	
61	66	2	6	
66	71	0	4	
77	84	4	6	
78	81	7	8	
80	100	3	4	
92	94	6	8	
100	105	0	6	
105	108	0	2	
108	111	0	1	
111	114	0	2	
114	118	0	4	
115	118	4	6	
118	127	1	6	
117	121	11	16	
121	127	6	16	
123	140	0	2	
127	131	2	16	
131	133	2	9	
130	133	14	16	
134	145	2	6	
133	139	14	16	
145	152	3	6	
142	152	9	16	
151	152	0	4	
0	6	16	21	
0	8	30	32	
0	24	15	16	
14	21	32	33	
24	25	16	17	
24	26	16	33	
23	24	29	33	
26	28	27	33	
26	28	16	18	

Table F-18 Chain drag survey field data for Marion Structure Number 100-0005 (Continued).

28	31	15	17	
28	34	20	21	
50	55	29	32	
103	113	29	32	
113	115	28	32	
115	120	27	30	
120	124	27	29	
120	124	22	24	
116	126	24	26	
116	126	26	28	
120	124	17	19	
120	123	28	32	
123	126	19	32	
126	130	16	32	
130	131	24	32	
131	134	16	24	
132	134	24	32	
134	143	25	33	
142	143	16	21	
133	147	16	18	
143	146	21	32	
145	146	19	21	
147	152	16	19	
151	152	19	32	
6	8	33	34	
6	8	34	36	
11	12	33	36	
12	19	32	33	
12	15	36	37	
21	22	41	45	
13	16	45	48	
22	31	44	48	
26	29	40	44	
26	30	32	37	
30	33	38	44	
31	34	40	41	
30	42	33	35	
37	42	35	36	
37	38	47	48	
42	48	46	47	
48	70	32	46	
53	55	37	39	
54	56	40	43	
53	68	45	48	
64	66	38	43	
68	71	45	47	
71	97	45	48	
70	76	32	35	
76	79	32	35	

Table F-18 Chain drag survey field data for Marion Structure Number 100-0005 (Continued).

78	79	41	43	
79	90	36	37	
89	97	33	35	
97	105	32	33	
97	104	36	37	
96	105	46	48	
105	119	45	47	
105	109	32	36	
113	118	32	35	
118	120	32	45	
120	122	37	45	
122	124	42	48	
120	126	32	34	
119	124	45	47	
124	132	45	48	
123	141	46	48	
141	152	45	48	
131	134	42	45	
133	136	38	42	
136	141	42	45	
135	152	33	35	
141	144	36	45	
144	146	36	42	
146	152	36	42	
150	152	42	45	
150	152	32	33	
120	126	19	23	concrete patches
123	126	23	27	concrete patches
119	123	29	32	concrete patches
126	130	16	32	concrete patches
130	132	26	32	concrete patches
133	142	16	21	concrete patches
146	152	19	32	concrete patches
13	16	33	36	concrete patches
22	27	32	45	concrete patches
71	77	34	36	concrete patches
79	90	34	36	concrete patches
98	105	33	36	concrete patches
118	120	34	36	concrete patches
120	124	34	38	concrete patches
124	127	34	45	concrete patches
127	132	32	45	concrete patches
132	135	34	36	concrete patches
134	137	42	45	concrete patches
144	150	42	45	concrete patches

